ELSEVIER

www.elsevier.nl/locate/jelechem

Journal of Electroanalytical Chemistry 479 (1999) 77–97

JOURNAL OF ELECTROANALYTICAL CHEMISTRY

Cumulative Author Index of Volumes 460–479

Abbessi, M., see Keita, B. **477**, 146

Abd El Meguid, E.A., Berenz, P. and Baltruschat, H.
Step decoration at Pt single crystal electrodes: role of the anion **467**, 50

Abdul-Redah, T., see Sperling, J. **477**, 62

Abe, M., Kondo, T., Uosaki, K. and Sasaki, Y.
Synthesis and electrochemical characterization of self-assembled monolayers of redox-active oxide-bridged triruthenium(III) clusters on Au(111) **473**, 93

Aberdam, D., see Pauporté, T. **465**, 88

Abruña, H.D., see Herrero, E. **460**, 121

Abruña, H.D., see Smith, S.P.E. **467**, 43

Adachi, K., see Talaie, A. **468**, 19

Adžić, R.R., see Marinković, N.S. **467**, 291

Aeiyach, S., see Lagrost, C. **476**, 1

Aeiyach, S., see Petitjean, J. **478**, 92

Agostinho, S.M.L., see Villamil, R.F.V. **472**, 112

Ahlberg, E., see Simic, N. **462**, 34

Akiba, U., see Azehara, H. **473**, 68

Al-Akl, A., Attard, G.A., Price, R. and Timothy, B.
Voltammetric and UHV characterisation of the (1 × 1) and reconstructed hex-R0.7° phases of Pt{100} **467**, 60

Alcobe, X., see Gómez, E. **475**, 66

Aldaz, A., see Climent, V. **467**, 20

Aldaz, A., see Climent, V. **461**, 65

Aldaz, A., see Huerta, F. **475**, 38

Aldaz, A., see Huerta, F. **469**, 159

Aldaz, A., see Huerta, F. **467**, 105

Alleman, K.S. and Peters, D.G.
Catalytic reduction of 1,8-diiodooctane by electrogenerated cobalt(I) salen and formation of μ-(1,8-*n*-octyl)-bis[(salen)cobalt(III)] **460**, 207

Alonso, B., see Casado, C.M. **463**, 87

Alpatova, N.M., see Semenikhin, O.A. **463**, 190

Alperson, B., Homyonfer, M. and Tenne, R.
Photoelectrochemical studies with inorganic cage structures of metal dichalcogenides **473**, 186

Amatore, C., Farsang, G., Maisonhaute, E. and Simon, P.
Voltammetric investigation of the anodic dimerization of *p*-halogenoanilines in DMF: Reactivity of their electrogenerated cation radicals **462**, 55

Amatore, C., see Haj Said, A. **464**, 85

Amatore, C., Thouin, L. and Fatima Bento, M.
Steady state voltammetry at low electrolyte/reactant concentration ratios: what it means and what it does not mean **463**, 45

Anaissi, F.J., Demets, G.J.-F., Toma, H.E. and Coelho, A.C.V.
Modified electrodes based on mixed bentonite vanadium(V) oxide xerogels **464**, 48

Anbu Kulandainathan, M., see Gorostiza, P. **469**, 48

Ando, S., see Müller, P. **467**, 282

Andrade, E.M., see Viva, F.A. **471**, 180

Andrauskas, D.M., see Stine, K.J. **472**, 147

Andrauskas, D.M., see Stine, K.J. **465**, 209

Andreasen, G., see Martins, M.E. **477**, 14

Andreasen, G., Vela, M.E., Salvarezza, R.C. and Arvia, A.J.
Influence of the electric potential on the structure of pyridine adlayers on Au(111) terraces from in-situ scanning tunnelling microscopy imaging **467**, 230

Andrieux, C.P., Savéant, J.-M. and Tardy, C.
Thermodynamic and kinetic basicities of the carbon and oxygen ends of enolates. Their role in the reductive cleavage electrochemistry of α-substituted acetophenones **476**, 81

Angnes, L., see Brito, M.S.L. **468**, 150

Aogaki, R., see Nakabayashi, S. **473**, 54

Aoki, A. and Miyashita, T.
A structural effect on electrochemical behavior of hetero-deposited redox polymer Langmuir–Blodgett films containing ferrocene and tris(bipyridine)ruthenium derivatives **473**, 125

Aoki, H., Bühlmann, P. and Umezawa, Y.
Self-assembly of a tricarboxylate receptor through thioamide groups and its use for electrochemical detection of protonated amines **473**, 105

Aoki, K. and Kakiuchi, T.
pK_a of an ω-carboxylalkanethiol self-assembled monolayer by interaction model **478**, 101

Aoki, K., Baars, A., Jaworski, A. and Osteryoung, J.
Chronoamperometry of strong acids without supporting electrolyte **472**, 1

Aoki, K., see Baars, A. **464**, 128

Aoki, K., see Teragishi, Y. **473**, 132

Aoki, K., Teragishi, Y. and Tokieda, M.
Light scattering of polyaniline films responding to electrochemical switching **460**, 254

Appetecchi, G.B., Croce, F., De Paolis, A. and Scrosati, B.
A poly(vinylidene fluoride)-based gel electrolyte membrane for lithium batteries **463**, 248

Arai, G., Noma, T., Habu, H. and Yasumori, I.
Pyruvate sensor based on pyruvate oxidase immobilized in a poly(mercapto-*p*-benzoquinone) film **464**, 143

Arai, K., see Takamura, K. **468**, 53

Aramata, A., see Fukuda, T. **467**, 112

Ardizzone, S. and Bianchi, C.L.
Electrochemical features of zirconia polymorphs. The interplay between structure and surface OH species **465**, 136

Arévalo, M.C., Rodríguez, J.L. and Pastor, E.
Adsorption, oxidation and reduction reactions of propargyl alcohol on palladium as studied by electrochemical mass spectrometry **472**, 71

Argyropoulos, P., see Scott, K. **477**, 97

Arihara, K., Kitamura, F., Nukanobu, K., Ohsaka, T. and Tokuda, K.
Voltammetric and spectroscopic study of the adsorption of alkyl viologens on a HOPG electrode **473**, 138

Ariño, C., see Berbel, F. **475**, 99

Ariño, C., see de Haro, C. **462**, 157

Armstrong, R.D. and Horrocks, B.R.
Thermodynamics for the situation where there is a discontinuous change of the electrode condition with potential due to the formation of a two dimensional condensed phase—diffuse layer effects **463**, 9

Arvia, A.J., see Andreasen, G. **467**, 230

Arvia, A.J., see Bolzán, A.E. **475**, 181

Arvia, A.J., see Bolzán, A.E. **461**, 40

Arvia, A.J., see Gómez, M.M. **474**, 74

Arvia, A.J., see Martins, M.E. **477**, 14

Ataka, K. and Osawa, M.
In situ infrared study of cytosine adsorption on gold electrodes **460**, 188

PII: S0022-0728(99)00466-0

Ataka, K., Hara, Y. and Osawa, M.
A new approach to electrode kinetics and dynamics by potential modulated Fourier transform infrared spectroscopy **473**, 34
Ataka, K., Hara, Y. and Osawa, M.
A new approach to electrode kinetics and dynamics by potential modulated Fourier transform infrared spectroscopy **473**, 34
Attard, G.A., see Al-Akl, A. **467**, 60
Attard, G.A., see Whelan, C.M. **474**, 138
Aubert, P.-H., Neudeck, A., Dunsch, L., Audebert, P., Capdevielle, P. and Maumy, M.
Electrochemical synthesis and structural studies of copolymers based on the electrooxidation of pyrrole and some salen compounds **470**, 77
Audebert, P., see Aubert, P.-H. **470**, 77
Aurbach, D., see Levi, M.D. **479**, 12
Aurbach, D., see Levi, M.D. **477**, 32
Aurbach, D., see Lu, Z. **466**, 203
Azcurra, A.I., Yudi, L.M. and Baruzzi, A.M.
Interfacial phenomena involving Fe(III)–ofloxacin complexes at the water|1,2-dichloroethane interface **461**, 194
Azechi, T., see Murakoshi, K. **473**, 117
Azehara, H., Yoshimoto, S., Hokari, H., Akiba, U., Taniguchi, I. and Fujihira, M.
Investigation of the structure of self-assembled monolayers of asymmetrical disulfides on Au(111) electrodes by electrochemical desorption **473**, 68

Baars, A., Aoki, K. and Watanabe, J.
The fast dropping oil | water electrode **464**, 128
Baars, A., see Aoki, K. **472**, 1
Babaei, A. and McQuillan, A.J.
An in situ UV-vis and IR spectroelectrochemical study of the deposition of a hydroquinone anion salt on platinum electrodes from dichloromethane solutions **462**, 266
Baba, R., see Ishibashi, K.-i. **465**, 195
Badiali, J.P., see Pecina, O. **475**, 46
Badiali, J.-P., see Vorotyntsev, M.A. **472**, 7
Baek, D., see Oh, K.-C. **468**, 98
Bae, Z.-U., Park, J.-H., Lee, S.-H. and Chang, H.-Y.
Nickel(II) tetraaza macrocycle modified electrodes for the electrocatalytic determination of L-ascorbic acid by the flow injection method **468**, 85
Bagel, O., L'Hostis, E., Lagger, G., Osborne, M.D., Seddon, B.J., Girault, H.H., Brack, D., Loyall, U. and Schäfer, H.
Rotograved carbon electrodes for amperometric cadmium and lead determination **469**, 189
Bakir, M.
Electrochemical properties of the first Re(I)–carbonyl compound of di-2-pyridyl ketone.oxime (dpk.oxime), *fac*-$Re(CO)_3$(dpk.oxime)Cl, in non-aqueous media **466**, 60
Baldo, M.A., see Daniele, S. **471**, 48
Ballarin, B., Seeber, R., Tonelli, D. and Vaccari, A.
Electrocatalytic properties of nickel(II) hydrotalcite-type anionic clay: application to methanol and ethanol oxidation **463**, 123
Baltruschat, H., see Abd El Meguid, E.A. **467**, 50
Baltruschat, H., see Vrestal, J. **461**, 90
Baranowski, B.
Electrochemical formation of nickel hydride in alkaline solutions **472**, 182
Baranski, A.S., see Basa, A. **463**, 200
Barba, F., see Batanero, B. **469**, 201
Barber, J. and Conway, B.E.
Response to discussion of the paper by Barber et al. [J. Electroanal. Chem. 446 (1998) 125] in the Short Communication by J.-P. Diard et al. [J. Electroanal. Chem. 466 (1999) 122] **466**, 124
Barber, J.H. and Conway, B.E.
Structural specificity of the kinetics of the hydrogen evolution reaction on the low-index surfaces of Pt single-crystal electrodes in 0.5 M dm^{-3} NaOH **461**, 80
Barbier, J., see Chollier-Brym, M.J. **474**, 147
Barnes, C.J., see Whelan, C.M. **474**, 138
Barthel, J., Neueder, R., Rawytsch, P. and Roch, H.
Conductivity study on lithium bromide in propylene carbonate + acetonitrile mixtures in dilute solutions from − 35 to 75°C **471**, 78
Bartlett, P.N., see Galceran, J. **476**, 132
Bartlett, P.N., see Galceran, J. **466**, 15
Baruzzi, A.M., see Azcurra, A.I. **461**, 194
Baruzzi, A.M., see Dassie, S.A. **464**, 54
Basa, A., Krogulec, T. and Baranski, A.S.
Kinetics of sulfide ion adsorption at copper amalgam electrode **463**, 200
Basura, V.I., see Beattie, P.D. **468**, 180
Batanero, B., Pérez, M.J. and Barba, F.
Electrosynthesis of 3-chloro-4-substituted-coumarins **469**, 201
Baute, N., Martinot, L. and Jérôme, R.
Investigation of the cathodic electropolymerization of acrylonitrile, ethylacrylate and methylmethacrylate by coupled quartz crystal microbalance analysis and cyclic voltammetry **472**, 83
Beattie, P.D., Basura, V.I. and Holdcroft, S.
Temperature and pressure dependence of O_2 reduction at Pt | Nafion® 117 and Pt | BAM® 407 interfaces **468**, 180
Becagli, S., see Pezzatini, G. **462**, 127
Platinum–palladium loaded polypyrrole film electrodes for the electrooxidation of D-glucose in neutral media **476**, 171
Bechtold, T., Burtscher, E. and Turcanu, A.
Anthraquinones as mediators for the indirect cathodic reduction of dispersed organic dyestuffs **465**, 80
Beck, F., see Boinowitz, T. **461**, 167
Behm, R.J., see Magnussen, O.M. **467**, 258
Belgsir, E.M., see Cherqaoui, A. **464**, 101
Bellec, N., Lorcy, D., Robert, A., Carlier, R. and Tallec, A.
Cathodic synthesis of powerful electron π-donors including dithiadiazafulvalenes **462**, 137
Bento, E.S., see de Azevedo, D.C. **466**, 99
Berbel, F., Díaz-Cruz, J.M., Ariño, C. and Esteban, M.
Voltammetry of sparingly soluble metal complexes: a differential pulse polarographic study of the Zn(II) + oxalate system **475**, 99
Berbel, F., see de Haro, C. **462**, 157
Berchmans, S., Yegnaraman, V., Sandhyarani, N., Murty, K.V.G.K. and Pradeep, T.
Formation of a nickel hydroxide monolayer on Au through a self-assembled monolayer of 5,5′-dithiobis(2-nitrobenzoic acid): voltammetric, SERS and XPS investigations of the modified electrodes **468**, 170
Berendson, J., see Nilsson, E. **460**, 88
Berenz, P., see Abd El Meguid, E.A. **467**, 50
Bergel, A., see Délécouls, K. **468**, 139
Bergelin, M., Herrero, E., Feliu, J.M. and Wasberg, M.
Oxidation of CO adlayers on Pt(111) at low potentials: an impinging jet study in H_2SO_4 electrolyte with mathematical modeling of the current transients **467**, 74
Berlouis, L.E.A., see Huerta, F. **463**, 109
Bernard, C., see Klíma, J. **462**, 181
Berthier, F., Diard, J.-P. and Montella, C.
Discontinuous immitance due to a saddle node bifurcation: II: Tangent bifurcation and critical slowdown during isotherm branch switching **460**, 226
Bertoncello, R., see Musiani, M. **465**, 160
Bertotti, M., see Kosminsky, L. **471**, 37
Bessone, J.B., see Salinas, D.R. **470**, 120
Betova, I., Bojinov, M., Lankinen, E. and Sundholm, G.
Studies on the redox behaviour of some polythiophene derivatives by impedance spectroscopy in symmetrical and asymmetrical configurations **472**, 20
Betova, I., see Bojinov, M. **475**, 58
Beyer, L., see Lubert, K.-H. **475**, 73
Beyer, L., see Lubert, K.-H. **462**, 174
Bianchi, C.L., see Ardizzone, S. **465**, 136
Bianchini, A., see Cataldi, T.R.I. **471**, 42
Bianco, P., see Lojou, E. **471**, 96

Bieniasz, L.K.
Finite-difference electrochemical kinetic simulations using the Rosenbrock time integration scheme **469**, 97
Biernat, J.F., see Zawisza, I. **471**, 156
Bilewicz, R., see Zawisza, I. **471**, 156
Bilger, C., see Chen, A. **467**, 342
Birss, V.I., see Bock, C. **475**, 20
Bisquert, J., Garcia-Belmonte, G., Fabregat-Santiago, F. and Bueno, P.R.
Theoretical models for ac impedance of finite diffusion layers exhibiting low frequency dispersion **475**, 152
Bizzotto, D., see Chen, A. **467**, 342
Bley-Escrich, J., see Gisselbrecht, J.P. **469**, 170
Bocarsly, A.B., see Chang, C.C. **470**, 99
Bock, C. and Birss, V.I.
Anion and water involvement in hydrous Ir oxide redox reactions in acidic solutions **475**, 20
Boinowitz, T. and Beck, F.
A quantitative discrimination between anion insertion- and surface redox-reactions at graphite with the rotating ring/disk-electrode **461**, 167
Bojarska, E. and Czochralska, B.
Electrooxidation of the antileukemic 2-chloro-2′-deoxyadenosine and related compounds **477**, 89
Bojinov, M., Betova, I., Fabricius, G., Laitinen, T. and Raicheff, R.
Passivation mechanism of iron in concentrated phosphoric acid **475**, 58
Bojinov, M., see Betova, I. **472**, 20
Bolzán, A.E., Florit, M.I. and Arvia, A.J.
The potentiodynamic behaviour of iridium electrodes in aqueous 3.7 M H_2SO_4 in the 293–195 K range **461**, 40
Bolzán, A.E., Wakenge, I.B., Salvarezza, R.C. and Arvia, A.J.
Electrochemical response of thiourea and formamidine disulphide on polycrystalline platinum in aqueous 0.5 M sulphuric acid **475**, 181
Bonfranceschi, A., Pérez Córdoba, A., Keunchkarian, S., Zapata, S. and Tucceri, R.
Transport across poly(*o*-aminophenol) modified electrodes in contact with media containing redox active couples. A study using rotating disc electrode voltammetry **477**, 1
Bontá, M., see Squella, J.A. **466**, 90
Boodts, J.F.C., see de Azevedo, D.C. **466**, 99
Borcherding, H., see Kirstein, D. **474**, 43
Bottecchia, O.L., see de Abreu, F.C. **462**, 195
Bouchard, G., see Reymond, F. **462**, 235
Bozkurt, V., Xu, Z., Brienne, S.H.R., Butler, I.S. and Finch, J.A.
In situ orientation study of xanthate on copper under potential control **475**, 124
Brack, D., see Bagel, O. **469**, 189
Bradley, J.C., Dengra, S., Gonzalez, G.A., Marshall, G. and Molina, F.V.
Ion transport and deposit growth in spatially coupled bipolar electrochemistry **478**, 128
Bragato, C., see Daniele, S. **471**, 48
Brandon, N.P., see Kelsall, G.H. **471**, 116
Braybrook, G.D., see Finot, M.O. **466**, 234
Brett, C.M.A., Fungaro, D.A., Morgado, J.M. and Gil, M.H.
Novel polymer-modified electrodes for batch injection sensors and application to environmental analysis **468**, 26
Brett, C.M.A., see Brito, M.S.L. **468**, 150
Brewster, J.D., see Gehring, A.G. **469**, 27
Brienne, S.H.R., see Bozkurt, V. **475**, 124
Brito, M.S.L., Angnes, L., Brett, C.M.A. and Gutz, I.G.R.
Determination of the surface charge density of a mercury electrode by extrusion: a new method for correction of the faradaic component **468**, 150
Broekmann, P., Wilms, M., Kruft, M., Stuhlmann, C. and Wandelt, K.
In-situ STM investigation of specific anion adsorption on Cu(111) **467**, 307
Brooksby, P.A., see Love, J.G. **464**, 93
Brown, R.B., see Yoon, I.J. **464**, 135
Brown, S., see Mahmoud, A. **463**, 129
Bruckenstein, S., see Zeng, X. **460**, 143
Bruckenstein, S., see Zeng, X. **460**, 131
Brunetti, B. and Ugo, P.
Factors influencing the ion-exchange preconcentration and voltammetric behaviour of redox cations at polyestersulfonated ionomer coated electrodes in acetonitrile solutions **460**, 38
Brust, M., see Simison, S. **470**, 89
Buck, M., see Tadjeddine, A. **473**, 25
Buda, M., Ion, A., Moutet, J.-C., Saint-Aman, E. and Ziessel, R.
Electrochemical response to anions by neutral ferrocenyl receptors containing 2,2′-bipyridyl arms **469**, 132
Bueno, P.R., see Bisquert, J. **475**, 152
Buess-Herman, C., see Vico, S. **475**, 1
Bühlmann, P., see Aoki, H. **473**, 105
Buller, L.J., see Herrero, E. **460**, 121
Bulska, E., see Grdeń, M. **460**, 30
Bureau, C.
Polymerization reaction coupled to the charge transfer: propagation versus termination as a source of permanent travelling waves and multi-peak voltammograms **479**, 43
Bureau, C., see Charlier, J. **465**, 200
Bureau, C., see Viel, P. **470**, 14
Burke, L.D. and Nagle, L.C.
Anomalous electrochemical behaviour of palladium in aqueous solution **461**, 52
Burtscher, E., see Bechtold, T. **465**, 80
Buschmann, H.-J. and Schollmeyer, E.
The complex formation of non-cyclic polyethers and crown ethers with Ag^+ in acetone and propylene carbonate studied by potentiometric and calorimetric methods **474**, 188
Butler, I.S., see Bozkurt, V. **475**, 124
Caix-Cecillon, C., Chardon-Noblat, S., Deronzier, A., Haukka, M., Pakkanen, T.A., Ziessel, R. and Zsoldos, D.
Electrochemical formation and spectroelectrochemical characterization of organometallic $[Ru(L)(CO)_2]_n$ polymers; L = disubstituted-2,2′-bipyridine **466**, 187
Calvente, J.J., see Marinković, N.S. **467**, 325
Calvente, J.J., see Molero, M. **460**, 100
Canny, J., see Keita, B. **478**, 76
Canny, J., see Keita, B. **477**, 146
Cao, H., see Yu, J. **474**, 69
Capdevielle, P., see Aubert, P.-H. **470**, 77
Caporali, S., see Pezzatini, G. **475**, 164
Carlier, R., see Bellec, N. **462**, 137
Carlier, V., see Vico, S. **475**, 1
Carrette, L.P.L., see Lampitt, R.A. **460**, 80
Carrier, M., see Zouaoui, A. **474**, 113
Carrupt, P.-A., see Reymond, F. **462**, 235
Cartaxo, M.A.M., see Tavares, A.C. **464**, 187
Casabó, J., see Lubert, K.-H. **475**, 73
Casado, C.M., Cuadrado, I., Alonso, B., Morán, M. and Losada, J.
Silicon-based ferrocenyl dendrimers as anion receptors in solution and immobilized onto electrode surfaces **463**, 87
Casella, I.G. and Guascito, M.R.
Anodic electrodeposition of conducting cobalt oxyhydroxide films on a gold surface. XPS study and electrochemical behaviour in neutral and alkaline solution **476**, 54
Casella, I.G., Guascito, M.R. and Sannazzaro, M.G.
Voltammetric and XPS investigations of nickel hydroxide electrochemically dispersed on gold surface electrodes **462**, 202
Cassir, M., see Chauvaut, V. **474**, 9
Cataldi, T.R.I., De Benedetto, G. and Bianchini, A.
Enhanced stability and electrocatalytic activity of a ruthenium-modified cobalt–hexacyanoferrate film electrode **471**, 42
Catalin Popescu, I., Dominguez, E., Narváez, A., Pavlov, V. and Katakis, I.
Electrocatalytic oxidation of NADH at graphite electrodes modified with osmium phenanthrolinedione **464**, 208
Cattaneo, C., Sanchez de Pinto, M.I., Mishima, H., López de Mishima, B.A., Lescano, D. and Cornaglia, L.
Characterization of platinum-rutheniun electrodeposits using XRD, AES and XPS analysis **460**, 32
Cattarin, S., Decker, F., Dini, D. and Margesin, B.
In-situ detection of stress in oxide films during Si electrodissolution in acidic fluoride electrolytes **474**, 182

Cavalcanti, J.C.M., see de Azevedo, D.C. **466**, 99
Cecilia, J., see Galceran, J. **472**, 42
Ceré, S., Vazquez, M., de Sánchez, S.R. and Schiffrin, D.J.
Surface redox catalysis and reduction kinetics of hydrogen peroxide on copper–nickel alloys **470**, 31
Cha, C.-S., see Liu, W.-J. **476**, 101
Cha, G.S., see Shin, J.H. **468**, 76
Cha, G.S., see Yoon, I.J. **464**, 135
Chambers, J.Q., see Johnston, R.F. **466**, 2
Champagne, G.Y., see Moretto, L.M. **467**, 193
Chane-Ching, K.I., see Just, P.E. **479**, 3
Chane-Ching, K.I., see Lagrost, C. **476**, 1
Chang, C.C. and Bocarsly, A.B.
Oxidation of halides by redox enhanced ferricyanide in the $[Fe^{II}–CN–Pt^{IV}]_n$ coordination polymer: an optically triggered process **470**, 99
Chang, H.-Y., see Bae, Z.-U. **468**, 85
Chang, S.-C., see Fan, L.-J. **477**, 111
Chang, S.-C., see Tang, C. **467**, 92
Chaparro, A.M.
Frequency dependent electrolyte electroreflectance at semiconductor | electrolyte interfaces **462**, 251
Chardon-Noblat, S., see Caix-Cecillon, C. **466**, 187
Charlier, J., Bureau, C. and Lecayon, G.
Electropolymerization of methacrylonitrile and *N*-vinyl-2-pyrrolidone as probed by an EQCM **465**, 200
Chatani, S., see Nishino, J. **473**, 217
Chatzidimitriou-Dreismann, C.A., see Sperling, J. **477**, 62
Chauvaut, V. and Cassir, M.
Behaviour of titanium species in molten $Li_2CO_3 + Na_2CO_3$ and $Li_2CO_3 + K_2CO_3$ in the anodic conditions used in molten carbonate fuel cells: II. Electrochemical intercalation of Li^+ in Li_2TiO_3 at 600 and 650°C **474**, 9
Chbihi, M.E.M., Takky, D., Hahn, F., Huser, H., Léger, J.M. and Lamy, C.
In-situ infrared reflectance spectroscopic study of propanediol electrooxidation at platinum and gold: Part 1. 1,3-Propanediol **463**, 63
Che, B., see Wan, X. **470**, 23
Chen, A., Shi, Z., Bizzotto, D., Lipkowski, J., Pettinger, B. and Bilger, C.
Iodide adsorption at the Au(111) electrode surface **467**, 342
Chen, A., Yang, D. and Lipkowski, J.
Electrochemical and FTIR studies of 4-cyanopyridine adsorption at the gold(111) | solution interface **475**, 130
Chen, B., see Yang, D. **470**, 114
Chen, C.F. and Wang, C.M.
Ruthenium purple-containing zeolite modified electrodes and their application for the detection of glucose **466**, 82
Chen, F., Cheng, S.-H., Yu, C.-H., Liu, M.-H. and Su, Y.O.
Electrochemical characterization and electrocatalysis of high valent manganese *meso*-tetrakis(*N*-methyl-2-pyridyl)porphyrin **474**, 52
Cheng, S.-H., see Chen, F. **474**, 52
Chen, H.-Y., see Fang, H. **465**, 219
Chen, H.-Y., see Hu, X.-Y. **466**, 26
Chen, K.Y., see Chen, Y. **471**, 151
Chen, S. and Schell, M.
A comparison of multistability in the electrocatalyzed oxidations of methanol and ethanol in acid and alkaline solutions **478**, 108
Chen Tsai, Y., Suárez, M.F., Compton, R.G., Ito, S. and Ono, N.
Electrochemical investigations and morphology of poly(4,9-dihydro-*o*-benzenonaphtho[2,3-c]pyrrole) and poly-(acenaphtho[1,2-c]pyrrole) **477**, 25
Chen, Y., Chen, K.Y. and Tseung, A.C.C.
An electrochemical alcohol sensor based on a co-electrodeposited Pt | WO_3 electrode **471**, 151
Chen, Y., see Yu, J. **474**, 69
Chen, Z., see Hojo, M. **468**, 110
Cheol Jeon, I., see Lee, C. **463**, 224
Cheol Jeon, I., see Moon, J.-M. **464**, 230
Cherqaoui, A., Takky, D., Kokoh, K.B., Hahn, F., Belgsir, E.M., Léger, J.-M. and Lamy, C.
Electro-oxidation of *meso*-erythritol on platinum in acid medium: analysis of the reaction products **464**, 101
Chevalet, J., see Moretto, L.M. **467**, 193
Chevrot, C., see Randriamahazaka, H. **472**, 103
Chia, L.S., see Li, J. **460**, 234
Chiba, M., see Seo, M. **473**, 49
Chollier-Brym, M.J., Epron, F., Lamy-Pitara, E. and Barbier, J.
Catalytic and electrocatalytic oxidation of oxalic acid in aqueous solutions of different compositions **474**, 147
Chopineaux-Courtois, V., see Reymond, F. **462**, 235
Chou, T.-J. and Tanioka, A.
Current–voltage curves of a composite bipolar membrane in organic acid–water solutions **462**, 12
Chrzanowski, W., see Tremiliosi-Filho, G. **467**, 143
Chu, J., see Shin, J.H. **468**, 76
Chung, C. and Lee, M.
Exchange of self-assembled thiol monolayers on gold: characterization by FT-IR external reflection spectroscopy **468**, 91
Ciszewski, A. and Milczarek, G.
Kinetics of electrocatalytic oxidation of formaldehyde on a nickel porphyrin-based glassy carbon electrode **469**, 18
Ciszkowska, M. and Stojek, Z.
Voltammetry in solutions of low ionic strength. Electrochemical and analytical aspects **466**, 129
Climent, V., Rodes, A., Orts, J.M., Aldaz, A. and Feliu, J.M.
Urea adsorption on Pt(111) electrodes **461**, 65
Climent, V., Rodes, A., Orts, J.M., Feliu, J.M. and Aldaz, A.
The electrochemistry of nitrogen-containing compounds at platinum single crystal electrodes: Part 3. Carbohydrazide on Pt(*hkl*) electrodes **467**, 20
Cobo, E.O., see Salinas, D.R. **470**, 120
Coche-Guérente, L., Desprez, V., Diard, J.-P. and Labbé, P.
Amplification of amperometric biosensor responses by electrochemical substrate recycling: Part I. Theoretical treatment of the catechol–polyphenol oxidase system **470**, 53
Coche-Guérente, L., Desprez, V., Labbé, P. and Therias, S.
Amplification of amperometric biosensor responses by electrochemical substrate recycling: Part II. Experimental study of the catechol–polyphenol oxidase system immobilized in a laponite clay matrix **470**, 61
Coelho, A.C.V., see Anaissi, F.J. **464**, 48
Cohen, Y., see Levi, M.D. **479**, 12
Collomb Dunand-Sauthier, M.-N., Deronzier, A. and Piron, A.
Electrochemical behaviour of $[Mn_2^{III,IV}O_2(phen)_4]^{3+}$ complex in aqueous phen + phenH$^+$ buffer; phen = 1,10-phenanthroline **463**, 119
Collomb Dunand-Sauthier, M.-N., Deronzier, A., Duboc Toia, C., Fontecave, M., Gorgy, K., Leprêtre, J.-C. and Ménage, S.
Electrochemical behaviour of (μ-oxo) diaqua diiron(III) complexes in organic media. Electrogeneration of mononuclear $[Fe^{II}(L)_2(S)_2]^{2+}$ complexes (L = 2,2′-bipyridine and (−)4,5-pinene-2,2′-bipyridine; S = H_2O or CH_3CN) **469**, 53
Colombini, M.P., see Pospišil, L. **472**, 33
Colomès, M., see Fabre, B. **460**, 119
Companys, E., see Galceran, J. **472**, 42
Compton, R.G., see Chen Tsai, Y. **477**, 25
Compton, R.G., see Del Campo, F.J. **477**, 71
Compton, R.G., see Prieto, F. **474**, 60
Compton, R.G., see Suárez, M.F. **462**, 211
Comte, P., see Cosnier, S. **469**, 176
Contant, R., see Keita, B. **478**, 76
Contant, R., see Keita, B. **477**, 146
Contant, R., see Mahmoud, A. **463**, 129
Conway, B.E., see Barber, J. **466**, 124
Conway, B.E., see Barber, J.H. **461**, 80
Conway, B.E., see Pierozynski, B. **467**, 30
Cordoba de Torresi, S.I., see Torresi, R.M. **475**, 193

Córdoba de Torresi, S.I., see Torresi, R.M. **460**, 161
Corio, P., see Villamil, R.F.V. **472**, 112
Cornaglia, L., see Cattaneo, C. **460**, 32
Correia dos Santos, M.M., Paes de Sousa, P.M., Simões Gonçalves, M.L., Lopes, H., Moura, I. and Moura, J.J.G.
Electrochemical studies on *c*-type cytochromes at microelectrodes **464**, 76
Cortona, M.N., Vettorazzi, N.R., Silber, J.J. and Sereno, L.E.
Electrochemical nitration of naphthalene in the presence of nitrite ion in aqueous non-ionic surfactant solutions **470**, 157
Cosnier, S., Senillou, A., Grätzel, M., Comte, P., Vlachopoulos, N., Jaffrezic Renault, N. and Martelet, C.
A glucose biosensor based on enzyme entrapment within polypyrrole films electrodeposited on mesoporous titanium dioxide **469**, 176
Costa, F.M., see Tavares, A.C. **464**, 187
Cousino, M.A., see Wijayawardhana, C.A. **468**, 2
Coutouli-Argyropoulou, E., Kelaidopoulou, A., Sideris, C. and Kokkinidis, G.
Electrochemical studies of ferrocene derivatives and their complexation by β-cyclodextrin **477**, 130
Creager, S.E., see O'Connor, S.D. **466**, 197
Croce, F., see Appetecchi, G.B. **463**, 248
Croce, F., see Tossici, R. **474**, 107
Cuadrado, I., see Casado, C.M. **463**, 87
Cuesta, A., Kibler, L.A. and Kolb, D.M.
A method to prepare single crystal electrodes of reactive metals: application to Pd(*hkl*) **466**, 165
Cuesta, A., see Ortiz, R. **465**, 234
Cui, X., Jiang, D., Diao, P., Li, J., Tong, R. and Wang, X.
Assessing the apparent effective thickness of alkanethiol self-assembled monolayers in different concentrations of $Fe(CN)_6^{3-}/Fe(CN)_6^{4-}$ by ac impedance spectroscopy **470**, 9
Cui, X., see Diao, P. **464**, 61
Čukman, D., see Vuković, M. **474**, 167
Cukrowski, I.
Experimental and calculated complex formation curves for mixed, dynamic and semi-dynamic, metal–ligand systems. A differential pulse polarographic study of Cu^{II}–sarcosine–OH and Cd^{II}–MIDA–OH systems at a fixed ligand to metal ratio and varied pH **460**, 197
Czapla, J., see Czerwiński, A. **471**, 190
Czerwiński, A., Kiersztyn, I., Grdeń, M. and Czapla, J.
The study of hydrogen sorption in palladium limited volume electrodes (Pd-LVE): I. Acidic solutions **471**, 190
Czerwiński, A., see Grdeń, M. **460**, 30
Czochralska, B., see Bojarska, E. **477**, 89

Dalas, E., see Tsamouras, D. **469**, 43
Daniele, S., Bragato, C. and Baldo, M.A.
Preparation and characterization of Nafion® coated sphere-cap mercury microelectrodes **471**, 48
da Silva Pereira, M.I., see Tavares, A.C. **464**, 187
Dassie, S.A., Yudi, L.M. and Baruzzi, A.M.
Voltammetric analysis of Cs^+-DB18C6 complex stoichiometry at the water | 1,2-dichloroethane interface **464**, 54
Davydov, A.D., see Modestov, A.D. **460**, 214
de Abreu, F.C., Tonholo, J., Bottecchia, O.L., Zani, C.L. and Goulart, M.O.F.
Cathodic reduction of 2-nitronaphthothiophen-4,9-quinone: evidence of catalysis by proton donors and its simulation **462**, 195
de Azevedo, D.C., Boodts, J.F.C., Cavalcanti, J.C.M., Santana, A.E.G., dos Santos, A.F., Bento, E.S., Tonholo, J. and Goulart, M.O.F.
Self-protonation mechanism in the electrochemical reduction of Jatropholone **466**, 99
De Benedetto, G., see Cataldi, T.R.I. **471**, 42
Decker, F., see Cattarin, S. **474**, 182
de Haro, C., Berbel, F., Manuel Díaz-Cruz, J., Ariño, C. and Esteban, M.
Voltammetric metal speciation in mixtures of inert and labile macromolecular complexes at any ligand-to-metal ratio: differential pulse polarographic study of the Zn(II)–nitrilotriacetate–polymethacrylate system **462**, 157
de Kouchkovsky, Y., see Mahmoud, A. **463**, 129
Del Campo, F.J., Neudeck, A., Compton, R.G. and Marken, F.
Low-temperature sonoelectrochemical processes: Part 1. Mass transport and cavitation effects of 20 kHz ultrasound in liquid ammonia **477**, 71
Délécouls, K., Saint-Aguet, P., Zaborosch, C. and Bergel, A.
Mechanism of the catalysis by *Alcaligenes eutrophus* H16 hydrogenase of direct electrochemical reduction of NAD^+ **468**, 139
de Levie, R., see Hromadova, M. **465**, 51
de Levie, R.
The electrolysis of water **476**, 92
Demets, G.J.-F., see Anaissi, F.J. **464**, 48
de Moraes, I.R. and Nart, F.C.
Sulfate ions adsorbed on Au(hkl) electrodes: in situ vibrational spectroscopy **460**, 110
Deng, J., see Sun, W. **469**, 63
Dengra, S., see Bradley, J.C. **478**, 128
Deng, Z.-X. and Lin, X.-Q.
Digital simulation of fast cyclic voltammogram by integration of the double layer charging current **464**, 215
Deniau, G., see Viel, P. **470**, 14
De Paolis, A., see Appetecchi, G.B. **463**, 248
Deronzier, A., see Caix-Cecillon, C. **466**, 187
Deronzier, A., see Collomb Dunand-Sauthier, M.-N. **469**, 53
Deronzier, A., see Collomb Dunand-Sauthier, M.-N. **463**, 119
de Rooij, N.F., see Michel, P.E. **474**, 192
de Sánchez, S.R., see Ceré, S. **470**, 31
Desprez, V., see Coche-Guérente, L. **470**, 61
Desprez, V., see Coche-Guérente, L. **470**, 53
Desvergne, J.-P., see Fabre, B. **460**, 119
de Wit, J.H.W., see Peelen, W.H.A. **470**, 39
Diao, P., Jiang, D., Cui, X., Gu, D., Tong, R. and Zhong, B.
Studies of structural disorder of self-assembled thiol monolayers on gold by cyclic voltammetry and ac impedance **464**, 61
Diao, P., see Cui, X. **470**, 9
Diard, J.-P., Le Gorrec, B. and Montella, C.
Discussion of the paper by Barber et al. [J. Electroanal. Chem. 446 (1998) 125] **466**, 122
Diard, J.-P., Le Gorrec, B. and Montella, C.
Linear diffusion impedance. General expression and applications **471**, 126
Diard, J.-P., Le Gorrec, B. and Montella, C.
Logistic differential equation: A general equation for electrointercalation processes? **475**, 190
Diard, J.-P., see Berthier, F. **460**, 226
Diard, J.-P., see Coche-Guérente, L. **470**, 53
Díaz-Cruz, J.M., see Berbel, F. **475**, 99
Diaz, R., see Gorostiza, P. **469**, 48
Diekmann, S., see Kirstein, D. **474**, 43
Dini, D., see Cattarin, S. **474**, 182
Dion, F. and Lasia, A.
The use of regularization methods in the deconvolution of underlying distributions in electrochemical processes **475**, 28
Dominguez, E., see Catalin Popescu, I. **464**, 208
Dong, L., see Jiang, Z. **469**, 1
dos Santos, A.F., see de Azevedo, D.C. **466**, 99
Doubova, L.M. and Trasatti, S.
Effect of the crystallographic orientation of Ag single crystal face electrodes on the kinetics of proton discharge **467**, 164
Dražić, D.M., Tripković, A.V., Popović, K.D. and Lović, J.D.
Kinetic and mechanistic study of hydroxyl ion electrosorption at the Pt(111) surface in alkaline media **466**, 155

Dretschkow, T. and Wandlowski, T.
Structural studies of 2,2′-bipyridine on Au(100) **467**, 207
D'Souza, V.T., see Stine, K.J. **472**, 147
D'Souza, V.T., see Stine, K.J. **465**, 209
Duah-Williams, L. and Hawkridge, F.M.
The temperature dependence of the kinetics of cyanide dissociation from the cyanide complex of myoglobin studied by cyclic voltammetry **466**, 177
Dubey, S., Fabre, B., Marchand, G., Pilard, J.-F. and Simonet, J.
Voltammetric investigation of new polythiophene derivatives possessing electrochemically cleavable arylsulfonamide groups as precursors for solid phase electrosynthesis **477**, 121
Duboc Toia, C., see Collomb Dunand-Sauthier, M.-N. **469**, 53
Dudek, D.A. and Fedkiw, P.S.
Electrodeposition of copper from cuprous cyanide electrolyte: I. Current distribution on a stationary disk **474**, 16
Dudek, D.A. and Fedkiw, P.S.
Electrodeposition of copper from cuprous cyanide electrolyte: II. Current distribution on a rotating disk **474**, 31
Dunsch, L., see Aubert, P.-H. **470**, 77
Duong, B., see Giz, M.J. **465**, 72
Durand, R., see Pauporté, T. **465**, 88

Eberhardt, D., Santos, E. and Schmickler, W.
Hydrogen evolution on silver single crystal electrodes—first results **461**, 76
Eickes, C., see Strasser, P. **462**, 19
Eikerling, M. and Kornyshev, A.A.
Electrochemical impedance of the cathode catalyst layer in polymer electrolyte fuel cells **475**, 107
Einaga, Y., see Ohkoshi, S.-i. **473**, 245
Eiswirth, M., see Strasser, P. **478**, 50
Eiswirth, M., see Strasser, P. **462**, 19
El-Deab, M.S., see Ohmori, T. **470**, 46
El-Shafei, A.A.
Electrocatalytic oxidation of methanol at a nickel hydroxide/glassy carbon modified electrode in alkaline medium **471**, 89
Endo, O., Kiguchi, M., Yokoyama, T., Ito, M. and Ohta, T.
In-situ X-ray absorption studies of bromine on the Ag(100) electrode **473**, 19
England, K.E.R., see Kelsall, G.H. **471**, 116
Epron, F., see Chollier-Brym, M.J. **474**, 147
Erk, M. and Raspor, B.
Electrochemical study on Cd binding to metallothioneins isolated from the mussel, *Mytilus galloprovincialis* **466**, 75
Ertl, G., see Xia, X.H. **460**, 102
Escriche, L., see Lubert, K.-H. **475**, 73
Esteban, M., Harlyk, C. and Rodríguez, A.R.
Cadmium binding properties of the C-terminal hexapeptide from mouse metallothionein: study by linear sweep voltammetry and multivariate curve resolution analysis **468**, 202
Esteban, M., see Berbel, F. **475**, 99
Esteban, M., see de Haro, C. **462**, 157
Esteso, M.A., see Fernández-Mérida, L. **466**, 38
Etcheberry, A., see Gonçalves, A.-M. **477**, 140
Etcheberry, A., see Gonçalves, A.-M. **462**, 88
Evans, D.H., see Oliver, E.W. **474**, 1

Fabre, B., Desvergne, J.-P., Colomès, M. and Simonet, J.
Electrochemical oxidation in different media of bis(*p*-phenylene crown ether) as a symmetrical molecule bearing two identical redox centers **460**, 119
Fabre, B., see Dubey, S. **477**, 121
Fabregat-Santiago, F., see Bisquert, J. **475**, 152
Fabricius, G., see Bojinov, M. **475**, 58
Fähnrich, K.A., see Michel, P.E. **474**, 192
Fang, H., Hu, X.-Y. and Chen, H.-Y.
Integration analysis of the cyclic voltammograms of the electrode reaction in a diffusionless system **465**, 219
Fan, L.-J., Wang, C., Chang, S.-C. and Yang, Y.-w.
Reaction of nitrobenzene on gold single-crystal electrodes: surface crystallographic orientation dependence **477** 111
Farnia, G., Marcuzzi, F. and Sandonà, G.
Electrochemical reduction of phenyl-substituted cyclopentadienes: a case of an 'indirect father–son' self-protonation process **460**, 160
Farsang, G., see Amatore, C. **462**, 55
Fatima Bento, M., see Amatore, C. **463**, 45
Fatouros, N. and Krulic, D.
Limiting current in normal pulse polarography with reactant adsorption obeying the Langmuir and the Frumkin isotherms **478**, 25
Faure, R., see Pauporté, T. **465**, 88
Fedkiw, P.S., see Dudek, D.A. **474**, 31
Fedkiw, P.S., see Dudek, D.A. **474**, 16
Fedorovich, N.V., see Ferapontova, E.E. **476**, 26
Feliu, J.M., see Bergelin, M. **467**, 74
Feliu, J.M., see Climent, V. **467**, 20
Feliu, J.M., see Climent, V. **461**, 65
Feliu, J.M., see Orts, J.M. **467**, 11
Ferapontova, E.E. and Fedorovich, N.V.
Effect of cation adsorption on the kinetics of anion electroreduction: Part I. Effect of the adsorption of inorganic cations in small concentrations on the kinetics of anion electroreduction with different elementary steps of discharge **476**, 26
Ferapontova, E.E.
Effect of cation adsorption on the kinetics of anion electroreduction: Part II. Effect of the adsorption of organic cations in small concentrations on the kinetics of anion electroreduction **476**, 37
Fermín, D.J., Ponomarev, E.A. and Peter, L.M.
A kinetic study of CdS photocorrosion by intensity modulated photocurrent and photoelectrochemical impedance spectroscopy **473**, 192
Fernández, H., see Zón, M.A. **465**, 225
Fernández-Mérida, L., García-García, G.E., Raposo, R.R. and Esteso, M.A.
Activity coefficients for aminoacid + electrolyte mixtures by using Pitzer equations: DL-α-amino-*n*-butyric acid in mixed electrolyte solutions of neutral, acid and alkaline pH values **466**, 38
Ferrigno, R., see Josserand, J. **468**, 42
Finch, J.A., see Bozkurt, V. **475**, 124
Finot, M.O., Braybrook, G.D. and McDermott, M.T.
Characterization of electrochemically deposited gold nanocrystals on glassy carbon electrodes **466**, 234
Florit, M.I., see Bolzán, A.E. **461**, 40
Florit, M.I., see Viva, F.A. **471**, 180
Fontecave, M., see Collomb Dunand-Sauthier, M.-N. **469**, 53
Fontes, E., see Nilsson, E. **460**, 88
Foresti, M.L., Innocenti, M., Guidelli, R. and Hamelin, A.
Electrochemical investigation of 1,5-pentanediol adsorption on the Ag(111) and Ag(110) faces **467**, 217
Foresti, M.L., see Pezzatini, G. **475**, 164
Foresti, M.L., see Pezzatini, G. **462**, 127
Forgo, P., see Stine, K.J. **472**, 147
Forgo, P., see Stine, K.J. **465**, 209
Formaro, L., see Longhi, M. **464**, 149
Forzani, E.S., Rivas, G.A. and Solís, V.M.
Kinetic behaviour of dopamine-polyphenol oxidase on electrodes of tetrathiafulvalenium tetracyanoquinodimethanide and tetracyanoquinodimethane species **461**, 174
Friedman, R.M., see Stine, K.J. **472**, 147
Friedrich, K.A., see Fujiwara, N. **472**, 120
Fujihira, M., see Azehara, H. **473**, 68
Fujii, H., see Nishimura, N. **473**, 75
Fujikura, H., see Hamamatsu, A. **473**, 223
Fujimoto, S., Kawachi, S., Nishio, T. and Shibata, T.
Impedance and photoelectrochemical properties of porous oxide film on Type304 stainless steel formed by square wave potential pulse polarisation **473**, 265
Fujishima, A., Rao, T.N., Popa, E., Sarada, B.V., Yagi, I. and Tryk, D.A.
Electroanalysis of dopamine and NADH at conductive diamond electrodes **473**, 179
Fujishima, A., see Ishibashi, K.-i. **465**, 195
Fujishima, A., see Ohkoshi, S.-i. **473**, 245
Fujishima, A., see Yagi, I. **473**, 173

Fujiwara, N., Friedrich, K.A. and Stimming, U.
Ethanol oxidation on PtRu electrodes studied by differential electrochemical mass spectrometry **472**, 120
Fukuda, K., see Masuda, H. **473**, 240
Fukuda, T. and Aramata, A.
The study of the adsorption/desorption of acetate anions on a Pt(111) electrode and the effect of counter cations in acidic media **467**, 112
Fungaro, D.A., see Brett, C.M.A. **468**, 26
Fuoco, R., see Pospíšil, L. **472**, 33
Furlanetto, F., see Musiani, M. **465**, 160
Furuichi, R., see Saeki, I. **464**, 238
Furuya, N. and Shibata, M.
Structural changes at various Pt single crystal surfaces with potential cycles in acidic and alkaline solutions **467**, 85
Furuya, N., Ichinose, M. and Shibata, M.
Structural changes at the Pt(100) surface with a great number of potential cycles **460**, 251
Fuse, T., see Takamura, K. **468**, 53

Gabriel, T., see Patolsky, F. **479**, 69
Gaigalas, A.K. and Ruzgas, T.
The role of the potential distribution at the electrode interface in determining the electron transfer rate constant **465**, 96
Gaigalas, A., see Ruzgas, T. **469**, 123
Gal, S., see Sargent, A. **470**, 144
Galceran, J., Cecília, J., Salvador, J., Monné, J., Torrent, M., Companys, E., Puy, J., Lluís Garcés, J. and Mas, F.
Voltammetric currents for any ligand-to-metal concentration ratio in fully labile metal-macromolecular complexation. Easy computations, analytical properties of the currents and a graphical method to estimate the stability constant **472**, 42
Galceran, J., Taylor, S.L. and Bartlett, P.N.
Application of Danckwerts' expression to first-order EC′ reactions. Transient currents at inlaid and recessed microdisc electrodes **466**, 15
Galceran, J., Taylor, S.L. and Bartlett, P.N.
Steady-state currents at inlaid and recessed microdisc electrodes for first-order EC′ reactions **476**, 132
Galus, Z., see Marczak, S. **471**, 62
Gamolsky, K., see Levi, M.D. **477**, 32
Gao, J., Njue, C.K., Mbindyo, J.K.N. and Rusling, J.F.
Mechanism of stereoselective production of *trans*-1-decalone by electrochemical catalysis in microemulsions **464**, 31
Gao, X.-X., see Xiao, Y.-J. **465**, 187
Gao, Z., see Yang, D. **470**, 114
Garay, F. and Solís, V.
Square wave stripping voltammetry of Cd–oxine complexes; surface redox reactions **476**, 165
Garay, F., Solís, V. and Lovrić, M.
Cathodic stripping square wave voltammetry of Cu(II)–oxine complexes. A mechanistic study **478**, 17
Garche, J., see Wilde, P.M. **460**, 154
García-García, G.E., see Fernández-Mérida, L. **466**, 38
García, S.G., see Salinas, D.R. **470**, 120
García-Belmonte, G., see Bisquert, J. **475**, 152
Garratt, P.J., see Ng, Y.-F. **464**, 263
Gasteiger, H.A., see Marković, N.M. **467**, 157
Gehring, A.G., Brewster, J.D., Irwin, P.L., Tu, S.-I. and Van Houten, L.J.
1-Naphthyl phosphate as an enzymatic substrate for enzyme-linked immunomagnetic electrochemistry **469**, 27
Giannarelli, S., see Pospíšil, L. **472**, 33
Gil, M.H., see Brett, C.M.A. **468**, 26
Girard, F., see Keita, B. **478**, 76
Girault, H.H., see Bagel, O. **469**, 189
Girault, H.H., see Josserand, J. **468**, 42
Girault, H.H., see Reymond, F. **462**, 235
Gisselbrecht, J.P., Bley-Escrich, J., Gross, M., Zander, L., Michels, M. and Vogel, E.
Electrochemical properties of 'figure-eight'-cyclooctapyrroles (octaphyrins) and their metal complexes **469**, 170
Giz, M.J., Duong, B. and Tao, N.J.
In situ STM study of self-assembled mercaptopropionic acid monolayers for electrochemical detection of dopamine **465**, 72
Glazier, S., see Herrero, E. **460**, 121
Gloaguen, F., Léger, J.-M. and Lamy, C.
An electrochemical quartz crystal microbalance study of the hydrogen underpotential deposition at a Pt electrode **467**, 186
Gofer, Y., see Levi, M.D. **479**, 12
Gofer, Y., see Schlindwein, W.S. **460**, 46
Goh, N.K., see Li, J. **460**, 234
Gojković, S.L., Gupta, S. and Savinell, R.F.
Heat-treated iron(III) tetramethoxyphenyl porphyrin chloride supported on high-area carbon as an electrocatalyst for oxygen reduction: Part II. Kinetics of oxygen reduction **462**, 63
Golabi, S.M. and Zare, H.R.
Electrocatalytic oxidation of hydrazine at a chlorogenic acid (CGA) modified glassy carbon electrode **465**, 168
Golabi, S.M., see Zare, H.R. **464**, 14
Goldenberg, L.M. and Neilands, O.
Hydrogen bond complexation of dimethyl-[1-butyl-2,4-dioxo(1H,3H)pyrimido]tetrathiafulvalene with aminopyridine derivatives probed by cyclic voltammetry **463**, 212
Golimowski, J., see Grdeń, M. **460**, 30
Gómez, E., Alcobe, X. and Vallés, E.
Electrodeposition of zinc + iron alloys: II. Relation between the stripping results and ex-situ characterization **475**, 66
Gómez, E., Guaus, E., Sanz, F. and Vallés, E.
Tin electrodeposition on carbon electrodes. From nuclei to microcrystallites **465**, 63
Gómez, E., Pelaez, E. and Vallés, E.
Electrodeposition of zinc + iron alloys: I. Analysis of the initial stages of the anomalous codeposition **469**, 139
Gómez, M.M., Vara, J.M., Hernández, J.C., Salvarezza, R.C. and Arvia, A.J.
Steric effects on molecular adsorption at columnar surfaces. A model for the adsorption of pyridine on gold electrodes **474**, 74
Gómez, R., see Orts, J.M. **467**, 11
Gómez, R., see Zou, S. **474**, 155
Gonçalves, A.-M., Mathieu, C., Herlem, M. and Etcheberry, A.
Oxygen reduction mechanisms at p-InP and p-GaAs electrodes in liquid ammonia in neutral buffered medium and acidic media **462**, 88
Gonçalves, A.-M., Mathieu, C., Herlem, M. and Etcheberry, A.
Using Pt microelectrodes in liquid ammonia for studying proton reduction **477**, 140
González-Arjona, D., see Molero, M. **460**, 100
Gonzalez, E.R., see Sena, D.R. **477**, 164
Gonzalez, E.R., see Torresi, R.M. **475**, 193
Gonzalez, E.R., see Torresi, R.M. **460**, 161
Gonzalez, G.A., see Bradley, J.C. **478**, 128
González, J.E.G. and Mirza-Rosca, J.C.
Study of the corrosion behavior of titanium and some of its alloys for biomedical and dental implant applications **471**, 109
Gonzalez, J., Hapiot, P., Konovalov, V. and Savéant, J.-M.
Investigating the reduction characteristics of transient free radicals by laser-pulse electron photo-injection—mechanism diagnostic criteria and determination of reactivity parameters from time-resolved experiments **463**, 157
González, J., see Serna, C. **468**, 158
Gorgy, K., see Collomb Dunand-Sauthier, M.-N. **469**, 53
Gorostiza, P., Díaz, R., Anbu Kulandainathan, M., Sanz, F. and Ramon Morante, J.
Simultaneous platinum deposition and formation of a photoluminescent porous silicon layer **469**, 48
Gorton, L., see Ruzgas, T. **469**, 123
Gorton, L., see Torto, N. **464**, 252
Goulart, M.O.F., see de Abreu, F.C. **462**, 195
Goulart, M.O.F., see de Azevedo, D.C. **466**, 99

Grafov, B.M.
The Shuttleworth equation for a finite surface strain **471**, 105
Grandell, D., Murtomäki, L. and Sundholm, G.
Ion transfer across a phospholipid monolayer adsorbed at the water | 1,2-dichloroethane interface under surface pressure control **469**, 72
Grandell, D., Murtomäki, L., Kontturi, K. and Sundholm, G.
Phospholipid monolayers studied by a combination of cyclic voltammetry and Langmuir techniques at the water | 1,2-dichloroethane interface **463**, 242
Granger, M.M., see Rault-Berthelot, J. **466**, 144
Granö, H., see Lankinen, E. **460**, 176
Grätzel, M., see Cosnier, S. **469**, 176
Grdeń, M., Czerwiński, A., Golimowski, J., Bulska, E., Krasnodębska-Ostręga, B., Marassi, R. and Zamponi, S.
Hydrogen electrosorption in Ni–Pd alloys **460**, 30
Grdeń, M., see Czerwiński, A. **471**, 190
Grgur, B.N., see Marković, N.M. **467**, 157
Gritzner, G., see Murauer, F. **470**, 1
Gross, M., see Gisselbrecht, J.P. **469**, 170
Grzybowska, B., see Tremiliosi-Filho, G. **467**, 143
Gu, D., see Diao, P. **464**, 61
Gu, Q., see Sun, W.-Y. **469**, 84
Guascito, M.R., see Casella, I.G. **476**, 54
Guascito, M.R., see Casella, I.G. **462**, 202
Guaus, E., see Gómez, E. **465**, 63
Guidelli, R.
A reply to the question of whether the internal energy of solid interfaces can be of a non-homogeneous nature **472**, 174
Guidelli, R., see Foresti, M.L. **467**, 217
Guidelli, R., see Pezzatini, G. **462**, 127
Guilbault, G.G., see Michel, P.E. **474**, 192
Gun, J., see Modestov, A.D. **476**, 118
Guo, S.X., see Khoo, S.B. **465**, 102
Gupta, S., see Gojković, S.L. **462**, 63
Gushikem, Y., see Pessôa, C.A. **477**, 158
Guther, T.J., see Wilde, P.M. **460**, 154
Gutiérrez, C., see Ortiz, R. **465**, 234
Guttmann, M., see Lubert, K.-H. **462**, 174
Gutz, I.G.R., see Brito, M.S.L. **468**, 150

Habu, H., see Arai, G. **464**, 143
Hahn, F., see Chbihi, M.E.M. **463**, 63
Hahn, F., see Cherqaoui, A. **464**, 101
Hahn, F., see Melendres, C.A. **463**, 258
Haj Said, A., Matoussi Mhalla, F., Amatore, C. and Verpeaux, J.-N.
Mechanistic investigation of the anodic oxidation of *p*-methoxytoluene in dry and wet acetonitrile **464**, 85
Halsall, H.B., see Wijayawardhana, C.A. **468**, 2
Hamamatsu, A., Kaneshiro, C., Fujikura, H. and Hasegawa, H.
Formation of ⟨001⟩-aligned nano-scale pores on (001) n-InP surfaces by photoelectrochemical anodization in HCl **473**, 223
Hamann, C.H., see Schwientek, M. **461**, 94
Hamelin, A., see Foresti, M.L. **467**, 217
Haoqing, W., see Tao, H. **463**, 24
Hapiot, P., see Gonzalez, J. **463**, 157
Hara, S., see Vidu, R. **475**, 171
Hara, Y., see Ataka, K. **473**, 34
Harima, Y., see Zhu, L. **464**, 158
Harima, Y., Tang, H., Zhu, L., Yamashita, K., Ohshita, J. and Kunai, A.
Electrochemical generation of cation radical π-dimers in polymer film composed of pentathiophenes bridged by monosilanylene units **472**, 157
Harlyk, C., see Esteban, M. **468**, 202
Hasegawa, H., see Hamamatsu, A. **473**, 223
Hashimoto, K., see Ishibashi, K. **465**, 195
Hashimoto, K., see Ohkoshi, S. **473**, 245
Hashimoto, Y., see Yoshimoto, S. **473**, 85
Ha, S.Y. and Kim, S.
Preparation and characterization of sol–gel derived carbon composite ceramic electrodes: electrochemical and XANES study of nitrite reduction **468**, 131
Haukka, M., see Caix-Cecillon, C. **466**, 187
Havran, L., see Tomschik, M. **476**, 71
Hawkridge, F.M., see Duah-Williams, L. **466**, 177
Hazemann, J.-L., see Pauporté, T. **465**, 88
He, G., see Yang, C. **471**, 32
Heerman, L. and Tarallo, A.
Theory of the chronoamperometric transient for electrochemical nucleation with diffusion-controlled growth **470**, 70
Heider, U., see Levi, M.D. **477**, 32
Heineman, W.R., see Wijayawardhana, C.A. **468**, 2
Hemmes, K., see Peelen, W.H.A. **470**, 39
Herlem, M., see Gonçalves, A.-M. **477**, 140
Herlem, M., see Gonçalves, A.-M. **462**, 88
Hernández, J.C., see Gómez, M.M. **474**, 74
Herrero, E., Glazier, S., Buller, L.J. and Abruña, H.D.
X-ray and electrochemical studies of Cu upd on single crystal electrodes in the presence of bromide: comparison between Au(111) and Pt(111) electrodes **460**, 121
Herrero, E., see Bergelin, M. **467**, 74
Hesse, K. and Schlettwein, D.
Spectroelectrochemical investigations on the reduction of thin films of hexadecafluorophthalocyaninatozinc ($F_{16}PcZn$) **476**, 148
Heusler, K.E., see Láng, G. **472**, 168
Higuera, M.J., Ruiz Montoya, M., Marín Galvín, R. and Rodríguez Mellado, J.M.
A contribution to the study of the electroreduction of 2-chloro-4,6-di(ethylamino)-1,3,5-triazine (simazine) on mercury electrodes **474**, 174
Hillman, A.R., see Saraswathi, R. **460**, 267
Himeno, S., Takamoto, M. and Ueda, T.
Synthesis, characterisation and voltammetric study of a β-Keggin-type $[PW_{12}O_{40}]^{3-}$ complex **465**, 129
Hinken, J.H., see Juzeliūnas, E. **477**, 171
Hinoue, T., Kuwamoto, N. and Watanabe, I.
Voltammetry using an electrode surface continuously renewed by laser ablation and its demonstration on electro-oxidation of L-ascorbic acid **466**, 31
Hirai, S., see Watanabe, K. **473**, 250
Hirata, Y., see Yabuki, S. **468**, 117
Hirayama, C., see Ohira, A. **472**, 163
Hitchman, M.L., see Ralph, T.R. **462**, 97
Hodgkinson, N.M., see Monk, P.M.S. **462**, 43
Hogarth, M.P., see Lampitt, R.A. **460**, 80
Hojo, M., Ueda, T., Chen, Z. and Nishimura, M.
Conductometric study of lithium halides and thiocyanate in the mixed solvents of tetrahydrofuran and 2-ethyl-1-hexanol **468**, 110
Hokari, H., see Azehara, H. **473**, 68
Holdcroft, S., see Beattie, P.D. **468**, 180
Holze, R., see Malinauskas, A. **461**, 184
Homyonfer, M., see Alperson, B. **473**, 186
Hong, H.-G., Park, W. and Yu, E.
Voltammetric determination of electron transfer kinetic parameters in hydroquinone-terminated self-assembled monolayers on gold **476**, 177
Hong, Y.-K., see Moon, J.-M. **464**, 230
Horányi, G., see Inzelt, G. **471**, 73
Hori, Y., see Hoshi, N. **467**, 67
Horikoshi, T., Itoh, M., Kurihara, M., Kubo, K. and Nishihara, H.
Synthesis, redox behavior and electrodeposition of biferrocene-modified gold clusters **473**, 113
Horrocks, B.R., see Armstrong, R.D. **463**, 9
Horvat-Radošević, V., Kvastek, K., Vuković, M. and Marijan, D.
Impedance of ruthenium electrodes in sulphuric acid solution **463**, 29
Hoshi, N., Kawatani, S., Kudo, M. and Hori, Y.
Significant enhancement of the electrochemical reduction of CO_2 at the kink sites on Pt(S)-[*n*(110) × (100)] and Pt(S)-[*n*(100) × (110)] **467**, 67
Hoshino, T., Oyama, M. and Okazaki, S.
Kinetic studies on ion pair formation between 2,3,5,6-tetrachloro-1,4 benzoquinone anion radical and alkaline earth metal cations (RPS 6708) **472**, 91
Hosokawa, H., see Murakoshi, K. **473**, 117
Hromadova, M. and de Levie, R.
A sodium-specific condensed film of α-cyclodextrin at the mercury | water interface **465**, 51
Hu, N., see Yang, J. **463**, 53
Hu, S.
Electrocatalytic reduction of molecular oxygen on a sodium montmorillonite-methyl viologen carbon paste chemically modified electrode **463**, 253

Hu, X.-Y., see Fang, H. **465**, 219
Hu, X.-Y., Xiao, Y. and Chen, H.-Y.
Adsorption characteristics of $Fe(CN)_6^{3-}/4-$ on Au colloids as monolayer films on cysteamine-modified gold electrode **466**, 26
Hu, Y., Tolmachev, Y.V. and Scherson, D.A.
Rotating ring-disk studies of oxidized nickel hydrous oxide: oxygen evolution and pseudocapacitance **468**, 64
Huang, J. and Korzeniewski, C.
A temperature controlled cell for in situ infrared spectroelectrochemical measurements and its use in the study of CO isothermal desorption **471**, 146
Huang, J., see Kardash, D. **476**, 95
Huber, T., Pecina, O. and Schmickler, W.
The influence of the ions on the capacity of liquid | liquid interfaces **467**, 203
Huerta, F., Morallón, E., Pérez, J.M., Vázquez, J.L. and Aldaz, A.
Oxidation of methylamine and ethylamine on Pt single crystal electrodes in acid medium **469**, 159
Huerta, F., Morallón, E., Quijada, C., Vázquez, J.L. and Berlouis, L.E.A.
Potential modulated reflectance spectroscopy of Pt(111) in acidic and alkaline media: cyanide adsorption **463**, 109
Huerta, F., Morallón, E., Quijada, C., Vázquez, J.L., Pérez, J.M. and Aldaz, A.
The adsorption of methylamine on Pt single crystal surfaces **467**, 105
Huerta, F., Morallón, E., Vázquez, J.L. and Aldaz, A.
Electrochemical behaviour of amino acids on Pt(*hkl*). A voltammetric and in situ FTIR study: Part IV. Serine and alanine on Pt(100) and Pt(110) **475**, 38
Humbert, C., see Tadjeddine, A. **473**, 25
Huser, H., see Chbihi, M.E.M. **463**, 63
Hush, N.S.
Electron transfer in retrospect and prospect: 1: Adiabatic electrode processes **460**, 5

Ianniello, R., Schmidt, V.M., Rodriguez, J.L. and Pastor, E.
Electrochemical surface reactions of intermediates formed in the oxidative ethanol adsorption on porous Pt and PtRu **471**, 167
Ichinose, M., see Furuya, N. **460**, 251
Igarashi, H., see Toda, T. **460**, 258
Iguchi, U., see Nakabayashi, S. **473**, 54
Ikeda, T., see Kinoshita, H. **478**, 33
Innocenti, M., see Foresti, M.L. **467**, 217
Innocenti, M., see Pezzatini, G. **475**, 164
Innocenti, M., see Pezzatini, G. **462**, 127
Inoue, H., see Iwakura, C. **463**, 116
Inzelt, G. and Horányi, G.
Direct experimental evidence proving the formation of surface layers in the course of the reduction of Cr(VI) species at a gold electrode **471**, 73
Inzelt, G., see Vorotyntsev, M.A. **472**, 7
Ion, A.C., Moutet, J.-C., Pailleret, A., Popescu, A., Saint-Aman, E., Siebert, E. and Ungureanu, E.M.
Electrochemical recognition of metal cations by poly(crown ether ferrocene) films investigated by cyclic voltammetry and electrochemical impedance spectroscopy **464**, 24
Ion, A., see Buda, M. **469**, 132
Irwin, P.L., see Gehring, A.G. **469**, 27
Ishibashi, K.-i., Sato, O., Baba, R., Hashimoto, K. and Fujishima, A.
Second harmonic generation investigation of rhodamine B derivatives in Langmuir–Blodgett films **465**, 195
Ishida, M., see Taniguchi, I. **460**, 245
Ishii, H., see Juodkazis, S. **473**, 235
Ishikawa, M., Machino, S.-i. and Morita, M.
Electrochemical control of a Li metal anode interface: improvement of Li cyclability by inorganic additives compatible with electrolytes **473**, 279
Ishizaki, T., see Ohira, A. **472**, 163
Itaya, K., see Müller, P. **467**, 282
Itaya, K., see Wan, L.-J. **473**, 10
Ito, M., see Endo, O. **473**, 19
Ito, M., see Momoi, K. **473**, 43
Ito, M., see Shingaya, Y. **467**, 299
Ito, S., see Chen Tsai, Y. **477**, 25
Ito, T., see Iwakura, C. **463**, 116
Itoh, J., Sasaki, T., Ohtsuka, T. and Osawa, M.
Surface layers formed initially on copper in air containing water vapor and SO_2 as determined by IR-RAS and 2D-IR **473**, 256
Itoh, M., see Horikoshi, T. **473**, 113
Itoh, S., see Sugiura, T. **473**, 204
Iwaku, M., see Tatsuma, T. **472**, 142
Iwakura, C., Ito, T. and Inoue, H.
Construction of a new dehydrogenation system using a two-compartment cell separated by a palladized Pd sheet electrode **463**, 116
Iyoda, T., see Kamata, K. **473**, 145

Jaeger, N.I., see Oekermann, T. **462**, 222
Jaffrezic Renault, N., see Cosnier, S. **469**, 176
Jang, J.-M., see Park, Y.-S. **468**, 70
Jarvi, T.D., see Sriramulu, S. **467**, 132
Jaworski, A., see Aoki, K. **472**, 1
Jaworski, J.S. and Leszczyński, P.
Solvent effect on kinetics of the chloride ion cleavage from anion radicals of 4-chlorobenzophenone **464**, 259
Jelen, F., see Tomschik, M. **476**, 71
Jerkiewicz, G., see Zolfaghari, A. **467**, 177
Jérôme, R., see Baute, N. **472**, 83
Jiang, D., see Cui, X. **470**, 9
Jiang, D., see Diao, P. **464**, 61
Jiang, Z., Zhang, J., Dong, L. and Zhuang, J.
Determination of the entropy change of the electrode reaction by an ac electrochemical–thermal method **469**, 1
Jin, L., see Sun, W. **469**, 63
Jin, S., see Sun, W. **469**, 63
Jin, S., see Wan, X. **470**, 23
John, S.A. and Ohsaka, T.
Electrochemical and EQCM studies on the assembly of asymmetric viologen on bare and alkanethiol-coated Au electrodes **477**, 52
John, S.A., Okajima, T. and Ohsaka, T.
A monomer–dimer equilibrium in self-assembled monolayers of *N*-ethyl-*N'*-octadecylviologen on the electrode surface. The influence of water content and hexafluorophosphate ion **466**, 67
Johnston, R.F., Lewis, D.M. and Chambers, J.Q.
Accumulation of Hg(II) by adsorbed polyuridylic acid: differentiation of coordinated Hg(II) and covalently mercurated species **466**, 2
Josserand, J., Morandini, J., Lee, H.J., Ferrigno, R. and Girault, H.H.
Finite element simulation of ion transfer reactions at a single micro-liquid | liquid interface supported on a thin polymer film **468**, 42
Jouini, M., see Lagrost, C. **476**, 1
Juodkazis, S., Ishii, H., Matsuo, S. and Misawa, H.
Photoelectrochemical submicrometer patterning of titanium dioxide by platinum **473**, 235
Jurczakowski, R. and Orlik, M.
On the source of oscillatory instabilities in the electroreduction of thiocyanate complexes of nickel(II) at mercury electrodes **478**, 118
Just, P.E., Chane-Ching, K.I., Lacroix, J.C. and Lacaze, P.C.
Anodic oxidation of dipyrrolyls linked with conjugated spacers: study of electronic interactions between the polypyrrole chain and the spacers **479**, 3
Jusys, Z., see Vaškelis, A. **465**, 142
Juzeliūnas, E. and Hinken, J.H.
Corrosion sensing by SQUID magnetometry **477**, 171

Kaczmarski, K., see Sanecki, P. **471**, 14
Kadırgan, F., see Becerik, İ. **476**, 171
Kakiuchi, T., see Aoki, K. **478**, 101
Kamata, K., Suzuki, T., Kawai, T. and Iyoda, T.
Voltammetric anion recognition by a highly cross-linked polyviologen film **473**, 145
Kaneko, M., see Yagi, M. **476**, 159
Kaneshiro, C., see Hamamatsu, A. **473**, 223
Kang, C., see Kim, S. **465**, 153
Kang, L., see Yu, J. **474**, 69
Kano, K., see Kinoshita, H. **478**, 33
Karantonis, A., see Nakabayashi, S. **473**, 54

Kardash, D., Huang, J. and Korzeniewski, C.
A jacketed cell for infrared spectroelectrochemistry at constant above ambient temperatures **476**, 95
Katakis, I., see Catalin Popescu, I. **464**, 208
Katano, H., see Senda, M. **468**, 34
Katz, E., Willner, I. and Kotlyar, A.B.
A non-compartmentalized glucose | O_2 biofuel cell by bioengineered ele
ctrode surfaces **479**, 64
Kawachi, S., see Fujimoto, S. **473**, 265
Kawai, T., see Kamata, K. **473**, 145
Kawatani, S., see Hoshi, N. **467**, 67
Kazarinov, V.E., see Semenikhin, O.A. **463**, 190
Kazitani, T., see Yoshida, T. **473**, 209
Keita, B., Girard, F., Nadjo, L., Contant, R., Canny, J. and Richet, M.
Metal ion complexes derived from the α_1 isomer of $(P_2W_{17}O_{61})^{10-}$: comparison with the corresponding α_2 species **478**, 76
Keita, B., Lu, Y.W., Nadjo, L., Contant, R., Abbessi, M., Canny, J. and Richet, M.
Electrochemical and catalytic behaviour of Dawson-type complexes derived from $[(1),2,3\text{-}P_2Mo_2W_{15}O_{61}]^{10-}$ and first transition metal ions **477**, 146
Keita, B., see Mahmoud, A. **463**, 129
Kelaidopoulou, A., see Coutouli-Argyropoulou, E. **477**, 130
Kelly, J.J., see van de Lagemaat, J. **475**, 139
Kelsall, G.H., Yin, Q., Vaughan, D.J., England, K.E.R. and Brandon, N.P.
Electrochemical oxidation of pyrite (FeS_2) in aqueous electrolytes **471**, 116
Kessler, R.W., see Kim, Y.-C. **468**, 121
Keunchkarian, S., see Bonfranceschi, A. **477**, 1
Khan, A.R., see Stine, K.J. **472**, 147
Khan, A.R., see Stine, K.J. **465**, 209
Khoo, S.B. and Guo, S.X.
Rapidly renewable and reproducible electropolymerized surface at a monomer modified carbon paste electrode **465**, 102
Kibler, L.A., Kleinert, M. and Kolb, D.M.
The initial stages of rhodium deposition on Au(111) **467**, 249
Kibler, L.A., see Cuesta, A. **466**, 165
Kiersztyn, I., see Czerwiński, A. **471**, 190
Kiguchi, M., see Endo, O. **473**, 19
Kim, H.-H., see Palmore, G.T.R. **464**, 110
Kim, H., see Tremiliosi-Filho, G. **467**, 143
Kim, K.-A., see Oh, K.-C. **468**, 98
Kim, S., see Ha, S.Y. **468**, 131
Kim, S., Yun, S.-E. and Kang, C.
Electrochemical evaluation of the reaction rate between methyl viologen mediator and diaphorase enzyme for the electrocatalytic reduction of NAD^+ and digital simulation for its voltammetric responses **465**, 153
Kim, Y.-C., Quint, B., Kessler, R.W. and Oelkrug, D.
Structural properties of electrochemically designed porous oxide films on AlMgl **468**, 121
Kinoshita, H., Torimura, M., Yamamoto, K., Kano, K. and Ikeda, T.
Amperometric determination of NAD(P)H with peroxidase-based H_2O_2-sensing electrodes and its application to isocitrate dehydrogenase activity assay in serum **478**, 33
Kirchner, V., see Xia, X.H. **460**, 102
Kirstein, D., Kirstein, L., Scheller, F., Borcherding, H., Ronnenberg, J., Diekmann, S. and Steinrücke, P.
Amperometric nitrate biosensors on the basis of *Pseudomonas stutzeri* nitrate reductase **474**, 43
Kirstein, L., see Kirstein, D. **474**, 43
Kišová, L., see Murauer, F. **470**, 1
Kitamura, F., see Arihara, K. **473**, 138
Kitamura, F., see Nanbu, N. **470**, 136
Kleinert, M., see Kibler, L.A. **467**, 249
Klíma, J. and Bernard, C.
Sonoassisted electrooxidative polymerisation of salicylic acid: role of acoustic streaming and microjetting **462**, 181
Kloss, A., see Marinković, N.S. **467**, 325
Klunker, J. and Schäfer, W.
Anodic behavior of copper in acetonitrile: the influence of carbon dioxide and dimethylamine **466**, 107
Kobayashi, M., see Ogura, K. **463**, 218
Kobayashi, S., see Yoshimoto, S. **473**, 85
Kobotiatis, L., see Tsamouras, D. **469**, 43
Koide, S. and Yokoyama, K.
Electrochemical characterization of an enzyme electrode based on a ferrocene-containing redox polymer **468**, 193
Kokkinidis, G., see Coutouli-Argyropoulou, E. **477**, 130
Kokoh, K.B., see Cherqaoui, A. **464**, 101
Kolb, D.M., see Cuesta, A. **466**, 165
Kolb, D.M., see Kibler, L.A. **467**, 249
Kolb, D.M., see Striegler, H. **471**, 9
Kolics, A., see Wieckowski, A. **464**, 118
Komenda, J., see Murauer, F. **470**, 1
Komura, T., Yokono, Y., Yamaguchi, T. and Takahashi, K.
Current enhancing effect of poly[1-methyl-3-(pyrrol-1-ylmethyl)pyridinium] films on the electrode reaction of anthraquinonedisulfonate **478**, 9
Kondo, T., see Abe, M. **473**, 93
Kondo, T., see Yagi, I. **473**, 173
Kong, J., see Sun, W. **469**, 63
Konishi, H., see Mukouyama, Y. **473**, 156
Konno, H., see Saeki, I. **464**, 238
Konovalov, V., see Gonzalez, J. **463**, 157
Kontturi, K., see Grandell, D. **463**, 242
Kontturi, K., see Murtomäki, L. **474**, 89
Kontturi, K., see Telaranta, R. **464**, 222
Koper, M.T.M. and van Santen, R.A.
Electric field effects on CO and NO adsorption at the Pt(111) surface **476**, 64
Koper, M.T.M. and van Santen, R.A.
Interaction of H, O and OH with metal surfaces **472**, 126
Koper, M.T.M., see Strasser, P. **478**, 50
Kornyshev, A.A., see Eikerling, M. **475**, 107
Korzeniewski, C., see Huang, J. **471**, 146
Korzeniewski, C., see Kardash, D. **476**, 95
Kosminsky, L. and Bertotti, M.
Studies on the catalytic reduction of iodate at glassy carbon electrodes modified by molybdenum oxides **471**, 37
Kostić, T.M., see Popov, K.I. **464**, 245
Kotlyar, A.B., see Katz, E. **479**, 64
Koudelka-Hep, M., see Michel, P.E. **474**, 192
Kovach, S.K., Olifirenko, S.N. and Vas'ko, A.T.
On the pH sensitivity of the galvanic tungsten–water interaction product **472**, 178
Kováčová, Z., see Marinković, N.S. **467**, 325
Krasnodębska-Ostręga, B., see Grdeń, M. **460**, 30
Krausa, M. and Schorb, K.
Trace detection of 2,4,6-trinitrotoluene in the gaseous phase by cyclic voltammetry **460**, 10
Kriván, E., see Visy, C. **462**, 1
Krogulec, T., see Basa, A. **463**, 200
Kruft, M., see Broekmann, P. **467**, 307
Krulic, D., see Fatouros, N. **478**, 25
Kubo, K., see Horikoshi, T. **473**, 113
Kudo, M., see Hoshi, N. **467**, 67
Kuhn, A., Mano, N. and Vidal, C.
Polyoxometalate modified electrodes: from a monolayer to multilayer structures **462**, 187
Kuhn, A., see Mano, N. **477**, 79
Kulesza, P., see Tremiliosi-Filho, G. **467**, 143
Kumazawa, N., Rafiqul Islam, M. and Takeuchi, M.
Photoresponse of a titanium dioxide chemical sensor **472**, 137
Kunai, A., see Harima, Y. **472**, 157
Kunai, A., see Zhu, L. **464**, 158
Kunitake, M., see Ohira, A. **472**, 163
Kuramitz, H., Sugawara, K., Nakamura, H. and Tanaka, S.
Control of electrocatalytic oxidation of NADH using an interaction between labeled biotin with dopamine and avidin **466**, 117
Kurihara, M., see Horikoshi, T. **473**, 113
Kuroda, K., see Sugiura, T. **473**, 204
Kusu, F., see Takamura, K. **468**, 53
Küver, A., see Wasmus, S. **460**, 14
Kuwabata, S., see Oyamatsu, D. **473**, 59
Kuwamoto, N., see Hinoue, T. **466**, 31
Kvastek, K., see Horvat-Radošević, V. **463**, 29
Kwak, J., see Lee, H. **468**, 104

Kyriacou, G., see Schizodimou, A. **471**, 26
Kyung Lee, Y., see Lee, C. **463**, 224

Labbé, P., see Coche-Guérente, L. **470**, 61
Labbé, P., see Coche-Guérente, L. **470**, 53
Lacasse, R., see Moretto, L.M. **467**, 193
Lacaze, P.C., see Just, P.E. **479**, 3
Lacaze, P.C., see Lagrost, C. **476**, 1
Lacaze, P.C., see Petitjean, J. **478**, 92
Lacroix, J.C., see Just, P.E. **479**, 3
Lacroix, J.C., see Lagrost, C. **476**, 1
Lacroix, J.C., see Petitjean, J. **478**, 92
Lagger, G., see Bagel, O. **469**, 189
Lagrost, C., Tanguy, J., Aeiyach, S., Lacroix, J.C., Jouini, M., Chane-Ching, K.I. and Lacaze, P.C.
Polymer chain encapsulation followed by a quartz microbalance during electropolymerization of bithiophene-β-cyclodextrin host–guest compounds in aqueous solution **476**, 1
Lahtinen, R., see Quinn, B. **460**, 149
Laitinen, T., see Bojinov, M. **475**, 58
Lamberts, L., see Walcarius, A. **463**, 100
Lambrou, C., see Schizodimou, A. **471**, 26
Lamperski, S. and Outhwaite, C.W.
A non-primitive model for the electrode | electrolyte interface based on the Percus–Yevick theory. Analysis of the different molecular sizes, ion valences and electrolyte concentrations **460**, 135
Lampitt, R.A., Carrette, L.P.L., Hogarth, M.P. and Russell, A.E.
In situ and model EXAFS studies of electrocatalysts for methanol oxidation **460**, 80
Lamy, C., see Chbihi, M.E.M. **463**, 63
Lamy, C., see Cherqaoui, A. **464**, 101
Lamy, C., see Gloaguen, F. **467**, 186
Lamy-Pitara, E., see Chollier-Brym, M.J. **474**, 147
Láng, G. and Heusler, K.E.
Can the internal energy function of solid interfaces be of a non-homogeneous nature? **472**, 168
Langmaier, J., see Samec, Z. **463**, 232
Langmaier, J., Trojánek, A., Weber, J. and Samec, Z.
Kinetics of the ferric/ferrous electrode reaction on Nafion®-coated electrodes **469**, 11
Lankinen, E., see Betova, I. **472**, 20
Lankinen, E., Sundholm, G., Talonen, P., Granö, H. and Sundholm, F.
Synthesis, electropolymerization and electrochemical characterization of some new acrylate substituted thiophene derivatives **460**, 176
Lasia, A., see Dion, F. **475**, 28
Lau, K.-W., see Shiu, K.-K. **476**, 109
Lecayon, G., see Charlier, J. **465**, 200
Lecayon, G., see Viel, P. **470**, 14
Lee, C., Kyung Lee, Y., Lee, Y. and Cheol Jeon, I.
Electrochemical study of methylalkylviologens using an electrochemical quartz crystal microbalance **463**, 224
Lee, C.-W., see Park, Y.-S. **468**, 70
Lee, D.K., see Yoon, I.J. **464**, 135
Lee, H.J., see Josserand, J. **468**, 42
Lee, H.J., see Shin, J.H. **468**, 76
Lee, H., Yang, H. and Kwak, J.
Mass transport behavior of polypyrrole and poly(*N*-methylpyrrole) films in acetonitrile solutions **468**, 104
Lee, J.S., see Shin, J.H. **468**, 76
Lee, J.-Y., see Talaie, A. **468**, 19
Lee, M., see Chung, C. **468**, 91
Lee, S.-H., see Bae, Z.-U. **468**, 85
Lee, Y.-K., see Moon, J.-M. **464**, 230
Lee, Y., see Lee, C. **463**, 224
Léger, J.M., see Chbihi, M.E.M. **463**, 63
Léger, J.-M., see Cherqaoui, A. **464**, 101
Léger, J.-M., see Gloaguen, F. **467**, 186
Le Gorrec, B., see Diard, J.-P. **475**, 190
Le Gorrec, B., see Diard, J.-P. **471**, 126
Le Gorrec, B., see Diard, J.-P. **466**, 122
Lelieur, J.-P., see Potteau, E. **476**, 15
Leprêtre, J.-C., see Collomb Dunand-Sauthier, M.-N. **469**, 53
Le Rille, A. and Tadjeddine, A.
In situ visible-infrared sum and difference frequency generation at the electrochemical interface **467**, 238
Le Rille, A., see Tadjeddine, A. **473**, 25
Lescano, D., see Cattaneo, C. **460**, 32
Leszczyński, P., see Jaworski, J.S. **464**, 259
Lev, O., see Modestov, A.D. **476**, 118
Lev, O., see Rabinovich, L. **466**, 45
Levi, M.D., Gamolsky, K., Aurbach, D., Heider, U. and Oesten, R.
Determination of the Li ion chemical diffusion coefficient for the topotactic solid-state reactions occurring via a two-phase or single-phase solid solution pathway **477**, 32
Levi, M.D., Lu, Z., Gofer, Y., Cohen, Y., Cohen, Y., Aurbach, D., Vieil, E. and Serose, J.
Simultaneous in-situ conductivity and cyclic voltammetry characterization of Li-ion intercalation into thin V_2O_5 films **479**, 12
Levillain, E., see Potteau, E. **476**, 15
Lewis, D.M., see Johnston, R.F. **466**, 2
L'Hostis, E., see Bagel, O. **469**, 189
Li, C.-z., see Taniguchi, I. **460**, 245
Li, H.-Q., Roscoe, S.G. and Lipkowski, J.
FTIR studies of benzoate adsorption on the Au(111) electrode **478**, 67
Li, J., Chia, L.S., Goh, N.K. and Tan, S.N.
Renewable silica sol–gel derived carbon composite based glucose biosensor **460**, 234
Li, J., see Cui, X. **470**, 9
Li, X., see Wang, Z. **464**, 181
Li, Y., see Yang, C. **471**, 32
Li, Z., see Xie, Q. **478**, 1
Liang, Y., see Wang, X. **470**, 95
Lieberman, S.H., see Mosier-Boss, P.A. **460**, 105
Lin, X.-Q., see Deng, Z.-X. **464**, 215
Lin, X., see Sun, W. **469**, 63
Lipkowski, J., see Chen, A. **475**, 130
Lipkowski, J., see Chen, A. **467**, 342
Lipkowski, J., see Li, H.-Q. **478**, 67
Liu, J., see Song, W. **476**, 85
Liu, J., see Stine, K.J. **472**, 147
Liu, M.-H., see Chen, F.-c. **474**, 52
Liu, P., Lu, J. and Yan, J.
Nitrite reduction at powder microelectrodes **469**, 196
Liu, W.-J., Wu, B.-L. and Cha, C.-S.
Surface diffusion and the spillover of H-adatoms and oxygen-containing surface species on the surface of carbon black and Pt/C porous electrodes **476**, 101
Liu, Y., see Song, W. **476**, 85
Lluis Garcés, J., see Galceran, J. **472**, 42
Löffler, T., see Vrestal, J. **461**, 90
Loi, T., see Sargent, A. **470**, 144
Lojou, E. and Bianco, P.
Electrocatalytic reduction of uranium by bacterial cytochromes: biochemical and chemical factors influencing the catalytic process **471**, 96
Longhi, M. and Formaro, L.
An old workhorse of oxide investigations: new features of Co_3O_4 **464**, 149
Loo, B.H., see Yang, Y.A. **462**, 259
Lopes, H., see Correia dos Santos, M.M. **464**, 76
Lopez, C., see Vieil, E. **466**, 218
López de Mishima, B.A., see Cattaneo, C. **460**, 32
López-Pérez, G., see Molero, M. **460**, 100
Lorcy, D., see Bellec, N. **462**, 137
Losada, J., see Casado, C.M. **463**, 87
Love, J.G., Brooksby, P.A. and McQuillan, A.J.
Infrared spectroelectrochemistry of the oxidation of absolute methanol at a platinum electrode **464**, 93
Lović, J.D., see Dražić, D.M. **466**, 155
Lovrić, M.
A minimum separating diffusion and adsorption waves in polarography using a static mercury drop electrode **465**, 30
Lovrić, M., see Garay, F. **478**, 17
Loyall, U., see Bagel, O. **469**, 189
Lu, J., see Liu, P. **469**, 196
Lu, Y.W., see Keita, B. **477**, 146
Lu, Z., Schechter, A., Moshkovich, M. and Aurbach, D.
On the electrochemical behavior of magnesium electrodes in polar aprotic electrolyte solutions **466**, 203
Lu, Z., see Levi, M.D. **479**, 12
Lubert, K.-H., Beyer, L., Casabó, J., Pérez-Jiménez, C. and Escriche, L.
Coordination of silver(I) at the surface of carbon paste electrodes modified with 2,5,8 - trithia[9] - *m* - cyclophane as studied by cyclic voltammetry **475**, 73
Lubert, K.-H., Guttmann, M. and Beyer, L.

Electrode reactions and accumulation of hydrogen at carbon paste electrodes in the presence of tetrachloropalladate **462**, 174
Lübke, M., see Strasser, P. **462**, 19
Luboch, E., see Zawisza, I. **471**, 156
Lukács, Z.
Evaluation of model and dispersion parameters and their effects on the formation of constant-phase elements in equivalent circuits **464**, 68
Lust, E., see Väärtnõu, M. **469**, 182
Lvov, S.N., Zhou, X.Y. and Macdonald, D.D.
Flow-through electrochemical cell for accurate pH measurements at temperatures up to 400°C **463**, 146

Ma, S., see Wang, Z. **464**, 181
Ma, S., Wu, Y. and Wang, Z.
Spectroelectrochemistry for a coupled chemical reaction in the channel cell: Part I. Theoretical simulation of an EC reaction **464**, 176
Macdonald, D.D., see Lvov, S.N. **463**, 146
Machino, S.-i., see Ishikawa, M. **473**, 279
Magnussen, O.M. and Behm, R.J.
Structure and growth in metal epitaxy on low-index Au surfaces—a comparison between solid|electrolyte and solid|vacuum interfaces **467**, 258
Mahmoud, A., Keita, B., Nadjo, L., Oung, O., Contant, R., Brown, S. and de Kouchkovsky, Y.
Coupled electron and proton transfers: compared behaviour of oxometalates in aqueous solution or after entrapment in polymer matrices **463**, 129
Mahon, P.J. and Oldham, K.B.
Convolutive modelling of electrochemical processes based on the relationship between the current and the surface concentration **464**, 1
Maisonhaute, E., see Amatore, C. **462**, 55
Malinauskas, A. and Holze, R.
A UV-vis spectroelectrochemical study of redox reactions of solution species at a polyaniline electrode in the conducting and the reduced state **461**, 184
Mano, N. and Kuhn, A.
Immobilized nitro-fluorenone derivatives as electrocatalysts for NADH oxidation **477**, 79
Mano, N., see Kuhn, A. **462**, 187
Manuel Díaz-Cruz, J., see de Haro, C. **462**, 157
Manzanares, J.A., see Telaranta, R. **464**, 222
Marassi, R., see Grdeń, M. **460**, 30
Marassi, R., see Tossici, R. **474**, 107
Marchand, G., see Dubey, S. **477**, 121
Marchiando, N.C., see Zón, M.A. **465**, 225
Marcuzzi, F., see Farnia, G. **460**, 160
Marczak, S., Wrona, P.K. and Galus, Z.
Analysis of the temperature dependence of the α and β coefficients of the electrode reactions in the Cr(III)/Cr(II) and Cr(II)/Cr(Hg) systems **471**, 62
Margesin, B., see Cattarin, S. **474**, 182
Mariaulle, P., see Walcarius, A. **463**, 100
Marijan, D., see Horvat-Radošević, V. **463**, 29
Marinković, J.S., see Marinković, N.S. **467**, 291
Marinković, N.S., Calvente, J.J., Kloss, A., Kováčová, Z. and Ronald Fawcett, W.
SNIFTIRS studies of the electrochemical double layer: Part II. Au(111) electrode in solutions with specifically adsorbed nitrate ions **467**, 325
Marinković, N.S., Marinković, J.S. and Adžić, R.R.
In situ infrared spectroscopic investigations of sulfate adsorption at the Ag(111) electrode surface **467**, 291
Marken, F., see Del Campo, F.J. **477**, 71
Marković, N.M., Gasteiger, H.A., Grgur, B.N. and Ross, P.N.
Oxygen reduction reaction on Pt(111): effects of bromide **467**, 157
Markwell, J., see Xiao, Y.-J. **465**, 187
Marín Galvín, R., see Higuera, M.J. **474**, 174
Márquez, J., see Ortiz, R. **465**, 234
Márquez, O.P., see Ortiz, R. **465**, 234
Marshall, G., see Bradley, J.C. **478**, 128
Martelet, C., see Cosnier, S. **469**, 176
Martinot, L., see Baute, N. **472**, 83
Martins, A., see Silva, F. **467**, 335
Martin, S.J., see Saraswathi, R. **460**, 267
Martins, M.E., Rodríguez Nieto, F.J., Salvarezza, R.C., Andreasen, G. and Arvia, A.J.
Voltammetric anodic stripping of silver from platinum electrodes consisting of an array of nm-sized voids **477**, 14
Martins, M.E., see Mendez, E. **477**, 41
Martínez-Ortiz, F., see Serna, C. **468**, 158
Mas, F., see Galceran, J. **472**, 42
Masuda, H. and Fukuda, K.
Change of hole size of Pd hole-array electrodes in a controlled fashion by cathodic polarization in acidic electrolyte **473**, 240
Masuda, T., see Oyama, M. **473**, 166
Mathieu, C., see Gonçalves, A.-M. **477**, 140
Mathieu, C., see Gonçalves, A.-M. **462**, 88
Matoussi Mhalla, F., see Haj Said, A. **464**, 85
Matsuo, S., see Juodkazis, S. **473**, 235
Maumy, M., see Aubert, P.-H. **470**, 77
Mbindyo, J.K.N., see Gao, J. **464**, 31
McCreery, R.L., see Ray, K.G., III **469**, 150
McDermott, M.T., see Finot, M.O. **466**, 234
McQuillan, A.J., see Babaei, A. **462**, 266
McQuillan, A.J., see Love, J.G. **464**, 93
Melendres, C.A. and Hahn, F.
'In-situ' observation of halide ion adsorption on a gold electrode using synchrotron far infrared spectroscopy **463**, 258
Ménage, S., see Collomb Dunand-Sauthier, M.-N. **469**, 53
Mendez, E., Martins, M.E. and Zinola, C.F.
New effects in the electrochemistry of carbon dioxide on platinum by the application of potential perturbations **477**, 41
Méndez, J.A., see Ortiz, R. **465**, 234
Michel, P.E., de Rooij, N.F., Koudelka-Hep, M., Fähnrich, K.A., O'Sullivan, C.K. and Guilbault, G.G.
Redox-cycling type electrochemiluminescence in aqueous medium. A new principle for the detection of proteins labeled with a ruthenium chelate **474**, 192
Michels, M., see Gisselbrecht, J.P. **469**, 170
Mickler, W., Mönner, A., Uhlemann, E., Wilke, S. and Müller, H.
Transfer of β-diketone and 4-acylpyrazolone anions across the electrified water|nitrobenzene interface **469**, 91
Mie, Y., see Taniguchi, I. **468**, 9
Miho, Y., see Ogura, K. **463**, 218
Milczarek, G., see Ciszewski, A. **469**, 18
Millington, J.P., see Ralph, T.R. **462**, 97
Milocco, R.H.
Structural identifiability of adsorption and electron transfer processes in metal dissolution and passivation mechanisms **471**, 1
Minoura, H., see Sugiura, T. **473**, 204
Minoura, H., see Yoshida, T. **473**, 209
Mirza-Rosca, J.C., see González, J.E.G. **471**, 109
Misawa, H., see Juodkazis, S. **473**, 235
Mishima, H., see Cattaneo, C. **460**, 32
Mitani, M., see Oyama, M. **473**, 166
Miyashita, T., see Aoki, A. **473**, 125
Miyawaki, T., see Yoshimoto, S. **473**, 85
Mizutani, F., see Sato, Y. **474**, 94
Mizutani, F., see Sato, Y. **473**, 99
Mizutani, F., see Yabuki, S. **468**, 117
Modestov, A.D. and Davydov, A.D.
Capacitance and photocurrent study of electronic properties of anodic oxide films on Nb and Ta. Evaluation of the ionized donor concentration profile in Nb_2O_5 film **460**, 214
Modestov, A.D., Gun, J. and Lev, O.
Graphite photoelectrochemistry 2. Photoelectrochemical studies of highly oriented pyrolitic graphite **476**, 118
Molero, M., González-Arjona, D., Calvente, J.J. and López-Pérez, G.
Activity coefficients of $Al(ClO_4)_3$ in aqueous solutions: a reexamination **460**, 100
Molina, A., see Serna, C. **468**, 158
Molina, A., see Serna, C. **466**, 8
Molina, F.V., see Bradley, J.C. **478**, 128
Molina, F.V., see Viva, F.A. **471**, 180
Momoi, K., Song, M.-B. and Ito, M.
Redox mechanisms of NO with water on the Pt(111) electrode studied by in-situ STM and IRAS **473**, 43

Monk, P.M.S. and Hodgkinson, N.M.
Electrochemical behaviour of *N*-aminopyridinium, and the viologens *N,N'*-diamino-4,4'-bipyridilium and *N,N'*-bis(4-aminophenyl)-4,4'-bipyridilium in aqueous acid: towards the formation of polymer hybrids of pyridine and aniline **462**, 43
Monné, J., see Galceran, J. **472**, 42
Mönner, A., see Mickler, W. **469**, 91
Montella, C.
Discussion on permeation transients in terms of insertion reaction mechanism and kinetics **465**, 37
Montella, C.
Review and theoretical analysis of ac–av methods for the investigation of hydrogen insertion I. Diffusion formalism **462**, 73
Montella, C., see Berthier, F. **460**, 226
Montella, C., see Diard, J.-P. **475**, 190
Montella, C., see Diard, J.-P. **471**, 126
Montella, C., see Diard, J.-P. **466**, 122
Moon, J.-M., Park, S., Lee, Y.-K., Sook Bang, G., Hong, Y.-K., Park, C. and Cheol Jeon, I.
Diamond-like carbon electrodes in electrochemical microgravimetry **464**, 230
Morallón, E., see Huerta, F. **475**, 38
Morallón, E., see Huerta, F. **469**, 159
Morallón, E., see Huerta, F. **467**, 105
Morallón, E., see Huerta, F. **463**, 109
Morandini, J., see Josserand, J. **468**, 42
Morán, M., see Casado, C.M. **463**, 87
Moretto, L.M., Ugo, P., Lacasse, R., Champagne, G.Y. and Chevalet, J.
Determination of methylmercury at Nafion® coated electrodes by single and multiple pulse voltammetric techniques **467**, 193
Morgado, J.M., see Brett, C.M.A. **468**, 26
Morin, S., see Pierozynski, B. **467**, 30
Morita, M., see Ishikawa, M. **473**, 279
Mortimer, R.J. and Warren, C.P.
Cyclic voltammetric studies of Prussian blue and viologens within a paper matrix for electrochromic printing applications **460**, 263
Moshkovich, M., see Lu, Z. **466**, 203
Mosiałek, M., see Tomczyk, P. **463**, 78
Mosiałek, M., see Tomczyk, P. **463**, 72
Mosier-Boss, P.A. and Lieberman, S.H.
Feasibility studies for the detection of volatile organic compounds in the gas phase using microelectrode sensors **460**, 105
Mostany, J., see Serruya, A. **464**, 39
Moura, I., see Correia dos Santos, M.M. **464**, 76
Moura, J.J.G., see Correia dos Santos, M.M. **464**, 76
Moutet, J.-C., see Buda, M. **469**, 132
Moutet, J.-C., see Ion, A.C. **464**, 24
Moutet, J.-C., see Zouaoui, A. **474**, 113
Mou Wang, C., see Sheng Ouyang, C. **474**, 82
Mukouyama, Y., Nakanishi, S., Konishi, H. and Nakato, Y.
Electrochemical oscillations of a new type in an $H_2O_2 + H_2SO_4$ | Pt-electrode system, appearing by addition of small amounts of halide ions **473**, 156
Mulder, W.H. and Sluyters, J.H.
Two mercury drops on a conducting surface in a mercurous ion solution as a model for electrochemical Ostwald ripening **468**, 127
Müller, H., see Mickler, W. **469**, 91
Müller, P., Ando, S., Yamada, T. and Itaya, K.
Formation of an ordered structure of iodine adsorbed on Ni(111) and the anodic dissolution processes: in-situ STM study **467**, 282
Müller, U., see Vrestal, J. **461**, 90
Murakoshi, K., Azechi, T., Hosokawa, H., Wada, Y. and Yanagida, S.
Chiroselective electron transfer at enantiomer-capped ZnO nanocrystalline surfaces **473**, 117
Murauer, F., Kišová, L., Komenda, J. and Gritzner, G.
Electrode kinetics of Eu^{3+} in dimethylsulfoxide **470**, 1
Murtomäki, L., Kontturi, K. and Schiffrin, D.J.
Some remarks on the double layer correction to the kinetics of ion transfer at the interface of immiscible electrolytes **474**, 89
Murtomäki, L., see Grandell, D. **469**, 72
Murtomäki, L., see Grandell, D. **463**, 242
Murtomäki, L., see Quinn, B. **460**, 149
Murty, K.V.G.K., see Berchmans, S. **468**, 170
Musiani, M., Furlanetto, F. and Bertoncello, R.
Electrodeposited $PbO_2 + RuO_2$: a composite anode for oxygen evolution from sulphuric acid solution **465**, 160

Nadjo, L., see Keita, B. **478**, 76
Nadjo, L., see Keita, B. **477**, 146
Nadjo, L., see Mahmoud, A. **463**, 129
Nagle, L.C., see Burke, L.D. **461**, 52
Nakabayashi, S., Aogaki, R., Karantonis, A., Iguchi, U., Ushida, K. and Nawa, M.
Two-dimensional metal deposition at the liquid|liquid interface; potential and magnetohydrodynamic pattern transition **473**, 54
Nakagiri, N., see Sugimura, H. **473**, 230
Nakamura, H., see Kuramitz, H. **466**, 117
Nakanishi, S., see Mukouyama, Y. **473**, 156
Nakaoka, K., see Ogura, K. **474**, 101
Nakato, Y., see Mukouyama, Y. **473**, 156
Nakayama, M., see Ogura, K. **474**, 101
Nakayama, M., see Ogura, K. **463**, 218
Nam, H., see Shin, J.H. **468**, 76
Nam, H., see Yoon, I.J. **464**, 135
Nanbu, N., Kitamura, F., Ohsaka, T. and Tokuda, K.
Adsorption of pyridine on a polycrystalline gold electrode surface studied by infrared reflection absorption spectroscopy **470**, 136
Nandhakumar, I., see Sorenson, T.A. **467**, 270
Naohara, H., Ye, S. and Uosaki, K.
Epitaxial growth of a palladium layer on an Au(100) electrode **473**, 2
Nart, F.C., see de Moraes, I.R. **460**, 110
Narula, P.M. and Noftle, R.E.
Investigation of the lifetimes of some pyrrole species by rapid scan cyclic voltammetry and double potential step techniques **464**, 123
Narváez, A., see Catalin Popescu, I. **464**, 208
Nawa, M., see Nakabayashi, S. **473**, 54
Neilands, O., see Goldenberg, L.M. **463**, 212
Neudeck, A., see Aubert, P.-H. **470**, 77
Neudeck, A., see Del Campo, F.J. **477**, 71
Neueder, R., see Barthel, J. **471**, 78
Ng, Y.-F., Strutwolf, J., Garratt, P.J. and Williams, D.E.
Cationic systems as self-assembled monolayers on gold surfaces **464**, 263
Nguyen, P.H. and Paasch, G.
Transfer matrix method for the electrochemical impedance of inhomogeneous porous electrodes and membranes **460**, 63
Nielsen, P.E., see Tomschik, M. **476**, 71
Nikolić, N.D., see Popov, K.I. **464**, 245
Nilsson, E., Berendson, J. and Fontes, E.
Electrochemical treatment of tumours: a simplified mathematical model **460**, 88
Nishihara, H., see Horikoshi, T. **473**, 113
Nishimura, M., see Hojo, M. **468**, 110
Nishimura, N., Ooi, M., Shimazu, K., Fujii, H. and Uosaki, K.
Post-assembly insertion of metal ions into thiol-derivatized porphyrin monolayers on gold **473**, 75
Nishino, J., Chatani, S., Uotani, Y. and Nosaka, Y.
Electrodeposition method for controlled formation of CdS films from aqueous solutions **473**, 217
Nishio, T., see Fujimoto, S. **473**, 265
Nishiyama, K., Tahara, S.-i., Uchida, Y., Tanoue, S. and Taniguchi, I.
Structural differences in self-assembled monolayers of anthraquinone derivatives on silver and gold electrodes studied by cyclic voltammetry and in situ SERS spectroscopy **478**, 83
Njue, C.K., see Gao, J. **464**, 31
Noël, V., see Randriamahazaka, H. **472**, 103
Noftle, R.E., see Narula, P.M. **464**, 123
Noma, T., see Arai, G. **464**, 143
Nosaka, Y., see Nishino, J. **473**, 217
Notsu, H., see Yagi, I. **473**, 173
Nozute, S., see Yoshimoto, S. **473**, 85
Nukanobu, K., see Arihara, K. **473**, 138
Núñez-Vergara, L.J., see Squella, J.A. **466**, 90

Nyokong, T., see Thamae, M. **470**, 126

O'Connor, S.D., Olsen, G.T. and Creager, S.E.
A Nernstian electron source model for the ac voltammetric response of a reversible surface redox reaction using large-amplitude ac voltages **466**, 197
Oekermann, T., Schlettwein, D. and Jaeger, N.I.
Role of surface states and adsorbates in time-resolved photocurrent measurements and photovoltage generation at phthalocyaninatozinc(II)-photocathodes **462**, 222
Oelkrug, D., see Kim, Y.-C. **468**, 121
Oesten, R., see Levi, M.D. **477**, 32
Oesten, R., see Wilde, P.M. **460**, 154
Oguni, S., see Toda, K. **479**, 57
Ogura, K., Kobayashi, M., Nakayama, M. and Miho, Y.
In-situ FTIR studies on the electrochemical oxidation of histidine and tyrosine **463**, 218
Ogura, K., Nakayama, M. and Nakaoka, K.
Electrochemical quartz crystal microbalance and in situ infrared spectroscopic studies on the redox reaction of Prussian blue **474**, 101
Oh, K.-C., Kim, K.-A., Paeng, I.R., Baek, D.-j. and Paeng, K.-J.
Anion-selective membrane electrodes based on polymer-supported metalloporphyrins **468**, 98
Ohira, A., Ishizaki, T., Sakata, M., Kunitake, M., Taniguchi, I. and Hirayama, C.
Self-organization of α-cyclodextrin on Au(111) surfaces induced by potential controlled adsorption **472**, 163
Ohkoshi, S.-i., Einaga, Y., Fujishima, A. and Hashimoto, K.
Magnetic properties and optical control of electrochemically prepared iron–chromium polycyanides **473**, 245
Ohmori, T., El-Deab, M.S. and Osawa, M.
Electroreduction of nitrate ion to nitrite and ammonia on a gold electrode in acidic and basic sodium and cesium nitrate solutions **470**, 46
Ohsaka, T., see Arihara, K. **473**, 138
Ohsaka, T., see John, S.A. **477**, 52
Ohsaka, T., see John, S.A. **466**, 67
Ohsaka, T., see Nanbu, N. **470**, 136
Ohsaka, T., see Okajima, T. **476**, 46
Ohsaka, T., see Vengatajalabathy Gobi, K. **465**, 177
Ohshita, J., see Harima, Y. **472**, 157
Ohshita, J., see Zhu, L. **464**, 158
Ohta, T., see Endo, O. **473**, 19
Ohtsuka, T. and Otsuki, T.
Effect of ultra-violet light irradiation on anodic oxide films on titanium in sulfuric acid solution **473**, 272
Ohtsuka, T., see Itoh, J. **473**, 256
Okada, T.
Theory for water management in membranes for polymer electrolyte fuel cells: Part 1. The effect of impurity ions at the anode side on the membrane performances **465**, 1
Okada, T.
Theory for water management in membranes for polymer electrolyte fuel cells: Part 2. The effect of impurity ions at the cathode side on the membrane performances **465**, 18
Okajima, T., see John, S.A. **466**, 67
Okajima, T., Tokuda, K. and Ohsaka, T.
Electrochemical behavior of a *Cypridina* luciferin analogue in acetonitrile solutions in the presence of proton acceptors **476**, 46
Okazaki, S., see Hoshino, T. **472**, 91
Okazaki, S., see Oyama, M. **473**, 166
Okuda, T., see Yamamoto, T. **460**, 242
Oldham, K.B., see Mahon, P.J. **464**, 1
Olifirenko, S.N., see Kovach, S.K. **472**, 178
Oliver, E.W. and Evans, D.H.
Electrochemical studies of six N–F electrophilic fluorinating reagents **474**, 1
Olsen, G.T., see O'Connor, S.D. **466**, 197
Ono, N., see Chen Tsai, Y. **477**, 25
Ooi, M., see Nishimura, N. **473**, 75
Ooi, T., see Sugiura, T. **473**, 204
Orlik, M., see Jurczakowski, R. **478**, 118
Ortiz, R., Cuesta, A., Márquez, O.P., Márquez, J., Méndez, J.A. and Gutiérrez, C.
Origin of the infrared reflectance increase produced by the adsorption of CO on particulate metals deposited on moderately reflecting substrates **465**, 234
Orts, J.M., Gómez, R. and Feliu, J.M.
Bromine monolayer adsorption on Pt(110) surfaces **467**, 11
Orts, J.M., see Climent, V. **467**, 20
Orts, J.M., see Climent, V. **461**, 65
Osawa, M., see Ataka, K. **473**, 34
Osawa, M., see Ataka, K. **460**, 188
Osawa, M., see Itoh, J. **473**, 256
Osawa, M., see Ohmori, T. **470**, 46
Osborne, M.D., see Bagel, O. **469**, 189
Osteryoung, J., see Aoki, K. **472**, 1
O'Sullivan, C.K., see Michel, P.E. **474**, 192
Other, A.N.
1799–1999: Alessandro Volta's 'Electric Pile': Two hundred years, but it doesn't seem like it **460**, 1
Otsuki, T., see Ohtsuka, T. **473**, 272
Oung, O., see Mahmoud, A. **463**, 129
Outhwaite, C.W., see Lamperski, S. **460**, 135
Ovsyannikova, E.V., see Semenikhin, O.A. **463**, 190
Oyama, M., Mitani, M., Washida, M., Masuda, T. and Okazaki, S.
Two-dimensional CCD detection of electrogenerated chemiluminescence (ECL) on an electrode surface. ECL reactions involving microcrystals of the perylene dimer cation radical salt **473**, 166
Oyama, M., see Hoshino, T. **472**, 91
Oyama, N., see Paulson, S.C. **470**, 166
Oyama, N., see Tatsuma, T. **472**, 142
Oyama, N., see Tatsuma, T. **469**, 34
Oyamatsu, D., Kuwabata, S. and Yoneyama, H.
Underpotential deposition behavior of metals onto gold electrodes coated with self-assembled monolayers of alkanethiols **473**, 59
Ozaki, M., see Tatsuma, T. **469**, 34

Paasch, G., see Nguyen, P.H. **460**, 63
Paeng, I.R., see Oh, K.-C. **468**, 98
Paeng, K.-J., see Oh, K.-C. **468**, 98
Paes de Sousa, P.M., see Correia dos Santos, M.M. **464**, 76
Paganin, V.A., see Sena, D.R. **477**, 164
Pagitsas, M. and Sazou, D.
Current oscillations induced by chlorides during the passive–active transition of iron in a sulfuric acid solution **471**, 132
Pailleret, A., see Ion, A.C. **464**, 24
Pakkanen, T.A., see Caix-Cecillon, C. **466**, 187
Paleček, E., see Tomschik, M. **476**, 71
Palmore, G.T.R. and Kim, H.-H.
Electro-enzymatic reduction of dioxygen to water in the cathode compartment of a biofuel cell **464**, 110
Park, C., see Moon, J.-M. **464**, 230
Park, J.-H., see Bae, Z.-U. **468**, 85
Park, S., see Moon, J.-M. **464**, 230
Park, W., see Hong, H.-G. **476**, 177
Park, Y.-S., Jang, J.-M. and Lee, C.-W.
Self-assembly of and charge transfer at *N*-docosyl-*N'*-methyl viologen on electrode surfaces **468**, 70
Pastor, E., see Arévalo, M.C. **472**, 71
Pastor, E., see Ianniello, R. **471**, 167
Patolsky, F., Gabriel, T. and Willner, I.
Controlled electrocatalysis by microperoxidase-11 and Au-nanoparticle superstructures on conductive supports **479**, 69
Paulson, S.C. and Oyama, N.
Addition of α-hydroxyalkylferrocenes to electrochemically oxidized poly(aniline) **470**, 166
Pauporté, T., Aberdam, D., Hazemann, J.-L., Faure, R. and Durand, R.
X-ray absorption in relation to valency of iridium in sputtered iridium oxide films **465**, 88
Pavlov, V., see Catalin Popescu, I. **464**, 208
Pavlović, M.G., see Popov, K.I. **464**, 245
Pecina, O. and Badiali, J.P.
Specific adsorption at modulated liquid | liquid interfaces **475**, 46
Pecina, O., see Huber, T. **467**, 203
Peelen, W.H.A., Hemmes, K. and de Wit, J.H.W.
Comparative study on the oxygen dissolution behaviour in 62/38 mol% Li/K and 52/48 mol% Li/Na carbonate **470**, 39

Peintler, G., see Visy, C. **462**, 1
Pelaez, E., see Gómez, E. **469**, 139
Pellicano, A., see Simison, S. **470**, 89
Pemberton, J.E., see Shen, A. **479**, 32
Pemberton, J.E., see Shen, A. **479**, 21
Peremans, A., see Tadjeddine, A. **473**, 25
Pérez Córdoba, A., see Bonfranceschi, A. **477**, 1
Pérez-Jiménez, C., see Lubert, K.-H. **475**, 73
Pérez, J.M., see Huerta, F. **469**, 159
Pérez, J.M., see Huerta, F. **467**, 105
Pérez, M.J., see Batanero, B. **469**, 201
Pessôa, C.A. and Gushikem, Y.
Cobalt(II) metallated hematoporphyrin IX and protoporphyrin IX immobilized on niobium(V) oxide grafted on a silica gel surface: electrochemical studies **477**, 158
Peter, L.M., see Fermín, D.J. **473**, 192
Peters, D.G., see Alleman, K.S. **460**, 207
Petitjean, J., Aeiyach, S., Lacroix, J.C. and Lacaze, P.C.
Ultra-fast electropolymerization of pyrrole in aqueous media on oxidizable metals in a one-step process **478**, 92
Pettinger, B., see Chen, A. **467**, 342
Pezzatini, G., Becagli, S., Innocenti, M., Foresti, M.L. and Guidelli, R.
Fumarodinitrile electrohydrodimerization and acrylonitrile electroreduction on liquid gallium: a comparison with mercury **462**, 127
Pezzatini, G., Caporali, S., Innocenti, M. and Foresti, M.L.
Formation of ZnSe on Ag(111) by electrochemical atomic layer epitaxy **475**, 164
Pierozynski, B., Morin, S. and Conway, B.E.
Influence of adsorption of guanidonium cations on H upd at Pt(*hkl*) surfaces: lattice-specific anion-mimetic effects **467**, 30
Pilard, J.-F., see Dubey, S. **477**, 121
Pinheiro, J.-P., see van Leeuwen, H.P. **471**, 55
Piron, A., see Collomb Dunand-Sauthier, M.-N. **463**, 119
Pletcher, D. and Thompson, H.
A microelectrode study of the catalysis of alkyl halide reduction by Co(II)(salen) **464**, 168
Pleus, S., see Schwientek, M. **461**, 94
Pluchery, O., see Tadjeddine, A. **473**, 25
Poehler, T.O., see Schlindwein, W.S. **460**, 46
Ponomarev, E.A., see Fermín, D.J. **473**, 192
Popa, E., see Fujishima, A. **473**, 179
Popescu, A., see Ion, A.C. **464**, 24
Popov, B.N., see Xie, Y. **466**, 169
Popov, K.I., Kostić, T.M., Nikolić, N.D., Stojilković, E.R. and Pavlović, M.G.
A new approach to metal electrodeposition at a periodically changing rate: Part I. The reversing overpotential method **464**, 245
Popović, K.D., see Dražić, D.M. **466**, 155
Pospíšil, L., Sokolová, R., Colombini, M.P., Giannarelli, S. and Fuoco, R.
Electrochemical properties of three dicarboximide-type pesticides: vinclozoline, iprodione and procymidone **472**, 33
Potteau, E., Levillain, E. and Lelieur, J.-P.
Mechanism of the electrochemical reduction of sulfur dioxide in non-aqueous solvents **476**, 15
Pourcelly, G., see Sistat, P. **460**, 53
Pradeep, T., see Berchmans, S. **468**, 170
Price, R., see Al-Akl, A. **467**, 60
Prieto, F., Rueda, M. and Compton, R.G.
Salt and isotope effects upon a multistep electrode reaction: the reduction of nitromethane on mercury **474**, 60
Purushothama, S., see Wijayawardhana, C.A. **468**, 2
Puy, J., see Galceran, J. **472**, 42
Pyun, H.-J., see Shin, J.H. **468**, 76

Quijada, C., see Huerta, F. **467**, 105
Quijada, C., see Huerta, F. **463**, 109
Quinn, B., Lahtinen, R. and Murtomäki, L.
Simultaneous ion transfer across the microhole ITIES: an example of ternary electrodiffusion **460**, 149
Quint, B., see Kim, Y.-C. **468**, 121

Rabinovich, L., Lev, O. and Tsirlina, G.A.
Electrochemical characterisation of Pd modified ceramic|carbon electrodes: partially flooded versus wetted channel hydrophobic gas electrodes **466**, 45
Rafiqul Islam, M., see Kumazawa, N. **472**, 137
Raicheff, R., see Bojinov, M. **475**, 58
Ralph, T.R., Hitchman, M.L., Millington, J.P. and Walsh, F.C.
Evaluation of a reactor model and cathode materials for batch electrolysis of L-cystine hydrochloride **462**, 97
Ramon Morante, J., see Gorostiza, P. **469**, 48
Randriamahazaka, H., Noël, V. and Chevrot, C.
Nucleation and growth of poly(3,4-ethylenedioxythiophene) in acetonitrile on platinum under potentiostatic conditions **472**, 103
Rao, T.N., see Fujishima, A. **473**, 179
Raoult, E., see Rault-Berthelot, J. **466**, 144
Raposo, R.R., see Fernández-Mérida, L. **466**, 38
Raspor, B., see Erk, M. **466**, 75
Rault-Berthelot, J., Rozé, C., Granger, M.M. and Raoult, E.
Anodic oxidation of various arylenecyanovinylenes made of alternating fluorenyl, thienyl and/or phenyl units **466**, 144
Rawytsch, P., see Barthel, J. **471**, 78
Ray, K.G., III and McCreery, R.L.
Characterization of the surface carbonyl and hydroxyl coverage on glassy carbon electrodes using Raman spectroscopy **469**, 150
Reymond, F., Chopineaux-Courtois, V., Steyaert, G., Bouchard, G., Carrupt, P.-A., Testa, B. and Girault, H.H.
Ionic partition diagrams of ionisable drugs: pH-lipophilicity profiles, transfer mechanisms and charge effects on solvation **462**, 235
Richet, M., see Keita, B. **478**, 76
Richet, M., see Keita, B. **477**, 146
Rivas, G.A., see Forzani, E.S. **461**, 174
Robert, A., see Bellec, N. **462**, 137
Roch, H., see Barthel, J. **471**, 78
Rodes, A., see Climent, V. **467**, 20
Rodes, A., see Climent, V. **461**, 65
Rodríguez, A.R., see Esteban, M. **468**, 202
Rodríguez, J.L., see Arévalo, M.C. **472**, 71
Rodríguez, J.L., see Ianniello, R. **471**, 167
Rodríguez Mellado, J.M., see Higuera, M.J. **474**, 174
Rodríguez Nieto, F.J., see Martins, M.E. **477**, 14
Romagnoli, J., see Talaie, A. **468**, 19
Ronald Fawcett, W., see Marinković, N.S. **467**, 325
Ronnenberg, J., see Kirstein, D. **474**, 43
Roscoe, S.G., see Li, H.-Q. **478**, 67
Ross, P.N., see Marković, N.M. **467**, 157
Rotenberg, Z.A., see Semenikhin, O.A. **463**, 190
Rozé, C., see Rault-Berthelot, J. **466**, 144
Rubim, J.C., see Villamil, R.F.V. **472**, 112
Rueda, M., see Prieto, F. **474**, 60
Ruiz Montoya, M., see Higuera, M.J. **474**, 174
Rusling, J.F., see Gao, J. **464**, 31
Rusling, J.F., see Yang, J. **463**, 53
Russell, A.E., see Lampitt, R.A. **460**, 80
Ruzgas, T., Gaigalas, A. and Gorton, L.
Diffusionless electron transfer of microperoxidase-11 on gold electrodes **469**, 123
Ruzgas, T., see Gaigalas, A.K. **465**, 96
Ruzgas, T., see Torto, N. **464**, 252

Sadik, O.A., see Sargent, A. **470**, 144
Sadkowski, A.
Small signal (local) analysis of electrocatalytic reaction. Pole-zero approach **465**, 119
Saeki, I., Setaka, J., Furuichi, R. and Konno, H.
Photoelectrochemical response and stability of titanium–zinc mixed oxide films formed by thermal oxidation **464**, 238
Saint-Aguet, P., see Délécouls, K. **468**, 139
Saint-Aman, E., see Buda, M. **469**, 132
Saint-Aman, E., see Ion, A.C. **464**, 24
Sakairi, M., see Watanabe, K. **473**, 250
Sakata, M., see Ohira, A. **472**, 163
Sakata, T., see Yasaki, Y. **469**, 116
Sakkopoulos, S., see Tsamouras, D. **469**, 43
Salinas, D.R., Cobo, E.O., Garcia, S.G. and Bessone, J.B.

Early stages of mercury electrodeposition on HOPG **470**, 120
Salvador, J., see Galceran, J. **472**, 42
Salvarezza, R.C., see Andreasen, G. **467**, 230
Salvarezza, R.C., see Bolzán, A.E. **475**, 181
Salvarezza, R.C., see Gómez, M.M. **474**, 74
Salvarezza, R.C., see Martins, M.E. **477**, 14
Samec, Z., Langmaier, J. and Trojánek, A.
Polarization phenomena at the water | *o*-nitrophenyl octyl ether interface: Part III. Kinetics of tetraethylammonium ion transfer across the polymer supported interfaces **463**, 232
Samec, Z., see Langmaier, J. **469**, 11
Sanchez de Pinto, M.I., see Cattaneo, C. **460**, 32
Sandhyarani, N., see Berchmans, S. **468**, 170
Sandonà, G., see Farnia, G. **460**, 160
Sanecki, P. and Kaczmarski, K.
The voltammetric reduction of some benzenesulfonyl fluorides, simulation of the ECE mechanism and determination of the potential variation of the transfer coefficient by using the compounds with two reducible groups **471**, 14
Sanemasa, I., see Toda, K. **479**, 57
Sannazzaro, M.G., see Casella, I.G. **462**, 202
Santana, A.E.G., see de Azevedo, D.C. **466**, 99
Santos, E., see Eberhardt, D. **461**, 76
Sanz, F., see Gómez, E. **465**, 63
Sanz, F., see Gorostiza, P. **469**, 48
Sarada, B.V., see Fujishima, A. **473**, 179
Saraswathi, R., Hillman, A.R. and Martin, S.J.
Mechanical resonance effects in electroactive polycarbazole films **460**, 267
Sargent, A., Loi, T., Gal, S. and Sadik, O.A.
The electrochemistry of antibody-modified conducting polymer electrodes **470**, 144
Sarker, H., see Schlindwein, W.S. **460**, 46
Sasaki, T., see Itoh, J. **473**, 256
Sasaki, Y., see Abe, M. **473**, 93
Sato, O., see Ishibashi, K.-i. **465**, 195
Sato, Y. and Mizutani, F.
Electrochemical behavior of gold electrodes modified with aminopurinethiol derivatives **473**, 99
Sato, Y., Mizutani, F., Shimazu, K., Ye, S. and Uosaki, K.
Mass transport accompanied with electron transfer between the gold electrode modified with 11-ferrocenylundecanethiol monolayer and redox species in solution — an electrochemical quartz crystal microbalance study **474**, 94
Savéant, J.-M., see Andrieux, C.P. **476**, 81
Savéant, J.-M., see Gonzalez, J. **463**, 157
Savinell, R.F., see Gojković, S.L. **462**, 63
Sazou, D., see Pagitsas, M. **471**, 132
Schäfer, H., see Bagel, O. **469**, 189
Schäfer, W., see Klunker, J. **466**, 107
Scharifker, B.R., see Serruya, A. **464**, 39
Schechter, A., see Lu, Z. **466**, 203
Scheller, F., see Kirstein, D. **474**, 43
Schell, M., see Chen, S. **478**, 108
Scherson, D.A., see Hu, Y. **468**, 64
Schiffrin, D.J., see Ceré, S. **470**, 31
Schiffrin, D.J., see Murtomäki, L. **474**, 89
Schiffrin, D.J., see Simison, S. **470**, 89
Schizodimou, A., Kyriacou, G. and Lambrou, C.
Electrochemical reduction of dichlorodifluoromethane in acetonitrile medium to useful fluorinated compounds **471**, 26
Schlereth, D.D.
Characterization of protein monolayers by surface plasmon resonance combined with cyclic voltammetry 'in situ' **464**, 198
Schlettwein, D., see Hesse, K. **476**, 148
Schlettwein, D., see Oekermann, T. **462**, 222
Schlindwein, W.S., Gofer, Y., Sarker, H., Poehler, T.O. and Searson, P.C.
The electrochemical properties of a series of phenylene-thienyl polymers in tetramethylene sulfone based electrolytes **460**, 46
Schmickler, W.
A model for assisted ion transfer across liquid | liquid interfaces **460**, 144
Schmickler, W., see Eberhardt, D. **461**, 76
Schmickler, W., see Huber, T. **467**, 203
Schmidt, V.M., see Ianniello, R. **471**, 167
Schollmeyer, E., see Buschmann, H.-J. **474**, 188
Schorb, K., see Krausa, M. **460**, 10
Schuster, R., see Xia, X.H. **460**, 102
Schwientek, M., Pleus, S. and Hamann, C.H.
Enantioselective electrodes: stereoselective electroreduction of 4-methylbenzophenone and acetophenone **461**, 94
Scott, K., Argyropoulos, P. and Sundmacher, K.
A model for the liquid feed direct methanol fuel cell **477**, 97
Scrosati, B., see Appetecchi, G.B. **463**, 248
Scrosati, B., see Tossici, R. **474**, 107
Searson, P.C., see Schlindwein, W.S. **460**, 46
Seddon, B.J., see Bagel, O. **469**, 189
Seeber, R., see Ballarin, B. **463**, 123
Sekine, K., see Sumiya, K. **462**, 150
Semenikhin, O.A., Ovsyannikova, E.V., Alpatova, N.M., Rotenberg, Z.A. and Kazarinov, V.E.
Electrochemical and photoelectrochemical behaviour of poly-3-methylthiophene and polybithiophene in non-aqueous solutions: 1. Dark and light processes in systems with and without cathodic doping **463**, 190
Sena, D.R., Ticianelli, E.A., Paganin, V.A. and Gonzalez, E.R.
Effect of water transport in a PEFC at low temperatures operating with dry hydrogen **477**, 164
Senda, M., Katano, H. and Yamada, M.
Amperometric ion-selective electrode. Voltammetric theory and analytical applications at high concentration and trace levels **468**, 34
Senillou, A., see Cosnier, S. **469**, 176
Seo, M., Chiba, M. and Suzuki, K.
Nano-mechano-electrochemistry of the iron (100) surface in solution **473**, 49
Sereno, L.E., see Cortona, M.N. **470**, 157
Serna, C. and Molina, A.
General solutions for the I/t response for reversible processes in the presence of product in a multipotential step experiment at planar and spherical electrodes whose areas increase with any power of time **466**, 8
Serna, C., Molina, A., Martínez-Ortiz, F. and González, J.
Study of a catalytic mechanism in double potential step techniques at spherical electrodes **468**, 158
Serose, J., see Levi, M.D. **479**, 12
Serruya, A., Mostany, J. and Scharifker, B.R.
The kinetics of mercury nucleation from Hg_2^{2+} and Hg^{2+} solutions on vitreous carbon electrodes **464**, 39
Setaka, J., see Saeki, I. **464**, 238
Shen, A. and Pemberton, J.E.
Interfacial structure of dimethylsulfoxide at Ag electrodes from surface enhanced Raman scattering and differential capacitance **479**, 21Shen, A. and Pemberton, J.E.
Surface Raman scattering of interfaces at Ag electrodes emersed from dimethylsulfoxide: spectroscopic evidence for an emersion-induced potential shift **479**, 32
Sheng Ouyang, C. and Mou Wang, C.
Electrochemical characterization of the clay-enhanced luminol ecl reaction **474**, 82
Shi, G., see Wang, X. **470**, 95
Shi, Z., see Chen, A. **467**, 342
Shibata, M., see Furuya, N. **467**, 85
Shibata, M., see Furuya, N. **460**, 251
Shibata, T., see Fujimoto, S. **473**, 265
Shimazu, K., see Nishimura, N. **473**, 75
Shimazu, K., see Sato, Y. **474**, 94
Shim, Y.-B., see Yeom, J.-S. **463**, 16
Shin, J.H., Lee, J.S., Lee, H.J., Chu, J., Pyun, H.-J., Nam, H. and Cha, G.S.
Trifluoroacetophenone derivative-based carbonate ion-selective electrodes: effect of diluent pH on the anion selectivity **468**, 76
Shingaya, Y. and Ito, M.
Comparison of a bisulfate anion adsorbed on M(111) (M = Pt, Rh, Au, Ag and Cu) **467**, 299
Shiu, K.-K., Song, F.-Y. and Lau, K.-W.
Effects of polymer thickness on the potentiometric pH responses of polypyrrole modified glassy carbon electrodes **476**, 109

Sideris, C., see Coutouli-Argyropoulou, E. **477**, 130
Siebert, E., see Ion, A.C. **464**, 24
Silber, J.J., see Cortona, M.N. **470**, 157
Silva, F. and Martins, A.
Surface structural effects on specific adsorption of oxoanions on gold single crystal electrodes **467**, 335
Simic, N. and Ahlberg, E.
Electrochemical, spectroscopic and structural investigations of the Cd/Cd(II) system in alkaline media: 2. Concentration effects **462**, 34
Simison, S., Pellicano, A., Brust, M. and Schiffrin, D.J.
Detection of near-wall hydrodynamic effects by electrochemiluminescence **470**, 89
Simões Gonçalves, M.L., see Correia dos Santos, M.M. **464**, 76
Simonet, J., see Dubey, S. **477**, 121
Simonet, J., see Fabre, B. **460**, 119
Simon, P., see Amatore, C. **462**, 55
Sistat, P. and Pourcelly, G.
Steady-state ion transport through homopolar ion-exchange membranes: an analytical solution of the Nernst–Planck equations for a 1:1 electrolyte under the electroneutrality assumption **460**, 53
Skoluda, P., see Striegler, H. **471**, 9
Sluyters, J.H., see Mulder, W.H. **468**, 127
Sluyters, J.H., see van Venrooij, T.G.J. **472**, 64
Sluyters, J.H., see van Venrooij, T.G.J. **472**, 53
Sluyters, J.H., see van Venrooij, T.G.J. **462**, 111
Sluyters-Rehbach, M., see van Venrooij, T.G.J. **472**, 64
Sluyters-Rehbach, M., see van Venrooij, T.G.J. **472**, 53
Sluyters-Rehbach, M., see van Venrooij, T.G.J. **462**, 111
Smith, S.P.E. and Abruña, H.D.
Structural effects on the oxidation of HCOOH by bismuth modified Pt(111) electrodes with (110) monatomic steps **467**, 43
Smoliński, S. and Sobkowski, J.
Adsorption of sulfate ions on monocrystalline copper electrodes: the structural effects **463**, 1
Smyth, M.R., see Whelan, C.M. **474**, 138
Sobkowski, J., see Smoliński, S. **463**, 1
Sokolová, R., see Pospíšil, L. **472**, 33
Solis, V., see Garay, F. **478**, 17
Solis, V.M., see Forzani, E.S. **461**, 174
Solis, V., see Garay, F. **476**, 165
Song, C. and Villemure, G.
Preparation of clay-modified electrodes by electrophoretic deposition of clay films **462**, 143
Song, F.-Y., see Shiu, K.-K. **476**, 109
Song, M.-B., see Momoi, K. **473**, 43
Song, W., Wang, X., Liu, Y., Liu, J. and Xu, H.
Electrochemical and electrocatalytic properties of tetra-iron substituted sandwich-type pentadecatungstodiphosphate heteropolyanions **476**, 85
Sonoda, K., see Taniguchi, I. **468**, 9
Sonoyama, N., see Yasaki, Y. **469**, 116
Sook Bang, G., see Moon, J.-M. **464**, 230
Sorenson, T.A., Wayne Suggs, D., Nandhakumar, I. and Stickney, J.L.
Phase transitions in the electrodeposition of tellurium atomic layers on Au(100) **467**, 270
Sotomura, T., see Tatsuma, T. **472**, 142
Sperling, J., Tributsch, H., Streffer, R.M.F., Abdul-Redah, T. and Chatzidimitriou-Dreismann, C.A.
Anomalous H/D isotopic effect in the kinetics of polarographic hydrogen evolution **477**, 62
Squella, J.A., Sturm, J.C., Weiss-Lopez, B., Bontá, M. and Núñez-Vergara, L.J.
Electrochemical study of β-nitrostyrene derivatives: steric and electronic effects on their electroreduction **466**, 90
Sriramulu, S., Jarvi, T.D. and Stuve, E.M.
Reaction mechanism and dynamics of methanol electrooxidation on platinum(111) **467**, 132
Stalnionis, G., see Vaškelis, A. **465**, 142
Steinrücke, P., see Kirstein, D. **474**, 43
Stéphan, O., see Zouaoui, A. **474**, 113
Steyaert, G., see Reymond, F. **462**, 235
Stickney, J.L., see Sorenson, T.A. **467**, 270
Stimming, U., see Fujiwara, N. **472**, 120
Stine, K.J., Andrauskas, D.M., Khan, A.R., Forgo, P. and D'Souza, V.T.
Electrochemical study of self-assembled monolayers of a β-cyclodextrin methyl sulfide covalently linked to anthraquinone **465**, 209
Stine, K.J., Andrauskas, D.M., Khan, A.R., Forgo, P., D'Souza, V.T., Liu, J. and Friedman, R.M.
Structure and electrochemical behavior of a flavin sulfide monolayer adsorbed on gold **472**, 147
Stojek, Z., see Ciszkowska, M. **466**, 129
Stojilković, E.R., see Popov, K.I. **464**, 245
Strasser, P., Eiswirth, M. and Koper, M.T.M.
Mechanistic classification of electrochemical oscillators — an operational experimental strategy **478**, 50
Strasser, P., Lübke, M., Eickes, C. and Eiswirth, M.
Modeling galvanostatic potential oscillations in the electrocatalytic iodate reduction system **462**, 19
Streffer, R.M.F., see Sperling, J. **477**, 62
Striegler, H., Skoluda, P. and Kolb, D.M.
On the stability of unreconstructed Au(100)-(1 × 1) at negative potentials in aqueous sulfate solution **471**, 9
Strong, T.D., see Yoon, I.J. **464**, 135
Strutwolf, J., see Ng, Y.-F. **464**, 263
Stuhlmann, C., see Broekmann, P. **467**, 307
Sturm, J.C., see Squella, J.A. **466**, 90
Stuve, E.M., see Sriramulu, S. **467**, 132
Suárez, M.F. and Compton, R.G.
In situ atomic force microscopy study of polypyrrole synthesis and the volume changes induced by oxidation and reduction of the polymer **462**, 211
Suárez, M.F., see Chen Tsai, Y. **477**, 25
Sugawara, K., see Kuramitz, H. **466**, 117
Sugimura, H., Takai, O. and Nakagiri, N.
Scanning probe lithography for electrode surface modification **473**, 230
Sugiura, T., Itoh, S., Ooi, T., Yoshida, T., Kuroda, K. and Minoura, H.
Evolution of a skeleton structured TiO_2 surface consisting of grain boundaries **473**, 204
Sugiura, T., see Yoshida, T. **473**, 209
Sumiya, K., Suzuki, J., Takasu, R., Sekine, K. and Takamura, T.
Enhancement of the electrochemical Li doping/undoping reaction rate of a graphitic material by an evaporated film of Sn, Zn or Pb **462**, 150
Sundholm, F., see Lankinen, E. **460**, 176
Sundholm, G., see Betova, I. **472**, 20
Sundholm, G., see Grandell, D. **469**, 72
Sundholm, G., see Grandell, D. **463**, 242
Sundholm, G., see Lankinen, E. **460**, 176
Sundmacher, K., see Scott, K. **477**, 97
Sun, S.-G. and Yang, Y.-Y.
Studies of kinetics of HCOOH oxidation on Pt(100), Pt(110), Pt(111), Pt(510) and Pt(911) single crystal electrodes **467**, 121
Sun, W.-Y., Zhang, L. and Gu, Q.
Electrochemical study of tetraphenylporphinato-iron(III)–thiolate complexes, NH···S hydrogen bonding in the cytochrome P-450 model system **469**, 84
Sun, W., Zhang, S., Lin, X., Jin, L., Jin, S., Deng, J. and Kong, J.
Electrocatalytic reduction of nitrite at a carbon fiber microelectrode chemically modified by palladium(II)-substituted Dawson type heptadecatungstodiphosphate **469**, 63
Su, Y.O., see Chen, F. **474**, 52
Suzuki, J., see Sumiya, K. **462**, 150
Suzuki, K., see Seo, M. **473**, 49
Suzuki, T., see Kamata, K. **473**, 145

Tadjeddine, A., Pluchery, O., Le Rille, A., Humbert, C., Buck, M., Peremans, A. and Zheng, W.Q.
What can we learn from the non-linear optical investigation of the liquid | solid interface? **473**, 25
Tadjeddine, A., see Le Rille, A. **467**, 238
Taguchi, M., see Tatsuma, T. **472**, 142
Taguchi, T., see Talaie, A. **468**, 19
Tahara, S.-i., see Nishiyama, K. **478**, 83
Takahashi, H., see Watanabe, K. **473**, 250
Takahashi, K., see Komura, T. **478**, 9

Takai, O., see Sugimura, H. **473**, 230
Takamatsu, Y., see Toda, K. **479**, 57
Takamoto, M., see Himeno, S. **465**, 129
Takamura, K., Fuse, T., Arai, K. and Kusu, F.
A review of a new voltammetric method for determining acids **468**, 53
Takamura, T., see Sumiya, K. **462**, 150
Takasu, R., see Sumiya, K. **462**, 150
Takata, A., see Zhu, L. **464**, 158
Takeuchi, M., see Kumazawa, N. **472**, 137
Takky, D., see Chbihi, M.E.M. **463**, 63
Takky, D., see Cherqaoui, A. **464**, 101
Talaie, A., Lee, J.-Y., Adachi, K., Taguchi, T. and Romagnoli, J.
Dynamic polymeric electrodes, dynamic computer modeling and dynamic electrochemical sensing **468**, 19
Tallec, A., see Bellec, N. **462**, 137
Talonen, P., see Lankinen, E. **460**, 176
Tan, S.N., see Li, J. **460**, 234
Tanaka, S., see Kuramitz, H. **466**, 117
Tang, C., Zou, S., Chang, S.-C. and Weaver, M.J.
Coadsorbate vibrational interactions within mixed carbon monoxide-nitric oxide adlayers on ordered low-index platinum-group electrodes **467**, 92
Tang, H., see Harima, Y. **472**, 157
Tang, H., see Zhu, L. **464**, 158
Tang, Y., see Wang, Z. **464**, 181
Tanguy, J., see Lagrost, C. **476**, 1
Taniguchi, I., Li, C.-z., Ishida, M. and Yao, Q.
Electrochemical and spectroelectrochemical properties of manganese reconstituted myoglobin **460**, 245
Taniguchi, I., see Azehara, H. **473**, 68
Taniguchi, I., see Nishiyama, K. **478**, 83
Taniguchi, I., see Ohira, A. **472**, 163
Taniguchi, I., see Yoshimoto, S. **473**, 85
Taniguchi, I., Sonoda, K. and Mie, Y.
Electroanalytical chemistry of myoglobin with modification of distal histidine by cyanated imidazole **468**, 9
Tanioka, A., see Chou, T.-J. **462**, 12
Tanoue, S., see Nishiyama, K. **478**, 83
Tao, H. and Haoqing, W.
Characterization of a new spinel Li–Cr–Mn–O for secondary lithium batteries **463**, 24
Tao, N.J., see Giz, M.J. **465**, 72
Tarallo, A., see Heerman, L. **470**, 70
Tardy, C., see Andrieux, C.P. **476**, 81
Tatsuma, T., Ozaki, M. and Oyama, N.
Electrochemically induced mass transfer and rheological changes of Nafion® coatings fully loaded with $[Os(bpy)_3]^{2+}$ **469**, 34
Tatsuma, T., Taguchi, M., Iwaku, M., Sotomura, T. and Oyama, N.
Inhibition effects of polyacrylonitrile gel electrolytes on lithium dendrite formation **472**, 142
Tavares, A.C., Cartaxo, M.A.M., da Silva Pereira, M.I. and Costa, F.M.
Effect of the partial replacement of Ni or Co by Cu on the electrocatalytic activity of the $NiCo_2O_4$ spinel oxide **464**, 187
Taylor, S.L., see Galceran, J. **476**, 132
Taylor, S.L., see Galceran, J. **466**, 15
Telaranta, R., Manzanares, J.A. and Kontturi, K.
Convective electrodiffusion processes through graft-modified charged porous membranes **464**, 222
Tenne, R., see Alperson, B. **473**, 186
Teragishi, Y. and Aoki, K.
Formation of conducting clusters of polyaniline films detected by light scattering **473**, 132
Teragishi, Y., see Aoki, K. **460**, 254
Testa, B., see Reymond, F. **462**, 235
Thamae, M. and Nyokong, T.
Cobalt(II) porphyrazine catalysed reduction of nitrite **470**, 126
Therias, S., see Coche-Guérente, L. **470**, 61
Thompson, H., see Pletcher, D. **464**, 168
Thouin, L., see Amatore, C. **463**, 45
Ticianelli, E.A., see Sena, D.R. **477**, 164
Timothy, B., see Al-Akl, A. **467**, 60
Toda, K., Oguni, S., Takamatsu, Y. and Sanemasa, I.
A wall-jet ring disk electrode fabricated within a thin-layered micromachined cell **479**, 57
Toda, T., Igarashi, H. and Watanabe, M.
Enhancement of the electrocatalytic O_2 reduction on Pt–Fe alloys **460**, 258
Tokieda, M., see Aoki, K. **460**, 254
Tokuda, K., see Arihara, K. **473**, 138
Tokuda, K., see Nanbu, N. **470**, 136
Tokuda, K., see Okajima, T. **476**, 46
Tolmachev, Y.V., see Hu, Y. **468**, 64
Toma, H.E., see Anaissi, F.J. **464**, 48
Tomczyk, P. and Mosiałek, M.
Electrochemistry of Ni oxidation in molten $Li_2CO_3 + Na_2CO_3$ eutectic **463**, 72
Tomczyk, P., Wyrwa, J. and Mosiałek, M.
Electrochemical behaviour of $Li_xNi_{1-x}O$ in molten $Li_2CO_3 + Na_2CO_3$ eutectic **463**, 78
Tomschik, M., Jelen, F., Havran, L., Trnková, L., Nielsen, P.E. and Paleček, E.
Reduction and oxidation of peptide nucleic acid and DNA at mercury and carbon electrodes **476**, 71
Tonelli, D., see Ballarin, B. **463**, 123
Tong, R., see Cui, X. **470**, 9
Tong, R., see Diao, P. **464**, 61
Tonholo, J., see de Abreu, F.C. **462**, 195
Tonholo, J., see de Azevedo, D.C. **466**, 99
Torimura, M., see Kinoshita, H. **478**, 33
Torrent, M., see Galceran, J. **472**, 42
Torresi, R.M., Cordoba de Torresi, S.I. and Gonzalez, E.R.
Comments on the paper "Logistical differential equation — a general equation for electrointercalation processes?" by J.-P. Diard, B. Le Gorrec and C. Montella **475**, 193
Torresi, R.M., Córdoba de Torresi, S.I. and Gonzalez, E.R.
On the use of the quadratic logistic differential equation for the interpretation of electrointercalation processes **460**, 161
Torto, N., Ruzgas, T. and Gorton, L.
Electrochemical oxidation of mono- and disaccharides at fresh as well as oxidized copper electrodes in alkaline media **464**, 252
Tossici, R., Croce, F., Scrosati, B. and Marassi, R.
An electrochemical impedance study on the interfacial behaviour of KC_8 electrodes in $LiClO_4$ containing electrolytes **474**, 107
Trasatti, S., see Doubova, L.M. **467**, 164
Trasatti, S.
Water electrolysis: who first? **476**, 90
Tremiliosi-Filho, G., Kim, H., Chrzanowski, W., Wieckowski, A., Grzybowska, B. and Kulesza, P.
Reactivity and activation parameters in methanol oxidation on platinum single crystal electrodes 'decorated' by ruthenium adlayers **467**, 143
Tributsch, H., see Sperling, J. **477**, 62
Tripković, A.V., see Dražić, D.M. **466**, 155
Trnková, L., see Tomschik, M. **476**, 71
Trojánek, A., see Langmaier, J. **469**, 11
Trojánek, A., see Samec, Z. **463**, 232
Tryk, D.A., see Fujishima, A. **473**, 179
Tryk, D.A., see Yagi, I. **473**, 173
Tsamouras, D., Kobotiatis, L., Dalas, E. and Sakkopoulos, S.
An impedance study of the metal sulfide $Cu_xZn_{(1-x)}S$ | electrolyte interface **469**, 43
Tseung, A.C.C., see Chen, Y. **471**, 151
Tsirlina, G.A., see Rabinovich, L. **466**, 45
Tu, S.-I., see Gehring, A.G. **469**, 27
Tucceri, R., see Bonfranceschi, A. **477**, 1
Turcanu, A., see Bechtold, T. **465**, 80

Uchida, Y., see Nishiyama, K. **478**, 83
Ueda, T., see Himeno, S. **465**, 129
Ueda, T., see Hojo, M. **468**, 110
Ugo, P., see Brunetti, B. **460**, 38
Ugo, P., see Moretto, L.M. **467**, 193
Uhlemann, E., see Mickler, W. **469**, 91
Umezawa, Y., see Aoki, H. **473**, 105
Ungureanu, E.M., see Ion, A.C. **464**, 24
Uosaki, K.
Preface **473**, 1
Uosaki, K., see Abe, M. **473**, 93
Uosaki, K., see Naohara, H. **473**, 2
Uosaki, K., see Nishimura, N. **473**, 75
Uosaki, K., see Sato, Y. **474**, 94
Uotani, Y., see Nishino, J. **473**, 217
Ushida, K., see Nakabayashi, S. **473**, 54

Väärtnõu, M. and Lust, E.
Calculation of thermodynamic and inner layer characteristics of halide ions adsorbed on bismuth single crystal planes from solutions in methanol **469**, 182

Vaccari, A., see Ballarin, B. **463**, 123
Valincius, G.
Electrocapillary equations of solid electrodes **478**, 40
Vallés, E., see Gómez, E. **475**, 66
Vallés, E., see Gómez, E. **469**, 139
Vallés, E., see Gómez, E. **465**, 63
van de Lagemaat, J., Vanmaekelbergh, D. and Kelly, J.J.
Electrochemistry of homoepitaxial CVD diamond: energetics and electrode kinetics in aqueous electrolytes **475**, 139
Van Houten, L.J., see Gehring, A.G. **469**, 27
van Leeuwen, H.P. and Pinheiro, J.-P.
Lability criteria for metal complexes in micro-electrode voltammetry **471**, 55
Vanmaekelbergh, D., see van de Lagemaat, J. **475**, 139
van Santen, R.A., see Koper, M.T.M. **476**, 64
van Santen, R.A., see Koper, M.T.M. **472**, 126
van Venrooij, T.G.J., Sluyters-Rehbach, M. and Sluyters, J.H.
Electrode kinetics and the nature of the metal electrode: Part 4. The Zn(II)/Zn electrode reaction studied at dropping Tl + Ga alloy electrodes **472**, 64
van Venrooij, T.G.J., Sluyters-Rehbach, M. and Sluyters, J.H.
Electrode kinetics and the nature of the metal electrode: Part 3. The Zn(II)/Zn electrode reaction studied at In + Ga dropping (micro)electrodes **472**, 53
van Venrooij, T.G.J., Sluyters-Rehbach, M. and Sluyters, J.H.
Indium adsorption at the surface of liquid In + Ga alloy electrodes in contact with an aqueous 1 M $NaClO_4$ solution **462**, 111
Vara, J.M., see Gómez, M.M. **474**, 74
Vaškelis, A., Stalnionis, G. and Jusys, Z.
Cyclic voltammetry and quartz crystal microgravimetry study of autocatalytic copper(II) reduction by cobalt(II) in ethylenediamine solutions **465**, 142
Vas'ko, A.T., see Kovach, S.K. **472**, 178
Vaughan, D.J., see Kelsall, G.H. **471**, 116
Vázquez, J.L., see Huerta, F. **475**, 38
Vázquez, J.L., see Huerta, F. **469**, 159
Vázquez, J.L., see Huerta, F. **467**, 105
Vázquez, J.L., see Huerta, F. **463**, 109
Vazquez, M., see Ceré, S. **470**, 31
Vela, M.E., see Andreasen, G. **467**, 230
Vengatajalabathy Gobi, K. and Ohsaka, T.
Enhanced electrostatic interactions for selective and controllable permeation of ionic species at a monolayer of self-assembled dicationic nickel complex **465**, 177
Verpeaux, J.-N., see Haj Said, A. **464**, 85
Vettorazzi, N.R., see Cortona, M.N. **470**, 157
Vico, S., Carlier, V. and Buess-Herman, C.
Spectroelectrochemical study of the influence of anions on the behaviour of poly(*N*-vinylcarbazole) films **475**, 1
Vidal, C., see Kuhn, A. **462**, 187
Vidu, R. and Hara, S.
Surface alloying at the Cd | Au(100) interface in the upd region. Electrochemical studies and in situ EC-AFM observation **475**, 171
Vieil, E. and Lopez, C.
Quantitative discrimination of mass fluxes at electrochemical interfaces by optical beam deflection **466**, 218
Vieil, E., see Levi, M.D. **479**, 12
Viel, P., Bureau, C., Deniau, G., Zalczer, G. and Lecayon, G.
Electropolymerization of methacrylonitrile on a rotating disk electrode at high spinning rate **470**, 14
Villamil, R.F.V., Corio, P., Agostinho, S.M.L. and Rubim, J.C.
Effect of sodium dodecylsulfate on copper corrosion in sulfuric acid media in the absence and presence of benzotriazole **472**, 112
Villemure, G., see Song, C. **462**, 143
Visy, C., Kriván, E. and Peintler, G.
MRA combined spectroelectrochemical studies on the redox stability of PPy/DS films **462**, 1
Viva, F.A., Andrade, E.M., Molina, F.V. and Florit, M.I.
Electropolymerization of 2-methoxy aniline. Electrochemical and spectroscopical product characterization **471**, 180
Vlachopoulos, N., see Cosnier, S. **469**, 176
Vogel, E., see Gisselbrecht, J.P. **469**, 170
Vorotyntsev, M.A., Badiali, J.-P. and Inzelt, G.
Electrochemical impedance spectroscopy of thin films with two mobile charge carriers: effects of the interfacial charging **472**, 7
Vrestal, J., Löffler, T., Müller, U. and Baltruschat, H.
Mass spectrometric study of desorption and hydrogenation of biphenyl, naphthalene and *t*-butylbenzene on poly- and monocrystalline platinum electrodes **461**, 90
Vuković, M. and Čukman, D.
Electrochemical quartz crystal microbalance study of electrodeposited ruthenium **474**, 167
Vuković, M., see Horvat-Radošević, V. **463**, 29

Wada, Y., see Murakoshi, K. **473**, 117
Wakenge, I.B., see Bolzán, A.E. **475**, 181
Walcarius, A., Mariaulle, P. and Lamberts, L.
Use of a zeolite-modified electrode for the study of the methylviologen–sodium ion-exchange in zeolite Y **463**, 100
Walsh, F.C., see Ralph, T.R. **462**, 97
Wan, L.-J. and Itaya, K.
In situ scanning tunneling microscopy of Cu(110): atomic structures of halide adlayers and anodic dissolution **473**, 10
Wan, X., Zhang, W., Jin, S., Xue, G., You, Q.-D. and Che, B.
The electrochemical copolymerization of pyrrole and furan in a novel binary solvent system **470**, 23
Wandelt, K., see Broekmann, P. **467**, 307
Wandlowski, T., see Dretschkow, T. **467**, 207
Wang, C.M., see Chen, C.F. **466**, 82
Wang, C., see Fan, L.-J. **477**, 111
Wang, H., see Wilke, S. **475**, 9
Wang, R., see Yang, C. **471**, 32
Wang, X., see Cui, X. **470**, 9
Wang, X., see Song, W. **476**, 85
Wang, X., Shi, G. and Liang, Y.
Synthesis of carbyne-like nano-particles by electrocatalytic dehydrochlorination of 1,1,2-trichloroethane **470**, 95
Wang, Z., Li, X., Wu, Y., Tang, Y. and Ma, S.
Spectroelectrochemistry for a coupled chemical reaction in the channel cell: Part II. Kinetics of hydrolysis and the absorption spectrum of *p*-benzoquinoneimine **464**, 181
Wang, Z., see Ma, S. **464**, 176
Warren, C.P., see Mortimer, R.J. **460**, 263
Wasberg, M., see Bergelin, M. **467**, 74
Washida, M., see Oyama, M. **473**, 166
Wasmus, S. and Küver, A.
Methanol oxidation and direct methanol fuel cells: A selective review **460**, 14
Watanabe, I., see Hinoue, T. **466**, 31
Watanabe, J., see Baars, A. **464**, 128
Watanabe, K., Sakairi, M., Takahashi, H., Hirai, S. and Yamaguchi, S.
Formation of Al–Zr composite oxide films on aluminum by sol–gel coating and anodizing **473**, 250
Watanabe, M., see Toda, T. **460**, 258
Wayne Suggs, D., see Sorenson, T.A. **467**, 270
Weaver, M.J., see Tang, C. **467**, 92
Weaver, M.J., see Zou, S. **474**, 155
Weber, J., see Langmaier, J. **469**, 11
Wei, Y.B., see Yang, Y.A. **462**, 259
Weiss-Lopez, B., see Squella, J.A. **466**, 90
Whelan, C.M., Smyth, M.R., Barnes, C.J., Attard, G.A. and Yang, X.
Surface structural transitions induced by repetitive underpotential deposition of Ag on Au(111) **474**, 138
White, R.E., see Xie, Y. **466**, 169
Wieckowski, A. and Kolics, A.
Comments on 'On the calculation of surface concentration from the measurement by the radiotracer 'electrode lowering' technique' by D. Poskus **464**, 118
Wieckowski, A., see Tremiliosi-Filho, G. **467**, 143
Wijayawardhana, C.A., Purushothama, S., Cousino, M.A., Halsall, H.B. and Heineman, W.R.

Rotating disk electrode amperometric detection for a bead-based immunoassay **468**, 2
Wilde, P.M., Guther, T.J., Oesten, R. and Garche, J.
Strontium ruthenate perovskite as the active material for supercapacitors **460**, 154
Wilke, S. and Wang, H.
Transfer of heavy metal ions across the water | nitrobenzene microinterface facilitated by the cadmium selective ionophore ETH1062 **475**, 9
Wilke, S., see Mickler, W. **469**, 91
Williams, D.E., see Ng, Y.-F. **464**, 263
Willner, I., see Katz, E. **479**, 64
Willner, I., see Patolsky, F. **479**, 69
Wilms, M., see Broekmann, P. **467**, 307
Won, M.-S., see Yeom, J.-S. **463**, 16
Wrona, P.K., see Marczak, S. **471**, 62
Wu, B.-L., see Liu, W.-J. **476**, 101
Wu, F., see Zhang, W.-S. **474**, 123
Wu, Y., see Ma, S. **464**, 176
Wu, Y., see Wang, Z. **464**, 181
Wyrwa, J., see Tomczyk, P. **463**, 78

Xia, X.H., Schuster, R., Kirchner, V. and Ertl, G.
The growth of size-determined Cu clusters in nanometer holes on Au(111) due to a balance between surface and electrochemical energy **460**, 102
Xiao, Y.-J., Gao, X.-X. and Markwell, J.
In-situ monitoring of the interaction of lactate dehydrogenase with NAD on a gold electrode by FT-SERS **465**, 187
Xiao, Y., see Hu, X.-Y. **466**, 26
Xie, Q., Zhang, Y., Xu, M., Li, Z., Yuan, Y. and Yao, S.
Combined quartz crystal impedance and electrochemical impedance measurements during adsorption of bovine serum albumin onto bare and cysteine- or thiophenol-modified gold electrodes **478**, 1
Xie, Y., Popov, B.N. and White, R.E.
A novel electrochemical method for the detection of nerve gases **466**, 169
Xu, H., see Song, W. **476**, 85
Xu, M., see Xie, Q. **478**, 1
Xu, Z., see Bozkurt, V. **475**, 124
Xue, G., see Wan, X. **470**, 23

Yabuki, S., Mizutani, F. and Hirata, Y.
Preparation of a microperoxidase and ferrocene-immobilized polyion complex membrane for the detection of hydrogen peroxide **468**, 117
Yagi, I., Notsu, H., Kondo, T., Tryk, D.A. and Fujishima, A.
Electrochemical selectivity for redox systems at oxygen-terminated diamond electrodes **473**, 173
Yagi, I., see Fujishima, A. **473**, 179
Yagi, M., Yamase, K. and Kaneko, M.
Temperature dependence of physical displacement and charge hopping in a polymer membrane incorporating a trinuclear ruthenium complex **476**, 159
Yamada, M., see Senda, M. **468**, 34
Yamada, T., see Müller, P. **467**, 282
Yamaguchi, K., see Yoshida, T. **473**, 209
Yamaguchi, S., see Watanabe, K. **473**, 250
Yamaguchi, T., see Komura, T. **478**, 9
Yamamoto, K., see Kinoshita, H. **478**, 33
Yamamoto, T. and Okuda, T.
Oligomeric poly(phenazine-2,7-diyl) and its electrochemical response **460**, 242
Yamase, K., see Yagi, M. **476**, 159
Yamashita, K., see Harima, Y. **472**, 157
Yamashita, K., see Zhu, L. **464**, 158
Yan, J., see Liu, P. **469**, 196
Yanagida, S., see Murakoshi, K. **473**, 117
Yang, C., He, G., Wang, R. and Li, Y.
Solid-state electrochemical investigation of poly[2-methoxy, 5-(2′-ethyl-hexyloxy)-1,4-phenylene vinylene] **471**, 32
Yang, D., see Chen, A. **475**, 130
Yang, D., Zi, M., Chen, B. and Gao, Z.
Separation of pinhole and tunneling electron transfer processes at self-assembled polymeric monolayers on gold electrodes **470**, 114
Yang, H., see Lee, H. **468**, 104
Yang, H., see Yu, J. **474**, 69
Yang, J., Hu, N. and Rusling, J.F.
Enhanced electron transfer for hemoglobin in poly (ester sulfonic acid) films on pyrolytic graphite electrodes **463**, 53
Yang, X., see Whelan, C.M. **474**, 138
Yang, Y.A., Wei, Y.B., Loo, B.H. and Yao, J.N.
Electroless copper plating on a glass substrate coated with ZnO film under UV illumination **462**, 259
Yang, Y.-w., see Fan, L.-J. **477**, 111
Yang, Y.-Y., see Sun, S.-G. **467**, 121
Yao, J.N., see Yang, Y.A. **462**, 259
Yao, Q., see Taniguchi, I. **460**, 245
Yao, S., see Xie, Q. **478**, 1
Yasaki, Y., Sonoyama, N. and Sakata, T.
Semiconductor sensitization of colloidal In_2S_3 on wide gap semiconductors **469**, 116
Yasumori, I., see Arai, G. **464**, 143
Ye, S., see Naohara, H. **473**, 2
Ye, S., see Sato, Y. **474**, 94
Yegnaraman, V., see Berchmans, S. **468**, 170
Yeom, J.-S., Won, M.-S. and Shim, Y.-B.
Voltammetric determination of the iodide ion with a quinine copper(II) complex modified carbon paste electrode **463**, 16
Yin, Q., see Kelsall, G.H. **471**, 116
Yokono, Y., see Komura, T. **478**, 9
Yokoyama, K., see Koide, S. **468**, 193
Yokoyama, T., see Endo, O. **473**, 19
Yoneyama, H., see Oyamatsu, D. **473**, 59
Yoon, I.J., Lee, D.K., Nam, H., Cha, G.S., Strong, T.D. and Brown, R.B.
Ion sensors using one-component room temperature vulcanized silicone rubber matrices **464**, 135
Yoshida, M., see Yoshimoto, S. **473**, 85
Yoshida, T., see Sugiura, T. **473**, 204
Yoshida, T., Yamaguchi, K., Kazitani, T., Sugiura, T. and Minoura, H.
Atom-by-atom growth of cadmium sulfide thin films by electroreduction of aqueous Cd^{2+}–SCN^- complex **473**, 209
Yoshimoto, S., see Azehara, H. **473**, 68
Yoshimoto, S., Yoshida, M., Kobayashi, S.-i., Nozute, S., Miyawaki, T., Hashimoto, Y. and Taniguchi, I.
Electrochemical study on competitive adsorption of pyridinethiol with sulfide onto Au(111) surfaces **473**, 85
You, Q.-D., see Wan, X. **470**, 23
Yu, C.-H., see Chen, F.-c. **474**, 52
Yu, E., see Hong, H.-G. **476**, 177
Yu, J., Cao, H., Chen, Y., Kang, L. and Yang, H.
A new approach to the estimation of electrocrystallization parameters **474**, 69
Yuan, Y., see Xie, Q. **478**, 1
Yudi, L.M., see Azcurra, A.I. **461**, 194
Yudi, L.M., see Dassie, S.A. **464**, 54
Yun, S.-E., see Kim, S. **465**, 153

Zaborosch, C., see Délécouls, K. **468**, 139
Zakroczymski, T.
Electrochemical determination of hydrogen in metals **475**, 82
Zalczer, G., see Viel, P. **470**, 14
Zamponi, S., see Grdeń, M. **460**, 30
Zander, L., see Gisselbrecht, J.P. **469**, 170
Zani, C.L., see de Abreu, F.C. **462**, 195
Zapata, S., see Bonfranceschi, A. **477**, 1
Zare, H.R. and Golabi, S.M.
Electrocatalytic oxidation of reduced nicotinamide adenine dinucleotide (NADH) at a chlorogenic acid modified glassy carbon electrode **464**, 14
Zare, H.R., see Golabi, S.M. **465**, 168
Zawisza, I., Bilewicz, R., Luboch, E. and Biernat, J.F.
Langmuir–Blodgett films of azocrown ethers on electrodes — voltammetric recognition of isomers **471**, 156
Zeng, X. and Bruckenstein, S.
Polycrystalline gold electrode redox behavior in an ammoniacal electrolyte: Part I. A parallel RRDE, EQCM, XPS and TOF-SIMS study of supporting electrolyte phenomena **460**, 131
Zeng, X. and Bruckenstein, S.
Polycrystalline gold electrode redox behavior in an ammoniacal electrolyte: Part II. A parallel RRDE, EQCM and TOF-SIMS study of copper underpotential deposition **460**, 143
Zeng, Y. and Zhou, S.
In situ surface Raman study of the phosphorus incorporation mechanism during electrodeposition of Ni–P alloys **469**, 79
Zhang, J., see Jiang, Z. **469**, 1
Zhang, L., see Sun, W.-Y. **469**, 84

Zhang, S., see Sun, W. **469**, 63
Zhang, W., see Wan, X. **470**, 23
Zhang, W.-S., Zhang, Z.-L. and Zhang, X.-W.
Effects of self-stress on the hydrogen absorption into palladium hydride electrodes of plate form under galvanostatic conditions **474**, 130
Zhang, W.-S., Zhang, Z.-L., Zhang, X.-W. and Wu, F.
Numerical simulation of hydrogen (deuterium) absorption into β-phase hydride (deuteride) palladium electrodes under galvanostatic conditions **474**, 123
Zhang, X.-W., see Zhang, W.-S. **474**, 123
Zhang, X.-W., see Zhang, W.-S. **474**, 130
Zhang, Y., see Xie, Q. **478**, 1
Zhang, Z.-L., see Zhang, W.-S. **474**, 123
Zhang, Z.-L., see Zhang, W.-S. **474**, 130
Zheng, W.Q., see Tadjeddine, A. **473**, 25
Zhong, B., see Diao, P. **464**, 61
Zhou, S., see Zeng, Y. **469**, 79
Zhou, X.Y., see Lvov, S.N. **463**, 146
Zhu, L., see Harima, Y. **472**, 157
Zhu, L., Tang, H., Harima, Y., Yamashita, K., Takata, A., Ohshita, J. and Kunai, A.
Electrochemical oxidation of poly[(hexamethyltrisilanylene)oligo(2,5 - thienylene)] films **464**, 158
Zhuang, J., see Jiang, Z. **469**, 1
Zi, M., see Yang, D. **470**, 114
Ziessel, R., see Buda, M. **469**, 132
Ziessel, R., see Caix-Cecillon, C. **466**, 187
Zinola, C.F., see Mendez, E. **477**, 41
Zolfaghari, A. and Jerkiewicz, G.
Temperature-dependent research on Pt(111) and Pt(100) electrodes in aqueous H_2SO_4 **467**, 177
Zón, M.A., Marchiando, N.C. and Fernández, H.
A study of the bielectronic electro-reduction of cercosporin phytotoxin in highly acidic non-aqueous medium **465**, 225
Zou, S., Gómez, R. and Weaver, M.J.
Infrared spectroscopy of carbon monoxide and nitric oxide on palladium(111) in aqueous solution: unexpected adlayer structural differences between electrochemical and ultrahigh-vacuum interfaces **474**, 155
Zou, S., see Tang, C. **467**, 92
Zouaoui, A., Stéphan, O., Carrier, M. and Moutet, J.-C.
Electrodeposition of copper into functionalized polypyrrole films **474**, 113
Zsoldos, D., see Caix-Cecillon, C. **466**, 187

ELSEVIER

www.elsevier.nl/locate/jelechem

Journal of Electroanalytical Chemistry 479 (1999) 99–150

JOURNAL OF ELECTROANALYTICAL CHEMISTRY

Cumulative Subject Index for Volumes 460–479

a-Axis orientation
Electrodeposition method for controlled formation of CdS films from aqueous solutions **473**, 217
Absence of supporting electrolyte
Voltammetry in solutions of low ionic strength. Electrochemical and analytical aspects **466**, 129
Absolute methanol
Infrared spectroelectrochemistry of the oxidation of absolute methanol at a platinum electrode **464**, 93
Absorbance
Light scattering of polyaniline films responding to electrochemical switching **460**, 254
Absorption
Discussion on permeation transients in terms of insertion reaction mechanism and kinetics **465**, 37
Electrochemical determination of hydrogen in metals **475**, 82
Review and theoretical analysis of ac–av methods for the investigation of hydrogen insertion I. Diffusion formalism **462**, 73
Acetate anions
The study of the adsorption/desorption of acetate anions on a Pt(111) electrode and the effect of counter cations in acidic media **467**, 112
Acetonitrile
Anodic behavior of copper in acetonitrile: the influence of carbon dioxide and dimethylamine **466**, 107
Factors influencing the ion-exchange preconcentration and voltammetric behaviour of redox cations at polyestersulfonated ionomer coated electrodes in acetonitrile solutions **460**, 38
Acetophenones
Thermodynamic and kinetic basicities of the carbon and oxygen ends of enolates. Their role in the reductive cleavage electrochemistry of α-substituted acetophenones **476**, 81
Acids
A review of a new voltammetric method for determining acids **468**, 53
Ac impedance
An electrochemical impedance study on the interfacial behaviour of KC_8 electrodes in $LiClO_4$ containing electrolytes **474**, 107
Evaluation of model and dispersion parameters and their effects on the formation of constant-phase elements in equivalent circuits **464**, 68
Studies of structural disorder of self-assembled thiol monolayers on gold by cyclic voltammetry and ac impedance **464**, 61
Theoretical models for ac impedance of finite diffusion layers exhibiting low frequency dispersion **475**, 152
Ac impedance spectroscopy
Assessing the apparent effective thickness of alkanethiol self-assembled monolayers in different concentrations of $Fe(CN)_6^{3-}$/$Fe(CN)_6^{4-}$ by ac impedance spectroscopy **470**, 9
Acrylonitrile
Investigation of the cathodic electropolymerization of acrylonitrile, ethylacrylate and methylmethacrylate by coupled quartz crystal microbalance analysis and cyclic voltammetry **472**, 83
Activated olefin
Self-protonation mechanism in the electrochemical reduction of Jatropholone **466**, 99
Active state
Anomalous electrochemical behaviour of palladium in aqueous solution **461**, 52
Activity coefficients
Activity coefficients for aminoacid + electrolyte mixtures by using Pitzer equations: DL-α-amino-*n*-butyric acid in mixed electrolyte solutions of neutral, acid and alkaline pH values **466**, 38
Activity coefficients of $Al(ClO_4)_3$ in aqueous solutions: a reexamination **460**, 100
Ac voltage
Photoresponse of a titanium dioxide chemical sensor **472**, 137
Ac voltammetry
A Nernstian electron source model for the ac voltammetric response of a reversible surface redox reaction using large-amplitude ac voltages **466**, 197
4-Acyl-5-pyrazolones
Transfer of β-diketone and 4-acylpyrazolone anions across the electrified water|nitrobenzene interface **469**, 91
Additive
Electrochemical control of a Li metal anode interface: improvement of Li cyclability by inorganic additives compatible with electrolytes **473**, 279
Adiabatic electrode processes
Electron transfer in retrospect and prospect: 1: Adiabatic electrode processes **460**, 5
Electron transfer in retrospect and prospect 1: Adiabatic electrode processes **470**, 170
Adlayer structures
In situ scanning tunneling microscopy of Cu(110): atomic structures of halide adlayers and anodic dissolution **473**, 10
Admittance
Electropolymerization of methacrylonitrile and *N*-vinyl-2-pyrrolidone as probed by an EQCM **465**, 200
Adsorbed cyanide
Potential modulated reflectance spectroscopy of Pt(111) in acidic and alkaline media: cyanide adsorption **463**, 109
The adsorption of methylamine on Pt single crystal surfaces **467**, 105
Adsorbed halides
'In-situ' observation of halide ion adsorption on a gold electrode using synchrotron far infrared spectroscopy **463**, 258
Adsorbed species
Surface diffusion and the spillover of H-adatoms and oxygen-containing surface species on the surface of carbon black and Pt/C porous electrodes **476**, 101
Adsorption
A contribution to the study of the electroreduction of 2-chloro-4,6-di(ethylamino)-1,3,5-triazine (simazine) on mercury electrodes **474**, 174
Adsorption of pyridine on a polycrystalline gold electrode surface studied by infrared reflection absorption spectroscopy **470**, 136

PII: S0022-0728(99)00467-2

Adsorption of sulfate ions on monocrystalline copper electrodes: the structural effects **463**, 1
A minimum separating diffusion and adsorption waves in polarography using a static mercury drop electrode **465**, 30
A sodium-specific condensed film of α-cyclodextrin at the mercury | water interface **465**, 51
Bromine monolayer adsorption on Pt(110) surfaces **467**, 11
Calculation of thermodynamic and inner layer characteristics of halide ions adsorbed on bismuth single crystal planes from solutions in methanol **469**, 182
Cathodic stripping square wave voltammetry of Cu(II)–oxine complexes. A mechanistic study **478**, 17
Electric field effects on CO and NO adsorption at the Pt(111) surface **476**, 64
Electrochemical behaviour of amino acids on Pt(*hkl*). A voltammetric and in situ FTIR study: Part IV. Serine and alanine on Pt(100) and Pt(110) **475**, 38
Electrochemical oscillations of a new type in an $H_2O_2 + H_2SO_4$ | Pt-electrode system, appearing by addition of small amounts of halide ions **473**, 156
Electrochemical surface reactions of intermediates formed in the oxidative ethanol adsorption on porous Pt and PtRu **471**, 167
Formation of an ordered structure of iodine adsorbed on Ni(111) and the anodic dissolution processes: in-situ STM study **467**, 282
FTIR studies of benzoate adsorption on the Au(111) electrode **478**, 67
In situ infrared spectroscopic investigations of sulfate adsorption at the Ag(111) electrode surface **467**, 291
In situ infrared study of cytosine adsorption on gold electrodes **460**, 188
In situ orientation study of xanthate on copper under potential control **475**, 124
In-situ X-ray absorption studies of bromine on the Ag(100) electrode **473**, 19
Iodide adsorption at the Au(111) electrode surface **467**, 342
Limiting current in normal pulse polarography with reactant adsorption obeying the Langmuir and the Frumkin isotherms **478**, 25
New effects in the electrochemistry of carbon dioxide on platinum by the application of potential perturbations **477**, 41
Phospholipid monolayers studied by a combination of cyclic voltammetry and Langmuir techniques at the water | 1,2-dichloroethane interface **463**, 242
Role of surface states and adsorbates in time-resolved photocurrent measurements and photovoltage generation at phthalocyaninatozinc(II)-photocathodes **462**, 222
Square wave stripping voltammetry of Cd–oxine complexes; surface redox reactions **476**, 165
Structural identifiability of adsorption and electron transfer processes in metal dissolution and passivation mechanisms **471**, 1
Sulfate ions adsorbed on Au(*hkl*) electrodes: in situ vibrational spectroscopy **460**, 110
Surface structural effects on specific adsorption of oxoanions on gold single crystal electrodes **467**, 335
The study of the adsorption/desorption of acetate anions on a Pt(111) electrode and the effect of counter cations in acidic media **467**, 112
Voltammetric and spectroscopic study of the adsorption of alkyl viologens on a HOPG electrode **473**, 138
What can we learn from the non-linear optical investigation of the liquid | solid interface? **473**, 25
X-ray absorption in relation to valency of iridium in sputtered iridium oxide films **465**, 88

Adsorption at Au(111)
Electrochemical and FTIR studies of 4-cyanopyridine adsorption at the gold(111) | solution interface **475**, 130

Adsorption at columnar surfaces
Steric effects on molecular adsorption at columnar surfaces. A model for the adsorption of pyridine on gold electrodes **474**, 74

Adsorption at ITIES
Interfacial phenomena involving Fe(III)–ofloxacin complexes at the water|1,2-dichloroethane interface **461**, 194

Adsorption-induced self-organization
Self-organization of α-cyclodextrin on Au(111) surfaces induced by potential controlled adsorption **472**, 163

Adsorption kinetics
In-situ STM investigation of specific anion adsorption on Cu(111) **467**, 307

Adsorption modeling
Steric effects on molecular adsorption at columnar surfaces. A model for the adsorption of pyridine on gold electrodes **474**, 74

Adsorption on platinum
Catalytic and electrocatalytic oxidation of oxalic acid in aqueous solutions of different compositions **474**, 147

Adsorption simulation
On the source of oscillatory instabilities in the electroreduction of thiocyanate complexes of nickel(II) at mercury electrodes **478**, 118

Adsorption thermodynamics
Temperature-dependent research on Pt(111) and Pt(100) electrodes in aqueous H_2SO_4 **467**, 177

AES
Characterization of platinum-rutheniun electrodeposits using XRD, AES and XPS analysis **460**, 32

Ag(111)
Formation of ZnSe on Ag(111) by electrochemical atomic layer epitaxy **475**, 164

Ag electrode
Effect of the crystallographic orientation of Ag single crystal face electrodes on the kinetics of proton discharge **467**, 164

Agrochemistry
Electrochemical properties of three dicarboximide-type pesticides: vinclozoline, iprodione and procymidone **472**, 33

Alanine
Electrochemical behaviour of amino acids on Pt(*hkl*). A voltammetric and in situ FTIR study: Part IV. Serine and alanine on Pt(100) and Pt(110) **475**, 38

Alcohol electroxidation
Electrocatalytic properties of nickel(II) hydrotalcite-type anionic clay: application to methanol and ethanol oxidation **463**, 123

Alcohols
Calculation of thermodynamic and inner layer characteristics of halide ions adsorbed on bismuth single crystal planes from solutions in methanol **469**, 182

Alcohol sensor
An electrochemical alcohol sensor based on a co-electrodeposited Pt | WO_3 electrode **471**, 151

Alkali cations
Voltammetric analysis of Cs^+-DB18C6 complex stoichiometry at the water | 1,2-dichloroethane interface **464**, 54

Alkaline medium
Electrocatalytic oxidation of methanol at a nickel hydroxide/glassy carbon modified electrode in alkaline medium **471**, 89

Alkaline solutions
Electrochemical, spectroscopic and structural investigations of the Cd/Cd(II) system in alkaline media: 2. Concentration effects **462**, 34
Kinetic and mechanistic study of hydroxyl ion electrosorption at the Pt(111) surface in alkaline media **466**, 155

Alkanethiol
Assessing the apparent effective thickness of alkanethiol self-assembled monolayers in different concentrations of $Fe(CN)_6^{3-}$/$Fe(CN)_6^{4-}$ by ac impedance spectroscopy **470**, 9
Exchange of self-assembled thiol monolayers on gold: characterization by FT-IR external reflection spectroscopy **468**, 91
Underpotential deposition behavior of metals onto gold electrodes coated with self-assembled monolayers of alkanethiols **473**, 59
n-Alkanethiols
Electrochemical and EQCM studies on the assembly of asymmetric viologen on bare and alkanethiol-coated Au electrodes **477**, 52
Alkyl halide reduction
A microelectrode study of the catalysis of alkyl halide reduction by Co(II)(salen) **464**, 168
Alloy
Corrosion sensing by SQUID magnetometry **477**, 171
Aluminium
Structural properties of electrochemically designed porous oxide films on AlMg1 **468**, 121
Al–Zr composite oxide film
Formation of Al–Zr composite oxide films on aluminum by sol–gel coating and anodizing **473**, 250
Amalgamation
General solutions for the *I*/*t* response for reversible processes in the presence of product in a multipotential step experiment at planar and spherical electrodes whose areas increase with any power of time **466**, 8
Aminopurinethiol
Electrochemical behavior of gold electrodes modified with aminopurinethiol derivatives **473**, 99
Ammonia
Cobalt(II) porphyrazine catalysed reduction of nitrite **470**, 126
Electroreduction of nitrate ion to nitrite and ammonia on a gold electrode in acidic and basic sodium and cesium nitrate solutions **470**, 46
Ammoniacal electrolyte
Polycrystalline gold electrode redox behavior in an ammoniacal electrolyte: Part I. A parallel RRDE, EQCM, XPS and TOF-SIMS study of supporting electrolyte phenomena **460**, 131
Amperometric detection
Rotating disk electrode amperometric detection for a bead-based immunoassay **468**, 2
DL-α-Amino-*n*-butyric acid
Activity coefficients for aminoacid + electrolyte mixtures by using Pitzer equations: DL-α-amino-*n*-butyric acid in mixed electrolyte solutions of neutral, acid and alkaline pH values **466**, 38
Amperometric sensor
Amperometric nitrate biosensors on the basis of *Pseudomonas stutzeri* nitrate reductase **474**, 43
Preparation of a microperoxidase and ferrocene-immobilized polyion complex membrane for the detection of hydrogen peroxide **468**, 117
Amperometry
Amperometric ion-selective electrode. Voltammetric theory and analytical applications at high concentration and trace levels **468**, 34
Amperometric ion-selective electrode. Voltammetric theory and analytical applications at high concentration and trace levels **475**, 90
Analysis of the iodide ion
Voltammetric determination of the iodide ion with a quinine copper(II) complex modified carbon paste electrode **463**, 16
α_1 and α_2 isomers
Metal ion complexes derived from the α_1 isomer of $(P_2W_{17}O_{61})^{10-}$: comparison with the corresponding α_2 species **478**, 76
α- and β-$[PW_{12}O_{40}]^{3-}$
Synthesis, characterisation and voltammetric study of a β-Keggin-type $[PW_{12}O_{40}]^{3-}$ complex **465**, 129
Anion adsorption
Catalytic and electrocatalytic oxidation of oxalic acid in aqueous solutions of different compositions **474**, 147
'In-situ' observation of halide ion adsorption on a gold electrode using synchrotron far infrared spectroscopy **463**, 258
Temperature-dependent research on Pt(111) and Pt(100) electrodes in aqueous H_2SO_4 **467**, 177
Anion complexation
Electrochemical response to anions by neutral ferrocenyl receptors containing 2,2′-bipyridyl arms **469**, 132
Anion-controlled redox process
Voltammetric anion recognition by a highly cross-linked polyviologen film **473**, 145
Anion effects
An electrochemical quartz crystal microbalance study of the hydrogen underpotential deposition at a Pt electrode **467**, 186
Spectroelectrochemical study of the influence of anions on the behaviour of poly(*N*-vinylcarbazole) films **475**, 1
Anion electroreduction
Effect of cation adsorption on the kinetics of anion electroreduction: Part I. Effect of the adsorption of inorganic cations in small concentrations on the kinetics of anion electroreduction with different elementary steps of discharge **476**, 26
Effect of cation adsorption on the kinetics of anion electroreduction: Part II. Effect of the adsorption of organic cations in small concentrations on the kinetics of anion electroreduction **476**, 37
Anion-imprinted electropolymerization
Voltammetric anion recognition by a highly cross-linked polyviologen film **473**, 145
Anion radicals
Solvent effect on kinetics of the chloride ion cleavage from anion radicals of 4-chlorobenzophenone **464**, 259
Anion receptors
Silicon-based ferrocenyl dendrimers as anion receptors in solution and immobilized onto electrode surfaces **463**, 87
Anion sorption
Direct experimental evidence proving the formation of surface layers in the course of the reduction of Cr(VI) species at a gold electrode **471**, 73
Anodic behavior
Anodic behavior of copper in acetonitrile: the influence of carbon dioxide and dimethylamine **466**, 107
Anodic electropolymerization
Electrochemical synthesis and structural studies of copolymers based on the electrooxidation of pyrrole and some salen compounds **470**, 77
Anodic film
Capacitance and photocurrent study of electronic properties of anodic oxide films on Nb and Ta. Evaluation of the ionized donor concentration profile in Nb_2O_5 film **460**, 214
Anodic oxidation
Mechanistic investigation of the anodic oxidation of *p*-methoxytoluene in dry and wet acetonitrile **464**, 85
Anodic oxide films
Impedance of ruthenium electrodes in sulphuric acid solution **463**, 29
Anodic porous alumina
Change of hole size of Pd hole-array electrodes in a controlled fashion by cathodic polarization in acidic electrolyte **473**, 240
Anodic stripping voltammetry
Novel polymer-modified electrodes for batch injection sensors and application to environmental analysis **468**, 26
Anodic treatment
Electroanalysis of dopamine and NADH at conductive diamond electrodes **473**, 179

Anodization
Formation of ⟨001⟩-aligned nano-scale pores on (001) n-InP surfaces by photoelectrochemical anodization in HCl **473**, 223
Anodizing of aluminum
Formation of Al–Zr composite oxide films on aluminum by sol–gel coating and anodizing **473**, 250
Anomalous behaviour
Anomalous electrochemical behaviour of palladium in aqueous solution **461**, 52
Anomalous co-deposition
Electrodeposition of zinc + iron alloys: I. Analysis of the initial stages of the anomalous codeposition **469**, 139
Anthraquinone
Anthraquinones as mediators for the indirect cathodic reduction of dispersed organic dyestuffs **465**, 80
Electrochemical study of self-assembled monolayers of a β-cyclodextrin methyl sulfide covalently linked to anthraquinone **465**, 209
Structural differences in self-assembled monolayers of anthraquinone derivatives on silver and gold electrodes studied by cyclic voltammetry and in situ SERS spectroscopy **478**, 83
Anthraquinonedisulfonate
Current enhancing effect of poly[1-methyl-3-(pyrrol-1-ylmethyl)pyridinium] films on the electrode reaction of anthraquinonedisulfonate **478**, 9
Antibody–antigen reactions
The electrochemistry of antibody-modified conducting polymer electrodes **470**, 144
Antileukemic agents
Electrooxidation of the antileukemic 2-chloro-2′-deoxyadenosine and related compounds **477**, 89
Apparent activation energy
Studies of kinetics of HCOOH oxidation on Pt(100), Pt(110), Pt(111), Pt(510) and Pt(911) single crystal electrodes **467**, 121
Apparent effective thickness
Assessing the apparent effective thickness of alkanethiol self-assembled monolayers in different concentrations of $Fe(CN)_6^{3-}$ / $Fe(CN)_6^{4-}$ by ac impedance spectroscopy **470**, 9
Aqueous electrolyte
Electrochemical oxidation of pyrite (FeS_2) in aqueous electrolytes **471**, 116
Aromatic ketone
Self-protonation mechanism in the electrochemical reduction of Jatropholone **466**, 99
Artificial neural networks
Dynamic polymeric electrodes, dynamic computer modeling and dynamic electrochemical sensing **468**, 19
Ascorbic acid
Voltammetry using an electrode surface continuously renewed by laser ablation and its demonstration on electro-oxidation of L-ascorbic acid **466**, 31
L-Ascorbic acid
Nickel(II) tetraaza macrocycle modified electrodes for the electrocatalytic determination of L-ascorbic acid by the flow injection method **468**, 85
Assisted ion transfer
A model for assisted ion transfer across liquid | liquid interfaces **460**, 144
Association
Conductometric study of lithium halides and thiocyanate in the mixed solvents of tetrahydrofuran and 2-ethyl-1-hexanol **468**, 110
Association constant
Conductivity study on lithium bromide in propylene carbonate + acetonitrile mixtures in dilute solutions from − 35 to 75°C **471**, 78
Asymmetrical disulfides
Investigation of the structure of self-assembled monolayers of asymmetrical disulfides on Au(111) electrodes by electrochemical desorption **473**, 68
Asymmetric viologen
A monomer–dimer equilibrium in self-assembled monolayers of *N*-ethyl-*N*′-octadecylviologen on the electrode surface. The influence of water content and hexafluorophosphate ion **466**, 67
Electrochemical and EQCM studies on the assembly of asymmetric viologen on bare and alkanethiol-coated Au electrodes **477**, 52
Atomic force microscopy
Electrochemical investigations and morphology of poly(4,9-dihydro-*o*-benzenonaphtho[2,3-c]pyrrole) and poly(acenaphtho[1,2-c]pyrrole) **477**, 25
In situ atomic force microscopy study of polypyrrole synthesis and the volume changes induced by oxidation and reduction of the polymer **462**, 211
Synthesis, electropolymerization and electrochemical characterization of some new acrylate substituted thiophene derivatives **460**, 176
Tin electrodeposition on carbon electrodes. From nuclei to microcrystallites **465**, 63
Atomic layer epitaxy
Formation of ZnSe on Ag(111) by electrochemical atomic layer epitaxy **475**, 164
Au(111)
Comments on 'On the calculation of surface concentration from the measurement by the radiotracer 'electrode lowering' technique' by D. Poskus **464**, 118
Au
Phase transitions in the electrodeposition of tellurium atomic layers on Au(100) **467**, 270
Au(111)
The initial stages of rhodium deposition on Au(111) **467**, 249
Au-colloids
Controlled electrocatalysis by microperoxidase-11 and Au-nanoparticle superstructures on conductive supports **479**, 69
Au electrode
Cationic systems as self-assembled monolayers on gold surfaces **464**, 263
In situ STM study of self-assembled mercaptopropionic acid monolayers for electrochemical detection of dopamine **465**, 72
In situ infrared study of cytosine adsorption on gold electrodes **460**, 188
Au(111) electrode
Iodide adsorption at the Au(111) electrode surface **467**, 342
FTIR studies of benzoate adsorption on the Au(111) electrode **478**, 67
Synthesis and electrochemical characterization of self-assembled monolayers of redox-active oxide-bridged triruthenium(III) clusters on Au(111) **473**, 93
Au(100) electrode
Epitaxial growth of a palladium layer on an Au(100) electrode **473**, 2
Surface alloying at the Cd | Au(100) interface in the upd region. Electrochemical studies and in situ EC-AFM observation **475**, 171
Au(111) single crystal
Electrochemical study on competitive adsorption of pyridinethiol with sulfide onto Au(111) surfaces **473**, 85
Au single-crystal electrodes
Reaction of nitrobenzene on gold single-crystal electrodes: surface crystallographic orientation dependence **477**, 111

Au(100) surface
On the stability of unreconstructed Au(100)-(1 × 1) at negative potentials in aqueous sulfate solution **471**, 9
Au(111) terraces
Influence of the electric potential on the structure of pyridine adlayers on Au(111) terraces from in-situ scanning tunnelling microscopy imaging **467**, 230
Autocatalysis
Electrochemical oscillations of a new type in an $H_2O_2 + H_2SO_4$ | Pt-electrode system, appearing by addition of small amounts of halide ions **473**, 156
Autocatalytic (electroless) deposition
Cyclic voltammetry and quartz crystal microgravimetry study of autocatalytic copper(II) reduction by cobalt(II) in ethylenediamine solutions **465**, 142
Azocrowns
Langmuir–Blodgett films of azocrown ethers on electrodes — voltammetric recognition of isomers **471**, 156

Backscattering factor
Comments on 'On the calculation of surface concentration from the measurement by the radiotracer 'electrode lowering' technique' by D. Poskus **464**, 118
Bacteria
1-Naphthyl phosphate as an enzymatic substrate for enzyme-linked immunomagnetic electrochemistry **469**, 27
Bandgap
Anodic oxidation of various arylene-cyanovinylenes made of alternating fluorenyl, thienyl and/or phenyl units **466**, 144
Batch injection analysis
Novel polymer-modified electrodes for batch injection sensors and application to environmental analysis **468**, 26
Batch reactor
Evaluation of a reactor model and cathode materials for batch electrolysis of L-cystine hydrochloride **462**, 97
Batch recycle operation
Evaluation of a reactor model and cathode materials for batch electrolysis of L-cystine hydrochloride **462**, 97
Battery
A poly(vinylidene fluoride)-based gel electrolyte membrane for lithium batteries **463**, 248
The electrochemical properties of a series of phenylene-thienyl polymers in tetramethylene sulfone based electrolytes **460**, 46
Bending beam method
In-situ detection of stress in oxide films during Si electrodissolution in acidic fluoride electrolytes **474**, 182
Bentonite
Modified electrodes based on mixed bentonite vanadium(V) oxide xerogels **464**, 48
Benzoate
FTIR studies of benzoate adsorption on the Au(111) electrode **478**, 67
Benzotriazole
Effect of sodium dodecylsulfate on copper corrosion in sulfuric acid media in the absence and presence of benzotriazole **472**, 112
p-Benzoquinoneimine
Spectroelectrochemistry for a coupled chemical reaction in the channel cell: Part II. Kinetics of hydrolysis and the absorption spectrum of *p*-benzoquinoneimine **464**, 181
Bethe's approximation
pK_a of an ω-carboxylalkanethiol self-assembled monolayer by interaction model **478**, 101
Biferrocene
Synthesis, redox behavior and electrodeposition of biferrocene-modified gold clusters **473**, 113
Bifurcation
Discontinuous immitance due to a saddle node bifurcation: II: Tangent bifurcation and critical slowdown during isotherm branch switching **460**, 226
Binary self-assembled monolayers
Investigation of the structure of self-assembled monolayers of asymmetrical disulfides on Au(111) electrodes by electrochemical desorption **473**, 68
Binary solvent system
The electrochemical copolymerization of pyrrole and furan in a novel binary solvent system **470**, 23
Bioelectrodes
Kinetic behaviour of dopamine-polyphenol oxidase on electrodes of tetrathiafulvalenium tetracyanoquinodimethanide and tetracyanoquinodimethane species **461**, 174
Biofuel cell
A non-compartmentalized glucose | O_2 biofuel cell by bioengineered electrode surfaces **479**, 64
Electro-enzymatic reduction of dioxygen to water in the cathode compartment of a biofuel cell **464**, 110
Biomedical implant alloys
Study of the corrosion behavior of titanium and some of its alloys for biomedical and dental implant applications **471**, 109
Biomimetism
Electrochemical behaviour of (μ-oxo) di-aqua diiron(III) complexes in organic media. Electrogeneration of mononuclear $[Fe^{II}(L)_2(S)_2]^{2+}$ complexes (L = 2,2′-bipyridine and (−)4,5-pinene-2,2′-bipyridine; S = H_2O or CH_3CN) **469**, 53
Biosensor
A glucose biosensor based on enzyme entrapment within polypyrrole films electrodeposited on mesoporous titanium dioxide **469**, 176
Amplification of amperometric biosensor responses by electrochemical substrate recycling: Part I. Theoretical treatment of the catechol–polyphenol oxidase system **470**, 53
Amplification of amperometric biosensor responses by electrochemical substrate recycling: Part II. Experimental study of the catechol–polyphenol oxidase system immobilized in a laponite clay matrix **470**, 61
Electroanalysis of dopamine and NADH at conductive diamond electrodes **473**, 179
Immobilized nitro-fluorenone derivatives as electrocatalysts for NADH oxidation **477**, 79
1-Naphthyl phosphate as an enzymatic substrate for enzyme-linked immunomagnetic electrochemistry **469**, 27
Preparation of a microperoxidase and ferrocene-immobilized polyion complex membrane for the detection of hydrogen peroxide **468**, 117
Renewable silica sol–gel derived carbon composite based glucose biosensor **460**, 234
Biphenyl
Mass spectrometric study of desorption and hydrogenation of biphenyl, naphthalene and *t*-butylbenzene on poly- and monocrystalline platinum electrodes **461**, 90
Bipolar electrochemistry
Ion transport and deposit growth in spatially coupled bipolar electrochemistry **478**, 128
Bipolaron
Electrochemical generation of cation radical π-dimers in polymer film composed of pentathiophenes bridged by monosiianylene units **472**, 157
Bipyridilium
Electrochemical behaviour of *N*-aminopyridinium, and the viologens *N*,*N*′-diamino-4,4′-bipyridilium and *N*,*N*′-bis(4-aminophenyl)-4,4′-bipyridilium in aqueous acid: towards the formation of polymer hybrids of pyridine and aniline **462**, 43

Bismuth
Calculation of thermodynamic and inner layer characteristics of halide ions adsorbed on bismuth single crystal planes from solutions in methanol **469**, 182
Structural effects on the oxidation of HCOOH by bismuth modified Pt(111) electrodes with (110) monatomic steps **467**, 43
Bistable
A comparison of multistability in the electrocatalyzed oxidations of methanol and ethanol in acid and alkaline solutions **478**, 108
Bisulphate anion
Comparison of a bisulfate anion adsorbed on M(111) (M = Pt, Rh, Au, Ag and Cu) **467**, 299
Bithiophene
Polymer chain encapsulation followed by a quartz microbalance during electropolymerization of bithiophene-β-cyclodextrin host–guest compounds in aqueous solution **476**, 1
Boltzmann statistics
Anomalous H/D isotopic effect in the kinetics of polarographic hydrogen evolution **477**, 62
Bond-breaking
Electron transfer in retrospect and prospect: 1: Adiabatic electrode processes **460**, 5
Electron transfer in retrospect and prospect 1: Adiabatic electrode processes **470**, 170
Boundary condition
Discussion of the paper by Barber et al. [J. Electroanal. Chem. 446 (1998) 125] **466**, 122
Bovine serum albumin
Combined quartz crystal impedance and electrochemical impedance measurements during adsorption of bovine serum albumin onto bare and cysteine- or thiophenol-modified gold electrodes **478**, 1
Redox-cycling type electrochemiluminescence in aqueous medium. A new principle for the detection of proteins labeled with a ruthenium chelate **474**, 192
Bromide
Oxygen reduction reaction on Pt(111): effects of bromide **467**, 157
Bromine
Bromine monolayer adsorption on Pt(110) surfaces **467**, 11
In-situ X-ray absorption studies of bromine on the Ag(100) electrode **473**, 19
Buffer effect
Trifluoroacetophenone derivative-based carbonate ion-selective electrodes: effect of diluent pH on the anion selectivity **468**, 76
Butler–Volmer kinetics
Integration analysis of the cyclic voltammograms of the electrode reaction in a diffusionless system **465**, 219

Cadmium
Cadmium binding properties of the C-terminal hexapeptide from mouse metallothionein: study by linear sweep voltammetry and multivariate curve resolution analysis **468**, 202
Electrochemical, spectroscopic and structural investigations of the Cd/Cd(II) system in alkaline media: 2. Concentration effects **462**, 34
Experimental and calculated complex formation curves for mixed, dynamic and semi-dynamic, metal–ligand systems. A differential pulse polarographic study of Cu^{II}–sarcosine–OH and Cd^{II}–MIDA–OH systems at a fixed ligand to metal ratio and varied pH **460**, 197
Rotograved carbon electrodes for amperometric cadmium and lead determination **469**, 189
Square wave stripping voltammetry of Cd–oxine complexes; surface redox reactions **476**, 165
Surface alloying at the Cd | Au(100) interface in the upd region. Electrochemical studies and in situ EC-AFM observation **475**, 171
Cadmium binding
Electrochemical study on Cd binding to metallothioneins isolated from the mussel, *Mytilus galloprovincialis* **466**, 75
Cadmium sulfide
A kinetic study of CdS photocorrosion by intensity modulated photocurrent and photoelectrochemical impedance spectroscopy **473**, 192
Atom-by-atom growth of cadmium sulfide thin films by electroreduction of aqueous Cd^{2+}–SCN^- complex **473**, 209
Calorimetry
The complex formation of non-cyclic polyethers and crown ethers with Ag^+ in acetone and propylene carbonate studied by potentiometric and calorimetric methods **474**, 188
Capacitance
Impedance and photoelectrochemical properties of porous oxide film on Type304 stainless steel formed by square wave potential pulse polarisation **473**, 265
Capacitive current
The fast dropping oil | water electrode **464**, 128
Carbohydrazine
The electrochemistry of nitrogen-containing compounds at platinum single crystal electrodes: Part 3. Carbohydrazide on Pt(*hkl*) electrodes **467**, 20
Carbon
Graphite photoelectrochemistry 2. Photoelectrochemical studies of highly oriented pyrolitic graphite **476**, 118
Carbonate ion-selective electrode
Trifluoroacetophenone derivative-based carbonate ion-selective electrodes: effect of diluent pH on the anion selectivity **468**, 76
Carbonate sensor
Ion sensors using one-component room temperature vulcanized silicone rubber matrices **464**, 135
Carbon black
Surface diffusion and the spillover of H-adatoms and oxygen-containing surface species on the surface of carbon black and Pt/C porous electrodes **476**, 101
Carbon composite ceramic electrodes
Preparation and characterization of sol–gel derived carbon composite ceramic electrodes: electrochemical and XANES study of nitrite reduction **468**, 131
Carbon dioxide
Anodic behavior of copper in acetonitrile: the influence of carbon dioxide and dimethylamine **466**, 107
New effects in the electrochemistry of carbon dioxide on platinum by the application of potential perturbations **477**, 41
Carbon electrodes
Reduction and oxidation of peptide nucleic acid and DNA at mercury and carbon electrodes **476**, 71
Carbon fiber microelectrode
Electrocatalytic reduction of nitrite at a carbon fiber microelectrode chemically modified by palladium(II)-substituted Dawson type heptadecatungstodiphosphate **469**, 63
Carbon monoxide
A temperature controlled cell for in situ infrared spectroelectrochemical measurements and its use in the study of CO isothermal desorption **471**, 146
Coadsorbate vibrational interactions within mixed carbon monoxide-nitric oxide adlayers on ordered low-index platinum-group electrodes **467**, 92
Infrared spectroscopy of carbon monoxide and nitric oxide on palladium(111) in aqueous solution: unexpected adlayer structural differences between electrochemical and ultrahigh-vacuum interfaces **474**, 155
Origin of the infrared reflectance increase produced by the adsorption of CO on particulate metals deposited on moderately reflecting substrates **465**, 234

Oxidation of CO adlayers on Pt(111) at low potentials: an impinging jet study in H_2SO_4 electrolyte with mathematical modeling of the current transients **467**, 74
Carbon paste electroactive electrodes
Electrochemical, spectroscopic and structural investigations of the Cd/Cd(II) system in alkaline media: 2. Concentration effects **462**, 34
Carbon paste electrode
Coordination of silver(I) at the surface of carbon paste electrodes modified with 2,5,8-trithia[9]-*m*-cyclophane as studied by cyclic voltammetry **475**, 73
Electrode reactions and accumulation of hydrogen at carbon paste electrodes in the presence of tetrachloropalladate **462**, 174
Use of a zeolite-modified electrode for the study of the methylviologen–sodium ion-exchange in zeolite Y **463**, 100
Voltammetric determination of the iodide ion with a quinine copper(II) complex modified carbon paste electrode **463**, 16
Carbonyl groups
Characterization of the surface carbonyl and hydroxyl coverage on glassy carbon electrodes using Raman spectroscopy **469**, 150
Carbyne
Synthesis of carbyne-like nano-particles by electrocatalytic dehydrochlorination of 1,1,2-trichloroethane **470**, 95
Catalysis
A microelectrode study of the catalysis of alkyl halide reduction by Co(II)(salen) **464**, 168
Cathodic reduction of 2-nitronaphthothiophen-4,9-quinone: evidence of catalysis by proton donors and its simulation **462**, 195
Electrochemical and catalytic behaviour of Dawson-type complexes derived from $[(1),2,3\text{-}P_2Mo_2W_{15}O_{61}]^{10-}$ and first transition metal ions **477**, 146
Mechanism of the catalysis by *Alcaligenes eutrophus* H16 hydrogenase of direct electrochemical reduction of NAD^+ **468**, 139
Methanol oxidation and direct methanol fuel cells: a selective review **460**, 14
Studies on the catalytic reduction of iodate at glassy carbon electrodes modified by molybdenum oxides **471**, 37
Surface redox catalysis and reduction kinetics of hydrogen peroxide on copper–nickel alloys **470**, 31
The use of regularization methods in the deconvolution of underlying distributions in electrochemical processes **475**, 28
Catalyst layer
Electrochemical impedance of the cathode catalyst layer in polymer electrolyte fuel cells **475**, 107
Catalytic mechanism
Study of a catalytic mechanism in double potential step techniques at spherical electrodes **468**, 158
Catalytic oxidation
Catalytic and electrocatalytic oxidation of oxalic acid in aqueous solutions of different compositions **474**, 147
Catalytic reduction
Catalytic reduction of 1,8-diiodooctane by electrogenerated cobalt(I) salen and formation of μ-(1,8-*n*-octyl)-bis[-(salen)cobalt(III)] **460**, 207
Catalytic reduction
Atom-by-atom growth of cadmium sulfide thin films by electroreduction of aqueous Cd^{2+}–SCN^- complex **473**, 209
Cathode
Electro-enzymatic reduction of dioxygen to water in the cathode compartment of a biofuel cell **464**, 110
Theory for water management in membranes for polymer electrolyte fuel cells: Part 2. The effect of impurity ions at the cathode side on the membrane performances **465**, 18
Cathodic coupling
Cathodic synthesis of powerful electron π-donors including dithiadiazafulvalenes **462**, 137
Cathodic reduction
Electrosynthesis of 3-chloro-4-substituted-coumarins **469**, 201
Cation-deficient spinel
Characterization of a new spinel Li–Cr–Mn–O for secondary lithium batteries **463**, 24
Cation radical
Voltammetric investigation of the anodic dimerization of *p*-halogenoanilines in DMF: Reactivity of their electrogenerated cation radicals **462**, 55
Cavitation
Low-temperature sonoelectrochemical processes: Part 1. Mass transport and cavitation effects of 20 kHz ultrasound in liquid ammonia **477**, 71
CCD detector
Two-dimensional CCD detection of electrogenerated chemiluminescence (ECL) on an electrode surface. ECL reactions involving microcrystals of the perylene dimer cation radical salt **473**, 166
CdS
Electrodeposition method for controlled formation of CdS films from aqueous solutions **473**, 217
Cell resistance
Steady state voltammetry at low electrolyte/reactant concentration ratios: what it means and what it does not mean **463**, 45
CE mechanism
Nitrite reduction at powder microelectrodes **469**, 196
Cercosporin phytotoxin
A study of the bielectronic electro-reduction of cercosporin phytotoxin in highly acidic non-aqueous medium **465**, 225
Cesium
Voltammetric analysis of Cs^+-DB18C6 complex stoichiometry at the water | 1,2-dichloroethane interface **464**, 54
CFC-12
Electrochemical reduction of dichlorodifluoromethane in acetonitrile medium to useful fluorinated compounds **471**, 26
Chalcogenide
Phase transitions in the electrodeposition of tellurium atomic layers on Au(100) **467**, 270
Channel flow cell
Spectroelectrochemistry for a coupled chemical reaction in the channel cell: Part I. Theoretical simulation of an EC reaction **464**, 176
Charge displacement
Urea adsorption on Pt(111) electrodes **461**, 65
Charge transfer
Polymerization reaction coupled to charge transfer: propagation versus termination as a source of permanent travelling waves and multi-peak voltammograms **479**, 43
Self-assembly of and charge transfer at *N*-docosyl-*N'*-methyl viologen on electrode surfaces **468**, 70
Charge transfer coefficient–potential variation
The voltammetric reduction of some benzenesulfonyl fluorides, simulation of the ECE mechanism and determination of the potential variation of the transfer coefficient by using the compounds with two reducible groups **471**, 14
Charge transfer kinetics
Electrochemistry of homoepitaxial CVD diamond: energetics and electrode kinetics in aqueous electrolytes **475**, 139
Charge transfer resistance
Electrochemical impedance spectroscopy of thin films with two mobile charge carriers: effects of the interfacial charging **472**, 7
Charge transport
Temperature dependence of physical displacement and charge hopping in a polymer membrane incorporating a trinuclear ruthenium complex **476**, 159
Chemically modified electrode
Cationic systems as self-assembled monolayers on gold surfaces **464**, 263

Electrocatalytic oxidation of hydrazine at a chlorogenic acid (CGA) modified glassy carbon electrode **465**, 168
Electrocatalytic reduction of molecular oxygen on a sodium montmorillonite-methyl viologen carbon paste chemically modified electrode **463**, 253
Electrocatalytic reduction of nitrite at a carbon fiber microelectrode chemically modified by palladium(II)-substituted Dawson type heptadecatungstodiphosphate **469**, 63
Self-assembly of a tricarboxylate receptor through thioamide groups and its use for electrochemical detection of protonated amines **473**, 105
Chemically modified electrodes
Electrocatalytic properties of nickel(II) hydrotalcite-type anionic clay: application to methanol and ethanol oxidation **463**, 123
Polyoxometalate modified electrodes: from a monolayer to multilayer structures **462**, 187
Chemical modification of electrode surfaces
Electrochemical behavior of gold electrodes modified with aminopurinethiol derivatives **473**, 99
Chemical oscillation
Electrochemical oscillations of a new type in an $H_2O_2 + H_2SO_4$ | Pt-electrode system, appearing by addition of small amounts of halide ions **473**, 156
Chemical sensor
Photoresponse of a titanium dioxide chemical sensor **472**, 137
Chemical warfare agents
Trace detection of 2,4,6-trinitrotoluene in the gaseous phase by cyclic voltammetry **460**, 10
Chemiluminescence
Detection of near-wall hydrodynamic effects by electrochemiluminescence **470**, 89
Chemisorption
Self-assembly of a tricarboxylate receptor through thioamide groups and its use for electrochemical detection of protonated amines **473**, 105
Chevreul's salt
Surface layers formed initially on copper in air containing water vapor and SO_2 as determined by IR-RAS and 2D-IR **473**, 256
Chiral pyrrole monomers
Enantioselective electrodes: stereoselective electroreduction of 4-methylbenzophenone and acetophenone **461**, 94
Chiral recognition
Chiroselective electron transfer at enantiomer-capped ZnO nanocrystalline surfaces **473**, 117
Chloride adsorption
In-situ STM investigation of specific anion adsorption on Cu(111) **467**, 307
Chloride attack
Current oscillations induced by chlorides during the passive–active transition of iron in a sulfuric acid solution **471**, 132
3-Chloro-4-alkyl(or aryl)-2H-1benzopyran-2-one
Electrosynthesis of 3-chloro-4-substituted-coumarins **469**, 201
2-Chloro-2′-deoxyadenosine
Electrooxidation of the antileukemic 2-chloro-2′-deoxyadenosine and related compounds **477**, 89
Chlorogenic acid
Electrocatalytic oxidation of hydrazine at a chlorogenic acid (CGA) modified glassy carbon electrode **465**, 168
Electrocatalytic oxidation of reduced nicotinamide adenine dinucleotide (NADH) at a chlorogenic acid modified glassy carbon electrode **464**, 14
Chromium
Analysis of the temperature dependence of the α and β coefficients of the electrode reactions in the Cr(III)/Cr(II) and Cr(II)/Cr(Hg) systems **471**, 62
Chromium enrichment
Impedance and photoelectrochemical properties of porous oxide film on Type304 stainless steel formed by square wave potential pulse polarisation **473**, 265
Chronoamperometry
Application of Danckwerts' expression to first-order EC′ reactions. Transient currents at inlaid and recessed microdisc electrodes **466**, 15
Chronoamperometry of strong acids without supporting electrolyte **472**, 1
Convolutive modelling of electrochemical processes based on the relationship between the current and the surface concentration **464**, 1
Electrocatalytic oxidation of hydrazine at a chlorogenic acid (CGA) modified glassy carbon electrode **465**, 168
The kinetics of mercury nucleation from Hg_2^{2+} and Hg^{2+} solutions on vitreous carbon electrodes **464**, 39
Theory of the chronoamperometric transient for electrochemical nucleation with diffusion-controlled growth **470**, 70
Chronocoulometry
Convolutive modelling of electrochemical processes based on the relationship between the current and the surface concentration **464**, 1
Electrochemical investigation of 1,5-pentanediol adsorption on the Ag(111) and Ag(110) faces **467**, 217
Iodide adsorption at the Au(111) electrode surface **467**, 342
On the source of oscillatory instabilities in the electroreduction of thiocyanate complexes of nickel(II) at mercury electrodes **478**, 118
Cladribine
Electrooxidation of the antileukemic 2-chloro-2′-deoxyadenosine and related compounds **477**, 89
Classification scheme
Mechanistic classification of electrochemical oscillators — an operational experimental strategy **478**, 50
Clay modified electrode
Amplification of amperometric biosensor responses by electrochemical substrate recycling: Part II. Experimental study of the catechol–polyphenol oxidase system immobilized in a laponite clay matrix **470**, 61
Electrochemical characterization of the clay-enhanced luminol ecl reaction **474**, 82
Clay-modified electrodes
Preparation of clay-modified electrodes by electrophoretic deposition of clay films **462**, 143
Cleavage
Voltammetric investigation of new polythiophene derivatives possessing electrochemically cleavable arylsulfonamide groups as precursors for solid phase electrosynthesis **477**, 121
Clusters
Formation of conducting clusters of polyaniline films detected by light scattering **473**, 132
The growth of size-determined Cu clusters in nanometer holes on Au(111) due to a balance between surface and electrochemical energy **460**, 102
Cobalt
Anodic electrodeposition of conducting cobalt oxyhydroxide films on a gold surface. XPS study and electrochemical behaviour in neutral and alkaline solution **476**, 54
Cobalt(II) porphyrazine catalysed reduction of nitrite **470**, 126
Enhanced stability and electrocatalytic activity of a ruthenium-modified cobalt–hexacyanoferrate film electrode **471**, 42
Cobalt(II)
Cyclic voltammetry and quartz crystal microgravimetry study of autocatalytic copper(II) reduction by cobalt(II) in ethylenediamine solutions **465**, 142

Cobalt(I) salen
Catalytic reduction of 1,8-diiodooctane by electrogenerated cobalt(I) salen and formation of μ-(1,8-*n*-octyl)-bis[(salen)-cobalt(III)] **460**, 207
Codeposition
Electrodeposited $PbO_2 + RuO_2$: a composite anode for oxygen evolution from sulphuric acid solution **465**, 160
Co(II)(salen)
A microelectrode study of the catalysis of alkyl halide reduction by Co(II)(salen) **464**, 168
Collection efficiency
A wall-jet ring disk electrode fabricated within a thin-layered micromachined cell **479**, 57
Colloidal gold
Adsorption characteristics of $Fe(CN)_6^{3-/4-}$ on Au colloids as monolayer films on cysteamine-modified gold electrode **466**, 26
Colloidal In_2S_3
Semiconductor sensitization of colloidal In_2S_3 on wide gap semiconductors **469**, 116
Competitive adsorption
Electrochemical study on competitive adsorption of pyridinethiol with sulfide onto Au(111) surfaces **473**, 85
Complex current oscillations
Current oscillations induced by chlorides during the passive–active transition of iron in a sulfuric acid solution **471**, 132
Complex formation curves
Experimental and calculated complex formation curves for mixed, dynamic and semi-dynamic, metal–ligand systems. A differential pulse polarographic study of Cu^{II}–sarcosine–OH and Cd^{II}–MIDA–OH systems at a fixed ligand to metal ratio and varied pH **460**, 197
Complex impedance
Electrochemical impedance of the cathode catalyst layer in polymer electrolyte fuel cells **475**, 107
Complexing capacity
Voltammetric metal speciation in mixtures of inert and labile macromolecular complexes at any ligand-to-metal ratio: differential pulse polarographic study of the Zn(II)–nitrilotriacetate–polymethacrylate system **462**, 157
Complexing properties
Transfer of heavy metal ions across the water | nitrobenzene microinterface facilitated by the cadmium selective ionophore ETH1062 **475**, 9
Composite
Renewable silica sol–gel derived carbon composite based glucose biosensor **460**, 234
Composite bipolar membrane
Current–voltage curves of a composite bipolar membrane in organic acid–water solutions **462**, 12
Computer modeling
Dynamic polymeric electrodes, dynamic computer modeling and dynamic electrochemical sensing **468**, 19
Concentration profiles
Voltammetric currents for any ligand-to-metal concentration ratio in fully labile metal-macromolecular complexation. Easy computations, analytical properties of the currents and a graphical method to estimate the stability constant **472**, 42
Conducting materials
Anodic oxidation of dipyrrolyls linked with conjugated spacers: study of electronic interactions between the polypyrrole chain and the spacers **479**, 3
Conducting polymer
Coupled electron and proton transfers: compared behaviour of oxometalates in aqueous solution or after entrapment in polymer matrices **463**, 129
Dynamic polymeric electrodes, dynamic computer modeling and dynamic electrochemical sensing **468**, 19
Electrochemical investigations and morphology of poly(4,9-dihydro-*o*-benzenonaphtho[2,3-c]pyrrole) and poly(acenaphtho[1,2-c]pyrrole) **477**, 25
Theoretical models for ac impedance of finite diffusion layers exhibiting low frequency dispersion **475**, 152
Conducting polymers
In situ atomic force microscopy study of polypyrrole synthesis and the volume changes induced by oxidation and reduction of the polymer **462**, 211
The electrochemical properties of a series of phenylene-thienyl polymers in tetramethylene sulfone based electrolytes **460**, 46
The electrochemistry of antibody-modified conducting polymer electrodes **470**, 144
Conductive polymer
Electrochemical behaviour of *N*-aminopyridinium, and the viologens *N,N'*-diamino-4,4'-bipyridilium and *N,N'*-bis(4-aminophenyl)-4,4'-bipyridilium in aqueous acid: towards the formation of polymer hybrids of pyridine and aniline **462**, 43
Pyruvate sensor based on pyruvate oxidase immobilized in a poly(mercapto-*p*-benzoquinone) film **464**, 143
Conductivity
Conductometric study of lithium halides and thiocyanate in the mixed solvents of tetrahydrofuran and 2-ethyl-1-hexanol **468**, 110
Simultaneous in-situ conductivity and cyclic voltammetry characterization of Li-ion intercalation into thin V_2O_5 films **479**, 12
Spectroelectrochemical study of the influence of anions on the behaviour of poly(*N*-vinylcarbazole) films **475**, 1
Confocal microscopy
Coupled electron and proton transfers: compared behaviour of oxometalates in aqueous solution or after entrapment in polymer matrices **463**, 129
π-Conjugated polymer
Oligomeric poly(phenazine-2,7-diyl) and its electrochemical response **460**, 242
σ–π-Conjugation
Electrochemical oxidation of poly[(hexamethyltrisilanylene)oligo(2,5-thienylene)] films **464**, 158
Constant phase element
Theoretical models for ac impedance of finite diffusion layers exhibiting low frequency dispersion **475**, 152
Contact electric resistance technique
Passivation mechanism of iron in concentrated phosphoric acid **475**, 58
Synthesis, electropolymerization and electrochemical characterization of some new acrylate substituted thiophene derivatives **460**, 176
Contact formation
Ion transport and deposit growth in spatially coupled bipolar electrochemistry **478**, 128
Convection
Ion transport and deposit growth in spatially coupled bipolar electrochemistry **478**, 128
Convective separation processes
Convective electrodiffusion processes through graft-modified charged porous membranes **464**, 222
Convolution
Quantitative discrimination of mass fluxes at electrochemical interfaces by optical beam deflection **466**, 218
Convolution integral
Convolutive modelling of electrochemical processes based on the relationship between the current and the surface concentration **464**, 1
Convolution voltammetry
Kinetics of sulfide ion adsorption at copper amalgam electrode **463**, 200

Co_3O_4
An old workhorse of oxide investigations: new features of Co_3O_4 **464**, 149
Cooperative phenomena
pK_a of an ω-carboxylalkanethiol self-assembled monolayer by interaction model **478**, 101
Coordination
Oxidation of halides by redox enhanced ferricyanide in the $[Fe^{II}–CN–Pt^{IV}]_n$ coordination polymer: an optically triggered process **470**, 99
Copolymers
Electrochemical synthesis and structural studies of copolymers based on the electrooxidation of pyrrole and some salen compounds **470**, 77
Copper
Adsorption of sulfate ions on monocrystalline copper electrodes: the structural effects **463**, 1
Anodic behavior of copper in acetonitrile: the influence of carbon dioxide and dimethylamine **466**, 107
Cathodic stripping square wave voltammetry of Cu(II)–oxine complexes. A mechanistic study **478**, 17
Effect of sodium dodecylsulfate on copper corrosion in sulfuric acid media in the absence and presence of benzotriazole **472**, 112
Electrodeposition of copper from cuprous cyanide electrolyte: I. Current distribution on a stationary disk **474**, 16
Electrodeposition of copper from cuprous cyanide electrolyte: II. Current distribution on a rotating disk **474**, 31
Electroless copper plating on a glass substrate coated with ZnO film under UV illumination **462**, 259
Experimental and calculated complex formation curves for mixed, dynamic and semi-dynamic, metal–ligand systems. A differential pulse polarographic study of Cu^{II}–sarcosine–OH and Cd^{II}–MIDA–OH systems at a fixed ligand to metal ratio and varied pH **460**, 197
In-situ STM investigation of specific anion adsorption on Cu(111) **467**, 307
Polycrystalline gold electrode redox behavior in an ammoniacal electrolyte: Part II. A parallel RRDE, EQCM and TOF-SIMS study of copper underpotential deposition **460**, 143
Copper amalgam electrode
Kinetics of sulfide ion adsorption at copper amalgam electrode **463**, 200
Copper complexes
Electrodeposition of copper into functionalized polypyrrole films **474**, 113
Copper determination
Rapidly renewable and reproducible electropolymerized surface at a monomer modified carbon paste electrode **465**, 102
Copper electrode
In situ orientation study of xanthate on copper under potential control **475**, 124
Copper electrodeposition
A new approach to metal electrodeposition at a periodically changing rate: Part I. The reversing overpotential method **464**, 245
Copper electrodes
Electrochemical oxidation of mono- and disaccharides at fresh as well as oxidized copper electrodes in alkaline media **464**, 252
Copper(II)
Cyclic voltammetry and quartz crystal microgravimetry study of autocatalytic copper(II) reduction by cobalt(II) in ethylenediamine solutions **465**, 142
Copper–nickel alloys
Surface redox catalysis and reduction kinetics of hydrogen peroxide on copper–nickel alloys **470**, 31
Copper sulfate
Surface layers formed initially on copper in air containing water vapor and SO_2 as determined by IR-RAS and 2D-IR **473**, 256
Corrosion
Corrosion sensing by SQUID magnetometry **477**, 171
Ultra-fast electropolymerization of pyrrole in aqueous media on oxidizable metals in a one-step process **478**, 92
Corrosion inhibition
Effect of sodium dodecylsulfate on copper corrosion in sulfuric acid media in the absence and presence of benzotriazole **472**, 112
Corrosion potential
Structural properties of electrochemically designed porous oxide films on AlMg1 **468**, 121
Corrosion products of copper
Surface layers formed initially on copper in air containing water vapor and SO_2 as determined by IR-RAS and 2D-IR **473**, 256
Coulomb interaction
pK_a of an ω-carboxylalkanethiol self-assembled monolayer by interaction model **478**, 101
Coumarins
Electrosynthesis of 3-chloro-4-substituted-coumarins **469**, 201
Crown ether
Electrochemical oxidation in different media of bis(*p*-phenylene crown ether) as a symmetrical molecule bearing two identical redox centers **460**, 119
Crown ether ferrocene
Electrochemical recognition of metal cations by poly(crown ether ferrocene) films investigated by cyclic voltammetry and electrochemical impedance spectroscopy **464**, 24
Crown ethers
Langmuir–Blodgett films of azocrown ethers on electrodes — voltammetric recognition of isomers **471**, 156
The complex formation of non-cyclic polyethers and crown ethers with Ag^+ in acetone and propylene carbonate studied by potentiometric and calorimetric methods **474**, 188
Cr(VI)
Direct experimental evidence proving the formation of surface layers in the course of the reduction of Cr(VI) species at a gold electrode **471**, 73
Crystal field potential
Electron transfer in retrospect and prospect: 1: Adiabatic electrode processes **460**, 5
Electron transfer in retrospect and prospect 1: Adiabatic electrode processes **470**, 170
Crystal impedance
Mechanical resonance effects in electroactive polycarbazole films **460**, 267
Crystallites
Tin electrodeposition on carbon electrodes. From nuclei to microcrystallites **465**, 63
Cu
Step decoration at Pt single crystal electrodes: role of the anion **467**, 50
Cu(110) electrode
In situ scanning tunneling microscopy of Cu(110): atomic structures of halide adlayers and anodic dissolution **473**, 10
Current distribution
Electrodeposition of copper from cuprous cyanide electrolyte: I. Current distribution on a stationary disk **474**, 16
Electrodeposition of copper from cuprous cyanide electrolyte: II. Current distribution on a rotating disk **474**, 31
Current transient
Step decoration at Pt single crystal electrodes: role of the anion **467**, 50
Current transients
Early stages of mercury electrodeposition on HOPG **470**, 120

Current–voltage curves
Current–voltage curves of a composite bipolar membrane in organic acid–water solutions **462**, 12
Cu upd
X-ray and electrochemical studies of Cu upd on single crystal electrodes in the presence of bromide: comparison between Au(111) and Pt(111) electrodes **460**, 121
Cyanated imidazole
Electroanalytical chemistry of myoglobin with modification of distal histidine by cyanated imidazole **468**, 9
Cyanide
Electrodeposition of copper from cuprous cyanide electrolyte: I. Current distribution on a stationary disk **474**, 16
Electrodeposition of copper from cuprous cyanide electrolyte: II. Current distribution on a rotating disk **474**, 31
What can we learn from the non-linear optical investigation of the liquid | solid interface? **473**, 25
Cyanide dissociation
The temperature dependence of the kinetics of cyanide dissociation from the cyanide complex of myoglobin studied by cyclic voltammetry **466**, 177
4-Cyanopyridine
Electrochemical and FTIR studies of 4-cyanopyridine adsorption at the gold(111) | solution interface **475**, 130
Cyclic voltammetry
An in situ UV-vis and IR spectroelectrochemical study of the deposition of a hydroquinone anion salt on platinum electrodes from dichloromethane solutions **462**, 266
Anodic electrodeposition of conducting cobalt oxyhydroxide films on a gold surface. XPS study and electrochemical behaviour in neutral and alkaline solution **476**, 54
Anthraquinones as mediators for the indirect cathodic reduction of dispersed organic dyestuffs **465**, 80
Cathodic reduction of 2-nitronaphthothiophen-4,9-quinone: evidence of catalysis by proton donors and its simulation **462**, 195
Cationic systems as self-assembled monolayers on gold surfaces **464**, 263
Characterization of protein monolayers by surface plasmon resonance combined with cyclic voltammetry 'in situ' **464**, 198
Convolutive modelling of electrochemical processes based on the relationship between the current and the surface concentration **464**, 1
Coordination of silver(I) at the surface of carbon paste electrodes modified with 2,5,8-trithia[9]-*m*-cyclophane as studied by cyclic voltammetry **475**, 73
Electrocatalytic oxidation of hydrazine at a chlorogenic acid (CGA) modified glassy carbon electrode **465**, 168
Electrochemical behavior of a *Cypridina* luciferin analogue in acetonitrile solutions in the presence of proton acceptors **476**, 46
Electrochemical behaviour of amino acids on Pt(*hkl*). A voltammetric and in situ FTIR study: Part IV. Serine and alanine on Pt(100) and Pt(110) **475**, 38
Electrochemical investigations and morphology of poly(4,9-dihydro-*o*-benzenonaphtho[2,3-c]pyrrole) and poly(acenaphtho[1,2-c]pyrrole) **477**, 25
Electrochemical oxidation in different media of bis(*p*-phenylene crown ether) as a symmetrical molecule bearing two identical redox centers **460**, 119
Electrochemical recognition of metal cations by poly(crown ether ferrocene) films investigated by cyclic voltammetry and electrochemical impedance spectroscopy **464**, 24
Electrochemical study of β-nitrostyrene derivatives: steric and electronic effects on their electroreduction **466**, 90
Electrode reactions and accumulation of hydrogen at carbon paste electrodes in the presence of tetrachloropalladate **462**, 174
Electropolymerization of 2-methoxy aniline. Electrochemical and spectroscopical product characterization **471**, 180
Enhanced electron transfer for hemoglobin in poly (ester sulfonic acid) films on pyrolytic graphite electrodes **463**, 53
Finite element simulation of ion transfer reactions at a single micro-liquid | liquid interface supported on a thin polymer film **468**, 42
Investigation of the lifetimes of some pyrrole species by rapid scan cyclic voltammetry and double potential step techniques **464**, 123
Langmuir–Blodgett films of azocrown ethers on electrodes — voltammetric recognition of isomers **471**, 156
Mechanism of the electrochemical reduction of sulfur dioxide in non-aqueous solvents **476**, 15
Reaction of nitrobenzene on gold single-crystal electrodes: surface crystallographic orientation dependence **477**, 111
Reduction and oxidation of peptide nucleic acid and DNA at mercury and carbon electrodes **476**, 71
Simultaneous in-situ conductivity and cyclic voltammetry characterization of Li-ion intercalation into thin V_2O_5 films **479**, 12
Solid-state electrochemical investigation of poly[2-methoxy, 5-(2′-ethyl-hexyloxy)-1,4-phenylene vinylene] **471**, 32
Studies of structural disorder of self-assembled thiol monolayers on gold by cyclic voltammetry and ac impedance **464**, 61
The adsorption of methylamine on Pt single crystal surfaces **467**, 105
The electrochemical properties of a series of phenylene-thienyl polymers in tetramethylene sulfone based electrolytes **460**, 46
The electrochemistry of antibody-modified conducting polymer electrodes **470**, 144
The electrochemistry of nitrogen-containing compounds at platinum single crystal electrodes: Part 3. Carbohydrazide on Pt(*hkl*) electrodes **467**, 20
The initial stages of rhodium deposition on Au(111) **467**, 249
The temperature dependence of the kinetics of cyanide dissociation from the cyanide complex of myoglobin studied by cyclic voltammetry **466**, 177
The voltammetric reduction of some benzenesulfonyl fluorides, simulation of the ECE mechanism and determination of the potential variation of the transfer coefficient by using the compounds with two reducible groups **471**, 14
Trace detection of 2,4,6-trinitrotoluene in the gaseous phase by cyclic voltammetry **460**, 10
Transfer of β-diketone and 4-acylpyrazolone anions across the electrified water|nitrobenzene interface **469**, 91
Urea adsorption on Pt(111) electrodes **461**, 65
Voltammetric investigation of new polythiophene derivatives possessing electrochemically cleavable arylsulfonamide groups as precursors for solid phase electrosynthesis **477**, 121
Cyclic voltammogram
Integration analysis of the cyclic voltammograms of the electrode reaction in a diffusionless system **465**, 219
Cycling efficiency
Electrochemical control of a Li metal anode interface: improvement of Li cyclability by inorganic additives compatible with electrolytes **473**, 279
Cyclization
Mechanism of stereoselective production of *trans*-1-decalone by electrochemical catalysis in microemulsions **464**, 31
Cyclodextrin
Electrochemical study of methylalkylviologens using an electrochemical quartz crystal microbalance **463**, 224
Electrochemical study of self-assembled monolayers of a β-cyclodextrin methyl sulfide covalently linked to anthraquinone **465**, 209

Polymer chain encapsulation followed by a quartz microbalance during electropolymerization of bithiophene-β-cyclodextrin host–guest compounds in aqueous solution **476**, 1
α-Cyclodextrin
A sodium-specific condensed film of α-cyclodextrin at the mercury | water interface **465**, 51
Self-organization of α-cyclodextrin on Au(111) surfaces induced by potential controlled adsorption **472**, 163
β-Cyclodextrin
Electrochemical studies of ferrocene derivatives and their complexation by β-cyclodextrin **477**, 130
Cyclopentadienes
Electrochemical reduction of phenyl-substituted cyclopentadienes: a case of an 'indirect father–son' self-protonation process **460**, 160
Cyclophane derivative
Coordination of silver(I) at the surface of carbon paste electrodes modified with 2,5,8-trithia[9]-*m*-cyclophane as studied by cyclic voltammetry **475**, 73
Cypridina luciferin analogues
Electrochemical behavior of a *Cypridina* luciferin analogue in acetonitrile solutions in the presence of proton acceptors **476**, 46
Cysteine
Combined quartz crystal impedance and electrochemical impedance measurements during adsorption of bovine serum albumin onto bare and cysteine- or thiophenol-modified gold electrodes **478**, 1
L-Cysteine
Evaluation of a reactor model and cathode materials for batch electrolysis of L-cystine hydrochloride **462**, 97
L-Cystine
Evaluation of a reactor model and cathode materials for batch electrolysis of L-cystine hydrochloride **462**, 97
Cytochrome *c*
A non-compartmentalized glucose | O_2 biofuel cell by bioengineered electrode surfaces **479**, 64
Electrochemical behavior of gold electrodes modified with aminopurinethiol derivatives **473**, 99
The role of the potential distribution at the electrode interface in determining the electron transfer rate constant **465**, 96
Cytochrome c_3
Electrocatalytic reduction of uranium by bacterial cytochromes: biochemical and chemical factors influencing the catalytic process **471**, 96
Cytochrome c_{552}
Electrochemical studies on *c*-type cytochromes at microelectrodes **464**, 76
Cytochrome c_{553}
Electrochemical studies on *c*-type cytochromes at microelectrodes **464**, 76
Cytochrome P-450
Electrochemical study of tetraphenylporphinato-iron(III)–thiolate complexes, NH···S hydrogen bonding in the cytochrome P-450 model system **469**, 84
Cytosine
In situ infrared study of cytosine adsorption on gold electrodes **460**, 188

Dawson-type complexes
Electrochemical and catalytic behaviour of Dawson-type complexes derived from $[(1),2,3\text{-}P_2Mo_2W_{15}O_{61}]^{10-}$ and first transition metal ions **477**, 146
Dawson-type heteropolytungstate
Electrocatalytic reduction of nitrite at a carbon fiber microelectrode chemically modified by palladium(II)-substituted Dawson type heptadecatungstodiphosphate **469**, 63
Dawson-type structure
Metal ion complexes derived from the α_1 isomer of $(P_2W_{17}O_{61})^{10-}$: comparison with the corresponding α_2 species **478**, 76
Defects
Assessing the apparent effective thickness of alkanethiol self-assembled monolayers in different concentrations of $Fe(CN)_6^{3-}$ / $Fe(CN)_6^{4-}$ by ac impedance spectroscopy **470**, 9
Dehydrogenation system
Construction of a new dehydrogenation system using a two-compartment cell separated by a palladized Pd sheet electrode **463**, 116
DEMS
Ethanol oxidation on PtRu electrodes studied by differential electrochemical mass spectrometry **472**, 120
Dendrimers
Silicon-based ferrocenyl dendrimers as anion receptors in solution and immobilized onto electrode surfaces **463**, 87
Deposition
Diamond-like carbon electrodes in electrochemical microgravimetry **464**, 230
Desorption
A temperature controlled cell for in situ infrared spectroelectrochemical measurements and its use in the study of CO isothermal desorption **471**, 146
Electrochemical determination of hydrogen in metals **475**, 82
In situ infrared study of cytosine adsorption on gold electrodes **460**, 188
Mass spectrometric study of desorption and hydrogenation of biphenyl, naphthalene and *t*-butylbenzene on poly- and monocrystalline platinum electrodes **461**, 90
The study of the adsorption/desorption of acetate anions on a Pt(111) electrode and the effect of counter cations in acidic media **467**, 112
Detection
1-Naphthyl phosphate as an enzymatic substrate for enzyme-linked immunomagnetic electrochemistry **469**, 27
Deuterium
Anomalous H/D isotopic effect in the kinetics of polarographic hydrogen evolution **477**, 62
The study of hydrogen sorption in palladium limited volume electrodes (Pd-LVE): I. Acidic solutions **471**, 190
Diamond
Electrochemistry of homoepitaxial CVD diamond: energetics and electrode kinetics in aqueous electrolytes **475**, 139
Diamond electrode
Electroanalysis of dopamine and NADH at conductive diamond electrodes **473**, 179
Electrochemical selectivity for redox systems at oxygen-terminated diamond electrodes **473**, 173
Diamond-like carbon
Diamond-like carbon electrodes in electrochemical microgravimetry **464**, 230
Diaphorase
Electrochemical evaluation of the reaction rate between methyl viologen mediator and diaphorase enzyme for the electrocatalytic reduction of NAD^+ and digital simulation for its voltammetric responses **465**, 153
Dibenzo-18-crown-6
Voltammetric analysis of Cs^+-DB18C6 complex stoichiometry at the water | 1,2-dichloroethane interface **464**, 54
Dicarbox-type pesticides
Electrochemical properties of three dicarboximide-type pesticides: vinclozoline, iprodione and procymidone **472**, 33

Dicationic nickel complex
Enhanced electrostatic interactions for selective and controllable permeation of ionic species at a monolayer of self-assembled dicationic nickel complex **465**, 177
Dichlorodifluoromethane
Electrochemical reduction of dichlorodifluoromethane in acetonitrile medium to useful fluorinated compounds **471**, 26
Dichloromethane
An in situ UV-vis and IR spectroelectrochemical study of the deposition of a hydroquinone anion salt on platinum electrodes from dichloromethane solutions **462**, 266
Diclofenac
Ionic partition diagrams of ionisable drugs: pH-lipophilicity profiles, transfer mechanisms and charge effects on solvation **462**, 235
Difference frequency generation
In situ visible-infrared sum and difference frequency generation at the electrochemical interface **467**, 238
Differential capacity
The fast dropping oil | water electrode **464**, 128
Differential electrochemical mass spectrometry
Adsorption, oxidation and reduction reactions of propargyl alcohol on palladium as studied by electrochemical mass spectrometry **472**, 71
Differential pulse anodic stripping voltammetry
Rotograved carbon electrodes for amperometric cadmium and lead determination **469**, 189
Differential pulse polarography
Voltammetric metal speciation in mixtures of inert and labile macromolecular complexes at any ligand-to-metal ratio: differential pulse polarographic study of the Zn(II)–nitrilotriacetate–polymethacrylate system **462**, 157
Differential pulse voltammetry
Study of a catalytic mechanism in double potential step techniques at spherical electrodes **468**, 158
Differential quadratic logistic equation
On the use of the quadratic logistic differential equation for the interpretation of electrointercalation processes **460**, 161
Diffusion
A minimum separating diffusion and adsorption waves in polarography using a static mercury drop electrode **465**, 30
Effects of self-stress on the hydrogen absorption into palladium hydride electrodes of plate form under galvanostatic conditions **474**, 130
Theoretical models for ac impedance of finite diffusion layers exhibiting low frequency dispersion **475**, 152
Diffusion coefficient
Determination of the Li ion chemical diffusion coefficient for the topotactic solid-state reactions occurring via a two-phase or single-phase solid solution pathway **477**, 32
Using Pt microelectrodes in liquid ammonia for studying proton reduction **477**, 140
Diffusion constant
Spectroelectrochemical investigations on the reduction of thin films of hexadecafluorophthalocyaninatozinc ($F_{16}PcZn$) **476**, 148
Diffusion impedance
Linear diffusion impedance. General expression and applications **471**, 126
Diffusionless system
Integration analysis of the cyclic voltammograms of the electrode reaction in a diffusionless system **465**, 219
Diffusivity
Electrochemical determination of hydrogen in metals **475**, 82
Difluoromethane
Electrochemical reduction of dichlorodifluoromethane in acetonitrile medium to useful fluorinated compounds **471**, 26
Digisim®
Mechanism of the electrochemical reduction of sulfur dioxide in non-aqueous solvents **476**, 15
Digital simulation
Digital simulation of fast cyclic voltammogram by integration of the double layer charging current **464**, 215
Electrochemical evaluation of the reaction rate between methyl viologen mediator and diaphorase enzyme for the electrocatalytic reduction of NAD^+ and digital simulation for its voltammetric responses **465**, 153
Finite-difference electrochemical kinetic simulations using the Rosenbrock time integration scheme **469**, 97
The voltammetric reduction of some benzenesulfonyl fluorides, simulation of the ECE mechanism and determination of the potential variation of the transfer coefficient by using the compounds with two reducible groups **471**, 14
Dihydroreduction
Electrochemical reduction of phenyl-substituted cyclopentadienes: a case of an 'indirect father–son' self-protonation process **460**, 160
1,8-Diiodooctane
Catalytic reduction of 1,8-diiodooctane by electrogenerated cobalt(I) salen and formation of μ-(1,8-*n*-octyl)-bis-[(salen)cobalt(III)] **460**, 207
β-Diketones
Transfer of β-diketone and 4-acylpyrazolone anions across the electrified water|nitrobenzene interface **469**, 91
π-Dimer
Electrochemical generation of cation radical π-dimers in polymer film composed of pentathiophenes bridged by monosilanylene units **472**, 157
Dimerization
Electrochemical behavior of a *Cypridina* luciferin analogue in acetonitrile solutions in the presence of proton acceptors **476**, 46
Voltammetric investigation of the anodic dimerization of *p*-halogenoanilines in DMF: Reactivity of their electrogenerated cation radicals **462**, 55
Dimethylamine
Anodic behavior of copper in acetonitrile: the influence of carbon dioxide and dimethylamine **466**, 107
Dimethylsulfoxide
Electrode kinetics of Eu^{3+} in dimethylsulfoxide **470**, 1
Dioxygen
Electro-enzymatic reduction of dioxygen to water in the cathode compartment of a biofuel cell **464**, 110
Dipyrrolyl monomers
Anodic oxidation of dipyrrolyls linked with conjugated spacers: study of electronic interactions between the polypyrrole chain and the spacers **479**, 3
Direct current
Electrochemical treatment of tumours: a simplified mathematical model **460**, 88
Directed wire growth
Ion transport and deposit growth in spatially coupled bipolar electrochemistry **478**, 128
Direct methanol fuel cell
A model for the liquid feed direct methanol fuel cell **477**, 97
Methanol oxidation and direct methanol fuel cells: a selective review **460**, 14
Disaccharides
Electrochemical oxidation of mono- and disaccharides at fresh as well as oxidized copper electrodes in alkaline media **464**, 252
Discrimination
Quantitative discrimination of mass fluxes at electrochemical interfaces by optical beam deflection **466**, 218

Disk electrode
Electrodeposition of copper from cuprous cyanide electrolyte: I. Current distribution on a stationary disk **474**, 16
Dissociation products
Interaction of H, O and OH with metal surfaces **472**, 126
Distance-dependence of electron transfer
Voltammetric determination of electron transfer kinetic parameters in hydroquinone-terminated self-assembled monolayers on gold **476**, 177
Distribution
Evaluation of model and dispersion parameters and their effects on the formation of constant-phase elements in equivalent circuits **464**, 68
Distribution function
A non-primitive model for the electrode | electrolyte interface based on the Percus–Yevick theory. Analysis of the different molecular sizes, ion valences and electrolyte concentrations **460**, 135
Dithiadiazafulvalene
Cathodic synthesis of powerful electron π-donors including dithiadiazafulvalenes **462**, 137
Dithiafulvene
Cathodic synthesis of powerful electron π-donors including dithiadiazafulvalenes **462**, 137
DME
General solutions for the I/t response for reversible processes in the presence of product in a multipotential step experiment at planar and spherical electrodes whose areas increase with any power of time **466**, 8
DNA oligomers
Reduction and oxidation of peptide nucleic acid and DNA at mercury and carbon electrodes **476**, 71
Dodecyl sulfate
MRA combined spectroelectrochemical studies on the redox stability of PPy/DS films **462**, 1
Donnan effects
Coupled electron and proton transfers: compared behaviour of oxometalates in aqueous solution or after entrapment in polymer matrices **463**, 129
Dopamine
Control of electrocatalytic oxidation of NADH using an interaction between labeled biotin with dopamine and avidin **466**, 117
Electroanalysis of dopamine and NADH at conductive diamond electrodes **473**, 179
In situ STM study of self-assembled mercaptopropionic acid monolayers for electrochemical detection of dopamine **465**, 72
Kinetic behaviour of dopamine-polyphenol oxidase on electrodes of tetrathiafulvalenium tetracyanoquinodimethanide and tetracyanoquinodimethane species **461**, 174
Dopants
Strontium ruthenate perovskite as the active material for supercapacitors **460**, 154
Doping
Electrochemical generation of cation radical π-dimers in polymer film composed of pentathiophenes bridged by monosilanylene units **472**, 157
Electrochemical oxidation of poly[(hexamethyltrisilanylene)oligo-(2,5-thienylene)] films **464**, 158
The electrochemical properties of a series of phenylene-thienyl polymers in tetramethylene sulfone based electrolytes **460**, 46
Double layer
An electrochemical quartz crystal microbalance study of the hydrogen underpotential deposition at a Pt electrode **467**, 186
Effect of the crystallographic orientation of Ag single crystal face electrodes on the kinetics of proton discharge **467**, 164
Double layer capacitances
Electrode kinetics of Eu^{3+} in dimethylsulfoxide **470**, 1
Double layer correction
Some remarks on the double layer correction to the kinetics of ion transfer at the interface of immiscible electrolytes **474**, 89
Double layer parameters
Indium adsorption at the surface of liquid In + Ga alloy electrodes in contact with an aqueous 1 M $NaClO_4$ solution **462**, 111
Double potential step chronoamperometry
Electrochemical behavior of a *Cypridina* luciferin analogue in acetonitrile solutions in the presence of proton acceptors **476**, 46
Investigation of the lifetimes of some pyrrole species by rapid scan cyclic voltammetry and double potential step techniques **464**, 123
Study of a catalytic mechanism in double potential step techniques at spherical electrodes **468**, 158
Doubling effect mechanism
Oxygen reduction mechanisms at p-InP and p-GaAs electrodes in liquid ammonia in neutral buffered medium and acidic media **462**, 88
DPP
Experimental and calculated complex formation curves for mixed, dynamic and semi-dynamic, metal–ligand systems. A differential pulse polarographic study of Cu^{II}–sarcosine–OH and Cd^{II}–MIDA–OH systems at a fixed ligand to metal ratio and varied pH **460**, 197
Dropping liquid metal electrodes
Indium adsorption at the surface of liquid In + Ga alloy electrodes in contact with an aqueous 1 M $NaClO_4$ solution **462**, 111
Dropping mercury electrode
A minimum separating diffusion and adsorption waves in polarography using a static mercury drop electrode **465**, 30
2D-structure
Anodic oxidation of dipyrrolyls linked with conjugated spacers: study of electronic interactions between the polypyrrole chain and the spacers **479**, 3
Dual integral equation
Steady-state currents at inlaid and recessed microdisc electrodes for first-order EC′ reactions **476**, 132
Dynamic sensing
Dynamic polymeric electrodes, dynamic computer modeling and dynamic electrochemical sensing **468**, 19

Eastman AQ
Enhanced electron transfer for hemoglobin in poly (ester sulfonic acid) films on pyrolytic graphite electrodes **463**, 53
ECE mechanism
The voltammetric reduction of some benzenesulfonyl fluorides, simulation of the ECE mechanism and determination of the potential variation of the transfer coefficient by using the compounds with two reducible groups **471**, 14
EC′ mechanism
Application of Danckwerts' expression to first-order EC′ reactions. Transient currents at inlaid and recessed microdisc electrodes **466**, 15
Steady-state currents at inlaid and recessed microdisc electrodes for first-order EC′ reactions **476**, 132
EC reaction
Spectroelectrochemistry for a coupled chemical reaction in the channel cell: Part I. Theoretical simulation of an EC reaction **464**, 176
Spectroelectrochemistry for a coupled chemical reaction in the channel cell: Part II. Kinetics of hydrolysis and the absorption spectrum of *p*-benzoquinoneimine **464**, 181
Effective hydrogen chemical potential
Electrochemical formation of nickel hydride in alkaline solutions **472**, 182
EIS
Determination of the Li ion chemical diffusion coefficient for the topotactic solid-state reactions occurring via a two-phase or single-phase solid solution pathway **477**, 32

Discussion of the paper by Barber et al. [J. Electroanal. Chem. 446 (1998) 125] **466**, 122
Linear diffusion impedance. General expression and applications **471**, 126
Review and theoretical analysis of ac–av methods for the investigation of hydrogen insertion I. Diffusion formalism **462**, 73
Study of the corrosion behavior of titanium and some of its alloys for biomedical and dental implant applications **471**, 109
E-isomers
Langmuir–Blodgett films of azocrown ethers on electrodes — voltammetric recognition of isomers **471**, 156
Electric contacts
Simultaneous platinum deposition and formation of a photoluminescent porous silicon layer **469**, 48
Electric double layer
Effect of cation adsorption on the kinetics of anion electroreduction: Part I. Effect of the adsorption of inorganic cations in small concentrations on the kinetics of anion electroreduction with different elementary steps of discharge **476**, 26
Effect of cation adsorption on the kinetics of anion electroreduction: Part II. Effect of the adsorption of organic cations in small concentrations on the kinetics of anion electroreduction **476**, 37
Electric field effects
Electric field effects on CO and NO adsorption at the Pt(111) surface **476**, 64
Electric potential
Influence of the electric potential on the structure of pyridine adlayers on Au(111) terraces from in-situ scanning tunnelling microscopy imaging **467**, 230
Electroactive films
On the use of the quadratic logistic differential equation for the interpretation of electrointercalation processes **460**, 161
Electroactive polymers
Anodic oxidation of various arylene-cyanovinylenes made of alternating fluorenyl, thienyl and/or phenyl units **466**, 144
Electrochemical impedance spectroscopy of thin films with two mobile charge carriers: effects of the interfacial charging **472**, 7
Electroactive species permeation
Transport across poly(*o*-aminophenol) modified electrodes in contact with media containing redox active couples. A study using rotating disc electrode voltammetry **477**, 1
Electroanalytical methods
Finite-difference electrochemical kinetic simulations using the Rosenbrock time integration scheme **469**, 97
Electrocapillary equations
Electrocapillary equations of solid electrodes **478**, 40
Electrocatalysis
A novel electrochemical method for the detection of nerve gases **466**, 169
Controlled electrocatalysis by microperoxidase-11 and Au-nanoparticle superstructures on conductive supports **479**, 69
Diffusionless electron transfer of microperoxidase-11 on gold electrodes **469**, 123
Effect of the crystallographic orientation of Ag single crystal face electrodes on the kinetics of proton discharge **467**, 164
Electrocatalytic oxidation of hydrazine at a chlorogenic acid (CGA) modified glassy carbon electrode **465**, 168
Electrocatalytic properties of nickel(II) hydrotalcite-type anionic clay: application to methanol and ethanol oxidation **463**, 123
Electrocatalytic reduction of uranium by bacterial cytochromes: biochemical and chemical factors influencing the catalytic process **471**, 96
Electrochemical and electrocatalytic properties of tetra-iron substituted sandwich-type pentadecatungstodiphosphate heteropolyanions **476**, 85
Electrochemical characterization and electrocatalysis of high valent manganese *meso*-tetrakis(*N*-methyl-2-pyridyl)porphyrin **474**, 52
Electrodeposited $PbO_2 + RuO_2$: a composite anode for oxygen evolution from sulphuric acid solution **465**, 160
Electrodeposition of copper into functionalized polypyrrole films **474**, 113
Enhanced electron transfer for hemoglobin in poly (ester sulfonic acid) films on pyrolytic graphite electrodes **463**, 53
Enhanced stability and electrocatalytic activity of a ruthenium-modified cobalt–hexacyanoferrate film electrode **471**, 42
Evaluation of a reactor model and cathode materials for batch electrolysis of L-cystine hydrochloride **462**, 97
Heat-treated iron(III) tetramethoxyphenyl porphyrin chloride supported on high-area carbon as an electrocatalyst for oxygen reduction: Part II. Kinetics of oxygen reduction **462**, 63
Immobilized nitro-fluorenone derivatives as electrocatalysts for NADH oxidation **477**, 79
On the source of oscillatory instabilities in the electroreduction of thiocyanate complexes of nickel(II) at mercury electrodes **478**, 118
Reaction mechanism and dynamics of methanol electrooxidation on platinum(111) **467**, 132
Small signal (local) analysis of electrocatalytic reaction. Pole-zero approach **465**, 119
Electrocatalysts
An electrochemical alcohol sensor based on a co-electrodeposited $Pt \mid WO_3$ electrode **471**, 151
Control of electrocatalytic oxidation of NADH using an interaction between labeled biotin with dopamine and avidin **466**, 117
Enhancement of the electrocatalytic O_2 reduction on Pt–Fe alloys **460**, 258
In situ and model EXAFS studies of electrocatalysts for methanol oxidation **460**, 80
Electrocatalytic activity
Cobalt(II) porphyrazine catalysed reduction of nitrite **470**, 126
Significant enhancement of the electrochemical reduction of CO_2 at the kink sites on Pt(S)-[n(110) × (100)] and Pt(S)-[n(100) × (110)] **467**, 67
Electrocatalytic dehydrochlorination
Synthesis of carbyne-like nano-particles by electrocatalytic dehydrochlorination of 1,1,2-trichloroethane **470**, 95
Electrocatalytic determination
Nickel(II) tetraaza macrocycle modified electrodes for the electrocatalytic determination of L-ascorbic acid by the flow injection method **468**, 85
Electrocatalytic effect
Current enhancing effect of poly[1-methyl-3-(pyrrol-1-ylmethyl)pyridinium] films on the electrode reaction of anthraquinonedisulfonate **478**, 9
Electrocatalytic oxidation
Catalytic and electrocatalytic oxidation of oxalic acid in aqueous solutions of different compositions **474**, 147
Electrocatalytic oxidation of NADH at graphite electrodes modified with osmium phenanthrolinedione **464**, 208
Electrocatalytic oxidation of reduced nicotinamide adenine dinucleotide (NADH) at a chlorogenic acid modified glassy carbon electrode **464**, 14
Electro-oxidation of *meso*-erythritol on platinum in acid medium: analysis of the reaction products **464**, 101
Ethanol oxidation on PtRu electrodes studied by differential electrochemical mass spectrometry **472**, 120
Oxidation of CO adlayers on Pt(111) at low potentials: an impinging jet study in H_2SO_4 electrolyte with mathematical modeling of the current transients **467**, 74
Electrocatalytic reduction
Electrocatalytic reduction of molecular oxygen on a sodium montmorillonite-methyl viologen carbon paste chemically modified electrode **463**, 253

Electrochemical activation
Structural changes at the Pt(100) surface with a great number of potential cycles **460**, 251
Structural changes at various Pt single crystal surfaces with potential cycles in acidic and alkaline solutions **467**, 85
Electrochemical amplification
Amplification of amperometric biosensor responses by electrochemical substrate recycling: Part I. Theoretical treatment of the catechol–polyphenol oxidase system **470**, 53
Amplification of amperometric biosensor responses by electrochemical substrate recycling: Part II. Experimental study of the catechol–polyphenol oxidase system immobilized in a laponite clay matrix **470**, 61
Electrochemical annealing
On the stability of unreconstructed Au(100)-(1 × 1) at negative potentials in aqueous sulfate solution **471**, 9
Electrochemical atomic force microscopy
Surface alloying at the Cd | Au(100) interface in the upd region. Electrochemical studies and in situ EC-AFM observation **475**, 171
Electrochemical behaviour
Solid-state electrochemical investigation of poly[2-methoxy, 5-(2′-ethyl-hexyloxy)-1,4-phenylene vinylene] **471**, 32
Electrochemical catalysis
Mechanism of stereoselective production of *trans*-1-decalone by electrochemical catalysis in microemulsions **464**, 31
Electrochemical copolymerization
The electrochemical copolymerization of pyrrole and furan in a novel binary solvent system **470**, 23
Electrochemical desorption
Investigation of the structure of self-assembled monolayers of asymmetrical disulfides on Au(111) electrodes by electrochemical desorption **473**, 68
Electrochemical detection
A review of a new voltammetric method for determining acids **468**, 53
Electrochemical impedance
Combined quartz crystal impedance and electrochemical impedance measurements during adsorption of bovine serum albumin onto bare and cysteine- or thiophenol-modified gold electrodes **478**, 1
Impedance of ruthenium electrodes in sulphuric acid solution **463**, 29
The role of the potential distribution at the electrode interface in determining the electron transfer rate constant **465**, 96
Electrochemical impedance spectroscopy
Electrochemical and photoelectrochemical behaviour of poly-3-methylthiophene and polybithiophene in non-aqueous solutions: I. Dark and light processes in systems with and without cathodic doping **463**, 190
Electrochemical characterization of the clay-enhanced luminol ecl reaction **474**, 82
Electrochemical recognition of metal cations by poly(crown ether ferrocene) films investigated by cyclic voltammetry and electrochemical impedance spectroscopy **464**, 24
Electropolymerization of 2-methoxy aniline. Electrochemical and spectroscopical product characterization **471**, 180
Passivation mechanism of iron in concentrated phosphoric acid **475**, 58
Studies on the redox behaviour of some polythiophene derivatives by impedance spectroscopy in symmetrical and asymmetrical configurations **472**, 20
Electrochemical in situ FTIR
FTIR studies of benzoate adsorption on the Au(111) electrode **478**, 67
Electrochemical intercalation
Behaviour of titanium species in molten $Li_2CO_3 + Na_2CO_3$ and $Li_2CO_3 + K_2CO_3$ in the anodic conditions used in molten carbonate fuel cells: II. Electrochemical intercalation of Li^+ in Li_2TiO_3 at 600 and 650°C **474**, 9
Electrochemical interface
Interfacial structure of dimethylsulfoxide at Ag electrodes from surface enhanced Raman scattering and differential capacitance **479**, 21, 32
Electrochemical kinetics
Finite-difference electrochemical kinetic simulations using the Rosenbrock time integration scheme **469**, 97
Electrochemical mechanism
Mechanistic investigation of the anodic oxidation of *p*-methoxytoluene in dry and wet acetonitrile **464**, 85
Electrochemical metal deposition
The growth of size-determined Cu clusters in nanometer holes on Au(111) due to a balance between surface and electrochemical energy **460**, 102
Electrochemical nucleation
Theory of the chronoamperometric transient for electrochemical nucleation with diffusion-controlled growth **470**, 70
Electrochemical oscillations
On the source of oscillatory instabilities in the electroreduction of thiocyanate complexes of nickel(II) at mercury electrodes **478**, 118
Electrochemical Ostwald ripening
Two mercury drops on a conducting surface in a mercurous ion solution as a model for electrochemical Ostwald ripening **468**, 127
Electrochemical oxidation
Electrochemical characterization and electrocatalysis of high valent manganese *meso*-tetrakis(*N*-methyl-2-pyridyl)porphyrin **474**, 52
Electrochemical oxidation of poly[(hexamethyltrisilanylene)-oligo(2,5-thienylene)] films **464**, 158
Electrochemical oxidation of pyrite (FeS_2) in aqueous electrolytes **471**, 116
In-situ infrared reflectance spectroscopic study of propanediol electrooxidation at platinum and gold: Part 1. 1,3-Propanediol **463**, 63
Electrochemical oxidation mechanism
Electrooxidation of the antileukemic 2-chloro-2′-deoxyadenosine and related compounds **477**, 89
Electrochemical properties
Electrochemical properties of 'figure-eight'-cyclooctapyrroles (octaphyrins) and their metal complexes **469**, 170
Electrochemical properties of the first Re(I)–carbonyl compound of di-2-pyridyl ketone.oxime (dpk.oxime), *fac*-$Re(CO)_3$-(dpk.oxime)Cl, in non-aqueous media **466**, 60
Electrochemical properties of three dicarboximide-type pesticides: vinclozoline, iprodione and procymidone **472**, 33
Electrochemical quartz crystal microbalance
Electrochemical quartz crystal microbalance study of electrodeposited ruthenium **474**, 167
Electropolymerization of methacrylonitrile and *N*-vinyl-2-pyrrolidone as probed by an EQCM **465**, 200
Electrochemical quartz microbalance
Electrochemical study of methylalkylviologens using an electrochemical quartz crystal microbalance **463**, 224
Electrochemical recognition
Electrochemical response to anions by neutral ferrocenyl receptors containing 2,2′-bipyridyl arms **469**, 132
Electrochemical reduction
Electrochemical reduction of dichlorodifluoromethane in acetonitrile medium to useful fluorinated compounds **471**, 26
Electrochemical reduction of phenyl-substituted cyclopentadienes: a case of an 'indirect father–son' self-protonation process **460**, 160

Mechanism of the catalysis by *Alcaligenes eutrophus* H16 hydrogenase of direct electrochemical reduction of NAD^+ **468**, 139
Oligomeric poly(phenazine-2,7-diyl) and its electrochemical response **460**, 242
Electrochemical reduction of carbon dioxide
Significant enhancement of the electrochemical reduction of CO_2 at the kink sites on Pt(S)-[n(110) × (100)] and Pt(S)-[n(100) × (110)] **467**, 67
Electrochemical reductive desorption
Electrochemical study on competitive adsorption of pyridinethiol with sulfide onto Au(111) surfaces **473**, 85
Electrochemical responses
Feasibility studies for the detection of volatile organic compounds in the gas phase using microelectrode sensors **460**, 105
Electrochemical sensor
A novel electrochemical method for the detection of nerve gases **466**, 169
Electrochemical supercapacitor
Electrochemical quartz crystal microbalance study of electrodeposited ruthenium **474**, 167
Electrochemical switching
Formation of conducting clusters of polyaniline films detected by light scattering **473**, 132
Light scattering of polyaniline films responding to electrochemical switching **460**, 254
Electrochemical synthesis
Magnetic properties and optical control of electrochemically prepared iron–chromium polycyanides **473**, 245
Electrochemical–thermal method
Determination of the entropy change of the electrode reaction by an ac electrochemical–thermal method **469**, 1
Electrochemical transformation
Electrochemical behaviour of $[Mn_2^{III,IV}O_2(phen)_4]^{3+}$ complex in aqueous phen + phenH$^+$ buffer; phen = 1,10-phenanthroline **463**, 119
Electrochemical treatment (ET)
Electrochemical treatment of tumours: a simplified mathematical model **460**, 88
Electrochemiluminescence
Redox-cycling type electrochemiluminescence in aqueous medium. A new principle for the detection of proteins labeled with a ruthenium chelate **474**, 192
Electrochemistry
A monomer–dimer equilibrium in self-assembled monolayers of *N*-ethyl-*N*′-octadecylviologen on the electrode surface. The influence of water content and hexafluorophosphate ion **466**, 67
A non-compartmentalized glucose | O_2 biofuel cell by bioengineered electrode surfaces **479**, 64
Detection of near-wall hydrodynamic effects by electrochemiluminescence **470**, 89
Electrochemical and EQCM studies on the assembly of asymmetric viologen on bare and alkanethiol-coated Au electrodes **477**, 52
Electrochemical studies on *c*-type cytochromes at microelectrodes **464**, 76
Electrochromic printing
Cyclic voltammetric studies of Prussian blue and viologens within a paper matrix for electrochromic printing applications **461**, 263
Electrochromism
Cyclic voltammetric studies of Prussian blue and viologens within a paper matrix for electrochromic printing applications **461**, 263
Logistic differential equation: A general equation for electrointercalation processes? **475**, 190
On the use of the quadratic logistic differential equation for the interpretation of electrointercalation processes **460**, 161
Spectroelectrochemical investigations on the reduction of thin films of hexadecafluorophthalocyaninatozinc (F_{16}PcZn) **476**, 148
Electrocoating
Investigation of the cathodic electropolymerization of acrylonitrile, ethylacrylate and methylmethacrylate by coupled quartz crystal microbalance analysis and cyclic voltammetry **472**, 83
Electrocrystallization parameters
A new approach to the estimation of electrocrystallization parameters **474**, 69
Electrode | electrolyte interface
A non-primitive model for the electrode | electrolyte interface based on the Percus–Yevick theory. Analysis of the different molecular sizes, ion valences and electrolyte concentrations **460**, 135
Electrode kinetics
A contribution to the study of the electroreduction of 2-chloro-4,6-di(ethylamino)-1,3,5-triazine (simazine) on mercury electrodes **474**, 174
Electrodeposition
An electrochemical alcohol sensor based on a co-electrodeposited Pt | WO_3 electrode **471**, 151
An in situ UV-vis and IR spectroelectrochemical study of the deposition of a hydroquinone anion salt on platinum electrodes from dichloromethane solutions **462**, 266
Anodic electrodeposition of conducting cobalt oxyhydroxide films on a gold surface. XPS study and electrochemical behaviour in neutral and alkaline solution **476**, 54
Atom-by-atom growth of cadmium sulfide thin films by electroreduction of aqueous Cd^{2+}–SCN^- complex **473**, 209
Electrochemical behaviour of *N*-aminopyridinium, and the viologens *N*,*N*′-diamino-4,4′-bipyridilium and *N*,*N*′-bis(4-aminophenyl)-4,4′-bipyridilium in aqueous acid: towards the formation of polymer hybrids of pyridine and aniline **462**, 43
Electrochemical quartz crystal microbalance study of electrodeposited ruthenium **474**, 167
Electrodeposition method for controlled formation of CdS films from aqueous solutions **473**, 217
Electrodeposition of copper from cuprous cyanide electrolyte: I. Current distribution on a stationary disk **474**, 16
Electrodeposition of copper from cuprous cyanide electrolyte: II. Current distribution on a rotating disk **474**, 31
Electrodeposition of zinc + iron alloys: I. Analysis of the initial stages of the anomalous codeposition **469**, 139
Electrodeposition of zinc + iron alloys: II. Relation between the stripping results and ex-situ characterization **475**, 66
In situ surface Raman study of the phosphorus incorporation mechanism during electrodeposition of Ni–P alloys **469**, 79
Nucleation and growth of poly(3,4-ethylenedioxythiophene) in acetonitrile on platinum under potentiostatic conditions **472**, 103
Synthesis, redox behavior and electrodeposition of biferrocene-modified gold clusters **473**, 113
The kinetics of mercury nucleation from Hg_2^{2+} and Hg^{2+} solutions on vitreous carbon electrodes **464**, 39
Tin electrodeposition on carbon electrodes. From nuclei to microcrystallites **465**, 63
Two-dimensional metal deposition at the liquid|liquid interface; potential and magnetohydrodynamic pattern transition **473**, 54
Electrode reaction
Analysis of the temperature dependence of the α and β coefficients of the electrode reactions in the Cr(III)/Cr(II) and Cr(II)/Cr(Hg) systems **471**, 62
Determination of the entropy change of the electrode reaction by an ac electrochemical–thermal method **469**, 1
Enhanced electrostatic interactions for selective and controllable permeation of ionic species at a monolayer of self-assembled dicationic nickel complex **465**, 177
Salt and isotope effects upon a multistep electrode reaction: the reduction of nitromethane on mercury **474**, 60

Electrode topography influence
Voltammetric anodic stripping of silver from platinum electrodes consisting of an array of nm-sized voids **477**, 14
Electrogenerated chemiluminescence
Two-dimensional CCD detection of electrogenerated chemiluminescence (ECL) on an electrode surface. ECL reactions involving microcrystals of the perylene dimer cation radical salt **473**, 166
Electrografting
Investigation of the cathodic electropolymerization of acrylonitrile, ethylacrylate and methylmethacrylate by coupled quartz crystal microbalance analysis and cyclic voltammetry **472**, 83
Electrohydrodimerization
Fumarodinitrile electrohydrodimerization and acrylonitrile electroreduction on liquid gallium: a comparison with mercury **462**, 127
Electroless metal deposition
Simultaneous platinum deposition and formation of a photoluminescent porous silicon layer **469**, 48
Electroless plating
Electroless copper plating on a glass substrate coated with ZnO film under UV illumination **462**, 259
Scanning probe lithography for electrode surface modification **473**, 230
Electrolysis
Cathodic reduction of 2-nitronaphthothiophen-4,9-quinone: evidence of catalysis by proton donors and its simulation **462**, 195
Electro-oxidation of *meso*-erythritol on platinum in acid medium: analysis of the reaction products **464**, 101
Mechanistic investigation of the anodic oxidation of *p*-methoxytoluene in dry and wet acetonitrile **464**, 85
Electrolysis: IR reflectance spectroscopy
In-situ infrared reflectance spectroscopic study of propanediol electrooxidation at platinum and gold: Part 1. 1,3-Propanediol **463**, 63
Electrolyte
An impedance study of the metal sulfide $Cu_xZn_{(1-x)}S$ | electrolyte interface **469**, 43
Inhibition effects of polyacrylonitrile gel electrolytes on lithium dendrite formation **472**, 142
Thermodynamics for the situation where there is a discontinuous change of the electrode condition with potential due to the formation of a two dimensional condensed phase—diffuse layer effects **463**, 9
Electrolyte conductivity
Conductivity study on lithium bromide in propylene carbonate + acetonitrile mixtures in dilute solutions from −35 to 75°C **471**, 78
Electrolyte phenomena
Polycrystalline gold electrode redox behavior in an ammoniacal electrolyte: Part I. A parallel RRDE, EQCM, XPS and TOF-SIMS study of supporting electrolyte phenomena **460**, 131
Electrolyte solutions
The influence of the ions on the capacity of liquid | liquid interfaces **467**, 203
Electrolytic capacitor
Formation of Al–Zr composite oxide films on aluminum by sol–gel coating and anodizing **473**, 250
Electron-conducting polymers
Electrochemical and photoelectrochemical behaviour of poly-3-methylthiophene and polybithiophene in non-aqueous solutions: 1. Dark and light processes in systems with and without cathodic doping **463**, 190
Electronic interactions
Anodic oxidation of dipyrrolyls linked with conjugated spacers: study of electronic interactions between the polypyrrole chain and the spacers **479**, 3
Electronic properties
Graphite photoelectrochemistry 2. Photoelectrochemical studies of highly oriented pyrolitic graphite **476**, 118
Electron microscopy
Structure and electrochemical behavior of a flavin sulfide monolayer adsorbed on gold **472**, 147
Electron transfer
A new approach to electrode kinetics and dynamics by potential modulated Fourier transform infrared spectroscopy **473**, 34
Chiroselective electron transfer at enantiomer-capped ZnO nanocrystalline surfaces **473**, 117
Electrochemical selectivity for redox systems at oxygen-terminated diamond electrodes **473**, 173
Electrochemical study of self-assembled monolayers of a β-cyclodextrin methyl sulfide covalently linked to anthraquinone **465**, 209
Electron transfer in retrospect and prospect: 1: Adiabatic electrode processes **460**, 5
Erratum to: Electron transfer in retrospect and prospect 1: Adiabatic electrode processes **470**, 170
Investigating the reduction characteristics of transient free radicals by laser-pulse electron photo-injection—mechanism diagnostic criteria and determination of reactivity parameters from time-resolved experiments **463**, 157
Mass transport accompanied with electron transfer between the gold electrode modified with 11-ferrocenylundecanethiol monolayer and redox species in solution — an electrochemical quartz crystal microbalance study **474**, 94
The role of the potential distribution at the electrode interface in determining the electron transfer rate constant **465**, 96
Structural identifiability of adsorption and electron transfer processes in metal dissolution and passivation mechanisms **471**, 1
Electron transfer kinetic parameter
Voltammetric determination of electron transfer kinetic parameters in hydroquinone-terminated self-assembled monolayers on gold **476**, 177
Electron-transfer kinetics
Electroanalytical chemistry of myoglobin with modification of distal histidine by cyanated imidazole **468**, 9
Electron tunneling
Assessing the apparent effective thickness of alkanethiol self-assembled monolayers in different concentrations of $Fe(CN)_6^{3-}$ / $Fe(CN)_6^{4-}$ by ac impedance spectroscopy **470**, 9
Separation of pinhole and tunneling electron transfer processes at self-assembled polymeric monolayers on gold electrodes **470**, 114
Electron tunneling constant
Voltammetric determination of electron transfer kinetic parameters in hydroquinone-terminated self-assembled monolayers on gold **476**, 177
Electrooxidation
Electrochemical nitration of naphthalene in the presence of nitrite ion in aqueous non-ionic surfactant solutions **470**, 157
Infrared spectroelectrochemistry of the oxidation of absolute methanol at a platinum electrode **464**,
Electrophoretic deposition
Preparation of clay-modified electrodes by electrophoretic deposition of clay films **462**, 143
Electropolymerisation
Electropolymerization of methacrylonitrile on a rotating disk electrode at high spinning rate **470**, 14
Kinetics of electrocatalytic oxidation of formaldehyde on a nickel porphyrin-based glassy carbon electrode **469**, 18

Sonoassisted electrooxidative polymerisation of salicylic acid: role of acoustic streaming and microjetting **462**, 181
Electropolymerization
A glucose biosensor based on enzyme entrapment within polypyrrole films electrodeposited on mesoporous titanium dioxide **469**, 176
Anodic oxidation of various arylene-cyanovinylenes made of alternating fluorenyl, thienyl and/or phenyl units **466**, 144
Electrochemical formation and spectroelectrochemical characterization of organometallic $[Ru(L)(CO)_2]_n$ polymers; L = disubstituted-2,2′-bipyridine **466**, 187
Electropolymerization of methacrylonitrile and *N*-vinyl-2-pyrrolidone as probed by an EQCM **465**, 200
Electropolymerization of 2-methoxy aniline. Electrochemical and spectroscopical product characterization **471**, 180
Nickel(II) tetraaza macrocycle modified electrodes for the electrocatalytic determination of L-ascorbic acid by the flow injection method **468**, 85
Polymer chain encapsulation followed by a quartz microbalance during electropolymerization of bithiophene-β-cyclodextrin host–guest compounds in aqueous solution **476**, 1
Rapidly renewable and reproducible electropolymerized surface at a monomer modified carbon paste electrode **465**, 102
Spectroelectrochemical study of the influence of anions on the behaviour of poly(*N*-vinylcarbazole) films **475**, 1
Ultra-fast electropolymerization of pyrrole in aqueous media on oxidizable metals in a one-step process **478**, 92
Electroreduction
A study of the bielectronic electro-reduction of cercosporin phytotoxin in highly acidic non-aqueous medium **465**, 225
Electrochemical study of β-nitrostyrene derivatives: steric and electronic effects on their electroreduction **466**, 90
Electroreduction of nitrate ion to nitrite and ammonia on a gold electrode in acidic and basic sodium and cesium nitrate solutions **470**, 46
Self-protonation mechanism in the electrochemical reduction of Jatropholone **466**, 99
The voltammetric reduction of some benzenesulfonyl fluorides, simulation of the ECE mechanism and determination of the potential variation of the transfer coefficient by using the compounds with two reducible groups **471**, 14
Electroreduction of dioxygen
Cobalt(II) metallated hematoporphyrin IX and protoporphyrin IX immobilized on niobium(V) oxide grafted on a silica gel surface: electrochemical studies **477**, 158
Electroreflectance
Frequency dependent electrolyte electroreflectance at semiconductor | electrolyte interfaces **462**, 251
The role of the potential distribution at the electrode interface in determining the electron transfer rate constant **465**, 96
Electrosorption
Discontinuous immitance due to a saddle node bifurcation: II: Tangent bifurcation and critical slowdown during isotherm branch switching **460**, 226
Electrochemical investigation of 1,5-pentanediol adsorption on the Ag(111) and Ag(110) faces **467**, 217
Influence of adsorption of guanidonium cations on H upd at Pt(*hkl*) surfaces: lattice-specific anion-mimetic effects **467**, 30
Kinetics of sulfide ion adsorption at copper amalgam electrode **463**, 200
Small signal (local) analysis of electrocatalytic reaction. Pole-zero approach **465**, 119
The potentiodynamic behaviour of iridium electrodes in aqueous 3.7 M H_2SO_4 in the 293–195 K range **461**, 40
Electrotherapy
Electrochemical treatment of tumours: a simplified mathematical model **460**,
Ellipsometry
Effect of ultra-violet light irradiation on anodic oxide films on titanium in sulfuric acid solution **473**, 272
Investigation of the cathodic electropolymerization of acrylonitrile, ethylacrylate and methylmethacrylate by coupled quartz crystal microbalance analysis and cyclic voltammetry **472**, 83
Emersed electrochemical interface
Surface Raman scattering of interfaces at Ag electrodes emersed from dimethylsulfoxide: spectroscopic evidence for an emersion-induced potential shift **479**, 32
Enantioselectivity
Enantioselective electrodes: stereoselective electroreduction of 4-methylbenzophenone and acetophenone **461**, 94
Encapsulation
Polymer chain encapsulation followed by a quartz microbalance during electropolymerization of bithiophene-β-cyclodextrin host–guest compounds in aqueous solution **476**, 1
Entropy change
Determination of the entropy change of the electrode reaction by an ac electrochemical–thermal method **469**, 1
Environmental electroanalysis
Novel polymer-modified electrodes for batch injection sensors and application to environmental analysis **468**, 26
Enzyme catalysis
A non-compartmentalized glucose | O_2 biofuel cell by bioengineered electrode surfaces **479**, 64
Electrochemical evaluation of the reaction rate between methyl viologen mediator and diaphorase enzyme for the electrocatalytic reduction of NAD^+ and digital simulation for its voltammetric responses **465**, 153
Enzyme immobilized electrode
Electrochemical characterization of an enzyme electrode based on a ferrocene-containing redox polymer **468**, 193
Epitaxial growth
Atom-by-atom growth of cadmium sulfide thin films by electorreduction of aqueous $Cd^{2+}-SCN^-$ complex **473**, 209
Epitaxial growth of a palladium layer on an Au(100) electrode **473**, 2
EQCM
An electrochemical quartz crystal microbalance study of the hydrogen underpotential deposition at a Pt electrode **467**, 186
A monomer–dimer equilibrium in self-assembled monolayers of *N*-ethyl-*N*′-octadecylviologen on the electrode surface. The influence of water content and hexafluorophosphate ion **466**, 67
Cyclic voltammetry and quartz crystal microgravimetry study of autocatalytic copper(II) reduction by cobalt(II) in ethylenediamine solutions **465**, 142
Diamond-like carbon electrodes in electrochemical microgravimetry **464**, 230
Direct experimental evidence proving the formation of surface layers in the course of the reduction of Cr(VI) species at a gold electrode **471**, 73
Electrochemical and EQCM studies on the assembly of asymmetric viologen on bare and alkanethiol-coated Au electrodes **477**, 52
Electrochemical quartz crystal microbalance and in situ infrared spectroscopic studies on the redox reaction of Prussian blue **474**, 101
Mass transport accompanied with electron transfer between the gold electrode modified with 11-ferrocenylundecanethiol monolayer and redox species in solution — an electrochemical quartz crystal microbalance study **474**, 94
Mass transport behavior of polypyrrole and poly(*N*-methylpyrrole) films in acetonitrile solutions **468**, 104

Polycrystalline gold electrode redox behavior in an ammoniacal electrolyte: Part II. A parallel RRDE, EQCM and TOF-SIMS study of copper underpotential deposition **460**, 143
Equivalent circuit
Theoretical models for ac impedance of finite diffusion layers exhibiting low frequency dispersion **475**, 152
Erythritol
Electro-oxidation of *meso*-erythritol on platinum in acid medium: analysis of the reaction products **464**, 101
Escherichia coli
1-Naphthyl phosphate as an enzymatic substrate for enzyme-linked immunomagnetic electrochemistry **469**, 27
Etching
Scanning probe lithography for electrode surface modification **473**, 230
Ethanol
A comparison of multistability in the electrocatalyzed oxidations of methanol and ethanol in acid and alkaline solutions **478**, 108
Ethanol oxidation on PtRu electrodes studied by differential electrochemical mass spectrometry **472**, 120
Ethylacrylate
Investigation of the cathodic electropolymerization of acrylonitrile, ethylacrylate and methylmethacrylate by coupled quartz crystal microbalance analysis and cyclic voltammetry **472**, 83
Ethylamine
Oxidation of methylamine and ethylamine on Pt single crystal electrodes in acid medium **469**, 159
Ethylenediamine
Cyclic voltammetry and quartz crystal microgravimetry study of autocatalytic copper(II) reduction by cobalt(II) in ethylenediamine solutions **465**, 142
Euler's theorem
A reply to the question of whether the internal energy of solid interfaces can be of a non-homogeneous nature **472**, 174
Can the internal energy function of solid interfaces be of a non-homogeneous nature? **472**, 168
Exchange current density
A new approach to metal electrodeposition at a periodically changing rate: Part I. The reversing overpotential method **464**, 245
Kinetic and mechanistic study of hydroxyl ion electrosorption at the Pt(111) surface in alkaline media **466**, 155
Excitors
Photoelectrochemical studies with inorganic cage structures of metal dichalcogenides **473**, 186
Experimental design
Structural properties of electrochemically designed porous oxide films on AlMgl **468**, 121
Extended X-ray absorption fine structure
In situ and model EXAFS studies of electrocatalysts for methanol oxidation **460**, 80
Extrusion
Determination of the surface charge density of a mercury electrode by extrusion: a new method for correction of the faradaic component **468**, 150

Facilitated ion transfer
Voltammetric analysis of Cs^+-DB18C6 complex stoichiometry at the water | 1,2-dichloroethane interface **464**, 54
Factor analysis
Cadmium binding properties of the C-terminal hexapeptide from mouse metallothionein: study by linear sweep voltammetry and multivariate curve resolution analysis **468**, 202
Far infrared spectroscopy
'In-situ' observation of halide ion adsorption on a gold electrode using synchrotron far infrared spectroscopy **463**, 258
Fast cyclic voltammetry
Digital simulation of fast cyclic voltammogram by integration of the double layer charging current **464**, 215
Fast dropping electrode
The fast dropping oil | water electrode **464**, 128
Fe/85% H_3PO_4 system
Passivation mechanism of iron in concentrated phosphoric acid **475**, 58
Ferric/ferrous electrode reaction
Kinetics of the ferric/ferrous electrode reaction on Nafion®-coated electrodes **469**, 11
Ferrocene
A structural effect on electrochemical behavior of hetero-deposited redox polymer Langmuir–Blodgett films containing ferrocene and tris(bipyridine)ruthenium derivatives **473**, 125
Electrochemical response to anions by neutral ferrocenyl receptors containing 2,2′-bipyridyl arms **469**, 132
Electrochemical studies of ferrocene derivatives and their complexation by β-cyclodextrin **477**, 130
Preparation of a microperoxidase and ferrocene-immobilized polyion complex membrane for the detection of hydrogen peroxide **468**, 117
Silicon-based ferrocenyl dendrimers as anion receptors in solution and immobilized onto electrode surfaces **463**, 87
Ferrocene derivative
Electrochemical characterization of an enzyme electrode based on a ferrocene-containing redox polymer **468**, 193
Ferrocenemethanol
Addition of α-hydroxyalkylferrocenes to electrochemically oxidized poly(aniline) **470**, 166
Ferrocene-terminated alkanethiol
Exchange of self-assembled thiol monolayers on gold: characterization by FT-IR external reflection spectroscopy **468**, 91
11-Ferrocenylundecanethiol
Mass transport accompanied with electron transfer between the gold electrode modified with 11-ferrocenylundecanethiol monolayer and redox species in solution — an electrochemical quartz crystal microbalance study **474**, 94
FeTMPP
Heat-treated iron(III) tetramethoxyphenyl porphyrin chloride supported on high-area carbon as an electrocatalyst for oxygen reduction: Part II. Kinetics of oxygen reduction **462**, 63
Film
Electrodeposition method for controlled formation of CdS films from aqueous solutions **473**, 217
Simultaneous in-situ conductivity and cyclic voltammetry characterization of Li-ion intercalation into thin V_2O_5 films **479**, 12
Film growth
Capacitance and photocurrent study of electronic properties of anodic oxide films on Nb and Ta. Evaluation of the ionized donor concentration profile in Nb_2O_5 film **460**, 214
Film resonance
Mechanical resonance effects in electroactive polycarbazole films **460**, 267
Film thickness
Effects of polymer thickness on the potentiometric pH responses of polypyrrole modified glassy carbon electrodes **476**, 109
Filter-press reactors
Evaluation of a reactor model and cathode materials for batch electrolysis of L-cystine hydrochloride **462**, 97
Finite element
Finite element simulation of ion transfer reactions at a single micro-liquid | liquid interface supported on a thin polymer film **468**, 42

Finite element method
Steady-state currents at inlaid and recessed microdisc electrodes for first-order EC′ reactions **476**, 132
Finite surface strain
The Shuttleworth equation for a finite surface strain **471**, 105
First transition metal cations
Metal ion complexes derived from the α_1 isomer of $(P_2W_{17}O_{61})^{10-}$: comparison with the corresponding α_2 species **478**, 76
Fitting of spectra
Spectroelectrochemistry for a coupled chemical reaction in the channel cell: Part II. Kinetics of hydrolysis and the absorption spectrum of *p*-benzoquinoneimine **464**, 181
Flat pyramidal islands
Structural changes at the Pt(100) surface with a great number of potential cycles **460**, 251
Flavins
Structure and electrochemical behavior of a flavin sulfide monolayer adsorbed on gold **472**, 147
Flow injection analysis
A review of a new voltammetric method for determining acids **468**, 53
Nickel(II) tetraaza macrocycle modified electrodes for the electrocatalytic determination of L-ascorbic acid by the flow injection method **468**, 85
Flow system
Oxidation of CO adlayers on Pt(111) at low potentials: an impinging jet study in H_2SO_4 electrolyte with mathematical modeling of the current transients **467**, 74
Flow-through electrochemical cell
Flow-through electrochemical cell for accurate pH measurements at temperatures up to 400°C **463**, 146
Fluorenone
Immobilized nitro-fluorenone derivatives as electrocatalysts for NADH oxidation **477**, 79
Fluoride solutions
Simultaneous platinum deposition and formation of a photoluminescent porous silicon layer **469**, 48
Fluorinating reagents
Electrochemical studies of six N–F electrophilic fluorinating reagents **474**, 1
Formaldehyde
Kinetics of electrocatalytic oxidation of formaldehyde on a nickel porphyrin-based glassy carbon electrode **469**, 18
Formamidine disulphide electrochemical reactions
Electrochemical response of thiourea and formamidine disulphide on polycrystalline platinum in aqueous 0.5 M sulphuric acid **475**, 181
Formic acid
Construction of a new dehydrogenation system using a two-compartment cell separated by a palladized Pd sheet electrode **463**, 116
Fourier transform infrared spectroscopy (FTIR)
Electrochemical oxidation of pyrite (FeS_2) in aqueous electrolytes **471**, 116
Fractionation factor
Anomalous H/D isotopic effect in the kinetics of polarographic hydrogen evolution **477**, 62
Frumkin isotherm
Discontinuous immitance due to a saddle node bifurcation: II: Tangent bifurcation and critical slowdown during isotherm branch switching **460**, 226
Kinetic and mechanistic study of hydroxyl ion electrosorption at the Pt(111) surface in alkaline media **466**, 155
Frumkin repulsion effect
Modeling galvanostatic potential oscillations in the electrocatalytic iodate reduction system **462**, 19
FT-IR
A new approach to electrode kinetics and dynamics by potential modulated Fourier transform infrared spectroscopy **473**, 34
Electrochemical and EQCM studies on the assembly of asymmetric viologen on bare and alkanethiol-coated Au electrodes **477**, 52
FT-IR external reflection spectroscopy
Exchange of self-assembled thiol monolayers on gold: characterization by FT-IR external reflection spectroscopy **468**, 91
FT-IRRAS
Oxidation of methylamine and ethylamine on Pt single crystal electrodes in acid medium **469**, 159
FTIRS
Urea adsorption on Pt(111) electrodes **461**, 65
FTIR spectroscopy
Electrochemical behaviour of amino acids on Pt(*hkl*). A voltammetric and in situ FTIR study: Part IV. Serine and alanine on Pt(100) and Pt(110) **475**, 38
In-situ FTIR studies on the electrochemical oxidation of histidine and tyrosine **463**, 218
In situ infrared spectroscopic investigations of sulfate adsorption at the Ag(111) electrode surface **467**, 291
In situ infrared study of cytosine adsorption on gold electrodes **460**, 188
The adsorption of methylamine on Pt single crystal surfaces **467**, 105
FT-SERS
In-situ monitoring of the interaction of lactate dehydrogenase with NAD on a gold electrode by FT-SERS **465**, 187
Fuel cell
Behaviour of titanium species in molten $Li_2CO_3 + Na_2CO_3$ and $Li_2CO_3 + K_2CO_3$ in the anodic conditions used in molten carbonate fuel cells: II. Electrochemical intercalation of Li^+ in Li_2TiO_3 at 600 and 650°C **474**, 9
Enhancement of the electrocatalytic O_2 reduction on Pt–Fe alloys **460**, 258
Fumarodinitrile
Fumarodinitrile electrohydrodimerization and acrylonitrile electroreduction on liquid gallium: a comparison with mercury **462**, 127
Functionalized polypyrrole
Electrochemical recognition of metal cations by poly(crown ether ferrocene) films investigated by cyclic voltammetry and electrochemical impedance spectroscopy **464**, 24
Electrodeposition of copper into functionalized polypyrrole films **474**, 113
Furan
The electrochemical copolymerization of pyrrole and furan in a novel binary solvent system **470**, 23

GaAs-p electrode
Oxygen reduction mechanisms at p-InP and p-GaAs electrodes in liquid ammonia in neutral buffered medium and acidic media **462**, 88
Gallium electrode
Electrode kinetics and the nature of the metal electrode: Part 4. The Zn(II)/Zn electrode reaction studied at dropping Tl + Ga alloy electrodes **472**, 64
Electrode kinetics and the nature of the metal electrode: Part 3. The Zn(II)/Zn electrode reaction studied at In + Ga dropping (micro)electrodes **472**, 53
Galvanic tungsten
On the pH sensitivity of the galvanic tungsten–water interaction product **472**, 178

Gas bubbles
Detection of near-wall hydrodynamic effects by electrochemiluminescence **470**, 89
Gas electrodes
Electrochemical characterisation of Pd modified ceramic | carbon electrodes: partially flooded versus wetted channel hydrophobic gas electrodes **466**, 45
D-Glucose
Platinum–palladium loaded polypyrrole film electrodes for the electrooxidation of D-glucose in neutral media **476**, 171
Genetic algorithm
A new approach to the estimation of electrocrystallization parameters **474**, 69
Gibbs adsorption equation
A reply to the question of whether the internal energy of solid interfaces can be of a non-homogeneous nature **472**, 174
GITT
Determination of the Li ion chemical diffusion coefficient for the topotactic solid-state reactions occurring via a two-phase or single-phase solid solution pathway **477**, 32
Glass substrates
Electroless copper plating on a glass substrate coated with ZnO film under UV illumination **462**, 259
Glassy carbon
Characterization of electrochemically deposited gold nanocrystals on glassy carbon electrodes **466**, 234
Electrocatalytic oxidation of methanol at a nickel hydroxide/glassy carbon modified electrode in alkaline medium **471**, 89
Origin of the infrared reflectance increase produced by the adsorption of CO on particulate metals deposited on moderately reflecting substrates **465**, 234
Glassy carbon electrodes
Catalytic reduction of 1,8-diiodooctane by electrogenerated cobalt(I) salen and formation of μ-(1,8-*n*-octyl)-bis[-(salen)cobalt(III)] **460**, 207
Characterization of the surface carbonyl and hydroxyl coverage on glassy carbon electrodes using Raman spectroscopy **469**, 150
Glucose
Renewable silica sol–gel derived carbon composite based glucose biosensor **460**, 234
Glucose detection
Ruthenium purple-containing zeolite modified electrodes and their application for the detection of glucose **466**, 82
Glucose oxidase
A glucose biosensor based on enzyme entrapment within polypyrrole films electrodeposited on mesoporous titanium dioxide **469**, 176
Glucose sensor
Electrochemical characterization of an enzyme electrode based on a ferrocene-containing redox polymer **468**, 193
Gold
Adsorption, oxidation and reduction reactions of propargyl alcohol on palladium as studied by electrochemical mass spectrometry **472**, 71
Direct experimental evidence proving the formation of surface layers in the course of the reduction of Cr(VI) species at a gold electrode **471**, 73
Investigation of the structure of self-assembled monolayers of asymmetrical disulfides on Au(111) electrodes by electrochemical desorption **473**, 68
Kinetics of the ferric/ferrous electrode reaction on Nafion®-coated electrodes **469**, 11
Surface structural transitions induced by repetitive underpotential deposition of Ag on Au(111) **474**, 138
Gold and silver electrodes
Structural differences in self-assembled monolayers of anthraquinone derivatives on silver and gold electrodes studied by cyclic voltammetry and in situ SERS spectroscopy **478**, 83
Gold cluster
Synthesis, redox behavior and electrodeposition of biferrocene-modified gold clusters **473**, 113
Gold electrode
Adsorption characteristics of $Fe(CN)_6^{3-/4-}$ on Au colloids as monolayer films on cysteamine-modified gold electrode **466**, 26
Adsorption of pyridine on a polycrystalline gold electrode surface studied by infrared reflection absorption spectroscopy **470**, 136
Anodic electrodeposition of conducting cobalt oxyhydroxide films on a gold surface. XPS study and electrochemical behaviour in neutral and alkaline solution **476**, 54
In-situ monitoring of the interaction of lactate dehydrogenase with NAD on a gold electrode by FT-SERS **465**, 187
'In-situ' observation of halide ion adsorption on a gold electrode using synchrotron far infrared spectroscopy **463**, 258
Mass transport accompanied with electron transfer between the gold electrode modified with 11-ferrocenylundecanethiol monolayer and redox species in solution — an electrochemical quartz crystal microbalance study **474**, 94
Separation of pinhole and tunneling electron transfer processes at self-assembled polymeric monolayers on gold electrodes **470**, 114
Surface structural effects on specific adsorption of oxoanions on gold single crystal electrodes **467**, 335
Voltammetric and XPS investigations of nickel hydroxide electrochemically dispersed on gold surface electrodes **462**, 202
Gold(111) electrode
SNIFTIRS studies of the electrochemical double layer: Part II. Au(111) electrode in solutions with specifically adsorbed nitrate ions **467**, 325
Gold nanocrystals
Characterization of electrochemically deposited gold nanocrystals on glassy carbon electrodes **466**, 234
Gold surface adsorption
Combined quartz crystal impedance and electrochemical impedance measurements during adsorption of bovine serum albumin onto bare and cysteine- or thiophenol-modified gold electrodes **478**, 1
Gold surfaces
Structure and growth in metal epitaxy on low-index Au surfaces—a comparison between solid | electrolyte and solid | vacuum interfaces **467**, 258
Grafting
Electropolymerization of methacrylonitrile and *N*-vinyl-2-pyrrolidone as probed by an EQCM **465**, 200
Electropolymerization of methacrylonitrile on a rotating disk electrode at high spinning rate **470**, 14
Grain boundary
Evolution of a skeleton structured TiO_2 surface consisting of grain boundaries **473**, 204
Graphite
Graphite photoelectrochemistry 2. Photoelectrochemical studies of highly oriented pyrolitic graphite **476**, 118
Graphite intercalation compounds
A quantitative discrimination between anion insertion- and surface redox-reactions at graphite with the rotating ring/disk-electrode **461**, 167
Graphitized carbon
Enhancement of the electrochemical Li doping/undoping reaction rate of a graphitic material by an evaporated film of Sn, Zn or Pb **462**, 150

Guanidonium ions
Influence of adsorption of guanidonium cations on H upd at Pt(*hkl*) surfaces: lattice-specific anion-mimetic effects **467**, 30

Halide
Electrochemical oscillations of a new type in an $H_2O_2 + H_2SO_4$ | Pt-electrode system, appearing by addition of small amounts of halide ions **473**, 156
In situ scanning tunneling microscopy of Cu(110): atomic structures of halide adlayers and anodic dissolution **473**, 10
Oxidation of halides by redox enhanced ferricyanide in the $[Fe^{II}–CN–Pt^{IV}]_n$ coordination polymer: an optically triggered process **470**, 99

Halide ion
Adsorption of pyridine on a polycrystalline gold electrode surface studied by infrared reflection absorption spectroscopy **470**, 136

Halide ion adsorption
Interfacial structure of dimethylsulfoxide at Ag electrodes from surface enhanced Raman scattering and differential capacitance **479**, 21

p-Halogenoanilines
Voltammetric investigation of the anodic dimerization of *p*-halogenoanilines in DMF: Reactivity of their electrogenerated cation radicals **462**, 55

Hardness
Nano-mechano-electrochemistry of the iron (100) surface in solution **473**, 49

HCOOH electrooxidation
Studies of kinetics of HCOOH oxidation on Pt(100), Pt(110), Pt(111), Pt(510) and Pt(911) single crystal electrodes **467**, 121

Hematoporphyrin IX
Cobalt(II) metallated hematoporphyrin IX and protoporphyrin IX immobilized on niobium(V) oxide grafted on a silica gel surface: electrochemical studies **477**, 158

Hemepeptide
Diffusionless electron transfer of microperoxidase-11 on gold electrodes **469**, 123

Hemeproteins
Characterization of protein monolayers by surface plasmon resonance combined with cyclic voltammetry 'in situ' **464**, 198

Hemoglobin
Enhanced electron transfer for hemoglobin in poly (ester sulfonic acid) films on pyrolytic graphite electrodes **463**, 53

Hetero-deposited Langmuir–Blodgett film
A structural effect on electrochemical behavior of hetero-deposited redox polymer Langmuir–Blodgett films containing ferrocene and tris(bipyridine)ruthenium derivatives **473**, 125

Heteropolyanion
Coupled electron and proton transfers: compared behaviour of oxometalates in aqueous solution or after entrapment in polymer matrices **463**, 129

Heteropolyoxometalates
Synthesis, characterisation and voltammetric study of a β-Keggin-type $[PW_{12}O_{40}]^{3-}$ complex **465**, 129

Hg electrodeposition
Early stages of mercury electrodeposition on HOPG **470**, 120

High-area carbon
Heat-treated iron(III) tetramethoxyphenyl porphyrin chloride supported on high-area carbon as an electrocatalyst for oxygen reduction: Part II. Kinetics of oxygen reduction **462**, 63

High concentration analysis
Amperometric ion-selective electrode. Voltammetric theory and analytical applications at high concentration and trace levels **468**, 34
Erratum to: Amperometric ion-selective electrode. Voltammetric theory and analytical applications at high concentration and trace levels **475**, 90

Higher Miller index
Structural changes at various Pt single crystal surfaces with potential cycles in acidic and alkaline solutions **467**, 85

Highly cross-linked polyviologen film
Voltammetric anion recognition by a highly cross-linked polyviologen film **473**, 145

High pressure electrolysis
Electrochemical formation of nickel hydride in alkaline solutions **472**, 182

High temperature
Behaviour of titanium species in molten $Li_2CO_3 + Na_2CO_3$ and $Li_2CO_3 + K_2CO_3$ in the anodic conditions used in molten carbonate fuel cells: II. Electrochemical intercalation of Li^+ in Li_2TiO_3 at 600 and 650°C **474**, 9

High temperature subcritical and supercritical aqueous solutions
Flow-through electrochemical cell for accurate pH measurements at temperatures up to 400°C **463**, 146

Histidine
In-situ FTIR studies on the electrochemical oxidation of histidine and tyrosine **463**, 218

Hole-array electrode
Change of hole size of Pd hole-array electrodes in a controlled fashion by cathodic polarization in acidic electrolyte **473**, 240

Homogeneous functions
Can the internal energy function of solid interfaces be of a non-homogeneous nature? **472**, 168

Homogeneous reaction
Application of Danckwerts' expression to first-order EC′ reactions. Transient currents at inlaid and recessed microdisc electrodes **466**, 15
Steady-state currents at inlaid and recessed microdisc electrodes for first-order EC′ reactions **476**, 132

Homopolar ion-exchange membranes
Steady-state ion transport through homopolar ion-exchange membranes: an analytical solution of the Nernst–Planck equations for a 1:1 electrolyte under the electroneutrality assumption **460**, 53

HOPG
Graphite photoelectrochemistry 2. Photoelectrochemical studies of highly oriented pyrolitic graphite **476**, 118
Voltammetric and spectroscopic study of the adsorption of alkyl viologens on a HOPG electrode **473**, 138

H_2O_2 reduction
Electrochemical and electrocatalytic properties of tetra-iron substituted sandwich-type pentadecatungstodiphosphate heteropolyanions **476**, 85

Horse heart cytochrome *c*
Electrochemical studies on *c*-type cytochromes at microelectrodes **464**, 76

Host–guest inclusion compounds
Polymer chain encapsulation followed by a quartz microbalance during electropolymerization of bithiophene-β-cyclodextrin host–guest compounds in aqueous solution **476**, 1

Hot electrons
Graphite photoelectrochemistry 2. Photoelectrochemical studies of highly oriented pyrolitic graphite **476**, 118

Hot holes
Graphite photoelectrochemistry 2. Photoelectrochemical studies of highly oriented pyrolitic graphite **476**, 118

HPLC analysis
Electrooxidation of the antileukemic 2-chloro-2′-deoxyadenosine and related compounds **477**, 89
Hydralazine
Ionic partition diagrams of ionisable drugs: pH-lipophilicity profiles, transfer mechanisms and charge effects on solvation **462**, 235
Hydrated ruthenium oxyhydroxide
Impedance of ruthenium electrodes in sulphuric acid solution **463**, 29
Hydration
MRA combined spectroelectrochemical studies on the redox stability of PPy/DS films **462**, 1
Hydrazine oxidation
Electrocatalytic oxidation of hydrazine at a chlorogenic acid (CGA) modified glassy carbon electrode **465**, 168
Hydrodynamic imaging
Detection of near-wall hydrodynamic effects by electrochemiluminescence **470**, 89
Hydrodynamic voltammetry
Electrochemical behavior of a *Cypridina* luciferin analogue in acetonitrile solutions in the presence of proton acceptors **476**, 46
Hydrogen
Discussion on permeation transients in terms of insertion reaction mechanism and kinetics **465**, 37
Electrochemical determination of hydrogen in metals **475**, 82
Electrode reactions and accumulation of hydrogen at carbon paste electrodes in the presence of tetrachloropalladate **462**, 174
Review and theoretical analysis of ac–av methods for the investigation of hydrogen insertion I. Diffusion formalism **462**, 73
The study of hydrogen sorption in palladium limited volume electrodes (Pd-LVE): I. Acidic solutions **471**, 190
Hydrogen absorption in Ni–Pd electrodes
Hydrogen electrosorption in Ni–Pd alloys **460**, 30
Hydrogen adsorption
Temperature-dependent research on Pt(111) and Pt(100) electrodes in aqueous H_2SO_4 **467**, 177
Hydrogenase
Mechanism of the catalysis by *Alcaligenes eutrophus* H16 hydrogenase of direct electrochemical reduction of NAD^+ **468**, 139
Hydrogenation
Mass spectrometric study of desorption and hydrogenation of biphenyl, naphthalene and *t*-butylbenzene on poly- and monocrystalline platinum electrodes **461**, 90
Hydrogen bond
Hydrogen bond complexation of dimethyl-[1-butyl-2,4-dioxo-(1H,3H)pyrimido]tetrathiafulvalene with aminopyridine derivatives probed by cyclic voltammetry **463**, 212
Hydrogen bonded complex
Electrochemical behavior of gold electrodes modified with aminopurinethiol derivatives **473**, 99
Hydrogen bonding
pK_a of an ω-carboxylalkanethiol self-assembled monolayer by interaction model **478**, 101
Hydrogen evolution
Anomalous H/D isotopic effect in the kinetics of polarographic hydrogen evolution **477**, 62
Effect of the crystallographic orientation of Ag single crystal face electrodes on the kinetics of proton discharge **467**, 164
Hydrogen evolution on silver single crystal electrodes—first results **461**, 76
Hydrogen evolution reaction
Structural specificity of the kinetics of the hydrogen evolution reaction on the low-index surfaces of Pt single-crystal electrodes in 0.5 M dm^{-3} NaOH **461**, 80
Hydrogen overpotential
Evaluation of a reactor model and cathode materials for batch electrolysis of L-cystine hydrochloride **462**, 97
Hydrogen peroxide
Amperometric determination of NAD(P)H with peroxidase-based H_2O_2-sensing electrodes and its application to isocitrate dehydrogenase activity assay in serum **478**, 33
Electrochemical oscillations of a new type in an $H_2O_2 + H_2SO_4$ | Pt-electrode system, appearing by addition of small amounts of halide ions **473**, 156
Preparation of a microperoxidase and ferrocene-immobilized polyion complex membrane for the detection of hydrogen peroxide **468**, 117
Hydrogen upd
An electrochemical quartz crystal microbalance study of the hydrogen underpotential deposition at a Pt electrode **467**, 186
Influence of adsorption of guanidonium cations on H upd at Pt(*hkl*) surfaces: lattice-specific anion-mimetic effects **467**, 30
Hydrolysis
Electrochemical studies of ferrocene derivatives and their complexation by β-cyclodextrin **477**, 130
Hydroquinone
An in situ UV-vis and IR spectroelectrochemical study of the deposition of a hydroquinone anion salt on platinum electrodes from dichloromethane solutions **462**, 266
Hydroquinone-terminated self-assembled monolayer
Voltammetric determination of electron transfer kinetic parameters in hydroquinone-terminated self-assembled monolayers on gold **476**, 177
Hydrous oxide
Anomalous electrochemical behaviour of palladium in aqueous solution **461**, 52
Hydroxylation
Electrochemical behavior of a *Cypridina* luciferin analogue in acetonitrile solutions in the presence of proton acceptors **476**, 46
Hydroxyl groups
Characterization of the surface carbonyl and hydroxyl coverage on glassy carbon electrodes using Raman spectroscopy **469**, 150

Ideally polarizable electrode
Studies of structural disorder of self-assembled thiol monolayers on gold by cyclic voltammetry and ac impedance **464**, 61
Immiscible
The influence of the ions on the capacity of liquid | liquid interfaces **467**, 203
Immittance
Small signal (local) analysis of electrocatalytic reaction. Pole-zero approach **465**, 119
Immunobeads
Rotating disk electrode amperometric detection for a bead-based immunoassay **468**, 2
Immunochemical sensor
The electrochemistry of antibody-modified conducting polymer electrodes **470**, 144
Immunomagnetic beads
1-Naphthyl phosphate as an enzymatic substrate for enzyme-linked immunomagnetic electrochemistry **469**, 27
Impedance
A kinetic study of CdS photocorrosion by intensity modulated photocurrent and photoelectrochemical impedance spectroscopy **473**, 192
An impedance study of the metal sulfide $Cu_xZn_{(1-x)}S$ | electrolyte interface **469**, 43
Discontinuous immittance due to a saddle node bifurcation: II: Tangent bifurcation and critical slowdown during isotherm branch switching **460**, 226
Electrochemical impedance spectroscopy of thin films with two mobile charge carriers: effects of the interfacial charging **472**, 7
Electrooxidation of the antileukemic 2-chloro-2′-deoxyadenosine and related compounds **477**, 89
Small signal (local) analysis of electrocatalytic reaction. Pole-zero approach **465**, 119

Structural properties of electrochemically designed porous oxide films on AlMg1 **468**, 121
Impedance analysis
Steady state voltammetry at low electrolyte/reactant concentration ratios: what it means and what it does not mean **463**, 45
Impedance response
Current enhancing effect of poly[1-methyl-3-(pyrrol-1-yl-methyl)-pyridinium] films on the electrode reaction of anthraquinonedisulfonate **478**, 9
Impedance spectroscopy
Electrochemical investigations and morphology of poly(4,9-dihydro-*o*-benzenonaphtho[2,3-c]pyrrole) and poly(acenaphtho[1,2-c]pyrrole) **477**, 25
The electrochemistry of antibody-modified conducting polymer electrodes **470**, 144
Transfer matrix method for the electrochemical impedance of inhomogeneous porous electrodes and membranes **460**, 63
Impinging jet
Oxidation of CO adlayers on Pt(111) at low potentials: an impinging jet study in H_2SO_4 electrolyte with mathematical modeling of the current transients **467**, 74
Implicit difference method
Spectroelectrochemistry for a coupled chemical reaction in the channel cell: Part I. Theoretical simulation of an EC reaction **464**, 176
Impurity ions
Theory for water management in membranes for polymer electrolyte fuel cells: Part 1. The effect of impurity ions at the anode side on the membrane performances **465**, 1
Theory for water management in membranes for polymer electrolyte fuel cells: Part 2. The effect of impurity ions at the cathode side on the membrane performances **465**, 18
Inclusion complexes
Electrochemical studies of ferrocene derivatives and their complexation by β-cyclodextrin **477**, 130
Indirect reduction
Anthraquinones as mediators for the indirect cathodic reduction of dispersed organic dyestuffs **465**, 80
Indium electrode
Electrode kinetics and the nature of the metal electrode: Part 3. The Zn(II)/Zn electrode reaction studied at In + Ga dropping (micro)electrodes **472**, 53
Indium–gallium alloys
Indium adsorption at the surface of liquid In + Ga alloy electrodes in contact with an aqueous 1 M $NaClO_4$ solution **462**, 111
Indium oxide
Electroanalytical chemistry of myoglobin with modification of distal histidine by cyanated imidazole **468**, 9
Inert complexes
Voltammetric metal speciation in mixtures of inert and labile macromolecular complexes at any ligand-to-metal ratio: differential pulse polarographic study of the Zn(II)–nitrilotriacetate–polymethacrylate system **462**, 157
Infrared reflectance
Origin of the infrared reflectance increase produced by the adsorption of CO on particulate metals deposited on moderately reflecting substrates **465**, 234
Infrared reflection absorption spectroscopy
Comparison of a bisulfate anion adsorbed on M(111) (M = Pt, Rh, Au, Ag and Cu) **467**, 299
FTIR studies of benzoate adsorption on the Au(111) electrode **478**, 67
Infrared spectroelectrochemistry
Infrared spectroelectrochemistry of the oxidation of absolute methanol at a platinum electrode **464**, 93
Infrared spectroscopy
Adsorption of pyridine on a polycrystalline gold electrode surface studied by infrared reflection absorption spectroscopy **470**, 136
Inhibition
Inhibition effects of polyacrylonitrile gel electrolytes on lithium dendrite formation **472**, 142
Ultra-fast electropolymerization of pyrrole in aqueous media on oxidizable metals in a one-step process **478**, 92
Ink-type electrode
Heat-treated iron(III) tetramethoxyphenyl porphyrin chloride supported on high-area carbon as an electrocatalyst for oxygen reduction: Part II. Kinetics of oxygen reduction **462**, 63
Inorganic film
Enhanced stability and electrocatalytic activity of a ruthenium-modified cobalt–hexacyanoferrate film electrode **471**, 42
Inorganic fullerene-like structures
Photoelectrochemical studies with inorganic cage structures of metal dichalcogenides **473**, 186
InP
Formation of ⟨001⟩-aligned nano-scale pores on (001) n-InP surfaces by photoelectrochemical anodization in HCl **473**, 223
InP-p electrode
Oxygen reduction mechanisms at p-InP and p-GaAs electrodes in liquid ammonia in neutral buffered medium and acidic media **462**, 88
Insertion
Discussion on permeation transients in terms of insertion reaction mechanism and kinetics **465**, 37
Review and theoretical analysis of ac–av methods for the investigation of hydrogen insertion I. Diffusion formalism **462**, 73
Theoretical models for ac impedance of finite diffusion layers exhibiting low frequency dispersion **475**, 152
In situ ESR/spectroelectrochemistry
Electrochemical synthesis and structural studies of copolymers based on the electrooxidation of pyrrole and some salen compounds **470**, 77
In situ FTIR
Electrochemical quartz crystal microbalance and in situ infrared spectroscopic studies on the redox reaction of Prussian blue **474**, 101
In situ FTIR spectroscopy
Synthesis, electropolymerization and electrochemical characterization of some new acrylate substituted thiophene derivatives **460**, 176
In-situ IRAS
Redox mechanisms of NO with water on the Pt(111) electrode studied by in-situ STM and IRAS **473**, 43
In situ Raman
In situ surface Raman study of the phosphorus incorporation mechanism during electrodeposition of Ni–P alloys **469**, 79
In-situ reflection IR spectroscopy
Electrochemical and FTIR studies of 4-cyanopyridine adsorption at the gold(111) | solution interface **475**, 130
In-situ scanning tunneling microscopy (STM)
Self-organization of α-cyclodextrin on Au(111) surfaces induced by potential controlled adsorption **472**, 163
In-situ STM
Early stages of mercury electrodeposition on HOPG **470**, 120
In-situ STM investigation of specific anion adsorption on Cu(111) **467**, 307
Structural changes at various Pt single crystal surfaces with potential cycles in acidic and alkaline solutions **467**, 85
Structural changes at the Pt(100) surface with a great number of potential cycles **460**, 251
Integration analysis
Integration analysis of the cyclic voltammograms of the electrode reaction in a diffusionless system **465**, 219

Intensity modulated photocurrent spectroscopy
A kinetic study of CdS photocorrosion by intensity modulated photocurrent and photoelectrochemical impedance spectroscopy **473**, 192
Intercalation
Logistic differential equation: A general equation for electrointercalation processes? **475**, 190
Interface
An impedance study of the metal sulfide $Cu_xZn_{(1-x)}S$ | electrolyte interface **469**, 43
A sodium-specific condensed film of α-cyclodextrin at the mercury | water interface **465**, 51
Infrared spectroscopy of carbon monoxide and nitric oxide on palladium(111) in aqueous solution: unexpected adlayer structural differences between electrochemical and ultrahigh-vacuum interfaces **474**, 155
In situ visible-infrared sum and difference frequency generation at the electrochemical interface **467**, 238
Temperature and pressure dependence of O_2 reduction at Pt | Nafion® 117 and Pt | BAM® 407 interfaces **468**, 180
Interface potential
The role of the potential distribution at the electrode interface in determining the electron transfer rate constant **465**, 96
Interfacial charging
Electrochemical impedance spectroscopy of thin films with two mobile charge carriers: effects of the interfacial charging **472**, 7
Interfacial chemistry
Activity coefficients of $Al(ClO_4)_3$ in aqueous solutions: a reexamination **460**, 100
Interfacial electron-transfer
Diffusionless electron transfer of microperoxidase-11 on gold electrodes **469**, 123
Interfacial structure
Frequency dependent electrolyte electroreflectance at semiconductor | electrolyte interfaces **462**, 251
Interfacial work
A reply to the question of whether the internal energy of solid interfaces can be of a non-homogeneous nature **472**, 174
Interferometric microscopy
Electrochemically induced mass transfer and rheological changes of Nafion® coatings fully loaded with $[Os(bpy)_3]^{2+}$ **469**, 34
Interferometry
Second harmonic generation investigation of rhodamine B derivatives in Langmuir–Blodgett films **465**, 195
Intrinsic rate constant
Solvent effect on kinetics of the chloride ion cleavage from anion radicals of 4-chlorobenzophenone **464**, 259
Iodate
Studies on the catalytic reduction of iodate at glassy carbon electrodes modified by molybdenum oxides **471**, 37
Iodide
Iodide adsorption at the Au(111) electrode surface **467**, 342
Iodide ion-selective electrode
Anion-selective membrane electrodes based on polymer-supported metalloporphyrins **468**, 98
Iodine
Formation of an ordered structure of iodine adsorbed on Ni(111) and the anodic dissolution processes: in-situ STM study **467**, 282
Ion-channel sensor
Self-assembly of a tricarboxylate receptor through thioamide groups and its use for electrochemical detection of protonated amines **473**, 105
Ion-exchange
Factors influencing the ion-exchange preconcentration and voltammetric behaviour of redox cations at polyestersulfonated ionomer coated electrodes in acetonitrile solutions **460**, 38
Use of a zeolite-modified electrode for the study of the methylviologen–sodium ion-exchange in zeolite Y **463**, 100
Ion-exchange voltammetry
Determination of methylmercury at Nafion® coated electrodes by single and multiple pulse voltammetric techniques **467**, 193
Ionic content
Quantitative discrimination of mass fluxes at electrochemical interfaces by optical beam deflection **466**, 218
Ionic interaction
Chronoamperometry of strong acids without supporting electrolyte **472**, 1
Ion intercalation
Spectroelectrochemical investigations on the reduction of thin films of hexadecafluorophthalocyaninatozinc ($F_{16}PcZn$) **476**, 148
Ionogenic reactions
Electron transfer in retrospect and prospect: 1: Adiabatic electrode processes **460**, 5
Electron transfer in retrospect and prospect 1: Adiabatic electrode processes **470**, 170
Ionophore
Transfer of heavy metal ions across the water | nitrobenzene microinterface facilitated by the cadmium selective ionophore ETH1062 **475**, 9
Ion pair formation
Kinetic studies on ion pair formation between 2,3,5,6-tetrachloro-1,4 benzoquinone anion radical and alkaline earth metal cations (RPS 6708) **472**, 91
Ions
Calculation of thermodynamic and inner layer characteristics of halide ions adsorbed on bismuth single crystal planes from solutions in methanol **469**, 182
Ion-selective electrode
Amperometric ion-selective electrode. Voltammetric theory and analytical applications at high concentration and trace levels **468**, 34
Amperometric ion-selective electrode. Voltammetric theory and analytical applications at high concentration and trace levels **475**, 90
Ion-selective membrane
Ion sensors using one-component room temperature vulcanized silicone rubber matrices **464**, 135
Ion transfer
Finite element simulation of ion transfer reactions at a single micro-liquid | liquid interface supported on a thin polymer film **468**, 42
Polarization phenomena at the water | *o*-nitrophenyl octyl ether interface: Part III. Kinetics of tetraethylammonium ion transfer across the polymer supported interfaces **463**, 232
Some remarks on the double layer correction to the kinetics of ion transfer at the interface of immiscible electrolytes **474**, 89
Transfer of β-diketone and 4-acylpyrazolone anions across the electrified water|nitrobenzene interface **469**, 91
Transfer of heavy metal ions across the water | nitrobenzene microinterface facilitated by the cadmium selective ionophore ETH1062 **475**, 9
Ion-transfer voltammetry
Amperometric ion-selective electrode. Voltammetric theory and analytical applications at high concentration and trace levels **468**, 34
Amperometric ion-selective electrode. Voltammetric theory and analytical applications at high concentration and trace levels **475**, 90
Ion transport
Mass transport behavior of polypyrrole and poly(*N*-methylpyrrole) films in acetonitrile solutions **468**, 104
Steady-state ion transport through homopolar ion-exchange membranes: an analytical solution of the Nernst–Planck equations for a 1:1 electrolyte under the electroneutrality assumption **460**, 53

IR drop
Simultaneous ion transfer across the microhole ITIES: an example of ternary electrodiffusion **460**, 149
Iridium
Origin of the infrared reflectance increase produced by the adsorption of CO on particulate metals deposited on moderately reflecting substrates **465**, 234
The potentiodynamic behaviour of iridium electrodes in aqueous 3.7 M H_2SO_4 in the 293–195 K range **461**, 40
Iridium oxide
Anion and water involvement in hydrous Ir oxide redox reactions in acidic solutions **475**, 20
Iron complexes
Electrochemical behaviour of (μ-oxo) di-aqua diiron(III) complexes in organic media. Electrogeneration of mononuclear $[Fe^{II}(L)_2(S)_2]^{2+}$ complexes (L = 2,2′-bipyridine and (−)4,5-pinene-2,2′-bipyridine; S = H_2O or CH_3CN) **469**, 53
Iron electrodissolution
Current oscillations induced by chlorides during the passive–active transition of iron in a sulfuric acid solution **471**, 132
Iron(III)/thiolate complexes
Electrochemical study of tetraphenylporphinato-iron(III)–thiolate complexes, NH···S hydrogen bonding in the cytochrome P-450 model system **469**, 84
Iron phthalocyanine
Preparation and characterization of sol–gel derived carbon composite ceramic electrodes: electrochemical and XANES study of nitrite reduction **468**, 131
Iron (100) surface
Nano-mechano-electrochemistry of the iron (100) surface in solution **473**, 49
Irradiation
Effect of ultra-violet light irradiation on anodic oxide films on titanium in sulfuric acid solution **473**, 272
IR spectroscopy
A temperature controlled cell for in situ infrared spectroelectrochemical measurements and its use in the study of CO isothermal desorption **471**, 146
Coadsorbate vibrational interactions within mixed carbon monoxide-nitric oxide adlayers on ordered low-index platinum-group electrodes **467**, 92
Infrared spectroscopy of carbon monoxide and nitric oxide on palladium(111) in aqueous solution: unexpected adlayer structural differences between electrochemical and ultrahigh-vacuum interfaces **474**, 155
SNIFTIRS studies of the electrochemical double layer: Part II. Au(111) electrode in solutions with specifically adsorbed nitrate ions **467**, 325
Sulfate ions adsorbed on Au(*hkl*) electrodes: in situ vibrational spectroscopy **460**, 110
Voltammetric and spectroscopic study of the adsorption of alkyl viologens on a HOPG electrode **473**, 138
Island formation
Underpotential deposition behavior of metals onto gold electrodes coated with self-assembled monolayers of alkanethiols **473**, 59
Isocitrate dehydrogenase
Amperometric determination of NAD(P)H with peroxidase-based H_2O_2-sensing electrodes and its application to isocitrate dehydrogenase activity assay in serum **478**, 33
Isoforms
Electrochemical study on Cd binding to metallothioneins isolated from the mussel, *Mytilus galloprovincialis* **466**, 75
Isomer recognition
Langmuir–Blodgett films of azocrown ethers on electrodes — voltammetric recognition of isomers **471**, 156
Isotherms
Adsorption of sulfate ions on monocrystalline copper electrodes: the structural effects **463**, 1
Use of a zeolite-modified electrode for the study of the methylviologen–sodium ion-exchange in zeolite Y **463**, 100
Isotope effect
Anomalous H/D isotopic effect in the kinetics of polarographic hydrogen evolution **477**, 62
Salt and isotope effects upon a multistep electrode reaction: the reduction of nitromethane on mercury **474**, 60
Isotropic electrode
The Shuttleworth equation for a finite surface strain **471**, 105
ITIE
Two-dimensional metal deposition at the liquid|liquid interface; potential and magnetohydrodynamic pattern transition **473**, 54
ITIES
A model for assisted ion transfer across liquid | liquid interfaces **460**, 144
Finite element simulation of ion transfer reactions at a single micro-liquid | liquid interface supported on a thin polymer film **468**, 42
Ionic partition diagrams of ionisable drugs: pH-lipophilicity profiles, transfer mechanisms and charge effects on solvation **462**, 235
Ion transfer across a phospholipid monolayer adsorbed at the water | 1,2-dichloroethane interface under surface pressure control **469**, 72
Phospholipid monolayers studied by a combination of cyclic voltammetry and Langmuir techniques at the water | 1,2-dichloroethane interface **463**, 242
Simultaneous ion transfer across the microhole ITIES: an example of ternary electrodiffusion **460**, 149
Some remarks on the double layer correction to the kinetics of ion transfer at the interface of immiscible electrolytes **474**, 89
Transfer of β-diketone and 4-acylpyrazolone anions across the electrified water|nitrobenzene interface **469**, 91
Voltammetric analysis of Cs^+-DB18C6 complex stoichiometry at the water | 1,2-dichloroethane interface **464**, 54

Jacketed cell
A jacketed cell for infrared spectroelectrochemistry at constant above ambient temperatures **476**, 95

KC_8 electrode
An electrochemical impedance study on the interfacial behaviour of KC_8 electrodes in $LiClO_4$ containing electrolytes **474**, 107
Kinetic model
Amplification of amperometric biosensor responses by electrochemical substrate recycling: Part II. Experimental study of the catechol–polyphenol oxidase system immobilized in a laponite clay matrix **470**, 61
Amplification of amperometric biosensor responses by electrochemical substrate recycling: Part I. Theoretical treatment of the catechol–polyphenol oxidase system **470**, 53
Oxidation of CO adlayers on Pt(111) at low potentials: an impinging jet study in H_2SO_4 electrolyte with mathematical modeling of the current transients **467**, 74
Passivation mechanism of iron in concentrated phosphoric acid **475**, 58
Small signal (local) analysis of electrocatalytic reaction. Pole-zero approach **465**, 119
Kinetics
A new approach to electrode kinetics and dynamics by potential modulated Fourier transform infrared spectroscopy **473**, 34
Effects of self-stress on the hydrogen absorption into palladium hydride electrodes of plate form under galvanostatic conditions **474**, 130

Electrode kinetics and the nature of the metal electrode: Part 4. The Zn(II)/Zn electrode reaction studied at dropping Tl + Ga alloy electrodes **472**, 64

Electrode kinetics and the nature of the metal electrode: Part 3. The Zn(II)/Zn electrode reaction studied at In + Ga dropping (micro)electrodes **472**, 53

Kinetics of sulfide ion adsorption at copper amalgam electrode **463**, 200

Kinetics of the ferric/ferrous electrode reaction on Nafion®-coated electrodes **469**, 11

Kinetic studies on ion pair formation between 2,3,5,6-tetrachloro-1,4 benzoquinone anion radical and alkaline earth metal cations (RPS 6708) **472**, 91

Numerical simulation of hydrogen (deuterium) absorption into β-phase hydride (deuteride) palladium electrodes under galvanostatic conditions **474**, 123

Polarization phenomena at the water | *o*-nitrophenyl octyl ether interface: Part III. Kinetics of tetraethylammonium ion transfer across the polymer supported interfaces **463**, 232

Reaction mechanism and dynamics of methanol electrooxidation on platinum(111) **467**, 132

Surface redox catalysis and reduction kinetics of hydrogen peroxide on copper–nickel alloys **470**, 31

Thermodynamic and kinetic basicities of the carbon and oxygen ends of enolates. Their role in the reductive cleavage electrochemistry of α-substituted acetophenones **476**, 81

The temperature dependence of the kinetics of cyanide dissociation from the cyanide complex of myoglobin studied by cyclic voltammetry **466**, 177

The use of regularization methods in the deconvolution of underlying distributions in electrochemical processes **475**, 28

Voltammetric investigation of the anodic dimerization of *p*-halogenoanilines in DMF: Reactivity of their electrogenerated cation radicals **462**, 55

Kink

Significant enhancement of the electrochemical reduction of CO_2 at the kink sites on Pt(S)-[*n*(110) × (100)] and Pt(S)-[*n*(100) × (110)] **467**, 67

Labeled biotin

Control of electrocatalytic oxidation of NADH using an interaction between labeled biotin with dopamine and avidin **466**, 117

Labeled proteins

Redox-cycling type electrochemiluminescence in aqueous medium. A new principle for the detection of proteins labeled with a ruthenium chelate **474**, 192

Lability

Lability criteria for metal complexes in micro-electrode voltammetry **471**, 55

Lactate dehydrogenase

In-situ monitoring of the interaction of lactate dehydrogenase with NAD on a gold electrode by FT-SERS **465**, 187

Lambert's function, Nernst–Planck equations

Steady-state ion transport through homopolar ion-exchange membranes: an analytical solution of the Nernst–Planck equations for a 1:1 electrolyte under the electroneutrality assumption **460**, 53

Lamellar composite

Modified electrodes based on mixed bentonite vanadium(V) oxide xerogels **464**, 48

Langmuir and Frumkin isotherms

Limiting current in normal pulse polarography with reactant adsorption obeying the Langmuir and the Frumkin isotherms **478**, 25

Langmuir–Blodgett films

Second harmonic generation investigation of rhodamine B derivatives in Langmuir–Blodgett films **465**, 195

Langmuir trough

Ion transfer across a phospholipid monolayer adsorbed at the water | 1,2-dichloroethane interface under surface pressure control **469**, 72

Phospholipid monolayers studied by a combination of cyclic voltammetry and Langmuir techniques at the water | 1,2-dichloroethane interface **463**, 242

Large bandgap semiconductors

Electrochemistry of homoepitaxial CVD diamond: energetics and electrode kinetics in aqueous electrolytes **475**, 139

Laser ablation

Voltammetry using an electrode surface continuously renewed by laser ablation and its demonstration on electro-oxidation of L-ascorbic acid **466**, 31

Laser fabrication

Photoelectrochemical submicrometer patterning of titanium dioxide by platinum **473**, 235

Lauric acid

Ionic partition diagrams of ionisable drugs: pH-lipophilicity profiles, transfer mechanisms and charge effects on solvation **462**, 235

Lead

Rotograved carbon electrodes for amperometric cadmium and lead determination **469**, 189

LEED

Phase transitions in the electrodeposition of tellurium atomic layers on Au(100) **467**, 270

Ligand

Electrochemical properties of the first Re(I)–carbonyl compound of di-2-pyridyl ketone.oxime (dpk.oxime), *fac*-$Re(CO)_3$-(dpk.oxime)Cl, in non-aqueous media **466**, 60

Light effect

Comments on 'On the calculation of surface concentration from the measurement by the radiotracer 'electrode lowering' technique' by D. Poskus **464**, 118

Light illumination

Photoresponse of a titanium dioxide chemical sensor **472**, 137

Light scattering

Formation of conducting clusters of polyaniline films detected by light scattering **473**, 132

Light scattering of polyaniline films responding to electrochemical switching **460**, 254

Li intercalation

Enhancement of the electrochemical Li doping/undoping reaction rate of a graphitic material by an evaporated film of Sn, Zn or Pb **462**, 150

Limited volume electrodes (LVE)

The study of hydrogen sorption in palladium limited volume electrodes (Pd-LVE): I. Acidic solutions **471**, 190

Linear analysis

Small signal (local) analysis of electrocatalytic reaction. Pole-zero approach **465**, 119

Linear sweep voltammetry

Logistic differential equation: A general equation for electrointercalation processes? **475**, 190

Linear Tafel approximation region

Kinetic and mechanistic study of hydroxyl ion electrosorption at the Pt(111) surface in alkaline media **466**, 155

$LiNiO_2$

Determination of the Li ion chemical diffusion coefficient for the topotactic solid-state reactions occurring via a two-phase or single-phase solid solution pathway **477**, 32

Lipid

Ion transfer across a phospholipid monolayer adsorbed at the water | 1,2-dichloroethane interface under surface pressure control **469**, 72

Phospholipid monolayers studied by a combination of cyclic voltammetry and Langmuir techniques at the water | 1,2-dichloroethane interface **463**, 242

Lipophilic additive
Anion-selective membrane electrodes based on polymer-supported metalloporphyrins **468**, 98
Lipophilicity
Ionic partition diagrams of ionisable drugs: pH-lipophilicity profiles, transfer mechanisms and charge effects on solvation **462**, 235
Lippmann equation
Can the internal energy function of solid interfaces be of a non-homogeneous nature? **472**, 168
Liquid ammonia
Low-temperature sonoelectrochemical processes: Part 1. Mass transport and cavitation effects of 20 kHz ultrasound in liquid ammonia **477**, 71
Oxygen reduction mechanisms at p-InP and p-GaAs electrodes in liquid ammonia in neutral buffered medium and acidic media **462**, 88
Using Pt microelectrodes in liquid ammonia for studying proton reduction **477**, 140
Liquid | liquid interface
A model for assisted ion transfer across liquid | liquid interfaces **460**, 144
Interfacial phenomena involving Fe(III)–ofloxacin complexes at the water|1,2-dichloroethane interface **461**, 194
Specific adsorption at modulated liquid | liquid interfaces **475**, 46
The influence of the ions on the capacity of liquid | liquid interfaces **467**, 203
Transfer of heavy metal ions across the water | nitrobenzene microinterface facilitated by the cadmium selective ionophore ETH1062 **475**, 9
Liquid | solid interface
What can we learn from the non-linear optical investigation of the liquid | solid interface? **473**, 25
Lithium
A poly(vinylidene fluoride)-based gel electrolyte membrane for lithium batteries **463**, 248
Inhibition effects of polyacrylonitrile gel electrolytes on lithium dendrite formation **472**, 142
Lithium bromide
Conductivity study on lithium bromide in propylene carbonate + acetonitrile mixtures in dilute solutions from −35 to 75°C **471**, 78
Lithium cell
Characterization of a new spinel Li–Cr–Mn–O for secondary lithium batteries **463**, 24
Lithium halides and thiocyanate
Conductometric study of lithium halides and thiocyanate in the mixed solvents of tetrahydrofuran and 2-ethyl-1-hexanol **468**, 110
Lithium incorporation and extraction, Molten carbonate fuel cell
Electrochemical behaviour of $Li_xNi_{1-x}O$ in molten $Li_2CO_3 + Na_2CO_3$ eutectic **463**, 78
Lithium intercalation
Determination of the Li ion chemical diffusion coefficient for the topotactic solid-state reactions occurring via a two-phase or single-phase solid solution pathway **477**, 32
Lithium ion
Simultaneous in-situ conductivity and cyclic voltammetry characterization of Li-ion intercalation into thin V_2O_5 films **479**, 12
Lithium-ion cell
An electrochemical impedance study on the interfacial behaviour of KC_8 electrodes in $LiClO_4$ containing electrolytes **474**, 107
Lithium metal anode
Electrochemical control of a Li metal anode interface: improvement of Li cyclability by inorganic additives compatible with electrolytes **473**, 279
Lithium titanate
Behaviour of titanium species in molten $Li_2CO_3 + Na_2CO_3$ and $Li_2CO_3 + K_2CO_3$ in the anodic conditions used in molten carbonate fuel cells: II. Electrochemical intercalation of Li^+ in Li_2TiO_3 at 600 and 650°C **474**, 9
Loaded ionomer
Current enhancing effect of poly[1-methyl-3-(pyrrol-1-ylmethyl)pyridinium] films on the electrode reaction of anthraquinonedisulfonate **478**, 9
Local active areas
Current oscillations induced by chlorides during the passive–active transition of iron in a sulfuric acid solution **471**, 132
Local charge density
Structural studies of 2,2′-bipyridine on Au(100) **467**, 207
Logistic equation
Logistic differential equation: A general equation for electrointercalation processes? **475**, 190
Low electrolyte/reactant ratio
Steady state voltammetry at low electrolyte/reactant concentration ratios: what it means and what it does not mean **463**, 45
Low index single crystal surfaces
In-situ STM investigation of specific anion adsorption on Cu(111) **467**, 307
Potential modulated reflectance spectroscopy of Pt(111) in acidic and alkaline media: cyanide adsorption **463**, 109
Low support ratio
Voltammetry in solutions of low ionic strength. Electrochemical and analytical aspects **466**, 129
Low temperature electrochemistry
Low-temperature sonoelectrochemical processes: Part 1. Mass transport and cavitation effects of 20 kHz ultrasound in liquid ammonia **477**, 71
Luminescence
Electrochemical characterization of the clay-enhanced luminol ecl reaction **474**, 82
Luminescent conjugated polymer
Solid-state electrochemical investigation of poly[2-methoxy, 5-(2′-ethyl-hexyloxy)-1,4-phenylene vinylene] **471**, 32
Luminol
Detection of near-wall hydrodynamic effects by electrochemiluminescence **470**, 89

Macro and microelectrodes
Electrochemical studies on *c*-type cytochromes at microelectrodes **464**, 76
Macromolecular complexation
Voltammetric currents for any ligand-to-metal concentration ratio in fully labile metal-macromolecular complexation. Easy computations, analytical properties of the currents and a graphical method to estimate the stability constant **472**, 42
Magnesium
On the electrochemical behavior of magnesium electrodes in polar aprotic electrolyte solutions **466**, 203
Magnetic thin film
Magnetic properties and optical control of electrochemically prepared iron–chromium polycyanides **473**, 245
Maldi-Tof spectrometry
Electrochemical synthesis and structural studies of copolymers based on the electrooxidation of pyrrole and some salen compounds **470**, 77
Manganese complexes
Electrochemical behaviour of $[Mn_2^{III,IV}O_2(phen)_4]^{3+}$ complex in aqueous phen + phenH$^+$ buffer; phen = 1,10-phenanthroline **463**, 119
Manganese porphyrin
Electrochemical characterization and electrocatalysis of high valent manganese *meso*-tetrakis(*N*-methyl-2-pyridyl)porphyrin **474**, 52

Mass transfer
Detection of near-wall hydrodynamic effects by electrochemiluminescence **470**, 89
Electrochemically induced mass transfer and rheological changes of Nafion® coatings fully loaded with $[Os(bpy)_3]^{2+}$ **469**, 34
Mass transport
A model for the liquid feed direct methanol fuel cell **477**, 97
Evaluation of a reactor model and cathode materials for batch electrolysis of L-cystine hydrochloride **462**, 97
Low-temperature sonoelectrochemical processes: Part 1. Mass transport and cavitation effects of 20 kHz ultrasound in liquid ammonia **477**, 71
Mass transport accompanied with electron transfer between the gold electrode modified with 11-ferrocenylundecanethiol monolayer and redox species in solution — an electrochemical quartz crystal microbalance study **474**, 94
Mathematical modelling
Electrochemical treatment of tumours: a simplified mathematical model **460**, 88
MCFC
Comparative study on the oxygen dissolution behaviour in 62/38 mol% Li/K and 52/48 mol% Li/Na carbonate **470**, 39
Mean field
A non-primitive model for the electrode | electrolyte interface based on the Percus–Yevick theory. Analysis of the different molecular sizes, ion valences and electrolyte concentrations **460**, 135
Mechanical property
Nano-mechano-electrochemistry of the iron (100) surface in solution **473**, 49
Mechanisms
In situ surface Raman study of the phosphorus incorporation mechanism during electrodeposition of Ni–P alloys **469**, 79
Voltammetric investigation of the anodic dimerization of *p*-halogenoanilines in DMF: Reactivity of their electrogenerated cation radicals **462**, 55
Mechano–electric oscillations
Polarization phenomena at the water | *o*-nitrophenyl octyl ether interface: Part III. Kinetics of tetraethylammonium ion transfer across the polymer supported interfaces **463**, 232
Mechano-electrochemistry
Nano-mechano-electrochemistry of the iron (100) surface in solution **473**, 49
M(111) electrodes
Comparison of a bisulfate anion adsorbed on M(111) (M = Pt, Rh, Au, Ag and Cu) **467**, 299
Membrane
A poly(vinylidene fluoride)-based gel electrolyte membrane for lithium batteries **463**, 248
Effect of water transport in a PEFC at low temperatures operating with dry hydrogen **477**, 164
Theory for water management in membranes for polymer electrolyte fuel cells: Part 1. The effect of impurity ions at the anode side on the membrane performances **465**, 1
Theory for water management in membranes for polymer electrolyte fuel cells: Part 2. The effect of impurity ions at the cathode side on the membrane performances **465**, 18
Membrane-covered electrode
Amperometric determination of NAD(P)H with peroxidase-based H_2O_2-sensing electrodes and its application to isocitrate dehydrogenase activity assay in serum **478**, 33
Preparation of a microperoxidase and ferrocene-immobilized polyion complex membrane for the detection of hydrogen peroxide **468**, 117
Membrane electrochemistry
Convective electrodiffusion processes through graft-modified charged porous membranes **464**, 222
Mercaptopropionic acid
In situ STM study of self-assembled mercaptopropionic acid monolayers for electrochemical detection of dopamine **465**, 72
4-Mercaptopyridine
A new approach to electrode kinetics and dynamics by potential modulated Fourier transform infrared spectroscopy **473**, 34
Mercury
Two mercury drops on a conducting surface in a mercurous ion solution as a model for electrochemical Ostwald ripening **468**, 127
Mercury electrode
Cathodic stripping square wave voltammetry of Cu(II)–oxine complexes. A mechanistic study **478**, 17
Determination of the surface charge density of a mercury electrode by extrusion: a new method for correction of the faradaic component **468**, 150
Reduction and oxidation of peptide nucleic acid and DNA at mercury and carbon electrodes **476**, 71
Mercury(I)
The kinetics of mercury nucleation from Hg_2^{2+} and Hg^{2+} solutions on vitreous carbon electrodes **464**, 39
Mercury(II)
The kinetics of mercury nucleation from Hg_2^{2+} and Hg^{2+} solutions on vitreous carbon electrodes **464**, 39
Mercury(II) electrode
Accumulation of Hg(II) by adsorbed polyuridylic acid: differentiation of coordinated Hg(II) and covalently mercurated species **466**, 2
Mercury microelectrodes
Preparation and characterization of Nafion® coated sphere-cap mercury microelectrodes **471**, 48
Metal complex
Lability criteria for metal complexes in micro-electrode voltammetry **471**, 55
Metal epitaxy
Structure and growth in metal epitaxy on low-index Au surfaces—a comparison between solid | electrolyte and solid | vacuum interfaces **467**, 258
Metal evaporation
Enhancement of the electrochemical Li doping/undoping reaction rate of a graphitic material by an evaporated film of Sn, Zn or Pb **462**, 150
Metallation
Post-assembly insertion of metal ions into thiol-derivatized porphyrin monolayers on gold **473**, 75
Metallothionein
Cadmium binding properties of the C-terminal hexapeptide from mouse metallothionein: study by linear sweep voltammetry and multivariate curve resolution analysis **468**, 202
Metallothioneins
Electrochemical study on Cd binding to metallothioneins isolated from the mussel, *Mytilus galloprovincialis* **466**, 75
Metal passivation
Structural identifiability of adsorption and electron transfer processes in metal dissolution and passivation mechanisms **471**, 1
Metal speciation
Voltammetric metal speciation in mixtures of inert and labile macromolecular complexes at any ligand-to-metal ratio: differential pulse polarographic study of the Zn(II)–nitrilotriacetate–polymethacrylate system **462**, 157
Metal surfaces
Interaction of H, O and OH with metal surfaces **472**, 126
Methacrylonitrile
Electropolymerization of methacrylonitrile and *N*-vinyl-2-pyrrolidone as probed by an EQCM **465**, 200

Methanol
A comparison of multistability in the electrocatalyzed oxidations of methanol and ethanol in acid and alkaline solutions **478**, 108
Calculation of thermodynamic and inner layer characteristics of halide ions adsorbed on bismuth single crystal planes from solutions in methanol **469**, 182
Reactivity and activation parameters in methanol oxidation on platinum single crystal electrodes 'decorated' by ruthenium adlayers **467**, 143
Methanol crossover
A model for the liquid feed direct methanol fuel cell **477**, 97
Methanol electrooxidation
Reaction mechanism and dynamics of methanol electrooxidation on platinum(111) **467**, 132
Methanol fuel cell
In situ and model EXAFS studies of electrocatalysts for methanol oxidation **460**, 80
Methanol oxidation
Electrocatalytic oxidation of methanol at a nickel hydroxide/glassy carbon modified electrode in alkaline medium **471**, 89
Methoxybenzenes
Mechanistic investigation of the anodic oxidation of *p*-methoxytoluene in dry and wet acetonitrile **464**, 85
Methylalkylviologens
Electrochemical study of methylalkylviologens using an electrochemical quartz crystal microbalance **463**, 224
Methylamine
Oxidation of methylamine and ethylamine on Pt single crystal electrodes in acid medium **469**, 159
The adsorption of methylamine on Pt single crystal surfaces **467**, 105
Methylene blue
Preparation of clay-modified electrodes by electrophoretic deposition of clay films **462**, 143
2-Methyl-8-hydroxyquinoline
Rapidly renewable and reproducible electropolymerized surface at a monomer modified carbon paste electrode **465**, 102
Methylmercury
Determination of methylmercury at Nafion® coated electrodes by single and multiple pulse voltammetric techniques **467**, 193
Methylmethacrylate
Investigation of the cathodic electropolymerization of acrylonitrile, ethylacrylate and methylmethacrylate by coupled quartz crystal microbalance analysis and cyclic voltammetry **472**, 83
Methylviologen
Electrocatalytic reduction of molecular oxygen on a sodium montmorillonite-methyl viologen carbon paste chemically modified electrode **463**, 253
Use of a zeolite-modified electrode for the study of the methylviologen–sodium ion-exchange in zeolite Y **463**, 100
MHD
Two-dimensional metal deposition at the liquid|liquid interface; potential and magnetohydrodynamic pattern transition **473**, 54
Micelles
Electrochemical nitration of naphthalene in the presence of nitrite ion in aqueous non-ionic surfactant solutions **470**, 157
Microband electrode
Cationic systems as self-assembled monolayers on gold surfaces **464**, 263
Microdisc
Application of Danckwerts' expression to first-order EC′ reactions. Transient currents at inlaid and recessed microdisc electrodes **466**, 15
Microdisc electrode
Steady-state currents at inlaid and recessed microdisc electrodes for first-order EC′ reactions **476**, 132
Microelectrode
A microelectrode study of the catalysis of alkyl halide reduction by Co(II)(salen) **464**, 168
General solutions for the I/t response for reversible processes in the presence of product in a multipotential step experiment at planar and spherical electrodes whose areas increase with any power of time **466**, 8
Lability criteria for metal complexes in micro-electrode voltammetry **471**, 55
Nitrite reduction at powder microelectrodes **469**, 196
Study of a catalytic mechanism in double potential step techniques at spherical electrodes **468**, 158
Trace detection of 2,4,6-trinitrotoluene in the gaseous phase by cyclic voltammetry **460**, 10
Using Pt microelectrodes in liquid ammonia for studying proton reduction **477**, 140
Voltammetry in solutions of low ionic strength. Electrochemical and analytical aspects **466**, 129
Microelectrode sensors
Feasibility studies for the detection of volatile organic compounds in the gas phase using microelectrode sensors **460**, 105
Microemulsions
Mechanism of stereoselective production of *trans*-1-decalone by electrochemical catalysis in microemulsions **464**, 31
Microhole
Simultaneous ion transfer across the microhole ITIES: an example of ternary electrodiffusion **460**, 149
Transfer of heavy metal ions across the water|nitrobenzene microinterface facilitated by the cadmium selective ionophore ETH1062 **475**, 9
Micromachining
A wall-jet ring disk electrode fabricated within a thin-layered micromachined cell **479**, 57
Microperoxidase-11
Diffusionless electron transfer of microperoxidase-11 on gold electrodes **469**, 123
Microperoxidase
Controlled electrocatalysis by microperoxidase-11 and Au-nanoparticle superstructures on conductive supports **479**, 69
MIDA
Experimental and calculated complex formation curves for mixed, dynamic and semi-dynamic, metal–ligand systems. A differential pulse polarographic study of Cu^{II}–sarcosine–OH and Cd^{II}–MIDA–OH systems at a fixed ligand to metal ratio and varied pH **460**, 197
Migration
Chronoamperometry of strong acids without supporting electrolyte **472**, 1
Ion transport and deposit growth in spatially coupled bipolar electrochemistry **478**, 128
Simultaneous ion transfer across the microhole ITIES: an example of ternary electrodiffusion **460**, 149
Steady state voltammetry at low electrolyte/reactant concentration ratios: what it means and what it does not mean **463**, 45
Voltammetry in solutions of low ionic strength. Electrochemical and analytical aspects **466**, 129
Mild steel
Ultra-fast electropolymerization of pyrrole in aqueous media on oxidizable metals in a one-step process **478**, 92
Mirage
Quantitative discrimination of mass fluxes at electrochemical interfaces by optical beam deflection **466**, 218

Mixed conductivity
Electrochemical impedance spectroscopy of thin films with two mobile charge carriers: effects of the interfacial charging **472**, 7
Mixed electrolyte solutions
Activity coefficients for aminoacid + electrolyte mixtures by using Pitzer equations: DL-α-amino-*n*-butyric acid in mixed electrolyte solutions of neutral, acid and alkaline pH values **466**, 38
Mixed solvents of THF
Conductometric study of lithium halides and thiocyanate in the mixed solvents of tetrahydrofuran and 2-ethyl-1-hexanol **468**, 110
Mixtures of ligands
Voltammetric metal speciation in mixtures of inert and labile macromolecular complexes at any ligand-to-metal ratio: differential pulse polarographic study of the Zn(II)–nitrilotriacetate–polymethacrylate system **462**, 157
Mn(III) reconstituted myoglobin
Electrochemical and spectroelectrochemical properties of manganese reconstituted myoglobin **460**, 245
Model
A model for the liquid feed direct methanol fuel cell **477**, 97
Modeling
Quantitative discrimination of mass fluxes at electrochemical interfaces by optical beam deflection **466**, 218
Reaction mechanism and dynamics of methanol electrooxidation on platinum(111) **467**, 132
Modification of distal histidine
Electroanalytical chemistry of myoglobin with modification of distal histidine by cyanated imidazole **468**, 9
Modified conducting polymer
Addition of α-hydroxyalkylferrocenes to electrochemically oxidized poly(aniline) **470**, 166
Modified electrode
Controlled electrocatalysis by microperoxidase-11 and Au-nanoparticle superstructures on conductive supports **479**, 69
Coordination of silver(I) at the surface of carbon paste electrodes modified with 2,5,8-trithia[9]-*m*-cyclophane as studied by cyclic voltammetry **475**, 73
Electrocatalytic oxidation of methanol at a nickel hydroxide/glassy carbon modified electrode in alkaline medium **471**, 89
Electrocatalytic oxidation of NADH at graphite electrodes modified with osmium phenanthrolinedione **464**, 208
Electrocatalytic oxidation of reduced nicotinamide adenine dinucleotide (NADH) at a chlorogenic acid modified glassy carbon electrode **464**, 14
Electrochemical recognition of metal cations by poly(crown ether ferrocene) films investigated by cyclic voltammetry and electrochemical impedance spectroscopy **464**, 24
Electrodeposition of copper into functionalized polypyrrole films **474**, 113
Enhanced stability and electrocatalytic activity of a ruthenium-modified cobalt–hexacyanoferrate film electrode **471**, 42
Immobilized nitro-fluorenone derivatives as electrocatalysts for NADH oxidation **477**, 79
Kinetics of electrocatalytic oxidation of formaldehyde on a nickel porphyrin-based glassy carbon electrode **469**, 18
Modified electrodes based on mixed bentonite vanadium(V) oxide xerogels **464**, 48
Silicon-based ferrocenyl dendrimers as anion receptors in solution and immobilized onto electrode surfaces **463**, 87
Studies on the catalytic reduction of iodate at glassy carbon electrodes modified by molybdenum oxides **471**, 37
Molecular electrochemistry
Electrochemical behaviour of (μ-oxo) di-aqua diiron(III) complexes in organic media. Electrogeneration of mononuclear $[Fe^{II}(L)_2(S)_2]^{2+}$ complexes (L = 2,2′-bipyridine and (−)4,5-pinene-2,2′-bipyridine; S = H_2O or CH_3CN) **469**, 53
Molecular imprint
Voltammetric anion recognition by a highly cross-linked polyviologen film **473**, 145
Molecular modelling
Anodic oxidation of dipyrrolyls linked with conjugated spacers: study of electronic interactions between the polypyrrole chain and the spacers **479**, 3
Molecular orientation
Second harmonic generation investigation of rhodamine B derivatives in Langmuir–Blodgett films **465**, 195
Molecular recognition
Hydrogen bond complexation of dimethyl-[1-butyl-2,4-dioxo(1H,3H)pyrimido]tetrathiafulvalene with aminopyridine derivatives probed by cyclic voltammetry **463**, 212
Silicon-based ferrocenyl dendrimers as anion receptors in solution and immobilized onto electrode surfaces **463**, 87
Molecular semiconductor
Role of surface states and adsorbates in time-resolved photocurrent measurements and photovoltage generation at phthalocyaninatozinc(II)-photocathodes **462**, 222
Molten carbonate
Behaviour of titanium species in molten $Li_2CO_3 + Na_2CO_3$ and $Li_2CO_3 + K_2CO_3$ in the anodic conditions used in molten carbonate fuel cells: II. Electrochemical intercalation of Li^+ in Li_2TiO_3 at 600 and 650°C **474**, 9
Comparative study on the oxygen dissolution behaviour in 62/38 mol% Li/K and 52/48 mol% Li/Na carbonate **470**, 39
Molten carbonate fuel cell
Electrochemistry of Ni oxidation in molten $Li_2CO_3 + Na_2CO_3$ eutectic **463**, 72
Molten carbonates
Electrochemical behaviour of $Li_xNi_{1-x}O$ in molten $Li_2CO_3 + Na_2CO_3$ eutectic **463**, 78
Electrochemistry of Ni oxidation in molten $Li_2CO_3 + Na_2CO_3$ eutectic **463**, 72
Molybdenum oxide
Studies on the catalytic reduction of iodate at glassy carbon electrodes modified by molybdenum oxides **471**, 37
Monocrystalline electrodes
Adsorption of sulfate ions on monocrystalline copper electrodes: the structural effects **463**, 1
Monolayers
A monomer–dimer equilibrium in self-assembled monolayers of *N*-ethyl-*N*′-octadecylviologen on the electrode surface. The influence of water content and hexafluorophosphate ion **466**, 67
A non-compartmentalized glucose | O_2 biofuel cell by bioengineered electrode surfaces **479**, 64
Enhanced electrostatic interactions for selective and controllable permeation of ionic species at a monolayer of self-assembled dicationic nickel complex **465**, 177
Cationic systems as self-assembled monolayers on gold surfaces **464**, 263
Characterization of protein monolayers by surface plasmon resonance combined with cyclic voltammetry 'in situ' **464**, 198
Langmuir–Blodgett films of azocrown ethers on electrodes — voltammetric recognition of isomers **471**, 156
Polyoxometalate modified electrodes: from a monolayer to multilayer structures **462**, 187
Self-assembly of a tricarboxylate receptor through thioamide groups and its use for electrochemical detection of protonated amines **473**, 105

Separation of pinhole and tunneling electron transfer processes at self-assembled polymeric monolayers on gold electrodes **470**, 114
Structure and electrochemical behavior of a flavin sulfide monolayer adsorbed on gold **472**, 147
Monomer–dimer
A monomer–dimer equilibrium in self-assembled monolayers of *N*-ethyl-*N'*-octadecylviologen on the electrode surface. The influence of water content and hexafluorophosphate ion **466**, 67
Monomer modified carbon paste
Rapidly renewable and reproducible electropolymerized surface at a monomer modified carbon paste electrode **465**, 102
Monosaccharides
Electrochemical oxidation of mono- and disaccharides at fresh as well as oxidized copper electrodes in alkaline media **464**, 252
Monte-Carlo
A non-primitive model for the electrode|electrolyte interface based on the Percus–Yevick theory. Analysis of the different molecular sizes, ion valences and electrolyte concentrations **460**, 135
Multi-electron transfer reaction
The voltammetric reduction of some benzenesulfonyl fluorides, simulation of the ECE mechanism and determination of the potential variation of the transfer coefficient by using the compounds with two reducible groups **471**, 14
Multiple pulse voltammetries
Determination of methylmercury at Nafion® coated electrodes by single and multiple pulse voltammetric techniques **467**, 193
Multipulse
General solutions for the I/t response for reversible processes in the presence of product in a multipotential step experiment at planar and spherical electrodes whose areas increase with any power of time **466**, 8
Multivariate analysis
Cadmium binding properties of the C-terminal hexapeptide from mouse metallothionein: study by linear sweep voltammetry and multivariate curve resolution analysis **468**, 202
Myoglobin
Electroanalytical chemistry of myoglobin with modification of distal histidine by cyanated imidazole **468**, 9
Electrochemical and spectroelectrochemical properties of manganese reconstituted myoglobin **460**, 245
Mytilus galloprovincialis
Electrochemical study on Cd binding to metallothioneins isolated from the mussel, *Mytilus galloprovincialis* **466**, 75

NAD^+
Electrochemical evaluation of the reaction rate between methyl viologen mediator and diaphorase enzyme for the electrocatalytic reduction of NAD^+ and digital simulation for its voltammetric responses **465**, 153
NAD
In-situ monitoring of the interaction of lactate dehydrogenase with NAD on a gold electrode by FT-SERS **465**, 187
NADH
Control of electrocatalytic oxidation of NADH using an interaction between labeled biotin with dopamine and avidin **466**, 117
Electroanalysis of dopamine and NADH at conductive diamond electrodes **473**, 179
Electrocatalytic oxidation of NADH at graphite electrodes modified with osmium phenanthrolinedione **464**, 208
Electrocatalytic oxidation of reduced nicotinamide adenine dinucleotide (NADH) at a chlorogenic acid modified glassy carbon electrode **464**, 14
Electrochemical evaluation of the reaction rate between methyl viologen mediator and diaphorase enzyme for the electrocatalytic reduction of NAD^+ and digital simulation for its voltammetric responses **465**, 153
NADH oxidation
Immobilized nitro-fluorenone derivatives as electrocatalysts for NADH oxidation **477**, 79
NAD(P)H
Amperometric determination of NAD(P)H with peroxidase-based H_2O_2-sensing electrodes and its application to isocitrate dehydrogenase activity assay in serum **478**, 33
Nafion®
Kinetics of the ferric/ferrous electrode reaction on Nafion®-coated electrodes **469**, 11
Preparation and characterization of Nafion® coated sphere-cap mercury microelectrodes **471**, 48
Nafion® coated electrodes
Determination of methylmercury at Nafion® coated electrodes by single and multiple pulse voltammetric techniques **467**, 193
Nafion® coating
Electrochemically induced mass transfer and rheological changes of Nafion® coatings fully loaded with $[Os(bpy)_3]^{2+}$ **469**, 34
Nafion® membrane
Temperature dependence of physical displacement and charge hopping in a polymer membrane incorporating a trinuclear ruthenium complex **476**, 159
Nano-crystalline
Impedance and photoelectrochemical properties of porous oxide film on Type304 stainless steel formed by square wave potential pulse polarisation **473**, 265
Nanoindentation
Nano-mechano-electrochemistry of the iron (100) surface in solution **473**, 49
Nanolithography
Scanning probe lithography for electrode surface modification **473**, 230
Nanoparticles
Controlled electrocatalysis by microperoxidase-11 and Au-nanoparticle superstructures on conductive supports **479**, 69
Nanostructures
Formation of ⟨001⟩-aligned nano-scale pores on (001) n-InP surfaces by photoelectrochemical anodization in HCl **473**, 223
Nanostructuring
The growth of size-determined Cu clusters in nanometer holes on Au(111) due to a balance between surface and electrochemical energy **460**, 102
Naphthalene
Electrochemical nitration of naphthalene in the presence of nitrite ion in aqueous non-ionic surfactant solutions **470**, 157
Mass spectrometric study of desorption and hydrogenation of biphenyl, naphthalene and *t*-butylbenzene on poly- and monocrystalline platinum electrodes **461**, 90
1,2-Naphthoquinone-4-sulfonate
A UV-vis spectroelectrochemical study of redox reactions of solution species at a polyaniline electrode in the conducting and the reduced state **461**, 184
Nb_2O_5
Capacitance and photocurrent study of electronic properties of anodic oxide films on Nb and Ta. Evaluation of the ionized donor concentration profile in Nb_2O_5 film **460**, 214
n-doping
Oligomeric poly(phenazine-2,7-diyl) and its electrochemical response **460**, 242
Nernstian distribution
A Nernstian electron source model for the ac voltammetric response of a reversible surface redox reaction using large-amplitude ac voltages **466**, 197

Nernst–Planck equation
Chronoamperometry of strong acids without supporting electrolyte **472**, 1
Nerve gases
A novel electrochemical method for the detection of nerve gases **466**, 169
NH···S hydrogen bond
Electrochemical study of tetraphenylporphinato-iron(III)–thiolate complexes, NH···S hydrogen bonding in the cytochrome P-450 model system **469**, 84
Nickel
Electrocatalytic oxidation of methanol at a nickel hydroxide/glassy carbon modified electrode in alkaline medium **471**, 89
Hydrogen electrosorption in Ni–Pd alloys **460**, 30
Nickel electrode
Formation of an ordered structure of iodine adsorbed on Ni(111) and the anodic dissolution processes: in-situ STM study **467**, 282
Nickel hydrides
Electrochemical formation of nickel hydride in alkaline solutions **472**, 182
Nickel oxidation
Electrochemistry of Ni oxidation in molten $Li_2CO_3 + Na_2CO_3$ eutectic **463**, 72
Nickel oxide electrode
Rotating ring-disk studies of oxidized nickel hydrous oxide: oxygen evolution and pseudocapacitance **468**, 64
Nickel–palladium alloys
Hydrogen electrosorption in Ni–Pd alloys **460**, 30
Ni–Co–Cu oxides
Effect of the partial replacement of Ni or Co by Cu on the electrocatalytic activity of the $NiCo_2O_4$ spinel oxide **464**, 187
Nicotine
Ionic partition diagrams of ionisable drugs: pH-lipophilicity profiles, transfer mechanisms and charge effects on solvation **462**, 235
Ni(II) hydrotalcites
Electrocatalytic properties of nickel(II) hydrotalcite-type anionic clay: application to methanol and ethanol oxidation **463**, 123
Ni(II) tetraaza macrocycle
Nickel(II) tetraaza macrocycle modified electrodes for the electrocatalytic determination of L-ascorbic acid by the flow injection method **468**, 85
Niobium(V) oxide
Cobalt(II) metallated hematoporphyrin IX and protoporphyrin IX immobilized on niobium(V) oxide grafted on a silica gel surface: electrochemical studies **477**, 158
Ni–P alloy
In situ surface Raman study of the phosphorus incorporation mechanism during electrodeposition of Ni–P alloys **469**, 79
Nitrate
Amperometric nitrate biosensors on the basis of *Pseudomonas stutzeri* nitrate reductase **474**, 43
Nitrate ion
Electroreduction of nitrate ion to nitrite and ammonia on a gold electrode in acidic and basic sodium and cesium nitrate solutions **470**, 46
SNIFTIRS studies of the electrochemical double layer: Part II. Au(111) electrode in solutions with specifically adsorbed nitrate ions **467**, 325
Nitrate reductase
Amperometric nitrate biosensors on the basis of *Pseudomonas stutzeri* nitrate reductase **474**, 43
Nitration
Electrochemical nitration of naphthalene in the presence of nitrite ion in aqueous non-ionic surfactant solutions **470**, 157
Nitric oxide
Coadsorbate vibrational interactions within mixed carbon monoxide-nitric oxide adlayers on ordered low-index platinum-group electrodes **467**, 92
Infrared spectroscopy of carbon monoxide and nitric oxide on palladium(111) in aqueous solution: unexpected adlayer structural differences between electrochemical and ultrahigh-vacuum interfaces **474**, 155
Nitrilotriacetate
Voltammetric metal speciation in mixtures of inert and labile macromolecular complexes at any ligand-to-metal ratio: differential pulse polarographic study of the Zn(II)–nitrilotriacetate–polymethacrylate system **462**, 157
Nitrite
Cobalt(II) porphyrazine catalysed reduction of nitrite **470**, 126
Nitrite ion
Electroreduction of nitrate ion to nitrite and ammonia on a gold electrode in acidic and basic sodium and cesium nitrate solutions **470**, 46
Nitrite reduction
Electrocatalytic reduction of nitrite at a carbon fiber microelectrode chemically modified by palladium(II)-substituted Dawson type heptadecatungstodiphosphate **469**, 63
Nitrite reduction at powder microelectrodes **469**, 196
Preparation and characterization of sol–gel derived carbon composite ceramic electrodes: electrochemical and XANES study of nitrite reduction **468**, 131
Nitrobenzene
Low-temperature sonoelectrochemical processes: Part 1. Mass transport and cavitation effects of 20 kHz ultrasound in liquid ammonia **477**, 71
Reaction of nitrobenzene on gold single-crystal electrodes: surface crystallographic orientation dependence **477**, 111
Nitromethane
Salt and isotope effects upon a multistep electrode reaction: the reduction of nitromethane on mercury **474**, 60
Nitrosobenzene
Reaction of nitrobenzene on gold single-crystal electrodes: surface crystallographic orientation dependence **477**, 111
β-Nitrostyrene derivatives
Electrochemical study of β-nitrostyrene derivatives: steric and electronic effects on their electroreduction **466**, 90
Nitrothiophenequinone
Cathodic reduction of 2-nitronaphthothiophen-4,9-quinone: evidence of catalysis by proton donors and its simulation **462**, 195
NO
Redox mechanisms of NO with water on the Pt(111) electrode studied by in-situ STM and IRAS **473**, 43
Non-aqueous solutions
Interfacial structure of dimethylsulfoxide at Ag electrodes from surface enhanced Raman scattering and differential capacitance **479**, 21
On the electrochemical behavior of magnesium electrodes in polar aprotic electrolyte solutions **466**, 203
Surface Raman scattering of interfaces at Ag electrodes emersed from dimethylsulfoxide: spectroscopic evidence for an emersion-induced potential shift **479**, 32
Non-aqueous solvent
Mechanism of the electrochemical reduction of sulfur dioxide in non-aqueous solvents **476**, 15
Non-linear diffusion
Voltammetric currents for any ligand-to-metal concentration ratio in fully labile metal-macromolecular complexation. Easy computations, analytical properties of the currents and a graphical method to estimate the stability constant **472**, 42

Non-linearity
Discontinuous immitance due to a saddle node bifurcation: II: Tangent bifurcation and critical slowdown during isotherm branch switching **460**, 226
Non-primitive model
A non-primitive model for the electrode | electrolyte interface based on the Percus–Yevick theory. Analysis of the different molecular sizes, ion valences and electrolyte concentrations **460**, 135
NO oxidation
Redox mechanisms of NO with water on the Pt(111) electrode studied by in-situ STM and IRAS **473**, 43
NO_2 reduction
Redox mechanisms of NO with water on the Pt(111) electrode studied by in-situ STM and IRAS **473**, 43
NO_2^- reduction
Electrochemical and electrocatalytic properties of tetra-iron substituted sandwich-type pentadecatungstodiphosphate heteropolyanions **476**, 85
Normal pulse polarography
Limiting current in normal pulse polarography with reactant adsorption obeying the Langmuir and the Frumkin isotherms **478**, 25
N-shaped potential dependence
Modeling galvanostatic potential oscillations in the electrocatalytic iodate reduction system **462**, 19
Nucleation
The growth of size-determined Cu clusters in nanometer holes on Au(111) due to a balance between surface and electrochemical energy **460**, 102
Tin electrodeposition on carbon electrodes. From nuclei to microcrystallites **465**, 63
Nucleation and growth
Early stages of mercury electrodeposition on HOPG **470**, 120
Nucleation and growth mechanisms
Nucleation and growth of poly(3,4-ethylenedioxythiophene) in acetonitrile on platinum under potentiostatic conditions **472**, 103

Octaphyrins
Electrochemical properties of 'figure-eight'-cyclooctapyrroles (octaphyrins) and their metal complexes **469**, 170
μ-(1,8-*n*-Octyl)-bis[(salen)cobalt(III)]
Catalytic reduction of 1,8-diiodooctane by electrogenerated cobalt(I) salen and formation of μ-(1,8-*n*-octyl)-bis-[(salen)cobalt(III)] **460**, 207
Ofloxacin
Interfacial phenomena involving Fe(III)–ofloxacin complexes at the water|1,2-dichloroethane interface **461**, 194
Ofloxacin–Fe complexes
Interfacial phenomena involving Fe(III)–ofloxacin complexes at the water|1,2-dichloroethane interface **461**, 194
Ohmic drop
Digital simulation of fast cyclic voltammogram by integration of the double layer charging current **464**, 215
Steady state voltammetry at low electrolyte/reactant concentration ratios: what it means and what it does not mean **463**, 45
Oil | water interface
The fast dropping oil | water electrode **464**, 128
Olefin oxidation
Electrochemical characterization and electrocatalysis of high valent manganese *meso*-tetrakis(*N*-methyl-2-pyridyl)porphyrin **474**, 52
Opd
Early stages of mercury electrodeposition on HOPG **470**, 120
Organic acid–water
Current–voltage curves of a composite bipolar membrane in organic acid–water solutions **462**, 12
Organic conducting salts
Kinetic behaviour of dopamine-polyphenol oxidase on electrodes of tetrathiafulvalenium tetracyanoquinodimethanide and tetracyanoquinodimethane species **461**, 174
Organometallic polymers
Electrochemical formation and spectroelectrochemical characterization of organometallic $[Ru(L)(CO)_2]_n$ polymers; L = disubstituted-2,2′-bipyridine **466**, 187
Organosilane self-assembled monolayer
Scanning probe lithography for electrode surface modification **473**, 230
Organosilicon polymer
Electrochemical generation of cation radical π-dimers in polymer film composed of pentathiophenes bridged by monosilanylene units **472**, 157
Oriented surfaces
New effects in the electrochemistry of carbon dioxide on platinum by the application of potential perturbations **477**, 41
orr
Enhancement of the electrocatalytic O_2 reduction on Pt–Fe alloys **460**, 258
Oscillations
A comparison of multistability in the electrocatalyzed oxidations of methanol and ethanol in acid and alkaline solutions **478**, 108
Oscillators
Mechanistic classification of electrochemical oscillators — an operational experimental strategy **478**, 50
Oscillatory electrocatalytic iodate reduction system
Modeling galvanostatic potential oscillations in the electrocatalytic iodate reduction system **462**, 19
Os-phendione
Electrocatalytic oxidation of NADH at graphite electrodes modified with osmium phenanthrolinedione **464**, 208
Osteryoung square wave voltammetry
1-Naphthyl phosphate as an enzymatic substrate for enzyme-linked immunomagnetic electrochemistry **469**, 27
Overlap models
Theory of the chronoamperometric transient for electrochemical nucleation with diffusion-controlled growth **470**, 70
Overvoltage
Electrochemical formation of nickel hydride in alkaline solutions **472**, 182
Oxalic acid
Catalytic and electrocatalytic oxidation of oxalic acid in aqueous solutions of different compositions **474**, 147
Oxidation
A comparison of multistability in the electrocatalyzed oxidations of methanol and ethanol in acid and alkaline solutions **478**, 108
Anomalous electrochemical behaviour of palladium in aqueous solution **461**, 52
Cationic systems as self-assembled monolayers on gold surfaces **464**, 263
Electrochemical and catalytic behaviour of Dawson-type complexes derived from $[(1),2,3\text{-}P_2Mo_2W_{15}O_{61}]^{10-}$ and first transition metal ions **477**, 146
Electrochemical behaviour of amino acids on Pt(*hkl*). A voltammetric and in situ FTIR study: Part IV. Serine and alanine on Pt(100) and Pt(110) **475**, 38
Electrochemical oxidation of mono- and disaccharides at fresh as well as oxidized copper electrodes in alkaline media **464**, 252
In-situ FTIR studies on the electrochemical oxidation of histidine and tyrosine **463**, 218
Oxidation of halides by redox enhanced ferricyanide in the $[Fe^{II}\text{–}CN\text{–}Pt^{IV}]_n$ coordination polymer: an optically triggered process **470**, 99

Reactivity and activation parameters in methanol oxidation on platinum single crystal electrodes 'decorated' by ruthenium adlayers **467**, 143
Structural effects on the oxidation of HCOOH by bismuth modified Pt(111) electrodes with (110) monatomic steps **467**, 43
Oxidative dimerization
Cathodic synthesis of powerful electron π-donors including dithiadiazafulvalenes **462**, 137
Oxide layer
Structural properties of electrochemically designed porous oxide films on AlMgl **468**, 121
Oxide-matrix composite
Electrodeposited $PbO_2 + RuO_2$: a composite anode for oxygen evolution from sulphuric acid solution **465**, 160
Oxides
Electrodeposited $PbO_2 + RuO_2$: a composite anode for oxygen evolution from sulphuric acid solution **465**, 160
Oxine
Cathodic stripping square wave voltammetry of Cu(II)–oxine complexes. A mechanistic study **478**, 17
Square wave stripping voltammetry of Cd–oxine complexes; surface redox reactions **476**, 165
Oxoanions
Surface structural effects on specific adsorption of oxoanions on gold single crystal electrodes **467**, 335
Oxo bridged complexes
Electrochemical behaviour of (μ-oxo) di-aqua diiron(III) complexes in organic media. Electrogeneration of mononuclear $[Fe^{II}(L)_2(S)_2]^{2+}$ complexes (L = 2,2'-bipyridine and (−)4,5-pinene-2,2'-bipyridine; S = H_2O or CH_3CN) **469**, 53
Oxo complexes
Electrochemical behaviour of $[Mn_2^{III,IV}O_2(phen)_4]^{3+}$ complex in aqueous phen + phenH$^+$ buffer; phen = 1,10-phenanthroline **463**, 119
Oxygen
Electrocatalytic reduction of molecular oxygen on a sodium montmorillonite-methyl viologen carbon paste chemically modified electrode **463**, 253
Oxygen evolution
Effect of the partial replacement of Ni or Co by Cu on the electrocatalytic activity of the $NiCo_2O_4$ spinel oxide **464**, 187
Oxygen evolution reaction
Rotating ring-disk studies of oxidized nickel hydrous oxide: oxygen evolution and pseudocapacitance **468**, 64
Oxygen photoreduction
Oxygen reduction mechanisms at p-InP and p-GaAs electrodes in liquid ammonia in neutral buffered medium and acidic media **462**, 88
Oxygen reduction
Electrochemical characterisation of Pd modified ceramic | carbon electrodes: partially flooded versus wetted channel hydrophobic gas electrodes **466**, 45
Enhancement of the electrocatalytic O_2 reduction on Pt–Fe alloys **460**, 258
Heat-treated iron(III) tetramethoxyphenyl porphyrin chloride supported on high-area carbon as an electrocatalyst for oxygen reduction: Part II. Kinetics of oxygen reduction **462**, 63
Rotating ring-disk studies of oxidized nickel hydrous oxide: oxygen evolution and pseudocapacitance **468**, 64
Temperature and pressure dependence of O_2 reduction at Pt | Nafion® 117 and Pt | BAM® 407 interfaces **468**, 180
Oxygen reduction reaction
Oxygen reduction reaction on Pt(111): effects of bromide **467**, 157
Oxygen solubility
Comparative study on the oxygen dissolution behaviour in 62/38 mol% Li/K and 52/48 mol% Li/Na carbonate **470**, 39

Palladium
Adsorption, oxidation and reduction reactions of propargyl alcohol on palladium as studied by electrochemical mass spectrometry **472**, 71
Anomalous electrochemical behaviour of palladium in aqueous solution **461**, 52
Electrocatalytic reduction of nitrite at a carbon fiber microelectrode chemically modified by palladium(II)-substituted Dawson type heptadecatungstodiphosphate **469**, 63
Electrochemical characterisation of Pd modified ceramic | carbon electrodes: partially flooded versus wetted channel hydrophobic gas electrodes **466**, 45
Electrode reactions and accumulation of hydrogen at carbon paste electrodes in the presence of tetrachloropalladate **462**, 174
Hydrogen electrosorption in Ni–Pd alloys **460**, 30
The study of hydrogen sorption in palladium limited volume electrodes (Pd-LVE): I. Acidic solutions **471**, 190
Palladium electrode
Construction of a new dehydrogenation system using a two-compartment cell separated by a palladized Pd sheet electrode **463**, 116
Palladium(111) electrode
Infrared spectroscopy of carbon monoxide and nitric oxide on palladium(111) in aqueous solution: unexpected adlayer structural differences between electrochemical and ultrahigh-vacuum interfaces **474**, 155
Palladium layer
Epitaxial growth of a palladium layer on an Au(100) electrode **473**, 2
p- and n-doping processes
Anodic oxidation of various arylene-cyanovinylenes made of alternating fluorenyl, thienyl and/or phenyl units **466**, 144
Parameters estimation
A new approach to the estimation of electrocrystallization parameters **474**, 69
Para-methoxytoluene
Mechanistic investigation of the anodic oxidation of *p*-methoxytoluene in dry and wet acetonitrile **464**, 85
Partial differential equations
Finite-difference electrochemical kinetic simulations using the Rosenbrock time integration scheme **469**, 97
Passivation
An electrochemical impedance study on the interfacial behaviour of KC_8 electrodes in $LiClO_4$ containing electrolytes **474**, 107
On the electrochemical behavior of magnesium electrodes in polar aprotic electrolyte solutions **466**, 203
Passivation mechanism of iron in concentrated phosphoric acid **475**, 58
Study of the corrosion behavior of titanium and some of its alloys for biomedical and dental implant applications **471**, 109
Passive–active region
Current oscillations induced by chlorides during the passive–active transition of iron in a sulfuric acid solution **471**, 132
Passive film
Impedance and photoelectrochemical properties of porous oxide film on Type304 stainless steel formed by square wave potential pulse polarisation **473**, 265
Nano-mechano-electrochemistry of the iron (100) surface in solution **473**, 49
Pd | D electrode
Numerical simulation of hydrogen (deuterium) absorption into β-phase hydride (deuteride) palladium electrodes under galvanostatic conditions **474**, 123

Pd electrode
Change of hole size of Pd hole-array electrodes in a controlled fashion by cathodic polarization in acidic electrolyte **473**, 240
Pd | H electrode
Effects of self-stress on the hydrogen absorption into palladium hydride electrodes of plate form under galvanostatic conditions **474**, 130
Numerical simulation of hydrogen (deuterium) absorption into β-phase hydride (deuteride) palladium electrodes under galvanostatic conditions **474**, 123
Pd(*hkl*) electrodes
A method to prepare single crystal electrodes of reactive metals: application to Pd(*hkl*) **466**, 165
PEM fuel cell
Heat-treated iron(III) tetramethoxyphenyl porphyrin chloride supported on high-area carbon as an electrocatalyst for oxygen reduction: Part II. Kinetics of oxygen reduction **462**, 63
1,5-Pentanediol
Electrochemical investigation of 1,5-pentanediol adsorption on the Ag(111) and Ag(110) faces **467**, 217
Pentathiophene
Electrochemical generation of cation radical π-dimers in polymer film composed of pentathiophenes bridged by monosilanylene units **472**, 157
Peptide
Cadmium binding properties of the C-terminal hexapeptide from mouse metallothionein: study by linear sweep voltammetry and multivariate curve resolution analysis **468**, 202
Peptide-modified electrodes
Diffusionless electron transfer of microperoxidase-11 on gold electrodes **469**, 123
Percus–Yevick
A non-primitive model for the electrode | electrolyte interface based on the Percus–Yevick theory. Analysis of the different molecular sizes, ion valences and electrolyte concentrations **460**, 135
Performance indicators
Evaluation of a reactor model and cathode materials for batch electrolysis of L-cystine hydrochloride **462**, 97
Permeation
Discussion on permeation transients in terms of insertion reaction mechanism and kinetics **465**, 37
Electrochemical determination of hydrogen in metals **475**, 82
Perovskite
Strontium ruthenate perovskite as the active material for supercapacitors **460**, 154
Perylene dimer cation radical
Two-dimensional CCD detection of electrogenerated chemiluminescence (ECL) on an electrode surface. ECL reactions involving microcrystals of the perylene dimer cation radical salt **473**, 166
Phase separation
Formation of conducting clusters of polyaniline films detected by light scattering **473**, 132
Investigation of the structure of self-assembled monolayers of asymmetrical disulfides on Au(111) electrodes by electrochemical desorption **473**, 68
Phenylalanine
Ionic partition diagrams of ionisable drugs: pH-lipophilicity profiles, transfer mechanisms and charge effects on solvation **462**, 235
Phenylene
Electrochemical oxidation in different media of bis(*p*-phenylene crown ether) as a symmetrical molecule bearing two identical redox centers **460**, 119
pH Measurements
Flow-through electrochemical cell for accurate pH measurements at temperatures up to 400°C **463**, 146
Photo-catalysis
Photoelectrochemical submicrometer patterning of titanium dioxide by platinum **473**, 235
Photochemistry
Oxidation of halides by redox enhanced ferricyanide in the $[Fe^{II}–CN–Pt^{IV}]_n$ coordination polymer: an optically triggered process **470**, 99
Photocorrosion
A kinetic study of CdS photocorrosion by intensity modulated photocurrent and photoelectrochemical impedance spectroscopy **473**, 192
Effect of ultra-violet light irradiation on anodic oxide films on titanium in sulfuric acid solution **473**, 272
Photocurrent
Electrochemical and photoelectrochemical behaviour of poly-3-methylthiophene and polybithiophene in non-aqueous solutions: 1. Dark and light processes in systems with and without cathodic doping **463**, 190
Impedance and photoelectrochemical properties of porous oxide film on Type304 stainless steel formed by square wave potential pulse polarisation **473**, 265
Investigating the reduction characteristics of transient free radicals by laser-pulse electron photo-injection—mechanism diagnostic criteria and determination of reactivity parameters from time-resolved experiments **463**, 157
Photoelectrochemical studies with inorganic cage structures of metal dichalcogenides **473**, 186
Photoeffect
Magnetic properties and optical control of electrochemically prepared iron–chromium polycyanides **473**, 245
Photoelectrochemistry
A kinetic study of CdS photocorrosion by intensity modulated photocurrent and photoelectrochemical impedance spectroscopy **473**, 192
Capacitance and photocurrent study of electronic properties of anodic oxide films on Nb and Ta. Evaluation of the ionized donor concentration profile in Nb_2O_5 film **460**, 214
Electrochemical and photoelectrochemical behaviour of poly-3-methylthiophene and polybithiophene in non-aqueous solutions: 1. Dark and light processes in systems with and without cathodic doping **463**, 190
Evolution of a skeleton structured TiO_2 surface consisting of grain boundaries **473**, 204
Frequency dependent electrolyte electroreflectance at semiconductor | electrolyte interfaces **462**, 251
Graphite photoelectrochemistry 2. Photoelectrochemical studies of highly oriented pyrolitic graphite **476**, 118
Photoelectrochemical response and stability of titanium–zinc mixed oxide films formed by thermal oxidation **464**, 238
Role of surface states and adsorbates in time-resolved photocurrent measurements and photovoltage generation at phthalocyaninatozinc(II)-photocathodes **462**, 222
Photo-injected charge
Investigating the reduction characteristics of transient free radicals by laser-pulse electron photo-injection—mechanism diagnostic criteria and determination of reactivity parameters from time-resolved experiments **463**, 157
Photoluminescence
Formation of ⟨001⟩-aligned nano-scale pores on (001) n-InP surfaces by photoelectrochemical anodization in HCl **473**, 223
Photoselective etching
Evolution of a skeleton structured TiO_2 surface consisting of grain boundaries **473**, 204

pH Response
Effects of polymer thickness on the potentiometric pH responses of polypyrrole modified glassy carbon electrodes **476**, 109
pH sensitivity
On the pH sensitivity of the galvanic tungsten–water interaction product **472**, 178
Phthalocyaninatozinc
Role of surface states and adsorbates in time-resolved photocurrent measurements and photovoltage generation at phthalocyaninatozinc(II)-photocathodes **462**, 222
Phthalocyanine
Spectroelectrochemical investigations on the reduction of thin films of hexadecafluorophthalocyaninatozinc ($F_{16}PcZn$) **476**, 148
Picrate
Ion transfer across a phospholipid monolayer adsorbed at the water | 1,2-dichloroethane interface under surface pressure control **469**, 72
PITT
Determination of the Li ion chemical diffusion coefficient for the topotactic solid-state reactions occurring via a two-phase or single-phase solid solution pathway **477**, 32
Pitting corrosion
Anodic behavior of copper in acetonitrile: the influence of carbon dioxide and dimethylamine **466**, 107
pK_a of carboxylic acids
pK_a of an ω-carboxylalkanethiol self-assembled monolayer by interaction model **478**, 101
Plasma treatment
Electrochemical selectivity for redox systems at oxygen-terminated diamond electrodes **473**, 173
Platinum
Adsorption, oxidation and reduction reactions of propargyl alcohol on palladium as studied by electrochemical mass spectrometry **472**, 71
An electrochemical alcohol sensor based on a co-electrodeposited Pt | WO_3 electrode **471**, 151
Electrochemical oscillations of a new type in an $H_2O_2 + H_2SO_4$ | Pt-electrode system, appearing by addition of small amounts of halide ions **473**, 156
Electrochemical response of thiourea and formamidine disulphide on polycrystalline platinum in aqueous 0.5 M sulphuric acid **475**, 181
Electrochemical studies of six N–F electrophilic fluorinating reagents **474**, 1
Electrochemical surface reactions of intermediates formed in the oxidative ethanol adsorption on porous Pt and PtRu **471**, 167
Electro-oxidation of *meso*-erythritol on platinum in acid medium: analysis of the reaction products **464**, 101
Kinetics of the ferric/ferrous electrode reaction on Nafion®-coated electrodes **469**, 11
New effects in the electrochemistry of carbon dioxide on platinum by the application of potential perturbations **477**, 41
Photoelectrochemical submicrometer patterning of titanium dioxide by platinum **473**, 235
Potential modulated reflectance spectroscopy of Pt(111) in acidic and alkaline media: cyanide adsorption **463**, 109
Step decoration at Pt single crystal electrodes: role of the anion **467**, 50
Temperature and pressure dependence of O_2 reduction at Pt | Nafion® 117 and Pt | BAM® 407 interfaces **468**, 180
The adsorption of methylamine on Pt single crystal surfaces **467**, 105
Platinum alloy
Enhancement of the electrocatalytic O_2 reduction on Pt–Fe alloys **460**, 258
Platinum catalyst
Catalytic and electrocatalytic oxidation of oxalic acid in aqueous solutions of different compositions **474**, 147
Platinum electrodes
Mass spectrometric study of desorption and hydrogenation of biphenyl, naphthalene and *t*-butylbenzene on poly- and monocrystalline platinum electrodes **461**, 90
Oxidation of methylamine and ethylamine on Pt single crystal electrodes in acid medium **469**, 159
Structural effects on the oxidation of HCOOH by bismuth modified Pt(111) electrodes with (110) monatomic steps **467**, 43
Platinum-group electrodes
Coadsorbate vibrational interactions within mixed carbon monoxide-nitric oxide adlayers on ordered low-index platinum-group electrodes **467**, 92
Platinum/palladium particles
Platinum–palladium loaded polypyrrole film electrodes for the electrooxidation of D-glucose in neutral media **476**, 171
Platinum ruthenium alloys
Electrochemical surface reactions of intermediates formed in the oxidative ethanol adsorption on porous Pt and PtRu **471**, 167
Platinum single crystal electrodes
The electrochemistry of nitrogen-containing compounds at platinum single crystal electrodes: Part 3. Carbohydrazide on Pt(*hkl*) electrodes **467**, 20
PNA oligomers
Reduction and oxidation of peptide nucleic acid and DNA at mercury and carbon electrodes **476**, 71
Point of zero charge
Electrochemical features of zirconia polymorphs. The interplay between structure and surface OH species **465**, 136
Poisoning
Reaction mechanism and dynamics of methanol electrooxidation on platinum(111) **467**, 132
Polarography
A minimum separating diffusion and adsorption waves in polarography using a static mercury drop electrode **465**, 30
Polyacrylonitrile
Inhibition effects of polyacrylonitrile gel electrolytes on lithium dendrite formation **472**, 142
Poly(3-alkylthiophene)
Separation of pinhole and tunneling electron transfer processes at self-assembled polymeric monolayers on gold electrodes **470**, 114
Polyaniline
A UV-vis spectroelectrochemical study of redox reactions of solution species at a polyaniline electrode in the conducting and the reduced state **461**, 184
Electrochemical behaviour of *N*-aminopyridinium, and the viologens *N,N'*-diamino-4,4'-bipyridilium and *N,N'*-bis(4-aminophenyl)-4,4'-bipyridilium in aqueous acid: towards the formation of polymer hybrids of pyridine and aniline **462**, 43
Poly(aniline)
Addition of α-hydroxyalkylferrocenes to electrochemically oxidized poly(aniline) **470**, 166
Polyaniline films
Formation of conducting clusters of polyaniline films detected by light scattering **473**, 132
Light scattering of polyaniline films responding to electrochemical switching **460**, 254
Polybithiophene
Electrochemical and photoelectrochemical behaviour of poly-3-methylthiophene and polybithiophene in non-aqueous solu-

tions: 1. Dark and light processes in systems with and without cathodic doping **463**, 190
Polymer chain encapsulation followed by a quartz microbalance during electropolymerization of bithiophene-β-cyclodextrin host–guest compounds in aqueous solution **476**, 1
Polycarbazole
Mechanical resonance effects in electroactive polycarbazole films **460**, 267
Polycrystalline gold
Polycrystalline gold electrode redox behavior in an ammoniacal electrolyte: Part II. A parallel RRDE, EQCM and TOF-SIMS study of copper underpotential deposition **460**, 143
Polycrystalline gold electrode
Polycrystalline gold electrode redox behavior in an ammoniacal electrolyte: Part I. A parallel RRDE, EQCM, XPS and TOF-SIMS study of supporting electrolyte phenomena **460**, 131
Poly(estersulfonate)
Factors influencing the ion-exchange preconcentration and voltammetric behaviour of redox cations at polyestersulfonated ionomer coated electrodes in acetonitrile solutions **460**, 38
Polyethers
The complex formation of non-cyclic polyethers and crown ethers with Ag^+ in acetone and propylene carbonate studied by potentiometric and calorimetric methods **474**, 188
Poly(3,4-ethylenedioxythiophene)
Nucleation and growth of poly(3,4-ethylenedioxythiophene) in acetonitrile on platinum under potentiostatic conditions **472**, 103
Poly[(hexamethyltrisilanylene)oligo(2,5-thienylene)]
Electrochemical oxidation of poly[(hexamethyltrisilanylene)oligo(2,5-thienylene)] films **464**, 158
Polymer
Oxidation of halides by redox enhanced ferricyanide in the $[Fe^{II}–CN–Pt^{IV}]_n$ coordination polymer: an optically triggered process **470**, 99
Polymer-coated electrodes
Novel polymer-modified electrodes for batch injection sensors and application to environmental analysis **468**, 26
Temperature dependence of physical displacement and charge hopping in a polymer membrane incorporating a trinuclear ruthenium complex **476**, 159
Polymer electrodes
Platinum–palladium loaded polypyrrole film electrodes for the electrooxidation of D-glucose in neutral media **476**, 171
Polymer electrolyte fuel cell
Effect of water transport in a PEFC at low temperatures operating with dry hydrogen **477**, 164
Electrochemical impedance of the cathode catalyst layer in polymer electrolyte fuel cells **475**, 107
Theory for water management in membranes for polymer electrolyte fuel cells: Part 1. The effect of impurity ions at the anode side on the membrane performances **465**, 1
Theory for water management in membranes for polymer electrolyte fuel cells: Part 2. The effect of impurity ions at the cathode side on the membrane performances **465**, 18
Polymer electrolytes
Methanol oxidation and direct methanol fuel cells: a selective review **460**, 14
Polymerization reaction
Polymerization reaction coupled to charge transfer: propagation versus termination as a source of permanent travelling waves and multi-peak voltammograms **479**, 43
Polymer Langmuir–Blodgett film
A structural effect on electrochemical behavior of hetero-deposited redox polymer Langmuir–Blodgett films containing ferrocene and tris(bipyridine)ruthenium derivatives **473**, 125
Polymer modified electrodes
Preparation and characterization of Nafion® coated sphere-cap mercury microelectrodes **471**, 48
Rapidly renewable and reproducible electropolymerized surface at a monomer modified carbon paste electrode **465**, 102
Polymer modified glassy carbon electrodes
Factors influencing the ion-exchange preconcentration and voltammetric behaviour of redox cations at polyestersulfonated ionomer coated electrodes in acetonitrile solutions **460**, 38
Polymer supported manganese(III) protoporphyrin IX
Anion-selective membrane electrodes based on polymer-supported metalloporphyrins **468**, 98
Polymer supported membrane
Polarization phenomena at the water|*o*-nitrophenyl octyl ether interface: Part III. Kinetics of tetraethylammonium ion transfer across the polymer supported interfaces **463**, 232
Polymethacrylate
Voltammetric metal speciation in mixtures of inert and labile macromolecular complexes at any ligand-to-metal ratio: differential pulse polarographic study of the Zn(II)–nitrilotriacetate–polymethacrylate system **462**, 157
Polymethacrylonitrile
Electropolymerization of methacrylonitrile on a rotating disk electrode at high spinning rate **470**, 14
Poly(2-methoxyaniline)
Electropolymerization of 2-methoxy aniline. Electrochemical and spectroscopical product characterization **471**, 180
Poly[1-methyl-3-(pyrrol-1-ylmethyl)pyridinium] film
Current enhancing effect of poly[1-methyl-3-(pyrrol-1-ylmethyl)pyridinium] films on the electrode reaction of anthraquinonedisulfonate **478**, 9
Poly-3-methylthiophene
Electrochemical and photoelectrochemical behaviour of poly-3-methylthiophene and polybithiophene in non-aqueous solutions: 1. Dark and light processes in systems with and without cathodic doping **463**, 190
Poly(3-methyl thiophene)
Studies on the redox behaviour of some polythiophene derivatives by impedance spectroscopy in symmetrical and asymmetrical configurations **472**, 20
Poly(*N*-methylpyrrole)
Mass transport behavior of polypyrrole and poly(*N*-methylpyrrole) films in acetonitrile solutions **468**, 104
Poly(*N*-vinylcarbazole)
Spectroelectrochemical study of the influence of anions on the behaviour of poly(*N*-vinylcarbazole) films **475**, 1
Poly(*o*-aminophenol)
Transport across poly(*o*-aminophenol) modified electrodes in contact with media containing redox active couples. A study using rotating disc electrode voltammetry **477**, 1
Polyoxometalates
Metal ion complexes derived from the α_1 isomer of $(P_2W_{17}O_{61})^{10-}$: comparison with the corresponding α_2 species **478**, 76
Polyoxometalate modified electrodes: from a monolayer to multilayer structures **462**, 187
Poly(phenazine-2,7-diyl)
Oligomeric poly(phenazine-2,7-diyl) and its electrochemical response **460**, 242
Polyphenol oxidase
Amplification of amperometric biosensor responses by electrochemical substrate recycling: Part I. Theoretical treatment of the catechol–polyphenol oxidase system **470**, 53
Amplification of amperometric biosensor responses by electrochemical substrate recycling: Part II. Experimental study of the catechol–polyphenol oxidase system immobilized in a laponite clay matrix **470**, 61

Kinetic behaviour of dopamine-polyphenol oxidase on electrodes of tetrathiafulvalenium tetracyanoquinodimethanide and tetracyanoquinodimethane species **461**, 174
Polypyrrole
A glucose biosensor based on enzyme entrapment within polypyrrole films electrodeposited on mesoporous titanium dioxide **469**, 176
Effects of polymer thickness on the potentiometric pH responses of polypyrrole modified glassy carbon electrodes **476**, 109
In situ atomic force microscopy study of polypyrrole synthesis and the volume changes induced by oxidation and reduction of the polymer **462**, 211
Mass transport behavior of polypyrrole and poly(*N*-methylpyrrole) films in acetonitrile solutions **468**, 104
MRA combined spectroelectrochemical studies on the redox stability of PPy/DS films **462**, 1
Platinum–palladium loaded polypyrrole film electrodes for the electrooxidation of D-glucose in neutral media **476**, 171
Ultra-fast electropolymerization of pyrrole in aqueous media on oxidizable metals in a one-step process **478**, 92
Poly(pyrroles)
Enantioselective electrodes: stereoselective electroreduction of 4-methylbenzophenone and acetophenone **461**, 94
Poly(3-thienyl methacrylate)
Studies on the redox behaviour of some polythiophene derivatives by impedance spectroscopy in symmetrical and asymmetrical configurations **472**, 20
Poly((3-thienyl) methylacrylate)
Synthesis, electropolymerization and electrochemical characterization of some new acrylate substituted thiophene derivatives **460**, 176
Polythiophene
The electrochemical properties of a series of phenylene-thienyl polymers in tetramethylene sulfone based electrolytes **460**, 46
Voltammetric investigation of new polythiophene derivatives possessing electrochemically cleavable arylsulfonamide groups as precursors for solid phase electrosynthesis **477**, 121
Poly(thiophene-3-methanol)
Studies on the redox behaviour of some polythiophene derivatives by impedance spectroscopy in symmetrical and asymmetrical configurations **472**, 20
Polyuridylic acid
Accumulation of Hg(II) by adsorbed polyuridylic acid: differentiation of coordinated Hg(II) and covalently mercurated species **466**, 2
Pores
Formation of ⟨001⟩-aligned nano-scale pores on (001) n-InP surfaces by photoelectrochemical anodization in HCl **473**, 223
Porous electrodes
Transfer matrix method for the electrochemical impedance of inhomogeneous porous electrodes and membranes **460**, 63
Porous semiconductors
Formation of ⟨001⟩-aligned nano-scale pores on (001) n-InP surfaces by photoelectrochemical anodization in HCl **473**, 223
Porous silicon
Simultaneous platinum deposition and formation of a photoluminescent porous silicon layer **469**, 48
Porphyrazine
Cobalt(II) porphyrazine catalysed reduction of nitrite **470**, 126
Potential
Thermodynamics for the situation where there is a discontinuous change of the electrode condition with potential due to the formation of a two dimensional condensed phase—diffuse layer effects **463**, 9
ψ_1 Potential
Effect of cation adsorption on the kinetics of anion electroreduction: Part I. Effect of the adsorption of inorganic cations in small concentrations on the kinetics of anion electroreduction with different elementary steps of discharge **476**, 26
Effect of cation adsorption on the kinetics of anion electroreduction: Part II. Effect of the adsorption of organic cations in small concentrations on the kinetics of anion electroreduction **476**, 37
Potential perturbations
New effects in the electrochemistry of carbon dioxide on platinum by the application of potential perturbations **477**, 41
Potential-step chronocoulospectrometry
Temperature dependence of physical displacement and charge hopping in a polymer membrane incorporating a trinuclear ruthenium complex **476**, 159
Potentiodynamic behaviour
The potentiodynamic behaviour of iridium electrodes in aqueous 3.7 M H_2SO_4 in the 293–195 K range **461**, 40
Potentiometry
Effects of polymer thickness on the potentiometric pH responses of polypyrrole modified glassy carbon electrodes **476**, 109
The complex formation of non-cyclic polyethers and crown ethers with Ag^+ in acetone and propylene carbonate studied by potentiometric and calorimetric methods **474**, 188
Potentiostatic pulses
Hydrogen evolution on silver single crystal electrodes—first results **461**, 76
Powder | Nafion® interface
Surface diffusion and the spillover of H-adatoms and oxygen-containing surface species on the surface of carbon black and Pt/C porous electrodes **476**, 101
Preconcentration
Use of a zeolite-modified electrode for the study of the methylviologen–sodium ion-exchange in zeolite Y **463**, 100
Prepeak
Electrochemical characterization of an enzyme electrode based on a ferrocene-containing redox polymer **468**, 193
Presence of product
General solutions for the I/t response for reversible processes in the presence of product in a multipotential step experiment at planar and spherical electrodes whose areas increase with any power of time **466**, 8
Pressure
Temperature and pressure dependence of O_2 reduction at Pt | Nafion® 117 and Pt | BAM® 407 interfaces **468**, 180
Probe beam deflection
Quantitative discrimination of mass fluxes at electrochemical interfaces by optical beam deflection **466**, 218
Programmed potential step technique
Studies of kinetics of HCOOH oxidation on Pt(100), Pt(110), Pt(111), Pt(510) and Pt(911) single crystal electrodes **467**, 121
Promoter
Electrochemical behavior of gold electrodes modified with aminopurinethiol derivatives **473**, 99
Propanediol
In-situ infrared reflectance spectroscopic study of propanediol electrooxidation at platinum and gold: Part 1. 1,3-Propanediol **463**, 63
Propargyl alcohol
Adsorption, oxidation and reduction reactions of propargyl alcohol on palladium as studied by electrochemical mass spectrometry **472**, 71
Propranolol
Ion transfer across a phospholipid monolayer adsorbed at the water | 1,2-dichloroethane interface under surface pressure control **469**, 72
Propylene carbonate + acetonitrile mixtures
Conductivity study on lithium bromide in propylene carbonate + acetonitrile mixtures in dilute solutions from −35 to 75°C **471**, 78

Protonation
Electrochemical reduction of phenyl-substituted cyclopentadienes: a case of an 'indirect father–son' self-protonation process **460**, 160
Proton injection
A quantitative discrimination between anion insertion- and surface redox-reactions at graphite with the rotating ring/disk-electrode **461**, 167
Proton insertion
X-ray absorption in relation to valency of iridium in sputtered iridium oxide films **465**, 88
Protons
Anomalous H/D isotopic effect in the kinetics of polarographic hydrogen evolution **477**, 62
Protoporphyrin IX
Cobalt(II) metallated hematoporphyrin IX and protoporphyrin IX immobilized on niobium(V) oxide grafted on a silica gel surface: electrochemical studies **477**, 158
Prussian blue
Cyclic voltammetric studies of Prussian blue and viologens within a paper matrix for electrochromic printing applications **461**, 263
Electrochemical quartz crystal microbalance and in situ infrared spectroscopic studies on the redox reaction of Prussian blue **474**, 101
Prussian blue analog
Magnetic properties and optical control of electrochemically prepared iron–chromium polycyanides **473**, 245
Pseudocapacitance
Rotating ring-disk studies of oxidized nickel hydrous oxide: oxygen evolution and pseudocapacitance **468**, 64
Pseudomonas stutzeri
Amperometric nitrate biosensors on the basis of *Pseudomonas stutzeri* nitrate reductase **474**, 43
Pt(100)
Structural changes at the Pt(100) surface with a great number of potential cycles **460**, 251
Pt(111)
Oxidation of CO adlayers on Pt(111) at low potentials: an impinging jet study in H_2SO_4 electrolyte with mathematical modeling of the current transients **467**, 74
Reaction mechanism and dynamics of methanol electrooxidation on platinum(111) **467**, 132
Redox mechanisms of NO with water on the Pt(111) electrode studied by in-situ STM and IRAS **473**, 43
Pt/C catalyst
Surface diffusion and the spillover of H-adatoms and oxygen-containing surface species on the surface of carbon black and Pt/C porous electrodes **476**, 101
Pt electrode
An electrochemical quartz crystal microbalance study of the hydrogen underpotential deposition at a Pt electrode **467**, 186
An in situ UV-vis and IR spectroelectrochemical study of the deposition of a hydroquinone anion salt on platinum electrodes from dichloromethane solutions **462**, 266
Infrared spectroelectrochemistry of the oxidation of absolute methanol at a platinum electrode **464**, 93
Pt(111) electrodes
Reactivity and activation parameters in methanol oxidation on platinum single crystal electrodes 'decorated' by ruthenium adlayers **467**, 143
Temperature-dependent research on Pt(111) and Pt(100) electrodes in aqueous H_2SO_4 **467**, 177
The study of the adsorption/desorption of acetate anions on a Pt(111) electrode and the effect of counter cations in acidic media **467**, 112
Urea adsorption on Pt(111) electrodes **461**, 65
Pt{100} electrodes
Voltammetric and UHV characterisation of the (1 × 1) and reconstructed hex-R0.7° phases of Pt{100} **467**, 60
Pt(100) electrodes
Temperature-dependent research on Pt(111) and Pt(100) electrodes in aqueous H_2SO_4 **467**, 177
Pt(310) face
Structural changes at the Pt(100) surface with a great number of potential cycles **460**, 251
Pt–Fe
Enhancement of the electrocatalytic O_2 reduction on Pt–Fe alloys **460**, 258
Pt(*hkl*) surfaces
Influence of adsorption of guanidonium cations on H upd at Pt(*hkl*) surfaces: lattice-specific anion-mimetic effects **467**, 30
PtRu electrode
Ethanol oxidation on PtRu electrodes studied by differential electrochemical mass spectrometry **472**, 120
Pt–Ru electrodeposits
Characterization of platinum-ruthenium electrodeposits using XRD, AES and XPS analysis **460**, 32
Pt single crystal
Structural changes at various Pt single crystal surfaces with potential cycles in acidic and alkaline solutions **467**, 85
Pt single crystal electrodes
Structural specificity of the kinetics of the hydrogen evolution reaction on the low-index surfaces of Pt single-crystal electrodes in 0.5 M dm^{-3} NaOH **461**, 80
Studies of kinetics of HCOOH oxidation on Pt(100), Pt(110), Pt(111), Pt(510) and Pt(911) single crystal electrodes **467**, 121
Pt(S)-[*n*(110) × (100)]
Significant enhancement of the electrochemical reduction of CO_2 at the kink sites on Pt(S)-[*n*(110) × (100)] and Pt(S)-[*n*(100) × (110)] **467**, 67
Pt(S)-[*n*(100) × (110)]
Significant enhancement of the electrochemical reduction of CO_2 at the kink sites on Pt(S)-[*n*(110) × (100)] and Pt(S)-[*n*(100) × (110)] **467**, 67
Pt(111) surface
Electric field effects on CO and NO adsorption at the Pt(111) surface **476**, 64
Kinetic and mechanistic study of hydroxyl ion electrosorption at the Pt(111) surface in alkaline media **466**, 155
Pt(110) surfaces
Bromine monolayer adsorption on Pt(110) surfaces **467**, 11
Pt | WO_3
An electrochemical alcohol sensor based on a co-electrodeposited Pt | WO_3 electrode **471**, 151
Pulse electrolysis stopped-flow method
Kinetic studies on ion pair formation between 2,3,5,6-tetrachloro-1,4 benzoquinone anion radical and alkaline earth metal cations (RPS 6708) **472**, 91
Pulse polarography
Voltammetric currents for any ligand-to-metal concentration ratio in fully labile metal-macromolecular complexation. Easy computations, analytical properties of the currents and a graphical method to estimate the stability constant **472**, 42
Voltammetry of sparingly soluble metal complexes: a differential pulse polarographic study of the Zn(II) + oxalate system **475**, 99
PVC
Anion-selective membrane electrodes based on polymer-supported metalloporphyrins **468**, 98
pWO_4^{2-} sensitivity
On the pH sensitivity of the galvanic tungsten–water interaction product **472**, 178

Pyridine
Adsorption of pyridine on a polycrystalline gold electrode surface studied by infrared reflection absorption spectroscopy **470**, 136
Ionic partition diagrams of ionisable drugs: pH-lipophilicity profiles, transfer mechanisms and charge effects on solvation **462**, 235
Pyridine adlayers
Influence of the electric potential on the structure of pyridine adlayers on Au(111) terraces from in-situ scanning tunnelling microscopy imaging **467**, 230
Pyridine adsorption on gold
Steric effects on molecular adsorption at columnar surfaces. A model for the adsorption of pyridine on gold electrodes **474**, 74
Pyridine, Self-assembled molecule
What can we learn from the non-linear optical investigation of the liquid | solid interface? **473**, 25
Pyridinethiol
Electrochemical study on competitive adsorption of pyridinethiol with sulfide onto Au(111) surfaces **473**, 85
Pyrite (FeS_2)
Electrochemical oxidation of pyrite (FeS_2) in aqueous electrolytes **471**, 116
Pyrrole
Electrochemical synthesis and structural studies of copolymers based on the electrooxidation of pyrrole and some salen compounds **470**, 77
Investigation of the lifetimes of some pyrrole species by rapid scan cyclic voltammetry and double potential step techniques **464**, 123
The electrochemical copolymerization of pyrrole and furan in a novel binary solvent system **470**, 23
Pyruvate oxidase
Pyruvate sensor based on pyruvate oxidase immobilized in a poly(mercapto-*p*-benzoquinone) film **464**, 143
Pyruvate sensor
Pyruvate sensor based on pyruvate oxidase immobilized in a poly(mercapto-*p*-benzoquinone) film **464**, 143

Quartz crystal impedance
Combined quartz crystal impedance and electrochemical impedance measurements during adsorption of bovine serum albumin onto bare and cysteine- or thiophenol-modified gold electrodes **478**, 1
Quartz crystal microbalance
Coupled electron and proton transfers: compared behaviour of oxometalates in aqueous solution or after entrapment in polymer matrices **463**, 129
Electrochemically induced mass transfer and rheological changes of Nafion® coatings fully loaded with $[Os(bpy)_3]^{2+}$ **469**, 34
Investigation of the cathodic electropolymerization of acrylonitrile, ethylacrylate and methylmethacrylate by coupled quartz crystal microbalance analysis and cyclic voltammetry **472**, 83
Mechanical resonance effects in electroactive polycarbazole films **460**, 267
On the use of the quadratic logistic differential equation for the interpretation of electrointercalation processes **460**, 161
Polymer chain encapsulation followed by a quartz microbalance during electropolymerization of bithiophene-β-cyclodextrin host–guest compounds in aqueous solution **476**, 1
Quasi-equilibrium conditions
Kinetic and mechanistic study of hydroxyl ion electrosorption at the Pt(111) surface in alkaline media **466**, 155
Quinine copper complex
Voltammetric determination of the iodide ion with a quinine copper(II) complex modified carbon paste electrode **463**, 16
Quinone
A review of a new voltammetric method for determining acids **468**, 53

Radical anions
Electrochemical reduction of phenyl-substituted cyclopentadienes: a case of an 'indirect father–son' self-protonation process **460**, 160
Radical polarogram
Investigating the reduction characteristics of transient free radicals by laser-pulse electron photo-injection—mechanism diagnostic criteria and determination of reactivity parameters from time-resolved experiments **463**, 157
Radioactive labeling
Comments on 'On the calculation of surface concentration from the measurement by the radiotracer 'electrode lowering' technique' by D. Poskus **464**, 118
Radiometry
Adsorption of sulfate ions on monocrystalline copper electrodes: the structural effects **463**, 1
Radiotracer technique
Direct experimental evidence proving the formation of surface layers in the course of the reduction of Cr(VI) species at a gold electrode **471**, 73
Raman spectroscopy
Characterization of the surface carbonyl and hydroxyl coverage on glassy carbon electrodes using Raman spectroscopy **469**, 150
Rate constant
Electrochemical evaluation of the reaction rate between methyl viologen mediator and diaphorase enzyme for the electrocatalytic reduction of NAD^+ and digital simulation for its voltammetric responses **465**, 153
Rate-determining
Fumarodinitrile electrohydrodimerization and acrylonitrile electroreduction on liquid gallium: a comparison with mercury **462**, 127
Rate enhancement
Enhancement of the electrochemical Li doping/undoping reaction rate of a graphitic material by an evaporated film of Sn, Zn or Pb **462**, 150
Rayleigh scattering
Light scattering of polyaniline films responding to electrochemical switching **460**, 254
Reaction/diffusion
Application of Danckwerts' expression to first-order EC′ reactions. Transient currents at inlaid and recessed microdisc electrodes **466**, 15
Steady-state currents at inlaid and recessed microdisc electrodes for first-order EC′ reactions **476**, 132
Reaction–diffusion
Finite-difference electrochemical kinetic simulations using the Rosenbrock time integration scheme **469**, 97
Reaction kinetics
Studies of kinetics of HCOOH oxidation on Pt(100), Pt(110), Pt(111), Pt(510) and Pt(911) single crystal electrodes **467**, 121
Reaction mechanisms
Electro-oxidation of *meso*-erythritol on platinum in acid medium: analysis of the reaction products **464**, 101
Reaction rate
Discussion of the paper by Barber et al. [J. Electroanal. Chem. 446 (1998) 125] **466**, 122
Reactions at nm-sized voids
Voltammetric anodic stripping of silver from platinum electrodes consisting of an array of nm-sized voids **477**, 14

Reactive metals
A method to prepare single crystal electrodes of reactive metals: application to Pd(*hkl*) **466**, 165
Reactor models
Evaluation of a reactor model and cathode materials for batch electrolysis of L-cystine hydrochloride **462**, 97
Rechargeable lithium battery
Electrochemical control of a Li metal anode interface: improvement of Li cyclability by inorganic additives compatible with electrolytes **473**, 279
Recrystallisation
Two mercury drops on a conducting surface in a mercurous ion solution as a model for electrochemical Ostwald ripening **468**, 127
Rectangular wave voltage
Electrodeposition method for controlled formation of CdS films from aqueous solutions **473**, 217
Redox-active ligand
Electrochemical response to anions by neutral ferrocenyl receptors containing 2,2′-bipyridyl arms **469**, 132
Redox behaviour
Studies on the redox behaviour of some polythiophene derivatives by impedance spectroscopy in symmetrical and asymmetrical configurations **472**, 20
Redox-cycling
Redox-cycling type electrochemiluminescence in aqueous medium. A new principle for the detection of proteins labeled with a ruthenium chelate **474**, 192
Redox mechanism
Mechanism of the electrochemical reduction of sulfur dioxide in non-aqueous solvents **476**, 15
Redox mediator
Amperometric nitrate biosensors on the basis of *Pseudomonas stutzeri* nitrate reductase **474**, 43
A UV-vis spectroelectrochemical study of redox reactions of solution species at a polyaniline electrode in the conducting and the reduced state **461**, 184
Electrochemical and spectroelectrochemical properties of manganese reconstituted myoglobin **460**, 245
Redox polymer
Coupled electron and proton transfers: compared behaviour of oxometalates in aqueous solution or after entrapment in polymer matrices **463**, 129
Electrochemical characterization of an enzyme electrode based on a ferrocene-containing redox polymer **468**, 193
Redox potential
Electroanalytical chemistry of myoglobin with modification of distal histidine by cyanated imidazole **468**, 9
Electrochemical and spectroelectrochemical properties of manganese reconstituted myoglobin **460**, 245
Electrochemical study of tetraphenylporphinato-iron(III)–thiolate complexes, NH···S hydrogen bonding in the cytochrome P-450 model system **469**, 84
Redox reactions
Anion and water involvement in hydrous Ir oxide redox reactions in acidic solutions **475**, 20
Electrochemical behavior of a *Cypridina* luciferin analogue in acetonitrile solutions in the presence of proton acceptors **476**, 46
Structural differences in self-assembled monolayers of anthraquinone derivatives on silver and gold electrodes studied by cyclic voltammetry and in situ SERS spectroscopy **478**, 83
Transport across poly(*o*-aminophenol) modified electrodes in contact with media containing redox active couples. A study using rotating disc electrode voltammetry **477**, 1
Redox reactions of perylene
Two-dimensional CCD detection of electrogenerated chemiluminescence (ECL) on an electrode surface. ECL reactions involving microcrystals of the perylene dimer cation radical salt **473**, 166
Reduction
Cathodic reduction of 2-nitronaphthothiophen-4,9-quinone: evidence of catalysis by proton donors and its simulation **462**, 195
Direct experimental evidence proving the formation of surface layers in the course of the reduction of Cr(VI) species at a gold electrode **471**, 73
Electrochemical reduction of dichlorodifluoromethane in acetonitrile medium to useful fluorinated compounds **471**, 26
Electrochemical studies of six N–F electrophilic fluorinating reagents **474**, 1
Electro-enzymatic reduction of dioxygen to water in the cathode compartment of a biofuel cell **464**, 110
Mechanism of the electrochemical reduction of sulfur dioxide in non-aqueous solvents **476**, 15
Photoelectrochemical submicrometer patterning of titanium dioxide by platinum **473**, 235
Salt and isotope effects upon a multistep electrode reaction: the reduction of nitromethane on mercury **474**, 60
Surface redox catalysis and reduction kinetics of hydrogen peroxide on copper–nickel alloys **470**, 31
Reduction mechanisms
A contribution to the study of the electroreduction of 2-chloro-4,6-di(ethylamino)-1,3,5-triazine (simazine) on mercury electrodes **474**, 174
Reduction of Eu^{3+}
Electrode kinetics of Eu^{3+} in dimethylsulfoxide **470**, 1
Reduction of radicals
Investigating the reduction characteristics of transient free radicals by laser-pulse electron photo-injection—mechanism diagnostic criteria and determination of reactivity parameters from time-resolved experiments **463**, 157
Reductive cleavage
Solvent effect on kinetics of the chloride ion cleavage from anion radicals of 4-chlorobenzophenone **464**, 259
Thermodynamic and kinetic basicities of the carbon and oxygen ends of enolates. Their role in the reductive cleavage electrochemistry of α-substituted acetophenones **476**, 81
Reflection
Light scattering of polyaniline films responding to electrochemical switching **460**, 254
Regioselectivity
Self-protonation mechanism in the electrochemical reduction of Jatropholone **466**, 99
Regularization methods
The use of regularization methods in the deconvolution of underlying distributions in electrochemical processes **475**, 28
Replication
Change of hole size of Pd hole-array electrodes in a controlled fashion by cathodic polarization in acidic electrolyte **473**, 240
Reproducibility
An electrochemical alcohol sensor based on a co-electrodeposited $Pt|WO_3$ electrode **471**, 151
Reverse pulse voltammetry
Study of a catalytic mechanism in double potential step techniques at spherical electrodes **468**, 158
Reversible process
General solutions for the I/t response for reversible processes in the presence of product in a multipotential step experiment at planar and spherical electrodes whose areas increase with any power of time **466**, 8
Reversible redox
Synthesis and electrochemical characterization of self-assembled monolayers of redox-active oxide-bridged triruthenium(III) clusters on Au(111) **473**, 93

Reversing overpotential
A new approach to metal electrodeposition at a periodically changing rate: Part I. The reversing overpotential method **464**, 245
Rhenium–carbonyl compound
Electrochemical properties of the first Re(I)–carbonyl compound of di-2-pyridyl ketone.oxime (dpk.oxime), *fac*-$Re(CO)_3$-(dpk.oxime)Cl, in non-aqueous media **466**, 60
Rhodamine B derivative
Second harmonic generation investigation of rhodamine B derivatives in Langmuir–Blodgett films **465**, 195
Rhodium deposition
The initial stages of rhodium deposition on Au(111) **467**, 249
Rosenbrock method
Finite-difference electrochemical kinetic simulations using the Rosenbrock time integration scheme **469**, 97
Rotating disc
Kinetics of electrocatalytic oxidation of formaldehyde on a nickel porphyrin-based glassy carbon electrode **469**, 18
Rotating disk electrode
Electrocatalytic oxidation of hydrazine at a chlorogenic acid (CGA) modified glassy carbon electrode **465**, 168
Electrochemical studies of ferrocene derivatives and their complexation by β-cyclodextrin **477**, 130
Electrodeposition of copper from cuprous cyanide electrolyte: II. Current distribution on a rotating disk **474**, 31
Electropolymerization of methacrylonitrile on a rotating disk electrode at high spinning rate **470**, 14
Rotating disk electrode amperometric detection for a bead-based immunoassay **468**, 2
Rotating ring-disk electrode
A quantitative discrimination between anion insertion- and surface redox-reactions at graphite with the rotating ring/disk-electrode **461**, 167
Passivation mechanism of iron in concentrated phosphoric acid **475**, 58
Rotating ring-disk studies of oxidized nickel hydrous oxide: oxygen evolution and pseudocapacitance **468**, 64
Rotating ring-disk technique
Oxygen reduction reaction on Pt(111): effects of bromide **467**, 157
Rotogravure
Rotograved carbon electrodes for amperometric cadmium and lead determination **469**, 189
Roughness
Specific adsorption at modulated liquid | liquid interfaces **475**, 46
Rough platinum electrodes
Voltammetric anodic stripping of silver from platinum electrodes consisting of an array of nm-sized voids **477**, 14
RRDE
Polycrystalline gold electrode redox behavior in an ammoniacal electrolyte: Part II. A parallel RRDE, EQCM and TOF-SIMS study of copper underpotential deposition **460**, 143
$[Ru(bpy)_3]^{3+}$
Diamond-like carbon electrodes in electrochemical microgravimetry **464**, 230
$Ru(bpy)_3^{2+}$
Redox-cycling type electrochemiluminescence in aqueous medium. A new principle for the detection of proteins labeled with a ruthenium chelate **474**, 192
Ruthenium
Electrochemical quartz crystal microbalance study of electrodeposited ruthenium **474**, 167
Enhanced stability and electrocatalytic activity of a ruthenium-modified cobalt–hexacyanoferrate film electrode **471**, 42
Reactivity and activation parameters in methanol oxidation on platinum single crystal electrodes 'decorated' by ruthenium adlayers **467**, 143
Ruthenium adlayers
Reactivity and activation parameters in methanol oxidation on platinum single crystal electrodes 'decorated' by ruthenium adlayers **467**, 143
Ruthenium chelate
Redox-cycling type electrochemiluminescence in aqueous medium. A new principle for the detection of proteins labeled with a ruthenium chelate **474**, 192
Ruthenium complexes
A structural effect on electrochemical behavior of hetero-deposited redox polymer Langmuir–Blodgett films containing ferrocene and tris(bipyridine)ruthenium derivatives **473**, 125
Electrochemical formation and spectroelectrochemical characterization of organometallic $[Ru(L)(CO)_2]_n$ polymers; L = disubstituted-2,2′-bipyridine **466**, 187
Temperature dependence of physical displacement and charge hopping in a polymer membrane incorporating a trinuclear ruthenium complex **476**, 159
Ruthenium electrodes
Impedance of ruthenium electrodes in sulphuric acid solution **463**, 29
Ruthenium purple
Ruthenium purple-containing zeolite modified electrodes and their application for the detection of glucose **466**, 82

Salen
Electrochemical synthesis and structural studies of copolymers based on the electrooxidation of pyrrole and some salen compounds **470**, 77
Salicylate interference
Trifluoroacetophenone derivative-based carbonate ion-selective electrodes: effect of diluent pH on the anion selectivity **468**, 76
Salt effect
Salt and isotope effects upon a multistep electrode reaction: the reduction of nitromethane on mercury **474**, 60
SAM
A Nernstian electron source model for the ac voltammetric response of a reversible surface redox reaction using large-amplitude ac voltages **466**, 197
Sandwich immunoassay
Rotating disk electrode amperometric detection for a bead-based immunoassay **468**, 2
Sarcosine
Experimental and calculated complex formation curves for mixed, dynamic and semi-dynamic, metal–ligand systems. A differential pulse polarographic study of Cu^{II}–sarcosine–OH and Cd^{II}–MIDA–OH systems at a fixed ligand to metal ratio and varied pH **460**, 197
Scanning electron microscopy
Tin electrodeposition on carbon electrodes. From nuclei to microcrystallites **465**, 63
Scanning probe microscopy
Scanning probe lithography for electrode surface modification **473**, 230
Scanning tunnelling microscopy
Formation of an ordered structure of iodine adsorbed on Ni(111) and the anodic dissolution processes: in-situ STM study **467**, 282
Influence of the electric potential on the structure of pyridine adlayers on Au(111) terraces from in-situ scanning tunnelling microscopy imaging **467**, 230
In situ scanning tunneling microscopy of Cu(110): atomic structures of halide adlayers and anodic dissolution **473**, 10

In situ STM study of self-assembled mercaptopropionic acid monolayers for electrochemical detection of dopamine **465**, 72
Structural studies of 2,2′-bipyridine on Au(100) **467**, 207
Structure and growth in metal epitaxy on low-index Au surfaces—a comparison between solid | electrolyte and solid | vacuum interfaces **467**, 258
Underpotential deposition behavior of metals onto gold electrodes coated with self-assembled monolayers of alkanethiols **473**, 59
Second harmonic generation
Second harmonic generation investigation of rhodamine B derivatives in Langmuir–Blodgett films **465**, 195
SEI
Enhancement of the electrochemical Li doping/undoping reaction rate of a graphitic material by an evaporated film of Sn, Zn or Pb **462**, 150
Self-assembled monolayers
Adsorption characteristics of $Fe(CN)_6^{3-/4-}$ on Au colloids as monolayer films on cysteamine-modified gold electrode **466**, 26
A new approach to electrode kinetics and dynamics by potential modulated Fourier transform infrared spectroscopy **473**, 34
Assessing the apparent effective thickness of alkanethiol self-assembled monolayers in different concentrations of $Fe(CN)_6^{3-}$/$Fe(CN)_6^{4-}$ by ac impedance spectroscopy **470**, 9
Exchange of self-assembled thiol monolayers on gold: characterization by FT-IR external reflection spectroscopy **468**, 91
pK_a of an ω-carboxylalkanethiol self-assembled monolayer by interaction model **478**, 101
Post-assembly insertion of metal ions into thiol-derivatized porphyrin monolayers on gold **473**, 75
Structural differences in self-assembled monolayers of anthraquinone derivatives on silver and gold electrodes studied by cyclic voltammetry and in situ SERS spectroscopy **478**, 83
Studies of structural disorder of self-assembled thiol monolayers on gold by cyclic voltammetry and ac impedance **464**, 61
Synthesis and electrochemical characterization of self-assembled monolayers of redox-active oxide-bridged triruthenium(III) clusters on Au(111) **473**, 93
Underpotential deposition behavior of metals onto gold electrodes coated with self-assembled monolayers of alkanethiols **473**, 59
Self-assembly
Electrochemical study of self-assembled monolayers of a β-cyclodextrin methyl sulfide covalently linked to anthraquinone **465**, 209
Formation of a nickel hydroxide monolayer on Au through a self-assembled monolayer of 5,5′-dithiobis(2-nitrobenzoic acid): voltammetric, SERS and XPS investigations of the modified electrodes **468**, 170
In situ STM study of self-assembled mercaptopropionic acid monolayers for electrochemical detection of dopamine **465**, 72
Self-assembly of and charge transfer at *N*-docosyl-*N*′-methyl viologen on electrode surfaces **468**, 70
Separation of pinhole and tunneling electron transfer processes at self-assembled polymeric monolayers on gold electrodes **470**, 114
Self-protonation
Electrochemical reduction of phenyl-substituted cyclopentadienes: a case of an 'indirect father–son' self-protonation process **460**, 160
Self-protonation mechanism in the electrochemical reduction of Jatropholone **466**, 99
SEM
Characterization of electrochemically deposited gold nanocrystals on glassy carbon electrodes **466**, 234
Semiconductor
Impedance and photoelectrochemical properties of porous oxide film on Type304 stainless steel formed by square wave potential pulse polarisation **473**, 265
Semiconductor electrochemistry
Electrochemistry of homoepitaxial CVD diamond: energetics and electrode kinetics in aqueous electrolytes **475**, 139
Semiconductor electrode
Frequency dependent electrolyte electroreflectance at semiconductor | electrolyte interfaces **462**, 251
Semiconductor sensitization
Semiconductor sensitization of colloidal In_2S_3 on wide gap semiconductors **469**, 116
Semiintegration
Convolutive modelling of electrochemical processes based on the relationship between the current and the surface concentration **464**, 1
Sensor
Rotograved carbon electrodes for amperometric cadmium and lead determination **469**, 189
Serine
Electrochemical behaviour of amino acids on Pt(*hkl*). A voltammetric and in situ FTIR study: Part IV. Serine and alanine on Pt(100) and Pt(110) **475**, 38
SERS
Effect of sodium dodecylsulfate on copper corrosion in sulfuric acid media in the absence and presence of benzotriazole **472**, 112
Formation of a nickel hydroxide monolayer on Au through a self-assembled monolayer of 5,5′-dithiobis(2-nitrobenzoic acid): voltammetric, SERS and XPS investigations of the modified electrodes **468**, 170
SFG–DFG
What can we learn from the non-linear optical investigation of the liquid | solid interface? **473**, 25
Shuttleworth equation
The Shuttleworth equation for a finite surface strain **471**, 105
Silica gel
Cobalt(II) metallated hematoporphyrin IX and protoporphyrin IX immobilized on niobium(V) oxide grafted on a silica gel surface: electrochemical studies **477**, 158
Silicon anodic dissolution
In-situ detection of stress in oxide films during Si electrodissolution in acidic fluoride electrolytes **474**, 182
Silicone rubber
Ion sensors using one-component room temperature vulcanized silicone rubber matrices **464**, 135
Silicon oxide etching
In-situ detection of stress in oxide films during Si electrodissolution in acidic fluoride electrolytes **474**, 182
Silver
Coordination of silver(I) at the surface of carbon paste electrodes modified with 2,5,8-trithia[9]-*m*-cyclophane as studied by cyclic voltammetry **475**, 73
In-situ X-ray absorption studies of bromine on the Ag(100) electrode **473**, 19
Surface structural transitions induced by repetitive underpotential deposition of Ag on Au(111) **474**, 138
The complex formation of non-cyclic polyethers and crown ethers with Ag^+ in acetone and propylene carbonate studied by potentiometric and calorimetric methods **474**, 188
Silver anodic stripping
Voltammetric anodic stripping of silver from platinum electrodes consisting of an array of nm-sized voids **477**, 14
Silver(111) electrode
In situ infrared spectroscopic investigations of sulfate adsorption at the Ag(111) electrode surface **467**, 291

Simazine
A contribution to the study of the electroreduction of 2-chloro-4,6-di(ethylamino)-1,3,5-triazine (simazine) on mercury electrodes **474**, 174
Simulation
A model for assisted ion transfer across liquid | liquid interfaces **460**, 144
Cathodic reduction of 2-nitronaphthothiophen-4,9-quinone: evidence of catalysis by proton donors and its simulation **462**, 195
Evaluation of model and dispersion parameters and their effects on the formation of constant-phase elements in equivalent circuits **464**, 68
Finite element simulation of ion transfer reactions at a single micro-liquid | liquid interface supported on a thin polymer film **468**, 42
Ion transport and deposit growth in spatially coupled bipolar electrochemistry **478**, 128
Kinetics of sulfide ion adsorption at copper amalgam electrode **463**, 200
Single crystal
Calculation of thermodynamic and inner layer characteristics of halide ions adsorbed on bismuth single crystal planes from solutions in methanol **469**, 182
Single crystal electrodes
A method to prepare single crystal electrodes of reactive metals: application to Pd(*hkl*) **466**, 165
Effect of the crystallographic orientation of Ag single crystal face electrodes on the kinetics of proton discharge **467**, 164
Oxidation of methylamine and ethylamine on Pt single crystal electrodes in acid medium **469**, 159
Sulfate ions adsorbed on Au(*hkl*) electrodes: in situ vibrational spectroscopy **460**, 110
Step decoration at Pt single crystal electrodes: role of the anion **467**, 50
The adsorption of methylamine on Pt single crystal surfaces **467**, 105
X-ray and electrochemical studies of Cu upd on single crystal electrodes in the presence of bromide: comparison between Au(111) and Pt(111) electrodes **460**, 121
Slow relaxation
Formation of conducting clusters of polyaniline films detected by light scattering **473**, 132
SMDE
General solutions for the I/t response for reversible processes in the presence of product in a multipotential step experiment at planar and spherical electrodes whose areas increase with any power of time **466**, 8
Sodium dodecylsulfate
Effect of sodium dodecylsulfate on copper corrosion in sulfuric acid media in the absence and presence of benzotriazole **472**, 112
Sodium montmorillonite
Electrocatalytic reduction of molecular oxygen on a sodium montmorillonite-methyl viologen carbon paste chemically modified electrode **463**, 253
Sol–gel
Electrochemical characterisation of Pd modified ceramic | carbon electrodes: partially flooded versus wetted channel hydrophobic gas electrodes **466**, 45
Renewable silica sol–gel derived carbon composite based glucose biosensor **460**, 234
Sol–gel coating
Formation of Al–Zr composite oxide films on aluminum by sol–gel coating and anodizing **473**, 250
Sol–gel methods
Preparation and characterization of sol–gel derived carbon composite ceramic electrodes: electrochemical and XANES study of nitrite reduction **468**, 131
Solid electrodes
Electrocapillary equations of solid electrodes **478**, 40
Solid | liquid interfaces
In-situ STM investigation of specific anion adsorption on Cu(111) **467**, 307
Solid-state sensor
Ion sensors using one-component room temperature vulcanized silicone rubber matrices **464**, 135
Solvent effect
Solvent effect on kinetics of the chloride ion cleavage from anion radicals of 4-chlorobenzophenone **464**, 259
Solvent splitting
Current–voltage curves of a composite bipolar membrane in organic acid–water solutions **462**, 12
Solvent transport
Mass transport behavior of polypyrrole and poly(*N*-methylpyrrole) films in acetonitrile solutions **468**, 104
Sonoelectrochemistry
Low-temperature sonoelectrochemical processes: Part 1. Mass transport and cavitation effects of 20 kHz ultrasound in liquid ammonia **477**, 71
Sonoassisted electrooxidative polymerisation of salicylic acid: role of acoustic streaming and microjetting **462**, 181
Sonovoltammetry
Sonoassisted electrooxidative polymerisation of salicylic acid: role of acoustic streaming and microjetting **462**, 181
Sorption
Electrode reactions and accumulation of hydrogen at carbon paste electrodes in the presence of tetrachloropalladate **462**, 174
Sorption in palladium
The study of hydrogen sorption in palladium limited volume electrodes (Pd-LVE): I. Acidic solutions **471**, 190
Spatial distribution
The kinetics of mercury nucleation from Hg_2^{2+} and Hg^{2+} solutions on vitreous carbon electrodes **464**, 39
Speciation
Experimental and calculated complex formation curves for mixed, dynamic and semi-dynamic, metal–ligand systems. A differential pulse polarographic study of Cu^{II}–sarcosine–OH and Cd^{II}–MIDA–OH systems at a fixed ligand to metal ratio and varied pH **460**, 197
Voltammetric currents for any ligand-to-metal concentration ratio in fully labile metal-macromolecular complexation. Easy computations, analytical properties of the currents and a graphical method to estimate the stability constant **472**, 42
Specific adsorption
SNIFTIRS studies of the electrochemical double layer: Part II. Au(111) electrode in solutions with specifically adsorbed nitrate ions **467**, 325
Specific adsorption at modulated liquid | liquid interfaces **475**, 46
Spectroelectrochemical channel cell
Spectroelectrochemistry for a coupled chemical reaction in the channel cell: Part II. Kinetics of hydrolysis and the absorption spectrum of *p*-benzoquinoneimine **464**, 181
Spectroelectrochemistry
A jacketed cell for infrared spectroelectrochemistry at constant above ambient temperatures **476**, 95
An in situ UV-vis and IR spectroelectrochemical study of the deposition of a hydroquinone anion salt on platinum electrodes from dichloromethane solutions **462**, 266
Anthraquinones as mediators for the indirect cathodic reduction of dispersed organic dyestuffs **465**, 80
Electrochemical and spectroelectrochemical properties of manganese reconstituted myoglobin **460**, 245
Electrochemical oxidation of poly[(hexamethyltrisilanylene)oligo(2,5-thienylene)] films **464**, 158
Electrochemical study of methylalkylviologens using an electrochemical quartz crystal microbalance **463**, 224

MRA combined spectroelectrochemical studies on the redox stability of PPy/DS films **462**, 1
Spectroelectrochemical study of the influence of anions on the behaviour of poly(*N*-vinylcarbazole) films **475**, 1
Spectroelectrochemistry for a coupled chemical reaction in the channel cell: Part I. Theoretical simulation of an EC reaction **464**, 176
Spectroscopy
Electropolymerization of 2-methoxy aniline. Electrochemical and spectroscopical product characterization **471**, 180
Spherical electrodes
Study of a catalytic mechanism in double potential step techniques at spherical electrodes **468**, 158
Spillover
Surface diffusion and the spillover of H-adatoms and oxygen-containing surface species on the surface of carbon black and Pt/C porous electrodes **476**, 101
Spin coating method
Semiconductor sensitization of colloidal In_2S_3 on wide gap semiconductors **469**, 116
Spinel
Effect of the partial replacement of Ni or Co by Cu on the electrocatalytic activity of the $NiCo_2O_4$ spinel oxide **464**, 187
Sputtered iridium oxide films
X-ray absorption in relation to valency of iridium in sputtered iridium oxide films **465**, 88
Square wave voltammetry
Cathodic stripping square wave voltammetry of Cu(II)–oxine complexes. A mechanistic study **478**, 17
Enhanced electron transfer for hemoglobin in poly (ester sulfonic acid) films on pyrolytic graphite electrodes **463**, 53
Reduction and oxidation of peptide nucleic acid and DNA at mercury and carbon electrodes **476**, 71
Square wave stripping voltammetry of Cd–oxine complexes; surface redox reactions **476**, 165
SQUID magnetometer
Corrosion sensing by SQUID magnetometry **477**, 171
Stability
MRA combined spectroelectrochemical studies on the redox stability of PPy/DS films **462**, 1
Stability constant
Voltammetric currents for any ligand-to-metal concentration ratio in fully labile metal-macromolecular complexation. Easy computations, analytical properties of the currents and a graphical method to estimate the stability constant **472**, 42
Stain etch
Simultaneous platinum deposition and formation of a photoluminescent porous silicon layer **469**, 48
Stainless steel
Impedance and photoelectrochemical properties of porous oxide film on Type304 stainless steel formed by square wave potential pulse polarisation **473**, 265
Standard reaction rates
Electrode kinetics of Eu^{3+} in dimethylsulfoxide **470**, 1
Stationary state
Using Pt microelectrodes in liquid ammonia for studying proton reduction **477**, 140
Steady-state
Steady-state currents at inlaid and recessed microdisc electrodes for first-order EC′ reactions **476**, 132
Stereoselective electroreduction
Enantioselective electrodes: stereoselective electroreduction of 4-methylbenzophenone and acetophenone **461**, 94
Stereoselectivity
Mechanism of stereoselective production of *trans*-1-decalone by electrochemical catalysis in microemulsions **464**, 31
STM
Phase transitions in the electrodeposition of tellurium atomic layers on Au(100) **467**, 270
Redox mechanisms of NO with water on the Pt(111) electrode studied by in-situ STM and IRAS **473**, 43
Surface structural transitions induced by repetitive underpotential deposition of Ag on Au(111) **474**, 138
Stokes radius
Underpotential deposition behavior of metals onto gold electrodes coated with self-assembled monolayers of alkanethiols **473**, 59
Stress
Effects of self-stress on the hydrogen absorption into palladium hydride electrodes of plate form under galvanostatic conditions **474**, 130
Stripping
Electrodeposition of zinc + iron alloys: I. Analysis of the initial stages of the anomalous codeposition **469**, 139
Electrodeposition of zinc + iron alloys: II. Relation between the stripping results and ex-situ characterization **475**, 66
Strong acids
Chronoamperometry of strong acids without supporting electrolyte **472**, 1
Strontium ruthenate
Strontium ruthenate perovskite as the active material for supercapacitors **460**, 154
Structural change
Structural changes at various Pt single crystal surfaces with potential cycles in acidic and alkaline solutions **467**, 85
Structural distinguishability
Structural identifiability of adsorption and electron transfer processes in metal dissolution and passivation mechanisms **471**, 1
Structural identifiability
Structural identifiability of adsorption and electron transfer processes in metal dissolution and passivation mechanisms **471**, 1
Structural specificity
Structural specificity of the kinetics of the hydrogen evolution reaction on the low-index surfaces of Pt single-crystal electrodes in 0.5 M dm^{-3} NaOH **461**, 80
Structure
Formation of an ordered structure of iodine adsorbed on Ni(111) and the anodic dissolution processes: in-situ STM study **467**, 282
Structural studies of 2,2′-bipyridine on Au(100) **467**, 207
Substitute
Characterization of a new spinel Li–Cr–Mn–O for secondary lithium batteries **463**, 24
Substituted bipyridine.
Electrochemical formation and spectroelectrochemical characterization of organometallic $[Ru(L)(CO)_2]_n$ polymers; L = disubstituted-2,2′-bipyridine **466**, 187
Substituted heteropolyanions
Metal ion complexes derived from the α_1 isomer of $(P_2W_{17}O_{61})^{10-}$: comparison with the corresponding α_2 species **478**, 76
Substrate recycling
Amplification of amperometric biosensor responses by electrochemical substrate recycling: Part II. Experimental study of the catechol–polyphenol oxidase system immobilized in a laponite clay matrix **470**, 61
Amplification of amperometric biosensor responses by electrochemical substrate recycling: Part I. Theoretical treatment of the catechol–polyphenol oxidase system **470**, 53
Sulfate
In situ infrared spectroscopic investigations of sulfate adsorption at the Ag(111) electrode surface **467**, 291
Sulfate adsorption
In-situ STM investigation of specific anion adsorption on Cu(111) **467**, 307
Sulfate ion
Adsorption of sulfate ions on monocrystalline copper electrodes: the structural effects **463**, 1

Sulfide
Electrochemical study on competitive adsorption of pyridinethiol with sulfide onto Au(111) surfaces **473**, 85
Kinetics of sulfide ion adsorption at copper amalgam electrode **463**, 200
Sulfolane
The electrochemical properties of a series of phenylene-thienyl polymers in tetramethylene sulfone based electrolytes **460**, 46
Sulfonamide
Voltammetric investigation of new polythiophene derivatives possessing electrochemically cleavable arylsulfonamide groups as precursors for solid phase electrosynthesis **477**, 121
Sulfonyl fluoride
The voltammetric reduction of some benzenesulfonyl fluorides, simulation of the ECE mechanism and determination of the potential variation of the transfer coefficient by using the compounds with two reducible groups **471**, 14
Sulfur dioxide
Mechanism of the electrochemical reduction of sulfur dioxide in non-aqueous solvents **476**, 15
Surface layers formed initially on copper in air containing water vapor and SO_2 as determined by IR-RAS and 2D-IR **473**, 256
Sum frequency generation
In situ visible-infrared sum and difference frequency generation at the electrochemical interface **467**, 238
Superlattices
In-situ STM investigation of specific anion adsorption on Cu(111) **467**, 307
Supporting electrolyte
Chronoamperometry of strong acids without supporting electrolyte **472**, 1
Surface alloying
Surface alloying at the Cd | Au(100) interface in the upd region. Electrochemical studies and in situ EC-AFM observation **475**, 171
Surface alloys
Surface structural transitions induced by repetitive underpotential deposition of Ag on Au(111) **474**, 138
Surface area determination
Characterization of electrochemically deposited gold nanocrystals on glassy carbon electrodes **466**, 234
Surface charge density
Determination of the surface charge density of a mercury electrode by extrusion: a new method for correction of the faradaic component **468**, 150
Surface chemistry
On the electrochemical behavior of magnesium electrodes in polar aprotic electrolyte solutions **466**, 203
Role of surface states and adsorbates in time-resolved photocurrent measurements and photovoltage generation at phthalocyaninatozinc(II)-photocathodes **462**, 222
Surface complex
Coordination of silver(I) at the surface of carbon paste electrodes modified with 2,5,8-trithia[9]-*m*-cyclophane as studied by cyclic voltammetry **475**, 73
Surface conductivity
Surface diffusion and the spillover of H-adatoms and oxygen-containing surface species on the surface of carbon black and Pt/C porous electrodes **476**, 101
Surface electrochemistry
A Nernstian electron source model for the ac voltammetric response of a reversible surface redox reaction using large-amplitude ac voltages **466**, 197
Surface energy
Can the internal energy function of solid interfaces be of a non-homogeneous nature? **472**, 168
Surface-enhanced infrared absorption spectroscopy
A new approach to electrode kinetics and dynamics by potential modulated Fourier transform infrared spectroscopy **473**, 34
Surface enhanced Raman scattering
Interfacial structure of dimethylsulfoxide at Ag electrodes from surface enhanced Raman scattering and differential capacitance **479**, 21
Surface Raman scattering of interfaces at Ag electrodes emersed from dimethylsulfoxide: spectroscopic evidence for an emersion-induced potential shift **479**, 32
Surface enhanced Raman spectroscopy
Structural differences in self-assembled monolayers of anthraquinone derivatives on silver and gold electrodes studied by cyclic voltammetry and in situ SERS spectroscopy **478**, 83
Surface modification
Chiroselective electron transfer at enantiomer-capped ZnO nanocrystalline surfaces **473**, 117
Formation of a nickel hydroxide monolayer on Au through a self-assembled monolayer of 5,5′-dithiobis(2-nitrobenzoic acid): voltammetric, SERS and XPS investigations of the modified electrodes **468**, 170
Surface morphology
Surface structural transitions induced by repetitive underpotential deposition of Ag on Au(111) **474**, 138
Surface plasmon
Synthesis, redox behavior and electrodeposition of biferrocene-modified gold clusters **473**, 113
Surface plasmon resonance
Characterization of protein monolayers by surface plasmon resonance combined with cyclic voltammetry 'in situ' **464**, 198
Surface reaction
Electrochemical surface reactions of intermediates formed in the oxidative ethanol adsorption on porous Pt and PtRu **471**, 167
Surface reconstruction
On the stability of unreconstructed Au(100)-(1 × 1) at negative potentials in aqueous sulfate solution **471**, 9
Surface roughness
Studies of structural disorder of self-assembled thiol monolayers on gold by cyclic voltammetry and ac impedance **464**, 61
Surface state
Electrochemical features of zirconia polymorphs. The interplay between structure and surface OH species **465**, 136
Role of surface states and adsorbates in time-resolved photocurrent measurements and photovoltage generation at phthalocyaninatozinc(II)-photocathodes **462**, 222
Surface stoichiometry
An old workhorse of oxide investigations: new features of Co_3O_4 **464**, 149
Surface stress
A reply to the question of whether the internal energy of solid interfaces can be of a non-homogeneous nature **472**, 174
Electrocapillary equations of solid electrodes **478**, 40
Surface structural effects
Surface structural effects on specific adsorption of oxoanions on gold single crystal electrodes **467**, 335
Surface structure
Evolution of a skeleton structured TiO_2 surface consisting of grain boundaries **473**, 204
Photoelectrochemical submicrometer patterning of titanium dioxide by platinum **473**, 235
Structural differences in self-assembled monolayers of anthraquinone derivatives on silver and gold electrodes studied by cyclic voltammetry and in situ SERS spectroscopy **478**, 83
Surface alloying at the Cd | Au(100) interface in the upd region. Electrochemical studies and in situ EC-AFM observation **475**, 171
Surface termination
Electrochemical selectivity for redox systems at oxygen-terminated diamond electrodes **473**, 173

Surface work
Electrocapillary equations of solid electrodes **478**, 40
Synchrotron source
'In-situ' observation of halide ion adsorption on a gold electrode using synchrotron far infrared spectroscopy **463**, 258

Tafel equation
Evaluation of model and dispersion parameters and their effects on the formation of constant-phase elements in equivalent circuits **464**, 68
Tafel plots
Hydrogen evolution on silver single crystal electrodes—first results **461**, 76
Ta_2O_5
Capacitance and photocurrent study of electronic properties of anodic oxide films on Nb and Ta. Evaluation of the ionized donor concentration profile in Nb_2O_5 film **460**, 214
Tellurium
Phase transitions in the electrodeposition of tellurium atomic layers on Au(100) **467**, 270
Temperature
A jacketed cell for infrared spectroelectrochemistry at constant above ambient temperatures **476**, 95
Analysis of the temperature dependence of the α and β coefficients of the electrode reactions in the Cr(III)/Cr(II) and Cr(II)/Cr(Hg) systems **471**, 62
A temperature controlled cell for in situ infrared spectroelectrochemical measurements and its use in the study of CO isothermal desorption **471**, 146
Temperature and pressure dependence of O_2 reduction at Pt | Nafion® 117 and Pt | BAM® 407 interfaces **468**, 180
Temperature-dependent research on Pt(111) and Pt(100) electrodes in aqueous H_2SO_4 **467**, 177
The potentiodynamic behaviour of iridium electrodes in aqueous 3.7 M H_2SO_4 in the 293–195 K range **461**, 40
Temperature dependence
The temperature dependence of the kinetics of cyanide dissociation from the cyanide complex of myoglobin studied by cyclic voltammetry **466**, 177
Ternary diffusion
Simultaneous ion transfer across the microhole ITIES: an example of ternary electrodiffusion **460**, 149
Tetrachloropalladate
Electrode reactions and accumulation of hydrogen at carbon paste electrodes in the presence of tetrachloropalladate **462**, 174
Tetrafluoroethylene
Electrochemical reduction of dichlorodifluoromethane in acetonitrile medium to useful fluorinated compounds **471**, 26
Tetra-iron substituted sandwich-type heteropolytungstate
Electrochemical and electrocatalytic properties of tetra-iron substituted sandwich-type pentadecatungstodiphosphate heteropolyanions **476**, 85
Tetraphenylporphyrin
Electrochemical study of tetraphenylporphinato-iron(III)–thiolate complexes, NH···S hydrogen bonding in the cytochrome P-450 model system **469**, 84
Tetrathiafulvalene
Hydrogen bond complexation of dimethyl-[1-butyl-2,4-dioxo(1H,3H)pyrimido]tetrathiafulvalene with aminopyridine derivatives probed by cyclic voltammetry **463**, 212
Tetrathiafulvalenium tetracyanoquinodimethanide
Kinetic behaviour of dopamine-polyphenol oxidase on electrodes of tetrathiafulvalenium tetracyanoquinodimethanide and tetracyanoquinodimethane species **461**, 174
Thallium electrode
Electrode kinetics and the nature of the metal electrode: Part 4. The Zn(II)/Zn electrode reaction studied at dropping Tl + Ga alloy electrodes **472**, 64

Theory
Amperometric ion-selective electrode. Voltammetric theory and analytical applications at high concentration and trace levels **468**, 34
Amperometric ion-selective electrode. Voltammetric theory and analytical applications at high concentration and trace levels **475**, 90
Thermal oxidation
Photoelectrochemical response and stability of titanium–zinc mixed oxide films formed by thermal oxidation **464**, 238
Thermo-currents
Corrosion sensing by SQUID magnetometry **477**, 171
Thermodynamic analysis
Activity coefficients of $Al(ClO_4)_3$ in aqueous solutions: a reexamination **460**, 100
Temperature dependence of physical displacement and charge hopping in a polymer membrane incorporating a trinuclear ruthenium complex **476**, 159
Thermodynamics
Thermodynamics for the situation where there is a discontinuous change of the electrode condition with potential due to the formation of a two dimensional condensed phase—diffuse layer effects **463**, 9
Thickness shear mode resonator
Mechanical resonance effects in electroactive polycarbazole films **460**, 267
Thin clay films
Preparation of clay-modified electrodes by electrophoretic deposition of clay films **462**, 143
Thin films
Electrochemical impedance spectroscopy of thin films with two mobile charge carriers: effects of the interfacial charging **472**, 7
Linear diffusion impedance. General expression and applications **471**, 126
Spectroelectrochemical investigations on the reduction of thin films of hexadecafluorophthalocyaninatozinc ($F_{16}PcZn$) **476**, 148
Thin layer electrode cell
A wall-jet ring disk electrode fabricated within a thin-layered micromachined cell **479**, 57
Thiocyanate
Atom-by-atom growth of cadmium sulfide thin films by electroreduction of aqueous Cd^{2+}–SCN^- complex **473**, 209
Thiocyanate complexes of nickel(II)
On the source of oscillatory instabilities in the electroreduction of thiocyanate complexes of nickel(II) at mercury electrodes **478**, 118
Thiol-derivatized porphyrin
Post-assembly insertion of metal ions into thiol-derivatized porphyrin monolayers on gold **473**, 75
Thiophenol
Combined quartz crystal impedance and electrochemical impedance measurements during adsorption of bovine serum albumin onto bare and cysteine- or thiophenol-modified gold electrodes **478**, 1
Thiourea electro-oxidation
Electrochemical response of thiourea and formamidine disulphide on polycrystalline platinum in aqueous 0.5 M sulphuric acid **475**, 181
Thiourea–formamidine disulphide redox system
Electrochemical response of thiourea and formamidine disulphide on polycrystalline platinum in aqueous 0.5 M sulphuric acid **475**, 181
Time dependent signals
Dynamic polymeric electrodes, dynamic computer modelling and dynamic electrochemical sensing **468**, 19
Time-resolved infrared reflection absorption spectroscopy
Surface layers formed initially on copper in air containing water vapor and SO_2 as determined by IR-RAS and 2D-IR **473**, 256

Tin
Tin electrodeposition on carbon electrodes. From nuclei to microcrystallites **465**, 63
TiO_2
A glucose biosensor based on enzyme entrapment within polypyrrole films electrodeposited on mesoporous titanium dioxide **469**, 176
Effect of ultra-violet light irradiation on anodic oxide films on titanium in sulfuric acid solution **473**, 272
Titanium
Behaviour of titanium species in molten $Li_2CO_3 + Na_2CO_3$ and $Li_2CO_3 + K_2CO_3$ in the anodic conditions used in molten carbonate fuel cells: II. Electrochemical intercalation of Li^+ in Li_2TiO_3 at 600 and 650°C **474**, 9
Photoelectrochemical response and stability of titanium–zinc mixed oxide films formed by thermal oxidation **464**, 238
Study of the corrosion behavior of titanium and some of its alloys for biomedical and dental implant applications **471**, 109
Titanium dioxide
Photoelectrochemical submicrometer patterning of titanium dioxide by platinum **473**, 235
Photoresponse of a titanium dioxide chemical sensor **472**, 137
TOF-SIMS
Polycrystalline gold electrode redox behavior in an ammoniacal electrolyte: Part II. A parallel RRDE, EQCM and TOF-SIMS study of copper underpotential deposition **460**, 143
Total CO_2 measurement
Trifluoroacetophenone derivative-based carbonate ion-selective electrodes: effect of diluent pH on the anion selectivity **468**, 76
Trace analysis
Amperometric ion-selective electrode. Voltammetric theory and analytical applications at high concentration and trace levels **468**, 34
Amperometric ion-selective electrode. Voltammetric theory and analytical applications at high concentration and trace levels **475**, 90
Transference numbers
Quantitative discrimination of mass fluxes at electrochemical interfaces by optical beam deflection **466**, 218
Transfer function
Linear diffusion impedance. General expression and applications **471**, 126
Review and theoretical analysis of ac–av methods for the investigation of hydrogen insertion I. Diffusion formalism **462**, 73
Transfer matrix
Transfer matrix method for the electrochemical impedance of inhomogeneous porous electrodes and membranes **460**, 63
Transmission line model
Electrochemical investigations and morphology of poly(4,9-dihydro-*o*-benzenonaphtho[2,3-c]pyrrole) and poly(acenaphtho[1,2-c]pyrrole) **477**, 25
Transport equations
Effect of water transport in a PEFC at low temperatures operating with dry hydrogen **477**, 164
Theory for water management in membranes for polymer electrolyte fuel cells: Part 1. The effect of impurity ions at the anode side on the membrane performances **465**, 1
Theory for water management in membranes for polymer electrolyte fuel cells: Part 2. The effect of impurity ions at the cathode side on the membrane performances **465**, 18
Trapping
Electrochemical determination of hydrogen in metals **475**, 82
Triazine herbicides
A contribution to the study of the electroreduction of 2-chloro-4,6-di(ethylamino)-1,3,5-triazine (simazine) on mercury electrodes **474**, 174
1,1,2-Trichloroethane
Synthesis of carbyne-like nano-particles by electrocatalytic dehydrochlorination of 1,1,2-trichloroethane **470**, 95
Trifluoroacetophenone derivative
Trifluoroacetophenone derivative-based carbonate ion-selective electrodes: effect of diluent pH on the anion selectivity **468**, 76
Triple ion
Conductometric study of lithium halides and thiocyanate in the mixed solvents of tetrahydrofuran and 2-ethyl-1-hexanol **468**, 110
Triruthenium(III) cluster
Synthesis and electrochemical characterization of self-assembled monolayers of redox-active oxide-bridged triruthenium(III) clusters on Au(111) **473**, 93
Tris(2,2′-bipyridyl) ruthenium(II)
Preparation of clay-modified electrodes by electrophoretic deposition of clay films **462**, 143
Tumour
Electrochemical treatment of tumours: a simplified mathematical model **460**, 88
Two-compartment cell
Construction of a new dehydrogenation system using a two-compartment cell separated by a palladized Pd sheet electrode **463**, 116
Two-dimensional infrared correlation spectroscopy
Surface layers formed initially on copper in air containing water vapor and SO_2 as determined by IR-RAS and 2D-IR **473**, 256
Two-dimensional mapping of electrode surface
Two-dimensional CCD detection of electrogenerated chemiluminescence (ECL) on an electrode surface. ECL reactions involving microcrystals of the perylene dimer cation radical salt **473**, 166
Tyrosine
In-situ FTIR studies on the electrochemical oxidation of histidine and tyrosine **463**, 218

UHV
Voltammetric and UHV characterisation of the (1×1) and reconstructed hex-R0.7° phases of Pt{100} **467**, 60
Ultrafast voltammetry
Voltammetric investigation of the anodic dimerization of *p*-halogenoanilines in DMF: Reactivity of their electrogenerated cation radicals **462**, 55
Ultrasound
Low-temperature sonoelectrochemical processes: Part 1. Mass transport and cavitation effects of 20 kHz ultrasound in liquid ammonia **477**, 71
Ultra-violet
Effect of ultra-violet light irradiation on anodic oxide films on titanium in sulfuric acid solution **473**, 272
Underpotential deposition
Atom-by-atom growth of cadmium sulfide thin films by electroreduction of aqueous Cd^{2+}–SCN^- complex **473**, 209
Polycrystalline gold electrode redox behavior in an ammoniacal electrolyte: Part II. A parallel RRDE, EQCM and TOF-SIMS study of copper underpotential deposition **460**, 143
Surface alloying at the Cd | Au(100) interface in the upd region. Electrochemical studies and in situ EC-AFM observation **475**, 171
Underpotential deposition behavior of metals onto gold electrodes coated with self-assembled monolayers of alkanethiols **473**, 59
Upd
Phase transitions in the electrodeposition of tellurium atomic layers on Au(100) **467**, 270
Step decoration at Pt single crystal electrodes: role of the anion **467**, 50
Surface structural transitions induced by repetitive underpotential deposition of Ag on Au(111) **474**, 138

Upd lead
Characterization of electrochemically deposited gold nanocrystals on glassy carbon electrodes **466**, 234
Upd of alkali metal atoms
Electroreduction of nitrate ion to nitrite and ammonia on a gold electrode in acidic and basic sodium and cesium nitrate solutions **470**, 46
Urea adlayers
Urea adsorption on Pt(111) electrodes **461**, 65
UV illumination
Electroless copper plating on a glass substrate coated with ZnO film under UV illumination **462**, 259
UV-visible reflectance spectroscopy
Potential modulated reflectance spectroscopy of Pt(111) in acidic and alkaline media: cyanide adsorption **463**, 109
UV-vis spectroelectrochemistry
A UV-vis spectroelectrochemical study of redox reactions of solution species at a polyaniline electrode in the conducting and the reduced state **461**, 184
UV–vis spectroscopy
Spectroelectrochemical investigations on the reduction of thin films of hexadecafluorophthalocyaninatozinc ($F_{16}PcZn$) **476**, 148

Vanadium oxide
Modified electrodes based on mixed bentonite vanadium(V) oxide xerogels **464**, 48
Variable permeability membranes
Convective electrodiffusion processes through graft-modified charged porous membranes **464**, 222
Vat dyes
Anthraquinones as mediators for the indirect cathodic reduction of dispersed organic dyestuffs **465**, 80
Vibrational interactions
Coadsorbate vibrational interactions within mixed carbon monoxide-nitric oxide adlayers on ordered low-index platinum-group electrodes **467**, 92
Vinylogous TTF
Cathodic synthesis of powerful electron π-donors including dithiadiazafulvalenes **462**, 137
N-vinyl-2-pyrrolidone
Electropolymerization of methacrylonitrile and *N*-vinyl-2-pyrrolidone as probed by an EQCM **465**, 200
Viologens
A UV-vis spectroelectrochemical study of redox reactions of solution species at a polyaniline electrode in the conducting and the reduced state **461**, 184
Cyclic voltammetric studies of Prussian blue and viologens within a paper matrix for electrochromic printing applications **461**, 263
Electrochemical behaviour of *N*-aminopyridinium, and the viologens *N,N′*-diamino-4,4′-bipyridilium and *N,N′*-bis(4-aminophenyl)-4,4′-bipyridilium in aqueous acid: towards the formation of polymer hybrids of pyridine and aniline **462**, 43
Self-assembly of and charge transfer at *N*-docosyl-*N′*-methyl viologen on electrode surfaces **468**, 70
Voltammetric and spectroscopic study of the adsorption of alkyl viologens on a HOPG electrode **473**, 138
Vitamin B_{12}
Mechanism of stereoselective production of *trans*-1-decalone by electrochemical catalysis in microemulsions **464**, 31
Voltammetric analysis
Electrooxidation of the antileukemic 2-chloro-2′-deoxyadenosine and related compounds **477**, 89
Voltammetric anion recognition
Voltammetric anion recognition by a highly cross-linked polyviologen film **473**, 145
Voltammetric modelling
Convolutive modelling of electrochemical processes based on the relationship between the current and the surface concentration **464**, 1
Voltammetric oxidation
Voltammetric investigation of the anodic dimerization of *p*-halogenoanilines in DMF: Reactivity of their electrogenerated cation radicals **462**, 55
Voltammetric response
Hydrogen bond complexation of dimethyl-[1-butyl-2,4-dioxo(1H,3H)pyrimido]tetrathiafulvalene with aminopyridine derivatives probed by cyclic voltammetry **463**, 212
Voltammetry
Accumulation of Hg(II) by adsorbed polyuridylic acid: differentiation of coordinated Hg(II) and covalently mercurated species **466**, 2
A contribution to the study of the electroreduction of 2-chloro-4,6-di(ethylamino)-1,3,5-triazine (simazine) on mercury electrodes **474**, 174
An old workhorse of oxide investigations: new features of Co_3O_4 **464**, 149
Cadmium binding properties of the C-terminal hexapeptide from mouse metallothionein: study by linear sweep voltammetry and multivariate curve resolution analysis **468**, 202
Electrocatalytic reduction of uranium by bacterial cytochromes: biochemical and chemical factors influencing the catalytic process **471**, 96
Electrochemical and electrocatalytic properties of tetra-iron substituted sandwich-type pentadecatungstodiphosphate heteropolyanions **476**, 85
Electrochemical studies of ferrocene derivatives and their complexation by β-cyclodextrin **477**, 130
Electrochemical study on Cd binding to metallothioneins isolated from the mussel, *Mytilus galloprovincialis* **466**, 75
Electropolymerization of methacrylonitrile and *N*-vinyl-2-pyrrolidone as probed by an EQCM **465**, 200
Factors influencing the ion-exchange preconcentration and voltammetric behaviour of redox cations at polyestersulfonated ionomer coated electrodes in acetonitrile solutions **460**, 38
Feasibility studies for the detection of volatile organic compounds in the gas phase using microelectrode sensors **460**, 105
Formation of a nickel hydroxide monolayer on Au through a self-assembled monolayer of 5,5′-dithiobis(2-nitrobenzoic acid): voltammetric, SERS and XPS investigations of the modified electrodes **468**, 170
Lability criteria for metal complexes in micro-electrode voltammetry **471**, 55
Low-temperature sonoelectrochemical processes: Part 1. Mass transport and cavitation effects of 20 kHz ultrasound in liquid ammonia **477**, 71
Polymerization reaction coupled to charge transfer: propagation versus termination as a source of permanent travelling waves and multi-peak voltammograms **479**, 43
Preparation and characterization of Nafion® coated sphere-cap mercury microelectrodes **471**, 48
Surface structural transitions induced by repetitive underpotential deposition of Ag on Au(111) **474**, 138
Synthesis, characterisation and voltammetric study of a β-Keggin-type $[PW_{12}O_{40}]^{3-}$ complex **465**, 129
The potentiodynamic behaviour of iridium electrodes in aqueous 3.7 M H_2SO_4 in the 293–195 K range **461**, 40
Transfer of heavy metal ions across the water | nitrobenzene microinterface facilitated by the cadmium selective ionophore ETH1062 **475**, 9
Use of a zeolite-modified electrode for the study of the methylviologen–sodium ion-exchange in zeolite Y **463**, 100
Voltammetric and UHV characterisation of the (1 × 1) and reconstructed hex-R0.7° phases of Pt{100} **467**, 60
Voltammetric and XPS investigations of nickel hydroxide electrochemically dispersed on gold surface electrodes **462**, 202
Voltammetric currents for any ligand-to-metal concentration ratio in fully labile metal-macromolecular complexation. Easy

computations, analytical properties of the currents and a graphical method to estimate the stability constant **472**, 42
Voltammetric metal speciation in mixtures of inert and labile macromolecular complexes at any ligand-to-metal ratio: differential pulse polarographic study of the Zn(II)–nitrilotriacetate–polymethacrylate system **462**, 157
Voltammetry in solutions of low ionic strength. Electrochemical and analytical aspects **466**, 129
Voltammetry of sparingly soluble metal complexes: a differential pulse polarographic study of the Zn(II) + oxalate system **475**, 99
Voltammetry using an electrode surface continuously renewed by laser ablation and its demonstration on electro-oxidation of L-ascorbic acid **466**, 31

Wall-jet electrode
Detection of near-wall hydrodynamic effects by electrochemiluminescence **470**, 89
Wall-jet ring disk electrode
A wall-jet ring disk electrode fabricated within a thin-layered micromachined cell **479**, 57
Water
Interaction of H, O and OH with metal surfaces **472**, 126
Water decomposition
Redox mechanisms of NO with water on the Pt(111) electrode studied by in-situ STM and IRAS **473**, 43
Water electrolysis
Electrodeposited $PbO_2 + RuO_2$: a composite anode for oxygen evolution from sulphuric acid solution **465**, 160
Water management
Effect of water transport in a PEFC at low temperatures operating with dry hydrogen **477**, 164
Theory for water management in membranes for polymer electrolyte fuel cells: Part 1. The effect of impurity ions at the anode side on the membrane performances **465**, 1
Theory for water management in membranes for polymer electrolyte fuel cells: Part 2. The effect of impurity ions at the cathode side on the membrane performances **465**, 18

XANES
Preparation and characterization of sol–gel derived carbon composite ceramic electrodes: electrochemical and XANES study of nitrite reduction **468**, 131
Xanthate
In situ orientation study of xanthate on copper under potential control **475**, 124
Xanthine oxidase
Electrooxidation of the antileukemic 2-chloro-2′-deoxyadenosine and related compounds **477**, 89
XPS
Characterization of platinum-rutheniun electrodeposits using XRD, AES and XPS analysis **460**, 32
Characterization of platinum-rutheniun electrodeposits using XRD, AES and XPS analysis **460**, 32
Formation of a nickel hydroxide monolayer on Au through a self-assembled monolayer of 5,5′-dithiobis(2-nitrobenzoic acid): voltammetric, SERS and XPS investigations of the modified electrodes **468**, 170
X-ray absorption fine structure (XAFS)
In-situ X-ray absorption studies of bromine on the Ag(100) electrode **473**, 19
X-ray and electrochemical studies
X-ray and electrochemical studies of Cu upd on single crystal electrodes in the presence of bromide: comparison between Au(111) and Pt(111) electrodes **460**, 121
X-ray diffraction
Characterization of platinum-rutheniun electrodeposits using XRD, AES and XPS analysis **460**, 32
X-ray photoelectron spectroscopy
Anodic electrodeposition of conducting cobalt oxyhydroxide films on a gold surface. XPS study and electrochemical behaviour in neutral and alkaline solution **476**, 54
Effect of the partial replacement of Ni or Co by Cu on the electrocatalytic activity of the $NiCo_2O_4$ spinel oxide **464**, 187
Structure and electrochemical behavior of a flavin sulfide monolayer adsorbed on gold **472**, 147
Voltammetric and XPS investigations of nickel hydroxide electrochemically dispersed on gold surface electrodes **462**, 202
X-ray photoelectron spectroscopy (XPS)
Electrochemical oxidation of pyrite (FeS_2) in aqueous electrolytes **471**, 116
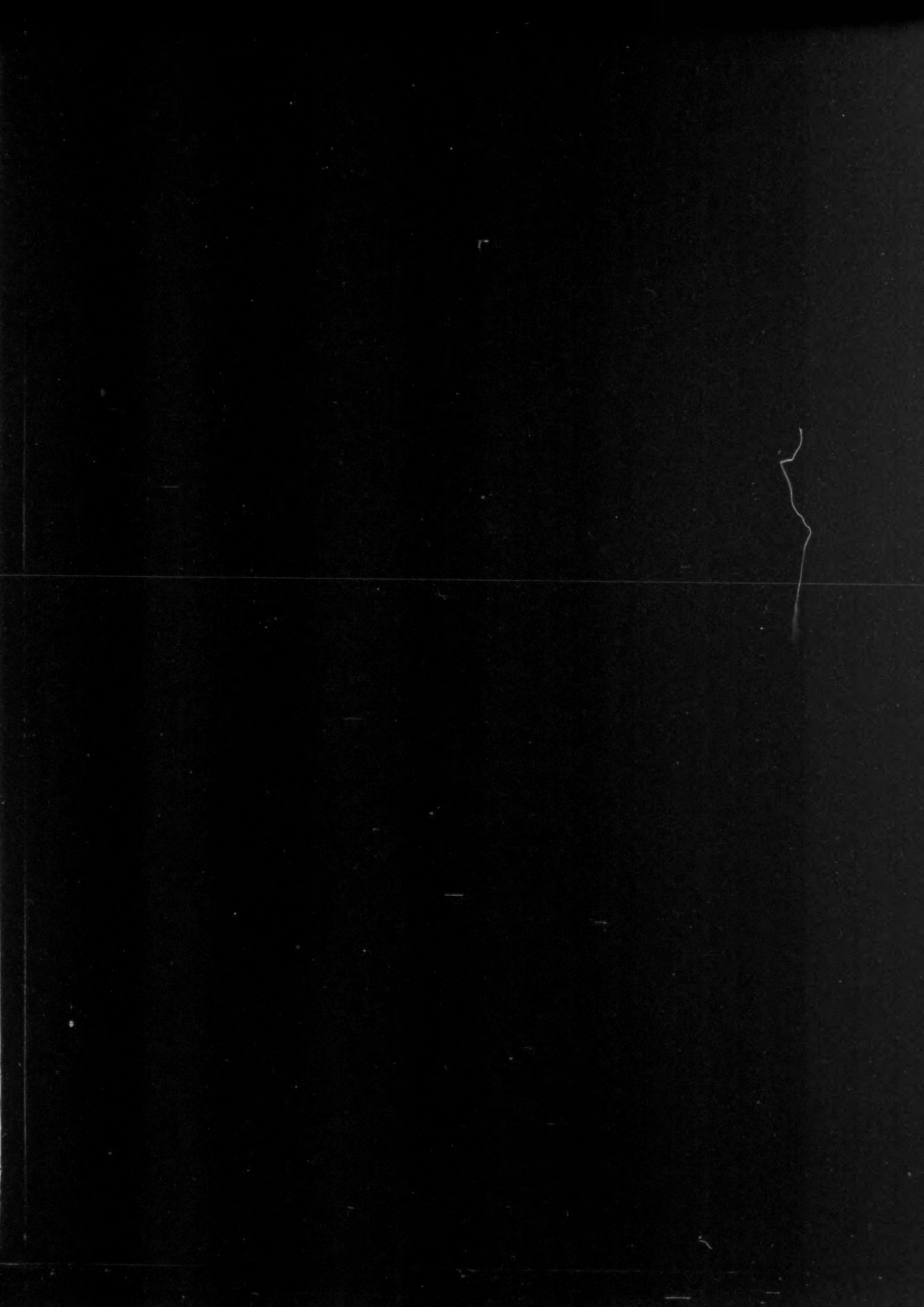
Zeolite electrodes
Ruthenium purple-containing zeolite modified electrodes and their application for the detection of glucose **466**, 82
Zeolites
Use of a zeolite-modified electrode for the study of the methylviologen–sodium ion-exchange in zeolite Y **463**, 100
Zinc
A new approach to the estimation of electrocrystallization parameters **474**, 69
Two-dimensional metal deposition at the liquid|liquid interface: potential and magnetohydrodynamic pattern transition **473**, 54
Ultra-fast electropolymerization of pyrrole in aqueous media on oxidizable metals in a one-step process **478**, 92
Voltammetric metal speciation in mixtures of inert and labile macromolecular complexes at any ligand-to-metal ratio: differential pulse polarographic study of the Zn(II)–nitrilotriacetate–polymethacrylate system **462**, 157
Zinc + iron alloys
Electrodeposition of zinc + iron alloys: I. Analysis of the initial stages of the anomalous codeposition **469**, 139
Electrodeposition of zinc + iron alloys: II. Relation between the stripping results and ex-situ characterization **475**, 66
Zinc oxide nancrystallites
Chiroselective electron transfer at enantiomer-capped ZnO nanocrystalline surfaces **473**, 117
Zirconia
Electrochemical features of zirconia polymorphs. The interplay between structure and surface OH species **465**, 136
Zirconium alkoxide
Formation of Al–Zr composite oxide films on aluminum by sol–gel coating and anodizing **473**, 250
Zirconium oxide
Formation of Al–Zr composite oxide films on aluminum by sol–gel coating and anodizing **473**, 250
Z-isomers
Langmuir–Blodgett films of azocrown ethers on electrodes — voltammetric recognition of isomers **471**, 156
Zn(II) + oxalate system
Voltammetry of sparingly soluble metal complexes: a differential pulse polarographic study of the Zn(II) + oxalate system **475**, 99
Zn(II) reduction
Electrode kinetics and the nature of the metal electrode: Part 4. The Zn(II)/Zn electrode reaction studied at dropping Tl + Ga alloy electrodes **472**, 64
Electrode kinetics and the nature of the metal electrode: Part 3. The Zn(II)/Zn electrode reaction studied at In + Ga dropping (micro)electrodes **472**, 53
ZnO
Electroless copper plating on a glass substrate coated with ZnO film under UV illumination **462**, 259
Photoelectrochemical response and stability of titanium–zinc mixed oxide films formed by thermal oxidation **464**, 238
ZnSe
Formation of ZnSe on Ag(111) by electrochemical atomic layer epitaxy **475**, 164